

**SEISMIC MODELING AND IMAGING FOR DETECTION OF CLANDESTINE
TUNNELS**

A Thesis Presented to
the Faculty of the Department of Earth and Atmospheric Sciences
University of Houston

In Partial Fulfillment
of the Requirements for the Degree
Master of Science

By
Seckin Polat
August 2017

**SEISMIC MODELING AND IMAGING FOR DETECTION OF CLANDESTINE
TUNNELS**

Seckin Polat

APPROVED:

Dr. Yingcai Zheng, Chairman

Dr. John Patrick Castagna, Member

Dr. Engin Alkan, Member

Dr. Dan E. Wells

Dean, College of Natural Sciences and Mathematics

Acknowledgements

I would like to express my thanks to the people who were involved and supported me during my Master's at the University of Houston.

First and foremost, I would like to recognize my advisor Dr. Yingcai Zheng, to whom I express deepest gratitude. It was truly an honor to be his first official graduate student, and I am indebted to him. I also wish to express my sincerest appreciation to my committee members, Dr. John Castagna and Dr. Engin Alkan, for their support and confidence in me and my research. I am thankful to Dr. Hu Hao for helping along the way through all the steps of my thesis, and providing enlightenment. I am also grateful to Turkish Petroleum for their financial contribution to my education at the University of Houston. I also would like to thank my girlfriend Megan E. Gryga for helping me with editing this thesis. Finally, I dedicate this master's thesis to my family who have supported me through everything.

**SEISMIC MODELING AND IMAGING FOR DETECTION OF CLANDESTINE
TUNNELS**

An Abstract of a Thesis Presented to
the Faculty of the Department of Earth and Atmospheric Sciences
University of Houston

In Partial Fulfillment
of the Requirements for the Degree
Master of Science

By
Seckin Polat
August 2017

Abstract

Covert subterranean tunnels have especially been used for drug smuggling and illegal trading across country borders such as the United States – Mexico, Egypt – Israel and so on over the years. Conventional border security measures and intel activities of border security agencies remain insufficient in stopping these illegal underground passageways. During the 2016 U.S. presidential election, arguments were particularly focused on constructing a wall that contains sensors to locate possible existing and future clandestine tunnels between the U.S. and Mexico. The reliability of a specific scientific method that can detect tunnel locations accurately has not been established yet. Among many proposed methods, seismic method is a promising technique for imaging those tunnels, despite its many potential drawbacks, such as low signal-to-noise ratio (S/N), scattering, absorption, and heterogeneity of complex subsurface structures. Instead, by assigning proper parameters into numerical modeling and projecting, the modeled results derived from these forward numerical model examples may allow us to investigate the seismic detection capability under optimal conditions and various data acquisition geometries. The experience acquired from the numerical modeling and imaging may lead us to locate the clandestine tunnels under realistic conditions.

In our modeling, we use the elastic full-wave finite-element method to simulate seismic wave interaction with subsurface tunnels. We test different frequencies and observational geometries including surface and borehole sources and receivers. We then used the modeled seismic data to implement the Kirchhoff migration. We have investigated various types of soils and boundary conditions. The modeling and imaging

can help us define the optimal seismic data acquisition scheme for detecting subsurface voids and tunnels.

Table of Contents

Table of Contents	vii
List of Figures.....	ix
List of Tables	xxvii
Chapter 1: Introduction	1
1.1 Motivation.....	1
1.2 Survey of Geophysical Tunnel Detection Methods	5
1.3 Proposed Work for This Thesis	8
1.4 Seismic Data Acquisition and Geometry	10
1.4.1 Seismic Methods.....	11
1.4.1.1 Surface Seismic Acquisition.....	11
1.4.1.2 Cross-Well Seismic Acquisition.....	13
1.4.2 Seismic Imaging.....	17
1.4.2.1 Kirchhoff Migration.....	17
1.5 Modeling and Imaging Procedure.....	18
1.5.1 Gmsh.....	19
1.5.2 Specfem2D.....	23
1.5.3 Seismic Un*x.....	29
Chapter 2: Tunnel Modeling with Subsurface Acquisition Geometry	31
2.1 Introduction.....	31
2.2 Models With a 14 m Deep Tunnel.....	33
2.2.1 One Layer Case.....	33
2.2.2 Two-Layered Case.....	52
2.3 Model of Tunnel Located at 19 Meters.....	71
2.3.1 One Layer Case.....	71
2.3.2 Two-Layered Case.....	87
Chapter 3: Tunnel Modeling with Cross-Well Seismic Method.....	104
3.1 Introduction.....	104
3.2 Example of Sources and Receivers Are Located in The Formation.....	104

3.2.1 Model of Tunnel Located at 14 Meters Depth.....	111
3.2.1.1 One Layer Case.....	111
3.2.1.2 Two-Layered Case.....	120
3.2.2 Model of Tunnel Located at 19 Meters Depth.....	129
3.2.2.1 One Layer Case.....	129
3.2.2.2 Two-Layered Case.....	137
Chapter 4: Recommended Acquisition Design to Locate Tunnels.....	146
4.1 Introduction.....	146
4.1.1 Model of Tunnel Located at 14 Meters Depth.....	147
4.1.1.1 One Layer Case.....	148
4.1.1.2 Two-Layered Case.....	156
Chapter 5: Discussion.....	166
Chapter 6: Conclusion.....	168
Chapter 7: Future Work.....	169
Chapter 8: References.....	170

List of Figures

Figure 1.1: A clandestine tunnel found in Otay Mesa, California in 2016 (from ice.gov).	2
Figure 1.2: A close caption shows the location of Otay Mesa (yellow rectangle) and Tijuana (red rectangle) (Captured by Google Earth Pro).....	3
Figure 1.3: A caption shows the location of Otay Mesa (yellow rectangle), Tijuana (red rectangle), and San Diego (blue rectangle) (Captured by Google Earth Pro).....	4
Figure 1.4: Snell Law (Modified from Lavergne, 1989).	11
Figure 1.5: Principle of Tunnel Seismic Imaging from Subsurface (Modified from Gao et al., 2014).	12
Figure 1.6: Acoustic Impedance (Modified from Lavergne, 1989).....	13
Figure 1.7: Principle of the cross-well seismic acquisition geometry.	14
Figure 1.8: An example of the wavelength.	15
Figure 1.9: The high resolution of the cross-well seismic result (left) compared with the surface seismic result (right) due to the cross-well seismic's high frequency source (Modified from Marion, 2014).	16
Figure 1.10: a) shows the seismic acquisition design for imaging the scatterer and b) displays the recorded waves from the scatterer that we summon to generate the Kirchhoff hyperbola (Retrieved from Pyun et al., 2008).....	18
Figure 1.11: An example of a .geo file used to generate a model via Gmsh.	21
Figure 1.12: Assigned points and lines of a .geo file in Gmsh software.	22
Figure 1.13: A screenshot of a meshed model with assigned points and lines in Gmsh software.....	23

Figure 1.14: Par_file of Specfem2D.....	25
Figure 1.15: SOURCE file of Specfem2D.....	26
Figure 1.16: process_the_Gmsh_file_once_and_for_all.sh script of Specfem2D.....	26
Figure 1.17: run_this_example.sh script of Specfem2D.....	27
Figure 1.18: A snapshot of Specfem2D while seismic waves propagate and interact with the tunnel inside of the numerical model.....	28
Figure 1.19: An example of visualization of a shot gather result using suximage program.....	30
Figure 2.1: Dimensions of the tunnel in our model.....	31
Figure 2.2: Fourteen meter deep tunnel model with one layer that has the absorbing boundary conditions for all boundaries with a single-force 400 Hz source (shown with a star) located at 25 meters on the surface.....	36
Figure 2.3: A snapshot of 14 meter deep tunnel model with one layer that has the absorbing boundary condition for all the boundaries run in Specfem2D at 5.5 ms with single-force 400 Hz source located on the surface.....	37
Figure 2.4: A snapshot of 14 meter deep tunnel model with one layer that has the absorbing boundary conditions for all boundaries while running in Specfem2D at 13.75 ms with a single-force 400 Hz source located at 25 meters on the surface.....	38
Figure 2.5: Fourteen-meter-deep tunnel model with one layer that has the absorbing boundary conditions for all boundaries with a single-force 400 Hz source (shown with a star).....	39

Figure 2.6: The seismogram (z-component) of a 14 meter deep tunnel model with a layer for absorbing boundary condition of all boundaries with a single-force 100 Hz source located at 25 meters distance and three meters depth (Figure 2.2). 40

Figure 2.7: The set of seismic shot gathers (z component) for the 14 meter depth one layer model with the absorbing boundary condition for 100 Hz sources, whose shot locations were displayed with stars..... 41

Figure 2.8: The migration velocity model for the homogenous medium that has one layer (vel represents velocity whose unit is m/sec). 42

Figure 2.9: Kirchhoff migration result of a 14 meter deep tunnel model with a layer with the absorbing boundary condition for all boundaries (Amp represents the amplitude, which is a measure of the contrast in density, seismic velocities of the formations and / or underground structures. Amplitude allows us to interpret the formations and the structures in the seismic data). 43

Figure 2.10: The seismogram (z-component) of a 14 meter deep tunnel model with one layer for the free surface boundary condition of the top boundary. The seismic source is a single-force 100 Hz source that located at 25 meters on the surface. 44

Figure 2.11: The set of shot gathers (z component) for a 14 meter depth one layer model with free surface boundary condition for 100 Hz seismic sources, whose shot locations were displayed with stars. 45

Figure 2.12: Kirchhoff migration result for the seismogram of a 14 meter deep tunnel model with a layer for the free surface boundary condition at the surface (Amp shows the

amplitude that is a measure of the contrast in density, seismic velocities of the formations and / or underground structures). 46

Figure 2.13: The seismogram (z-component) of a 14 meter deep tunnel model with a layer that has the absorbing boundary condition for all boundaries for a single-force 400 Hz source located at 25 meters distance on x-axis and three meters depth. 47

Figure 2.14: The set of seismic shot gathers (z-components) for a 14 meters depth one layer model that has the absorbing boundary condition for all boundaries with 400 Hz sources whose locations (on the surface) were marked with stars..... 48

Figure 2.15 Kirchhoff migration result of the 14 meter deep tunnel model with a layer has the absorbing boundary condition for all boundaries (Amp represents the amplitude, which is a measure of the contrast in density, seismic velocities of the formations and / or underground structures). 49

Figure 2.16: The seismogram (z-component) of 14 meter deep tunnel model with a layer with the free surface boundary condition at the surface (25 m) with a single force 400 Hz source. 50

Figure 2.17: The seismic shot gather (z-component) for a 14 meter depth one layer model with the free surface boundary condition (surface). We used single-force 400 Hz seismic sources, whose shot locations are displayed with stars on the surface. 51

Figure 2.18: Kirchhoff migration result of the 14 meter deep tunnel model with a layer for free surface boundary condition at the surface (Amp shows the amplitude, which is a measure of the contrast in density, seismic velocities of the formations and / or underground structures). 52

Figure 2.19: Fourteen meters depth tunnel model with two layers with the absorbing boundary condition for the all boundaries. The seismic source is a single-force with 400 Hz located on the surface (shown with the star).	55
Figure 2.20: Fourteen meters depth tunnel model with two layers run in Specfem2D at 5.75 ms.....	56
Figure 2.21: Fourteen meters depth tunnel model with one layer run in Specfem2D at 10 ms while seismic wave propagations are reflected from the deeper formation and the tunnel and travel back to the surface.....	57
Figure 2.22: Fourteen-meter-deep tunnel model with two layers that has the absorbing boundary conditions for all boundaries with a single-force 400 Hz source at three meters depth (shown with a star).....	58
Figure 2.23: The seismogram (z-component) of a 14 meters deep tunnel model with two layers for the absorbing boundary conditon at the surface with a single-force of 100 Hz source.....	59
Figure 2.24: The migration velocity model for the two-layered medium (vel represents velocities whose values are between 2500 m/sec to 3000 m/sec).	60
Figure 2.25: The seismic shot gather (z-component) for 14 meters depth two-layered model with the absorbing boundary condition for all the boundaries. Sources are single-forces with 100 Hz, shot locations were shown with stars.	61
Figure 2.26: Kirchhoff migration result of the 14 meters depth tunnel model with two layers for an absorbing boundary condition for all boundaries with 100 Hz seismic sources (Amp represents the amplitude, which is a measure of the contrast in density,	

seismic velocities of the formations and / or underground structures. Amplitude allows us to interpret the formations and the structures in the seismic data).....	62
Figure 2.27: The seismogram (z-component) of a 14 meters depth model for a free surface boundary condition with a parallel layer for a 100 Hz seismic source at 25 meters on the surface.	63
Figure 2.28: The set of shot gathers for the free boundary condition (surface) for 14 meters depth tunnel with a parallel layer with the seismic sources of 100 Hz (shown with stars).....	64
Figure 2.29: Kirchhoff migration result of the 14 meters depth tunnel model with two layers for the free surface boundary condition (surface) with single-force seismic sources of 100 Hz.....	65
Figure 2.30: The seismogram (z-component) of a 14 meters depth model with two layers for the absorbing boundary condition (all boundaries) with a single-force 400 Hz source at three meters depth from the surface.....	66
Figure 2.31: The set of shot gathers of 14 meters depth tunnel model with two layers that have the absorbing boundary condition (all boundaries) with single-force 400 Hz seismic sources (shown with stars) on the surface.....	67
Figure 2.32: Kirchhoff migration result of the 14 meters depth tunnel model with two layers model for the absorbing boundary condition (all boundaries) (Amp shows the amplitude, which is a measure of the contrast in density, seismic velocities of the formations and / or underground structures).....	68

Figure 2.33: The seismogram (z-component) of a 14 meters depth tunnel model with two layers for the free surface condition (surface) with a single-force 400Hz seismic source at 25 meters on x-axis at the surface. 69

Figure 2.34: The set of shot gathers of 14 meters depth tunnel with two layers for the free surface boundary condition with single-force seismic sources of 400 Hz (shown with stars). 70

Figure 2.35: The seismic shot gather for the free surface boundary condition for 14 meters depth tunnel with a parallel layer and a seismic source at 400 Hz (Amp represents the amplitude, which is a measure of the contrast in density, seismic velocities of the formations and / or underground structures). 71

Figure 2.36: 14 meter depth tunnel model with one layer. The source (shown with the star is a single-force with 400 Hz located at 25 meters on x-axis 75

Figure 2.37: Fourteen meters depth tunnel model with one layer. The shot location (25 meters on x-axis) is shown with the star. 76

Figure 2.38: The seismogram (z-component) of 14 meters depth model with one layer for the absorbing boundary condition (all boundaries) with a single-force 100 Hz seismic source located at 25 meters on x-axis, three meters depth from the surface. 77

Figure 2.39: The set of shot gathers (z-component) for the 19 meters depth tunnel model with one layer of the absorbing boundary condition (for all boundaries) with single-force 100 Hz sources (shown with stars). 78

Figure 2.40: The Kirchhoff migration result for 19 meters depth one layer model with absorbing boundary condition with the 100 Hz source (Amp represents the amplitude,

which is a measure of the contrast in density, seismic velocities of the formations and / or underground structures).	79
Figure 2.41: The seismogram (z-component) of 19 meters depth model with one layer for the free surface boundary condition (surface) with a single-force 100 Hz source located at 25 meters on the surface.	80
Figure 2.42: The set of shot gathers (z-component) for 19 meters depth one layer model with the free surface condition with the single-force 100 Hz sources (shown with stars).	80
Figure 2.43: The seismic shot gather (z-component) for 19 meters depth one layer model with free surface condition for 100 Hz source. The shot locations were showed with stars (Amp shows the amplitude, which is a measure of the contrast in density, seismic velocities of the formations and / or underground structures).	81
Figure 2.44: The seismogram for the model that has a tunnel at 19 Meters depth with one layer for the absorbing boundary condition (all boundaries) with a single-force 400 Hz source located at 25 m on x-axis and three meters depth.	82
Figure 2.45: The set of shot gathers for the model that has a tunnel at 19 meters depth with the single-force 400 Hz sources (shown with stars).	83
Figure 2.46: The Kirchhoff migration result for the model that has a tunnel at 19 meters depth (with extended top boundary-22 meters depth tunnel) with the single-force 400 Hz sources at the three meters depth from the surface (Amp shows the amplitude, which is a measure of the contrast in density, seismic velocities of the formations and / or underground structures).	84

Figure 2.47: The seismogram for the model that has a tunnel at 19 meters depth with one layer and the free surface condition (surface) with the single-force 400 Hz sources located at the surface.....	85
Figure 2.48: The set of shot gathers for the model that has a tunnel at 19 meters depth with single-force sources of 400 Hz (shown with stars).....	86
Figure 2.49: The Kirchhoff migration result for the model that has a tunnel at 19 meters depth with the 400 Hz source at the surface with the absorbing boundary condition (Amp represents the amplitude, which is a measure of the contrast in density, seismic velocities of the formations and / or underground structures).	87
Figure 2.50: Nineteen meters depth tunnel model with two layers for the absorbing boundary case. The source is a single-force with 400 Hz located at 25 meters on x-axis and shown with the star.....	91
Figure 2.51: Nineteen-meter-deep tunnel (22 meters with the extended top) model with two layers that has the absorbing boundary conditions for all boundaries with a single-force 400 Hz source at three meters depth (shown with a star).....	92
Figure 2.52: The seismogram (z-component) of the 19 meters depth tunnel model (22 meters with extended top) with two layers for the absorbing boundary condition with a single-force 100 Hz source at the three meters depth.	93
Figure 2.53: The set of shot gathers (z-component) for the 19 meters depth two-layered model with an absorbing boundary condition for single-force 100 Hz sources, shot locations are shown with stars.	94

Figure 2.54: Kirchhoff migration result of the 19 meters depth tunnel model with two layers for the absorbing boundary condition (all boundaries) with single-force 100 Hz sources on the surface (Amp represents the amplitude, which is a measure of the contrast in density, seismic velocities of the formations and / or underground structures). 95

Figure 2.55: The seismogram (z-component) of the 19 meters depth model with free surface boundary condition with two layers for a 100 Hz seismic source 25 meters on x-axis at the surface..... 96

Figure 2.56: The set of shot gathers for the free boundary condition for the 19 meters depth tunnel with two layers with seismic sources (shown with stars) of 100 Hz located on the surface. 97

Figure 2.57: Kirchhoff migration result of the 19 meters depth tunnel model with two layers for the free surface boundary condition at the surface with 100 Hz sources. (Amp shows the amplitude, which is a measure of the contrast in density, seismic velocities of the formations and / or underground structures)..... 97

Figure 2.58: The seismogram (z-component) of the 19 meters depth tunnel model for the absorbing boundary condition with a parallel layer and a single-force 400 Hz source located at 25 meters on the surface. 98

Figure 2.59: The set of shot gathers of the absorbing boundary condition for the 19 meters depth tunnel with a parallel layer seismic source at 400 Hz. 99

Figure 2.60: Kirchhoff migration result of the 19 meters depth tunnel (22 meters depth due to the extension) model with two layers model with the absorbing boundary

condition at the surface (Amp shows the amplitude, which is a measure of the contrast in density, seismic velocities of the formations and / or underground structures).....	100
Figure 2.61: The seismogram (z-component) of the 19 meters depth tunnel model for the free surface condition with a parallel layer and a 400 Hz seismic source at 25 meters on the surface.	101
Figure 2.62: The seismic shot gather for the free surface boundary condition for the 19 meters depth tunnel with a parallel layer and a seismic source of 400 Hz.	102
Figure 2.63: The seismic shot gather for the free surface boundary condition for the 19 meters depth tunnel with a parallel layer seismic source at 400 Hz (Amp represents the amplitude, which is a measure of the contrast in density, seismic velocities of the formations and / or underground structures).....	103
Figure 3.1: The geometry of the cross-well seismic with wells.	105
Figure 3.2: The 14 meters depth tunnel model with one layer run in Specfem2D at 10 ms.	107
Figure 3.3: The seismogram z-component of the 14 meter depth tunnel model with one layer.....	108
Figure 3.4: The geometry of the cross-well seismic method without wells.	109
Figure 3.5: 14 meters depth tunnel model with one layer run in Specfem2D at 10 ms..	110
Figure 3.6: The seismogram z-component of the 14 meters depth tunnel model with one layer.....	111
Figure 3.7: The acquisition geometry and model parameters of the 14 meters depth tunnel model with one layer.....	114

Figure 3.8: The seismogram (z-component) of the 14 meters depth tunnel model for the absorbing boundary condition with one layer and a 3000 Hz seismic source at 15 meters depth on the left side of the model..... 115

Figure 3.9: The seismic shot gather for the absorbing surface boundary condition for the 14 meters depth tunnel with a parallel layer and a seismic source of 3000 Hz. 116

Figure 3.10: Kirchhoff migration result of the 14 meters depth tunnel model with the one layer model with the absorbing surface boundary condition (all boundaries) with single-force 3000 Hz sources are located on the left boundary (Amp represents the amplitude, which is a measure of the contrast in density, seismic velocities of the formations and / or underground structures). 117

Figure 3.11: The seismogram (z-component) of the 14 meters depth tunnel model with the absorbing boundary (surface) with one layer and a 4000 Hz seismic source at 15 meters depth on the left side of the model. 118

Figure 3.12: The seismic shot gather for the absorbing surface boundary condition for the 14 meters depth tunnel with a parallel layer and a seismic source of 4000 Hz. 119

Figure 3.13: Kirchhoff migration result of the 14 meters depth tunnel model with the one layer model with the absorbing surface boundary condition at the surface and 4000 Hz sources (Amp shows the amplitude, which is a measure of the contrast in density, seismic velocities of the formations and / or underground structures). 120

Figure 3.14: The acquisition geometry design for the 14 meters depth tunnel with two layers for the cross-well seismic without wells. 121

Figure 3.15: The seismogram (z-component) of the 14 meters depth tunnel model with the absorbing boundary condition (surface) with two layers and a 3000 Hz seismic source at 15 meters depth on the left side of the model. 123

Figure 3.16: The set of shot gathers with the absorbing surface boundary condition (all boundaries) for the 14 meters depth tunnel with two layers for the seismic sources of 3000 Hz. 124

Figure 3.17: Kirchhoff migration result of the 14 meters depth tunnel model with two layers with the absorbing surface boundary condition at the surface and 3000Hz sources (Amp represents the amplitude, which is a measure of the contrast in density, seismic velocities of the formations and / or underground structures. Amplitude allows us to interpret the formations and the structures in the seismic data)..... 125

Figure 3.18: The seismogram (z-component) of the 14 meters depth tunnel model with two layers and with the absorbing boundary condition (surface) and a 4000 Hz seismic source at 15 meters depth on the left side of the model..... 126

Figure 3.19: The set of shot gathers with the absorbing surface boundary condition (surface) for the 14 meters depth tunnel with two layers with seismic sources of 4000 Hz. 127

Figure 3.20: Kirchhoff migration result of the 14 meters depth tunnel model with two layers with the absorbing surface boundary condition at the surface and 4000 Hz sources (Amp shows the amplitude, which is a measure of the contrast in density, seismic velocities of the formations and / or underground structures). 128

Figure 3.21: The acquisition geometry and parameters of the 14 meters depth tunnel model with one layer.....	131
Figure 3.22: The seismogram (z-component) of the 14 meters depth tunnel model for the absorbing boundary condition with one layer and a 3000 Hz seismic source at 15 meters depth on the left side of the model.....	132
Figure 3.23: The set of shot gathers for the absorbing surface boundary condition for the 19 meters depth tunnel within one layer and seismic sources of 3000 Hz.	133
Figure 3.24: Kirchhoff migration result of the 19 meters depth tunnel model with one layer with the absorbing surface boundary condition at the surface and 3000 Hz sources (Amp represents the amplitude, which is a measure of the contrast in density, seismic velocities of the formations and / or underground structures).	134
Figure 3.25: The seismogram (z-component) of the 19 meters depth tunnel model with the absorbing boundary condition (surface) with one layer and a 4000 Hz seismic source at 20 meters depth on the left side of the model.	135
Figure 3.26: The set of shot gathers for the absorbing surface boundary condition for the 19 meters depth tunnel with a parallel layer and a seismic source of 4000 Hz.	136
Figure 3.27: Kirchhoff migration result of the 19 meters depth tunnel model with one layer with the absorbing surface boundary condition at the surface and 4000 Hz sources (Amp shows the amplitude, which is a measure of the contrast in density, seismic velocities of the formations and / or underground structures).	137
Figure 3.28: The acquisition geometry design for the 19 meters depth tunnel with two layers for the cross-well seismic method without wells.	139

Figure 3.29: The seismogram (z-component) of the 19 meters depth tunnel model with the absorbing boundary (surface) with two layers and a 3000 Hz seismic source at 20 meters depth on the left side of the model. 140

Figure 3.30: The set of shot gathers with the absorbing surface boundary condition (surface) for the 19 meters depth tunnel with two layers for the seismic sources of 3000 Hz. 141

Figure 3.31: Kirchhoff migration result of the 14 meters depth tunnel model with two layers with the absorbing boundary condition (for all boundaries) and single-force 3000 Hz sources are located on the left boundary (Amp shows the amplitude, which is a measure of the contrast in density, seismic velocities of the formations and / or underground structures). 142

Figure 3.32: The seismogram (z-component) of the 19 meters depth tunnel model with the absorbing boundary condition (surface) with two layers and a 4000 Hz seismic source at 20 meters depth on the left side of the model. 143

Figure 3.33: The set of shot gathers with the absorbing surface boundary condition (for all boundaries) for the 19 meters depth tunnel with two layers. The seismic sources are single-force 4000 Hz sources that are located on the left boundary of the model. 144

Figure 3.34: Kirchhoff migration result of the 19 meters depth tunnel model with two layers with the absorbing surface boundary condition (for all boundaries) and the seismic sources are single-force 4000 Hz sources located on the left boundary of the model (Amp represents the amplitude, which is a measure of the contrast in density, seismic velocities of the formations and / or underground structures). 145

Figure 4.1: The acquisition geometry and parameters of the 14 meters depth tunnel model with one layer when the receivers and the source are located on the left boundary of the model..... 150

Figure 4.2: The acquisition geometry and parameters of the 14 meters depth tunnel model with one layer when the source is located on the left boundary and the receivers are placed on the right boundary of the model. 151

Figure 4.3: Kirchhoff migration result for the model in which single-force 3000 Hz sources and the receivers are located on the left boundary of the model (Amp represents the amplitude, which is a measure of the contrast in density, seismic velocities of the formations and / or underground structures)..... 152

Figure 4.4: Kirchhoff migration result for the model in which single-force 3000 Hz sources are located on the left boundary and the receivers are placed on the right boundary of the model (Amp shows the amplitude, which is a measure of the contrast in density, seismic velocities of the formations and / or underground structures)..... 153

Figure 4.5: Kirchhoff migration result for the model in which single-force 4000 Hz sources and the receivers are located on the left boundary of the model (Amp shows the amplitude, which is a measure of the contrast in density, seismic velocities of the formations and / or underground structures)..... 155

Figure 4.6: Kirchhoff migration result for the model in which single-force 4000 Hz sources are placed on the left boundary of the model and the receivers are located on the right boundary of the model (Amp represents the amplitude, which is a measure of the

contrast in density, seismic velocities of the formations and / or underground structures).	
.....	156
Figure 4.7: The acquisition geometry and parameters of the 14 meters depth tunnel model with two layers when the receivers and the source are located on the left boundary of the model.....	157
Figure 4.8: The acquisition geometry and parameters of the 14 meters depth tunnel model with two layers when the source is located on the left boundary and the receivers are placed on the right boundary of the model.	158
Figure 4.9: The velocity model of the two-layered model (vel represents velocities whose values are between 1100 m/sec to 2500 m/sec).....	160
Figure 4.10: Kirchhoff migration result for the model that has two layers in which single-force 3000 Hz sources and receivers are located on the left boundary of the model (Amp shows the amplitude, which is a measure of the contrast in density, seismic velocities of the formations and / or underground structures).....	161
Figure 4.11: Kirchhoff migration result for the model that has two layers in which single-force 3000 Hz sources are placed on the left boundary of the model and the receivers are located on the right boundary of the model (Amp represents the amplitude, which is a measure of the contrast in density, seismic velocities of the formations and / or underground structures).	162
Figure 4.12: Kirchhoff migration result for the model that has two layers in which single-force 4000 Hz sources and the receivers are located on the left boundary of the model	

(Amp shows the amplitude, which is a measure of the contrast in density, seismic velocities of the formations and / or underground structures).....	163
Figure 4.13: Kirchhoff migration result for the model that has two layers in which single-force 4000 Hz sources are placed on the left boundary of the model and the receivers are located on the right boundary of the model with 3000 Hz source (Amp shows the amplitude, which is a measure of the contrast in density, seismic velocities of the formations and / or underground structures).....	165

List of Tables

Table 1.1: Subsurface modeling and imaging parameters.....	9
Table 1.2: Cross-well tunnel imaging for 14 meters depth tunnel when source is located on surface.....	10
Table 1.3: Meshing scheme for Gmsh.....	20
Table 1.4: Running scheme for Specfem2D.....	29
Table 2.1: Typical Seismic Velocities and Densities of Different Rock Formations (Mavko, 2011).....	33
Table 2.2: Table 2.7 Table 2.8 Table 2.9The acquisition geometry parameters for the tunnel with a depth of 14 meters for subsurface seismic method.....	35
Table 2.3: The acquisition geometry parameters for the tunnel at 14 meters depth for a two-layered model for the subsurface seismic method.....	53
Table 2.4: The acquisition geometry parameters for the tunnel with a depth of 14 meters for subsurface seismic method.....	73
Table 2.5: The acquisition geometry parameters for the tunnel at 14 meters depth with two-layers model for the subsurface seismic method.....	90
Table 3.1: The acquisition geometry for the cross-well seismic method.....	106
Table 3.2: The acquisition geometry parameters for the 14 meters depth tunnel with one layer for the cross-well seismic without wells.....	113
Table 3.3: The acquisition geometry parameters for the 14 meters depth tunnel with two layers for the cross-well seismic without wells.....	122

Table 3.4: The acquisition geometry parameters for the 14 meters depth tunnel with one layer for the cross-well seismic without wells.....	130
Table 3.5: The acquisition geometry parameters for the 19 meters depth tunnel with two layers for the cross-well seismic method without wells.	138
Table 4.1: Orders of magnitudes of Q-factors of rocks of P-Waves (Modified and retrieved from Lavergne, 1989).....	147
Table 4.2: The acquisition geometry parameters for the 14 meters depth tunnel with one layer for the cross-well seismic method without wells.	149
Table 4.3: The acquisition geometry parameters for the 14 meters depth tunnel with one layer for the cross-well seismic without wells.....	159

Chapter 1: Introduction

1.1 Motivation

Since ancient times, hidden tunnels have enjoyed widespread use for a variety of purposes – from clandestine military operations to illicit smuggling. The Ottoman Empire conquered “Constantinople” (1452), the capital of the Byzantium Empire, due to the great contribution of miners. These miners were part of a military unit in charge of digging tunnels under the enemy city walls, organizing explosives throughout the tunnels to destroy the walls from beneath. There are hundreds of examples of military exploitation of covert tunnels, as recent as the first and second World Wars and the Vietnam War. Even the Battle of Mosul in Iraq revealed that terrorists were digging tunnels for surprise attacks against the Iraqi Army (McKirdy et al., 2017). However, during the late 1980s, covert tunnels began to be utilized far beyond their earlier military purposes towards more criminal activities, such as drug smuggling and human trafficking, especially between Mexico and the United States. The first drug tunnel, found in Arizona in 1990, was highly advanced compared to other tunnels; it had lifts, rails, and lighting to increase transportation productivity (Figure 1.1).



Figure 1.1: A clandestine tunnel found in Otay Mesa, California in 2016 (from ice.gov).

Between 1990 and 2015, U.S. law enforcement officials discovered nearly 170 drug smuggling tunnels along the almost 2000-mile-long border between the U.S. and Mexico (Steven et al., 2015), although officials do not have an exact number of how many tunnels actually pass under the border. Otay Mesa, California has a notable concentration of these tunnels due to two factors (Figure 1.2, Figure 1.3): its geographic location and near surface geology. Otay Mesa is near Tijuana, Mexico – a well-established drug smuggling hub – and the area’s geological formations. The earth underneath Otay Mesa is composed largely of bentonite which can be easily bored. The

bentonite clay is self-supportive mechanically and lowers the likelihood of tunnels collapsing (Dodds, 2016).

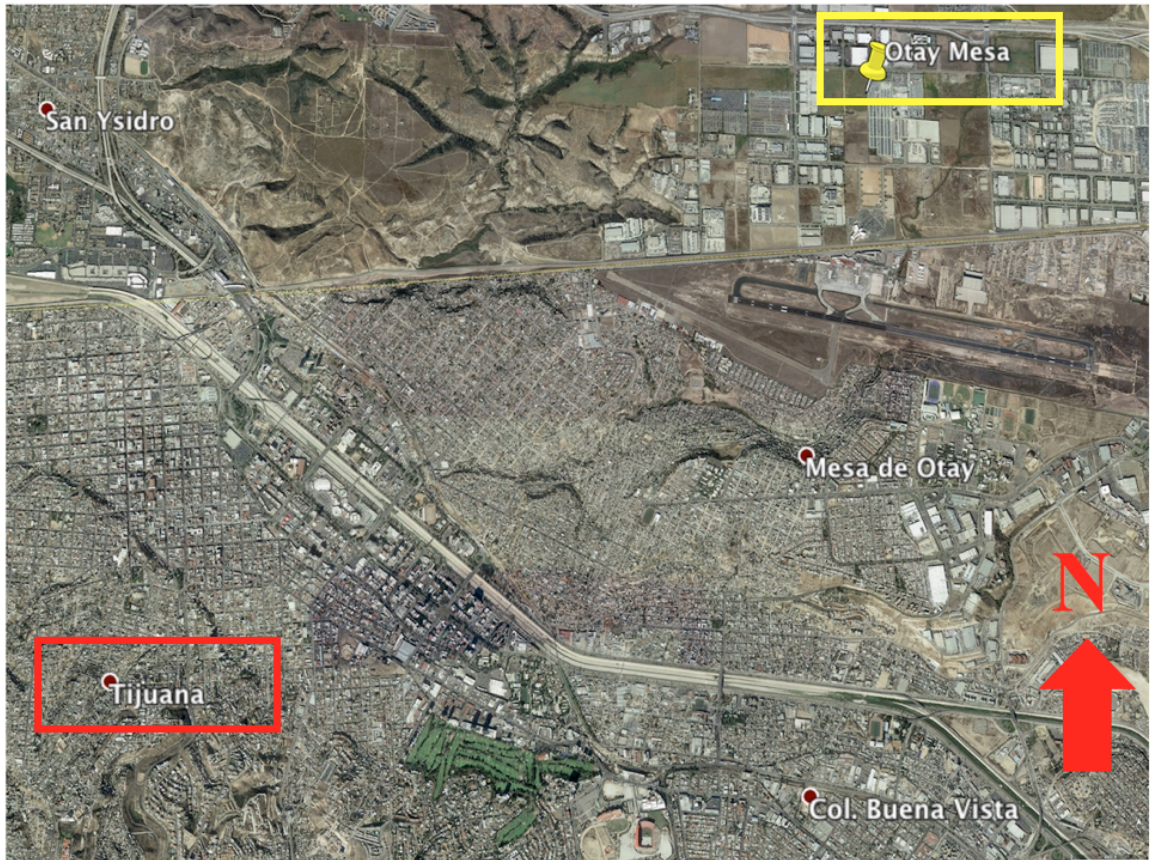


Figure 1.2: A close caption shows the location of Otay Mesa (yellow rectangle) and Tijuana (red rectangle) (Captured by Google Earth Pro).



Figure 1.3: A caption shows the location of Otay Mesa (yellow rectangle), Tijuana (red rectangle), and San Diego (blue rectangle) (Captured by Google Earth Pro).

During the 2016 U.S. presidential elections, then-candidate Donald Trump promised to build a wall between Mexico and the U.S. for border security. The secretary of Homeland Security, John F. Kelly included that the wall would need to be patrolled by law enforcement officers, sensors and observation devices (Smith, 2017). However, details of the construction of the wall and sensors were not shared with the public due to their highly classified content. Tunneling is so common along the U.S. Mexico border according to Border Patrol Agents, certain sections beneath the border, such as the Nogales area in Arizona, are like “Swiss Cheese” (Nixon, 2016).

1.2 Survey of Geophysical Tunnel Detection Methods

Geophysics offers various approaches to detect and image these covert tunnels, such as gravity, electro-magnetic, and seismic methods. Throughout the years, various research projects to detect tunnels using these numerous procedures have been published.

Using the gravity method, authors created a new system that uses an artificial neural network. They tested it with assorted sets of synthetic gravity data and applied their findings to a real data set from the Medford cavity site in Florida. Researchers' findings were promising, except that one complex anomaly occurred due to cavities at two different depth levels (Elawadi et al., 2001). Although the gravity method can be used for detecting clandestine tunnels, it would be expensive and time consuming to apply to the 1,989-mile border between the U.S. and Mexico.

To locate a tunnel in Otay Mesa, researchers Mahrer and List used three radio frequency electro-magnetic field surveys that have skin depth values between 0.47 m. to 1.9 m. for surface to surface, borehole to surface, and borehole to borehole acquisition geometries. Unfortunately, they were unable to produce reliable results with the surface to surface and borehole to surface surveys unless there was an electrical cable in the tunnel. Borehole to borehole survey gave the most accurate results for detecting the existence of an underground passage. This research showed that the electro-magnetic method can be used for the detection of existing tunnels (Mahrer et al., 1977).

In another electro-magnetic based tunnel detection research, Farid and other geoscientists generated numerical models using finite difference and ran an experimental test for cross-well radar (CRW). Since there is no real case study for verification, and a

PVC – which has a different dielectric constant – was used as a tunnel which made an anomaly occur (Farid et al., 2012), further research is needed to demonstrate this method's feasibility.

A distinct survey completed by Ballard focused on locating voids in Medford Cave and Manatee Springs, Florida, and Waverly, Kentucky. Ballard applied and compared various geophysical methods, including seismic refraction, refraction fan-shooting, seismic reflection, seismic cross-hole, and passive seismic. He also used electrical resistivity, cross-hole resistivity, ground penetrating radar, magnetic, micro-gravity, and cross-hole radar. The amount of contrasting methods applied, followed by a cross-method comparison, makes this research among the best. The author concludes that the cross-hole seismic method is the best method due to its high-resolution applications (Ballard, 1982). All these geophysical methods are applied to underground caves and mines that have similar geophysical anomalies to tunnels. In addition, if this research suggested that one of the methods used could be employed as a border security measure for locating drug tunnels, a wall with such sensors along the U.S. border with Mexico would not still be such a hotly-contended subject.

For another seismic method, Rechten and other researchers used the cross-well seismic method to locate an unknown tunnel. The authors compared real and synthetic cross-well seismic data to locate an unknown tunnel. By comparing the synthetic and real data, researchers located a tunnel using this method. The cross-well seismic method proves its reliability for detection of clandestine tunnels. However, the researchers did not share the location of the data possibly due to highly classified information (Rechten et

al., 1995). Furthermore, the authors only mentioned their acquisition geometry they used; they did not mention the recommended acquisition geometry for detection of the clandestine tunnel.

In a different study for tunnel detection using surface seismic method, researchers used reflected and diffracted backscattered waves for a tunnel that had been detected earlier in Otay Mesa by authorities. The authors used the detected tunnel as a calibration target for locating an underground passage whose location is unknown. Researchers located some possible clandestine tunnel locations after processing and interpreting the acquired seismic data set, and they achieved their goal of detecting two possible underground passages in Otay Mesa and one potential tunnel in San Ysidro (Miller, et al., 2003). Since no other method has been used to verify these possible tunnel locations, the accuracy of the author's findings for this research is unknown.

In a final study based on a subsurface seismic acquisition design, Steven and other researchers built a tunnel that was surrounded by formations similar to a dry-desert environment along the southwestern U.S. border to test the detectability of their manmade tunnel via body-wave diffractions and backscattered waves. The scientists used this manmade tunnel to calibrate their acquisition design in order to detect two clandestine tunnels whose locations were not known in Afghanistan (Steven et al., 2015). The authors were able to find a tunnel whose location is unknown using subsurface seismic imaging. On the other hand, even though researchers were able to discover tunnels whose previous location was unknown, their method is not likely to be used for detecting the clandestine tunnels in different locations since the researchers have to build

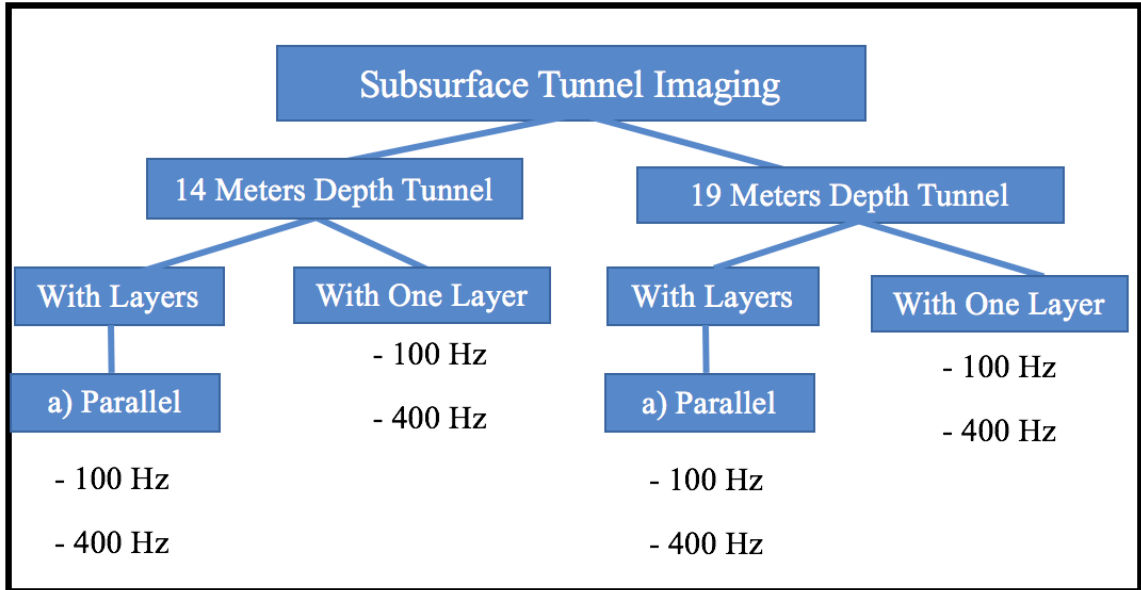
a new manmade tunnel to calibrate their acquisition design for a different tunnel detection survey.

1.3 Proposed Work for This Thesis

Instead, numerical modeling can help us to understand the detectability of clandestine tunnels. By generating numerical models with different parameters (density and seismic velocities of the formations) and various acquisition geometries (near surface seismic imaging, cross-well seismic imaging), we can achieve some outcomes from the numerical modeling that help us process and interpret the real geophysical data sets more accurately.

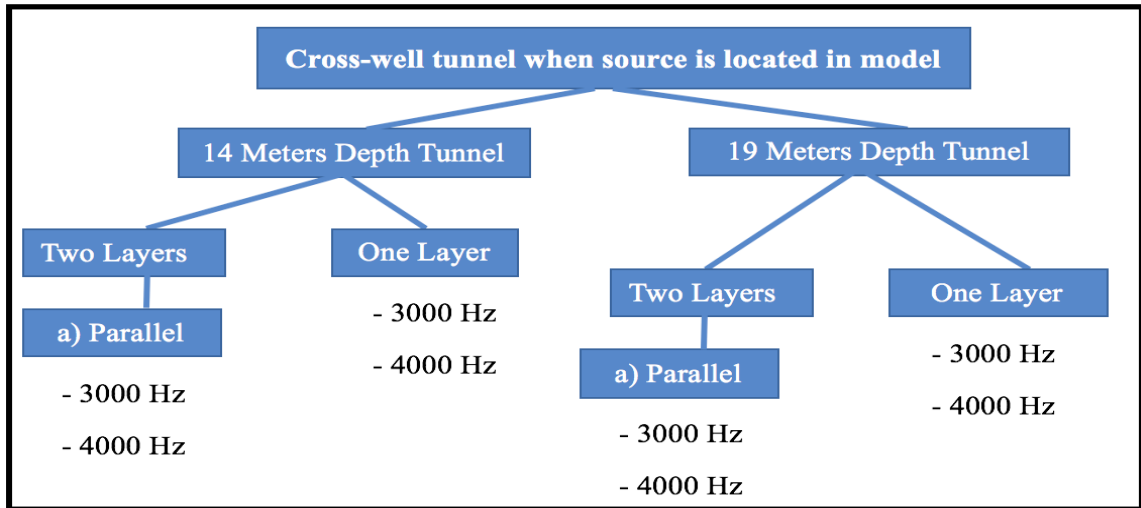
For this objective, we generated a suite of 2D forward numerical models where each of the models has a different geological structure with a clandestine tunnel inside the model at two different depths: 14 and 19 meters. All numerical models were generated using the “Gmsh” open software, which is a 2D / 3D finite-element mesh generator (Geuzaine et al., 2009). After generating the models, we used a finite-element modeling software, “Specfem2D”, to model seismic wave interaction with the tunnel (Komatitsch et al., 1997). We also have considered different acquisition geometries: surface seismic imaging and cross-well seismic imaging (Table 1.1, Table 1.2). For surface sources, we used the single-force seismic source where the source wavelet frequency varies from 100 Hz to 400 Hz (Table 1.1).

Table 1.1: Subsurface modeling and imaging parameters.



For the cross-well modeling geometry, we used the same 2D forward numerical models with the same parameters that we used for surface seismic imaging. For this modeling, we used two different source frequencies, 3 kHz and 4 kHz (Table 1.2).

Table 1.2: Cross-well tunnel imaging for 14 meters depth tunnel when source is located on surface.



After the modeled data has been computed, we applied the Kirchhoff migration to study the detectability of clandestine tunnels. We finalized our research by generating extra models with real parameters of bentonite (density, seismic velocities) (Tisato et al., 2013) and applied Kirchhoff migration to these extra models to find the most realistic acquisition design in order to locate the covert tunnels.

1.4 Seismic Data Acquisition and Geometry

We used two different seismic acquisition geometries, which are surface seismic acquisition geometry and cross-well seismic acquisition geometry for this research.

1.4.1 Seismic Methods

1.4.1.1 Surface Seismic Acquisition

Seismic waves (primary, secondary waves) are a form of energy generated by a controlled source (e.g., hammer, seismic vibrator, air-gun, dynamite). These generated waves propagate along the medium (i.e. geological formations, underground structures). According to Snell Law (Figure 1.4), seismic waves are reflected and / or refracted (Figure 1.5) when they encounter interfaces that have different physical properties (density, velocity) while they are travelling within the formations (Figure 1.6).

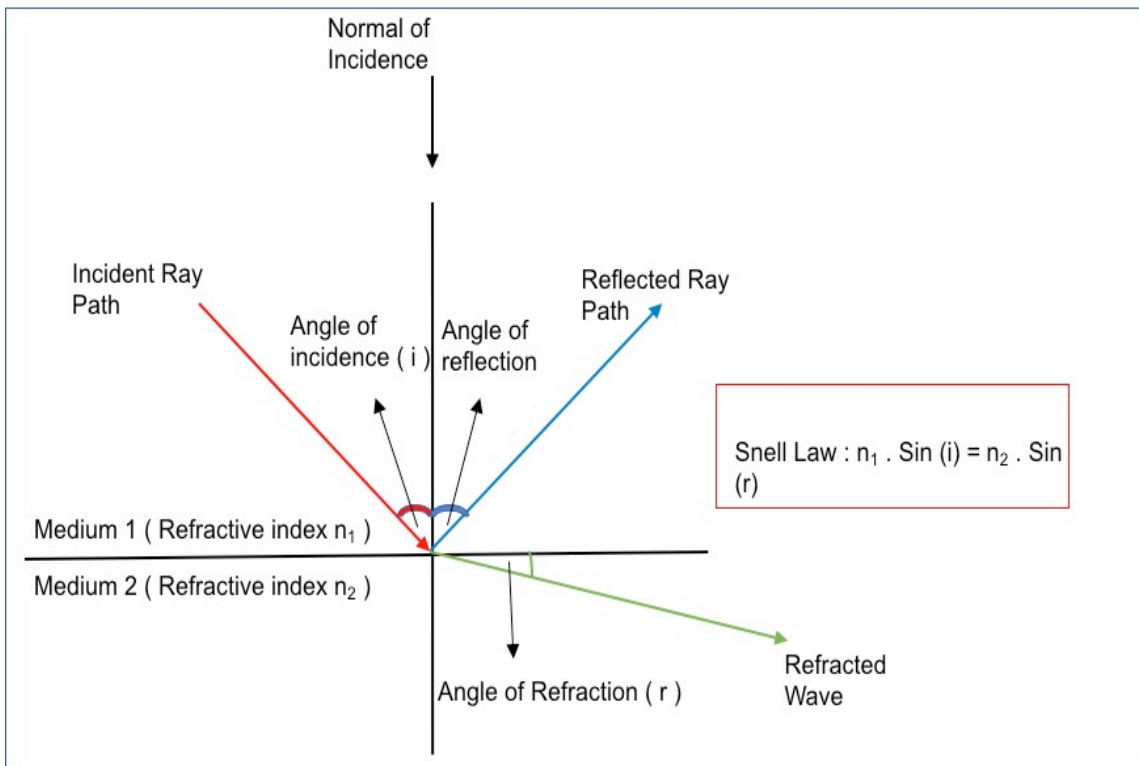


Figure 1.4: Snell Law (Modified from Lavergne, 1989).

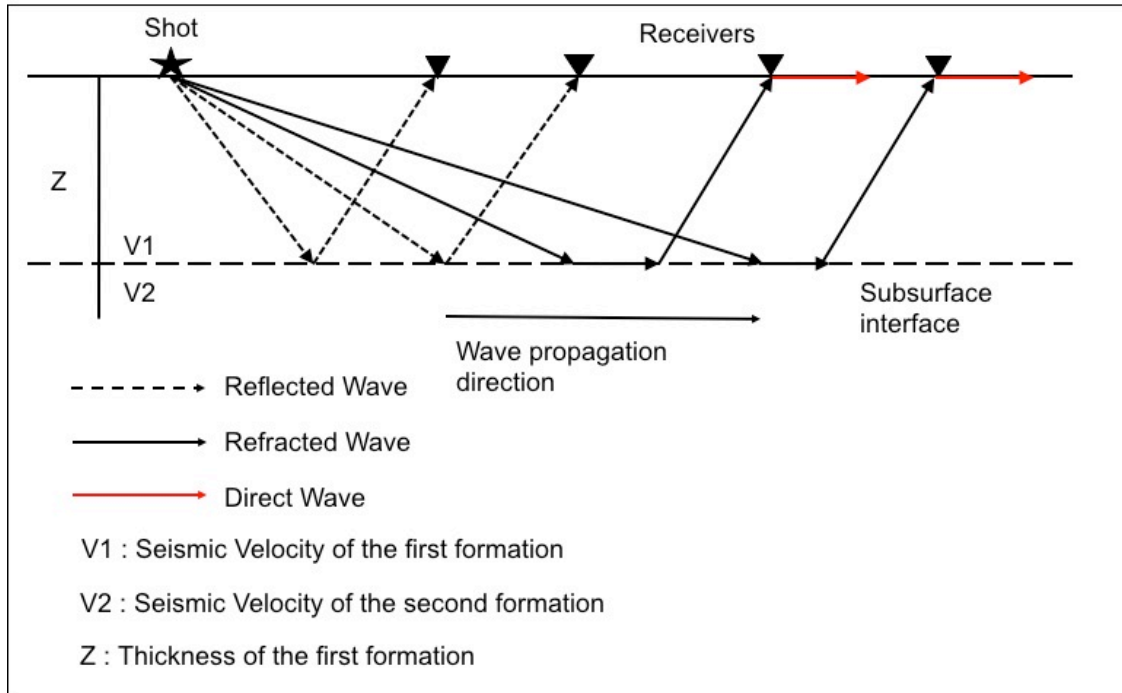


Figure 1.5: Principle of Tunnel Seismic Imaging from Subsurface (Modified from Gao et al., 2014).

Reflected and refracted waves are recorded when they reach receivers (i.e. geophones) from reflector surfaces. Since controlled sources are applied with this procedure, by having calculated travel times, we can determine a formation's seismic velocity, and with angles of reflection, calculate its dipping trend. The diverse characteristics of a formation – determined by its velocity and density values with reflection coefficients – will interact variously with propagated seismic waves in order to penetrate incoming seismic waves (Figure 1.6).

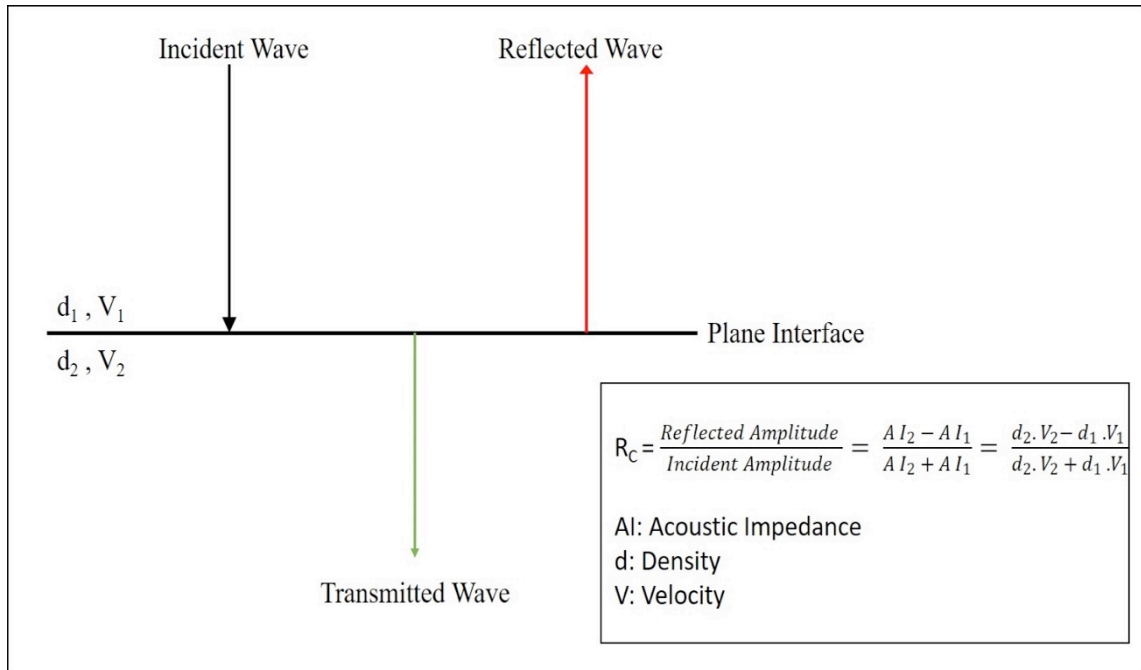


Figure 1.6: Acoustic Impedance (Modified from Lavergne, 1989).

The surface seismic method can be used to detect and locate clandestine tunnels because the existence of a tunnel in a geological formation changes the physical properties (continuity of waves and density) of the formation, so much as to generate seismic reflections and refractions that can be used towards identification of the tunnels in recorded seismograms.

1.4.1.2 Cross-Well Seismic Acquisition

The cross-well seismic is a high-resolution seismic acquisition design that uses a source (e.g., dynamite, electric arc discharge) which is placed inside of a well, while receivers are placed into a neighbor well. The seismic source generates seismic waves that travel along the direction of the wave propagation. When these seismic waves encounter a contrasting formation that has different physical quantities such as density

and porosity, these various physical differences will produce reflections and refractions from a layer that has different physical properties than the medium (Figure 1.7).

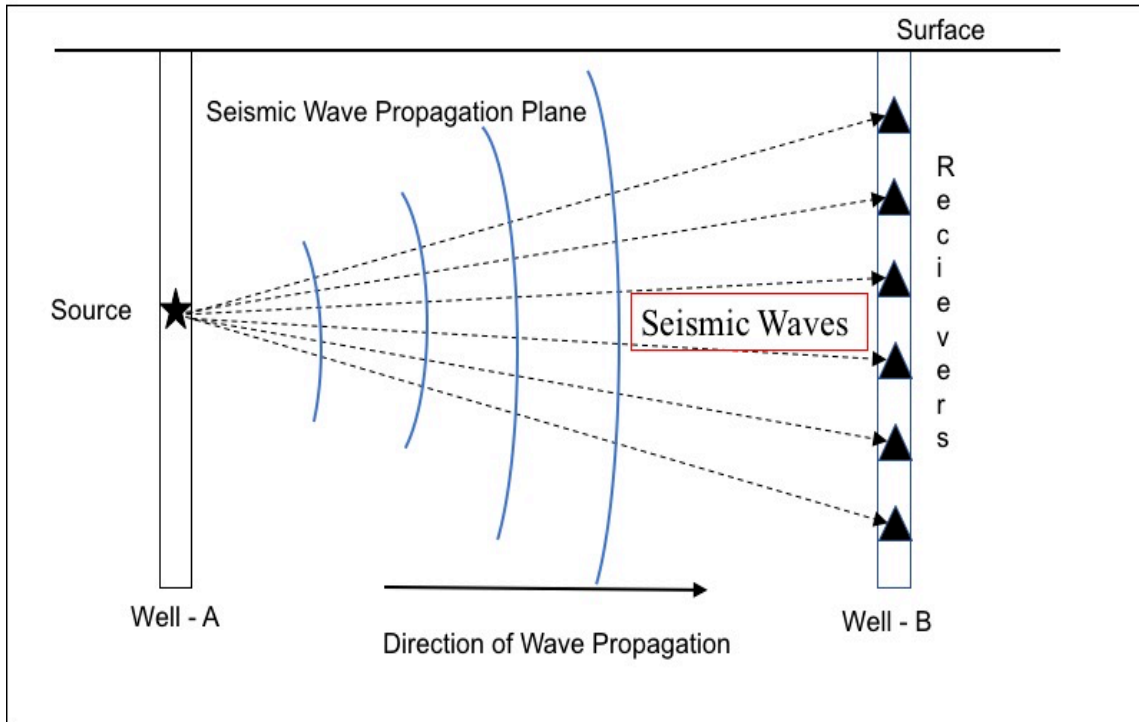


Figure 1.7: Principle of the cross-well seismic acquisition geometry.

In this method, the frequency of the source can reach up to 5 kHz (Marion, 2014) since the frequency of the cross-well is not affected with the weathering zone, which is located close to the surface and coupling problem of the surface sources. Seismic sources generate wavelets that excite particles while traveling through the medium.

The wavelength (λ) is described as the distance between two contiguous points on the wave that have similar displacement. (Figure 1.8).

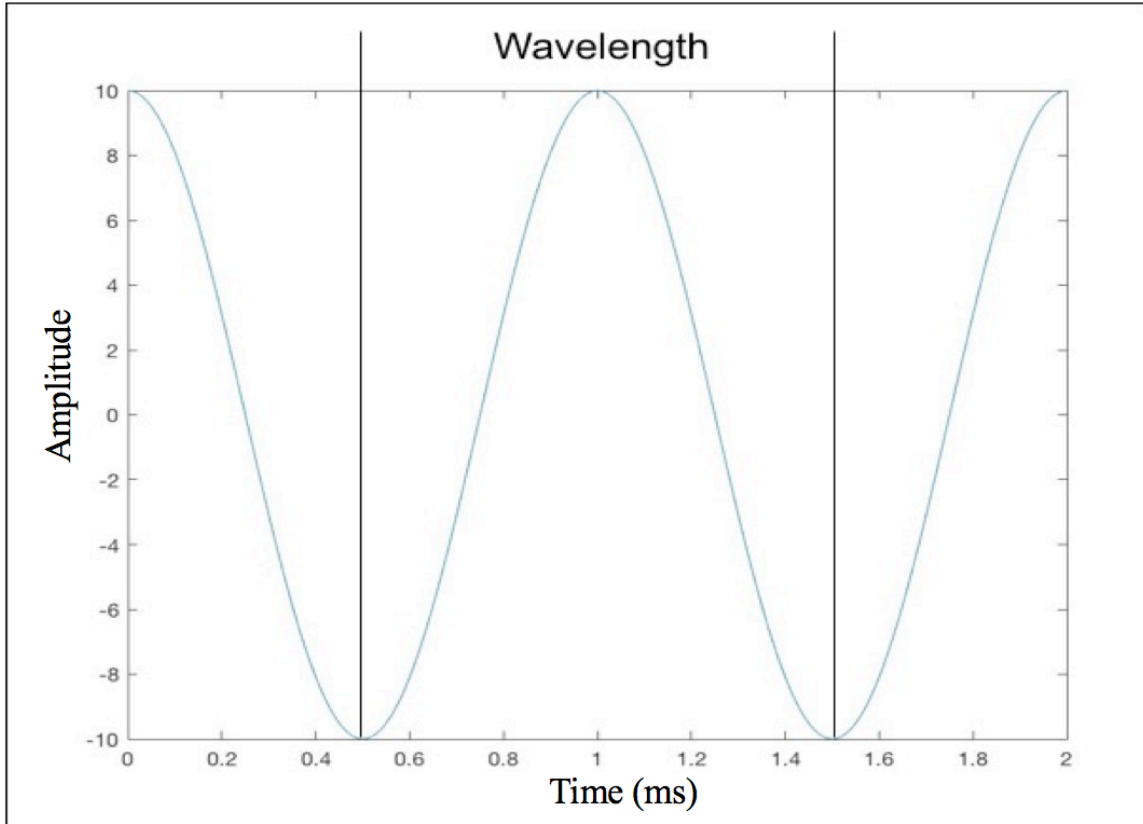


Figure 1.8: An example of the wavelength.

For instance, if our wavelength is 10 meters, the underground structure's thickness should be equal to or greater than 10 meters. Otherwise, the wavelet will penetrate through the formation without any reflections. The wavelength is calculated by the formula (1.1):

$$\lambda = \frac{v}{f} \quad (1.1)$$

where λ is wavelength, v is velocity, and f is frequency.

Smaller wavelengths have a higher vertical resolution according to the vertical resolution formula (1.2):

$$R = \frac{\lambda}{4} \quad (1.2)$$

where R is vertical resolution, λ is wavelength. The vertical resolution is important for our research since we use vertical sources to generate seismic modeling.

With its high frequency source, the cross-well seismic method can offer five to ten times higher resolution than conventional surface seismic surveys, depending on the source's frequency (Figure 1.9) (Marion, 2014). In addition to higher resolution, cross-well seismic has a high signal-to-noise ratio (S/N) because this method is not highly affected by ground rolls, source coupling, weathered shallow layers, shallow low velocities zones compared to conventional surface seismic surveys.

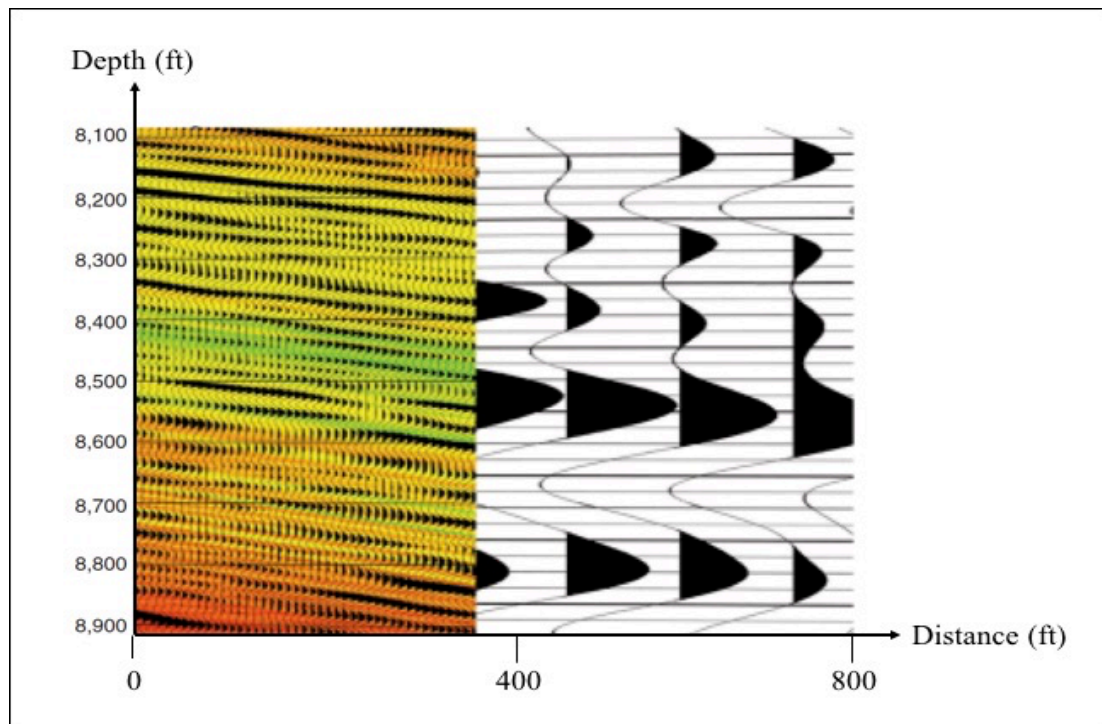


Figure 1.9: The high resolution of the cross-well seismic result (left) compared with the surface seismic result (right) due to the cross-well seismic's high frequency source (Modified from Marion, 2014).

Cross-well seismic is an effective seismic method to image the clandestine tunnels with highly accurate results. However, the application of this method is not common compared to the subsurface seismic method on account of the prohibitive cost (equipment, drilling cost for wells) and coverage limitation of this method.

1.4.2 Seismic Imaging

The purpose of recoding seismic data is to build up an image of the geological features in the subsurface (Biondi, 2005). For this purpose, seismic migration is to be used in seismic data processing to move out the distortions from reflections and put the changing events into their correct position to make seismic data similar to subsurface geological structures.

1.4.2.1 Kirchhoff Migration

In this research, we used the Kirchhoff depth migration to image the clandestine tunnels. The Kirchhoff migration uses the integral form of the wave equation to place the recorded reflectors from the surface into the region to be imaged. The Kirchhoff integral illustrates a field at a given point as a superposition of wave propagating from adjoining points and times. We need a smooth or a constant velocity model to place reflectors into their right location by using continuation of the wave-field (from oilfield.slb.com). Figure 1.10 illustrates the Kirchhoff migration principle. On the left side of the figure (a) due a scatterer we record the reflected waves from this scatterer then on the right side of the figure (b) we generate the Kirchhoff hyperbola according to the seismic recording from

the scatterer. We use this hyperbola to place the reflections to their right position (Figure 1.9).

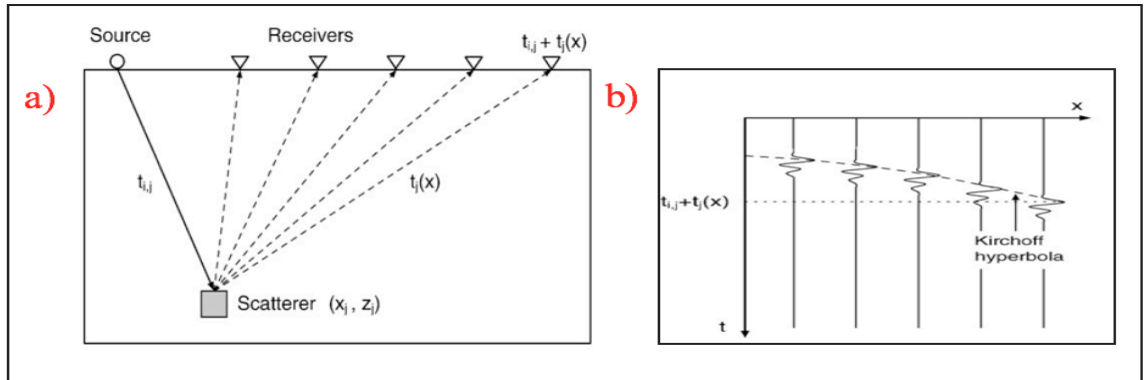


Figure 1.10: a) shows the seismic acquisition design for imaging the scatterer and b) displays the recorded waves from the scatterer that we sum to generate the Kirchhoff hyperbola (Retrieved from Pyun et al., 2008).

We used the Kirchhoff migration via Seismic Unix's `sukdmig2d` command (Cohen et. al, 2017) in our research.

1.5 Modeling and Imaging Procedure

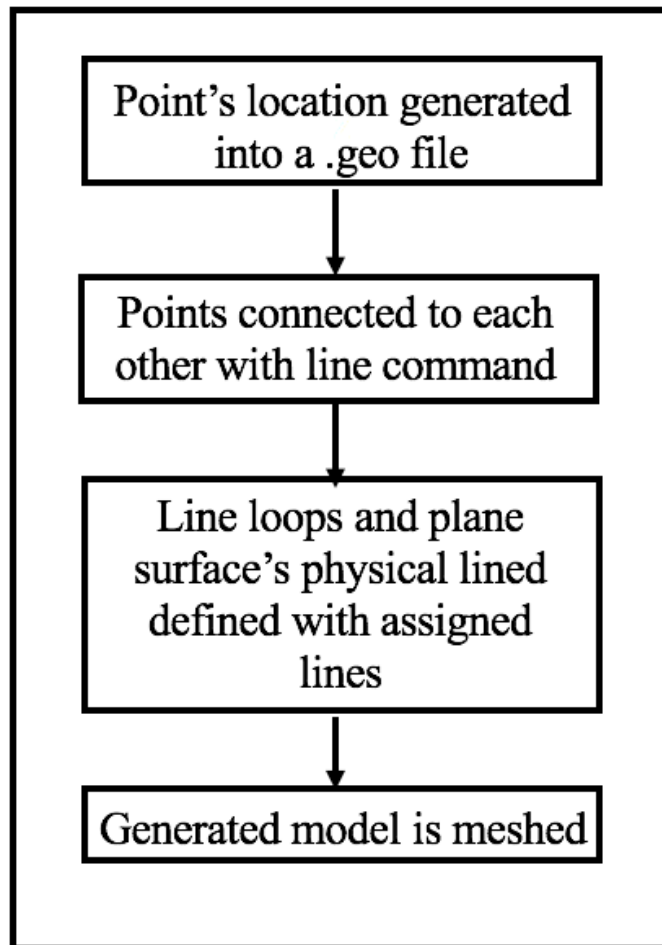
Gmsh open software was used to generate numerical models and mesh these models that have clandestine tunnels inside them. Then Specfem2D was used to model seismic wave propagations to observe interactions between seismic waves and the meshed models. Afterwards Seismic Unix software was used to visualize the recorded seismograms and to apply the Kirchhoff migration to these recorded seismograms to image the clandestine tunnels in our numerical models.

1.5.1 Gmsh

Gmsh is an open 3D finite-element generator that comes with efficient and light meshing and visualization features. Gmsh is built with four main modules. We only use two of them in our research: geometry for defining points, directed lines (circles, and splines), and oriented surfaces; meshing, which generates small meshes which allow us to use seismic modeling for the numerical models that were produced, and a post-processing feature and solver (Geuzaine, 2009).

Finite-element meshing blends fundamental geometrical elements which have different shapes, such as lines, triangles, and prisms, into a whole piece. Every geometrical element is connected to some other element from an edge or a node. The meshing procedure flows in a top-to-bottom formation (Table 1.3).

Table 1.3: Meshing scheme for Gmsh.



To begin with, we created a .geo file by assigning coordinates for each point in succession. Afterwards, we connected these assigned points to one another using line command and defined different plane surfaces and physical lines in the .geo file to designate different parameters in different formations (Figure 1.11).

```

// Geometry File of Perfect Shape Tunnel With Receiver and Source That is Not Located in Wells
c11=0.25;

//Boundary Points of Square
Point(1) = {0, 0, 0, c11};
Point(2) = {50, 0, 0, c11};
Point(3) = {50,46, 0, c11};
Point(4) = {50, 50, 0, c11};
Point(14) = {0, 50, 0, c11};
Point(15) = {0, 46, 0, c11};

//Connection Points
Point(5) = {25, 50, 0, c11};
Point(6) = {25, 46, 0, c11};

//Points of Boundary of Tunnel
Point(7) = {25, 36, 0, c11};
Point(8) = {24.5 , 35.5, 0, c11};
Point(9) = {24.5, 34.5, 0, c11};
Point(10) = {25.5, 34.5, 0, c11};
Point(11) = {25.5, 35.5, 0, c11};

//Points of Center of Tunnel and Its Circles
Point(12) = {25, 35.5, 0, c11};
Point(13) = {25, 34.5, 0, c11};

//Lines of Square
Line(1) = {1, 2};
Line(2) = {2, 3};
Line(3) = {3, 4};
Line(4) = {4, 5};
Line(14) = {5, 14};
Line(15) = {14, 15};
Line(16) = {15, 1};

//Lines of Connection
Line(5) = {5, 6};
Line(6) = {6, 7};

//Lines of Tunnel
Circle(7) = {7,12, 8};
Line(8) = {8, 9};
Circle(9) = {9, 13, 10};
Line(10) = {10, 11};
Circle(11) = {11, 12, 7};

//Second Layers Lines

//Loops
Line Loop(1) = {1, 2, 3, 4, 5, 6, 7, 8, 9, 10, 11, -6, -5, 14, 15, 16};
//Line Loop(1) = {1, 2, 3, 4, 14, 15, 16};

```

Figure 1.11: An example of a .geo file used to generate a model via Gmsh.

Conclusively, the .geo file is opened in Gmsh software (Figure 1.13) and we choose the parameters in the .geo file (Figure 1.13) within the software to complete the meshing procedure. The file is then saved for use in the Specfem2D software so that seismic propagations can be run with the meshed numerical models.

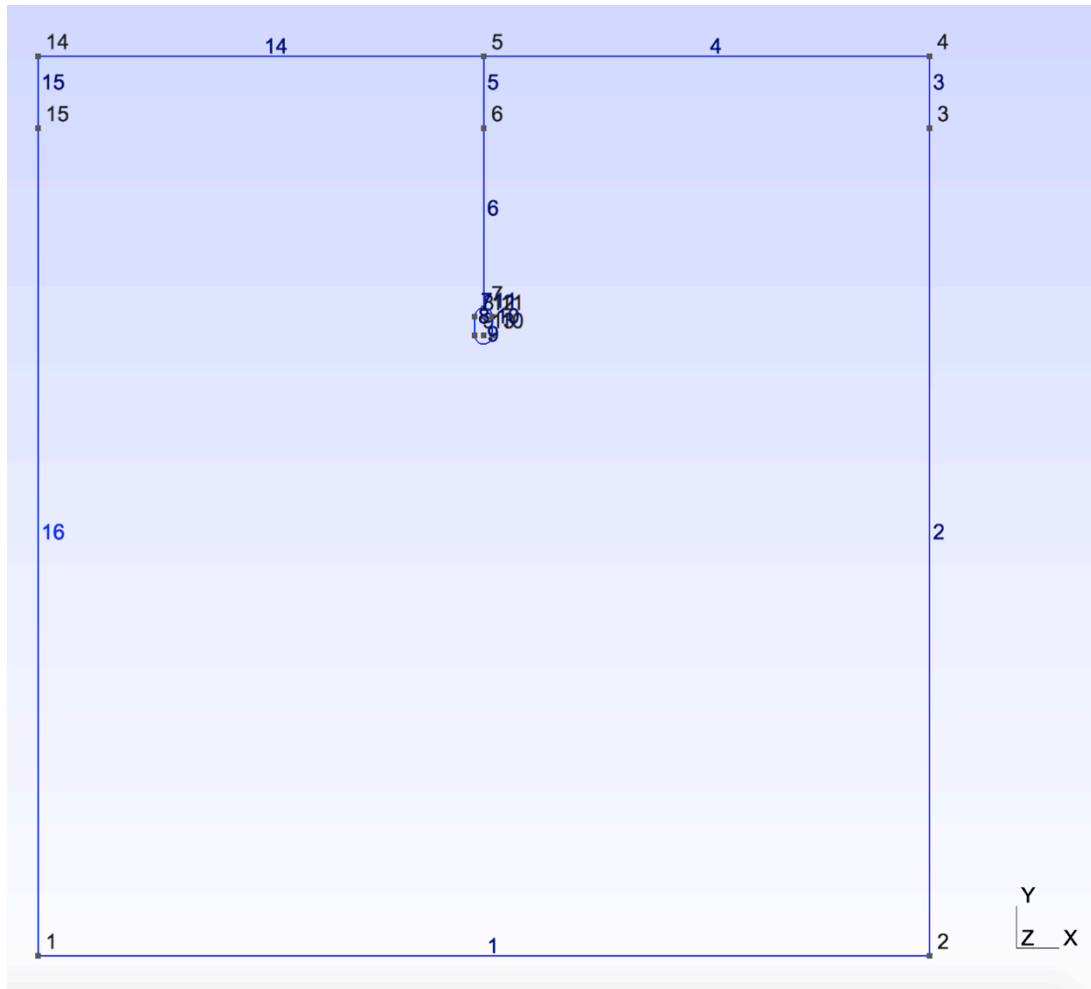


Figure 1.12: Assigned points and lines of a .geo file in Gmsh software.

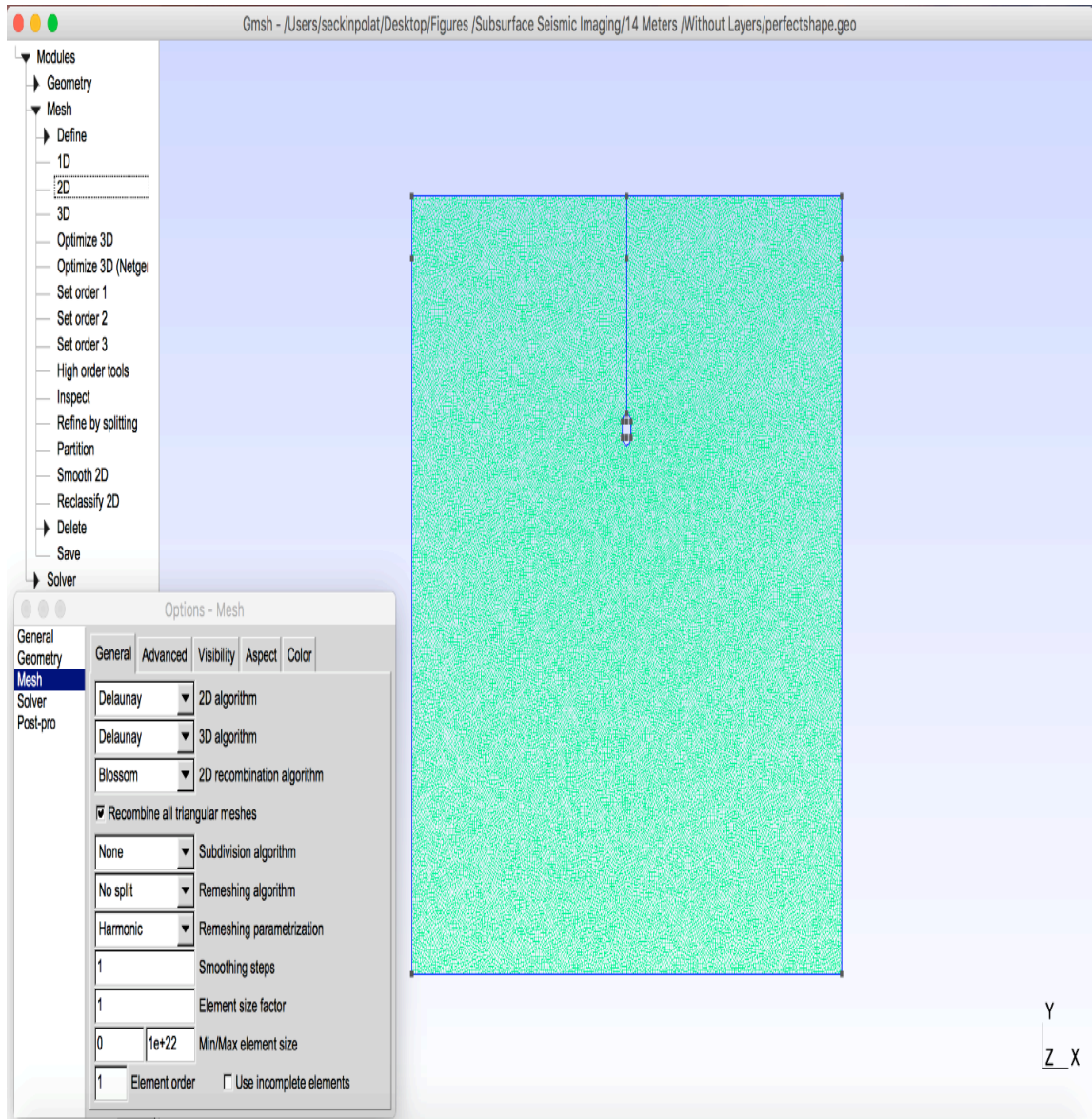


Figure 1.13: A screenshot of a meshed model with assigned points and lines in Gmsh software.

1.5.2 Specfem2D

Specfem2D is a spectral-element solver that also offers internal meshing software. It can operate with different external mesh generator packages such as Gmsh (Geuzaine,

2009) to create seismic models. Specfem2D simplifies acoustic, elastic and poroelastic seismic wave propagations for 2D cases. This software can run in both serial and parallel fashion on a computer cluster (Komatitsch, 1997).

Specfem2D is a spectral element method (SEM), which was developed from computational fluid dynamics (Patera, 1984, Maday and Patera, 1989) and used to address problems in seismic wave propagation. In spectral element method, the wave field is shown in terms of higher degree Lagrange polynomials on Gauss-Lobatto-Legendre interpolation points that establish minimum numerical grid dispersion and anisotropy. The biggest advantage of SEM is that it decreases computational cost due to the mass matrix, which is exactly diagonal by numeric construction.

For running scripts in Specfem2D, the first step is to assign parameters into `Par_file`. We enter parameters for acquisition geometry by entering the number of receivers and the locations, density, and velocity of the formations created with Gmsh. Afterwards, we can choose the number of cores that we want to use for each simulation. (Figure 1.14).

```

#-----
# simulation input parameters
#-----
# title of job
title = Subsurface Modeling for Detection of a Tunnel with One Receiver Set

# forward or adjoint simulation
# 1 = forward, 2 = adjoint, 3 = both simultaneously
# note: 2 is purposely UNUSED (for compatibility with the numbering of our 3D codes)
SIMULATION_TYPE = 1
# 0 = regular wave propagation simulation, 1/2/3 = noise simulation
NOISE_TOMOGRAPHY = 0
# save the last frame, needed for adjoint simulation
SAVE_FORWARD = .false.

# parameters concerning partitioning
NPROC = 112 # number of processes
partitioning_method = 3 # SCOTCH = 3, ascending order (very bad idea) = 1
# number of control nodes per element (4 or 9)
ngnod = 4

# time step parameters
# total number of time steps
NSTEP = 140000
# duration of a time step (see section "How to choose the time step" of the manual for how to do this)
DT = 5.d-7

# time stepping
# 1 = Newmark (2nd order), 2 = LDDRK4-6 (4th-order 6-stage low storage Runge-Kutta), 3 = classical RK4 4th-order 4-stage Runge-Kutta
time_stepping_scheme = 1

# axisymmetric (2.5D) or Cartesian planar (2D) simulation
AXISYM = .false.

# set the type of calculation (P-SV or SH/membrane waves)
P_SV = .true.

# set to true to use GPUs
GPU_MODE = .false.

# available models
# default - define model using nbmodels below
# ascii - read model from ascii database file
# binary - read model from binary database file
# binary_voigt - read Voigt model from binary database file
# external - define model using define_external_model subroutine
# gll - read GLL model from binary database file
# legacy - read model from model_velocity.dat_input
MODEL = default

```

Figure 1.14: Par_file of Specfem2D.

Then, parameters are entered into a SOURCE file that controls the source for each seismic modeling. We enter the number, location, type, and frequency of source (Figure 1.15). We used a single-force (double couple) source for our research.

```

#source 1. The components of a moment tensor source must be given in N.m, not in dyne.cm as in the DATA/CMTSOLUTION source file of the 3D version of the code.
source_surf      = .false.      # source inside the medium or at the surface
xs               = 0            # source location x in meters
zs               = ABCD        # source location z in meters
source_type      = 1            # elastic force or acoustic pressure = 1 or moment tensor = 2
time_function_type = 1          # Ricker = 1, first derivative = 2, Gaussian = 3, Dirac = 4, Heaviside = 5
# time_function_type == 8 source read from file, if time_function_type == 9 : burst
# If time_function_type == 8, enter below the custom source file to read (two columns file with time and amplitude) :
# (For the moment dt must be equal to the dt of the simulation. File name can't exceed 150 characters)
name_of_source_file = ""       # Only for option 8 : file containing the source wavelet
burst_band_width   = 0.        # Only for option 9 : band width of the burst
f0                 = 4000       # dominant source frequency (Hz) if not Dirac or Heaviside
tshift             = 0.0        # time shift when multi sources (if one source, must be zero)
anglesource        = 90.0       # angle of the source (for a force only)
Mxx                = 1.         # Mxx component (for a moment tensor source only)
Mzz                = 1.         # Mzz component (for a moment tensor source only)
Mxz                = 0.         # Mxz component (for a moment tensor source only)
factor             = 1.d10      # amplification factor

```

Figure 1.15: SOURCE file of Specfem2D.

Then we run “process_the_Gmsh_file_once_and_for_all.sh”, which converts external mesh into a form that Specfem2D can recognize the external mesh and is able to run the mesh file for the seismic simulations. This script also allows us to choose what sort of boundary conditions (absorbing or free surface) that we would like to use for our modeling (Figure 1.16).

```

#!/bin/bash
#
# create the absorbing and free surface files from the Gmsh file
#
python ../../UTILS/Gmsh/LibGmsh2Specfem_convert_Gmsh_to_Specfem2D_official.py SqrCirc.msh -t F -l A -b A -r A

```

Figure 1.16: process_the_Gmsh_file_once_and_for_all.sh script of Specfem2D.

For the last step, we run “run_this_example.sh” that reads all assigned parameters and runs the seismic simulation (Figure 1.17).

```

#!/bin/bash
#
# script runs mesher and solver (in serial)
# using this example setup
#
echo "running example: `date`"
currentdir=`pwd`

echo
echo "(will take about 2 minutes)"
echo

# sets up directory structure in current example directory
echo
echo "  setting up example..."
echo

mkdir -p OUTPUT_FILES
mkdir -p DATA

# sets up local DATA/ directory
cd DATA/
cp ../Par_file_Gmsh_SqrCircles.in Par_file
cp ../SOURCE.SqrCirc SOURCE
cd ../

# cleans output files
rm -rf OUTPUT_FILES/*

cd $currentdir

# links executables
rm -f xmeshfem2D xspecfem2D
ln -s ../../bin/xmeshfem2D
ln -s ../../bin/xspecfem2D

# stores setup
cp DATA/Par_file OUTPUT_FILES/
cp DATA/SOURCE OUTPUT_FILES/

# runs database generation
echo
echo "  running mesher..."
echo
./xmeshfem2D

# runs simulation
echo
echo "  running solver..."
echo
mpirun -np 4 ./xspecfem2D

"run_this_example.sh" 63L, 1037C

```

Figure 1.17: run_this_example.sh script of Specfem2D.

Specfem2D run script creates a figure of a specific time for the model and continues for the next time step figure. Figure 1.18 represents an example of an illustration from Specfem2D while it is running.

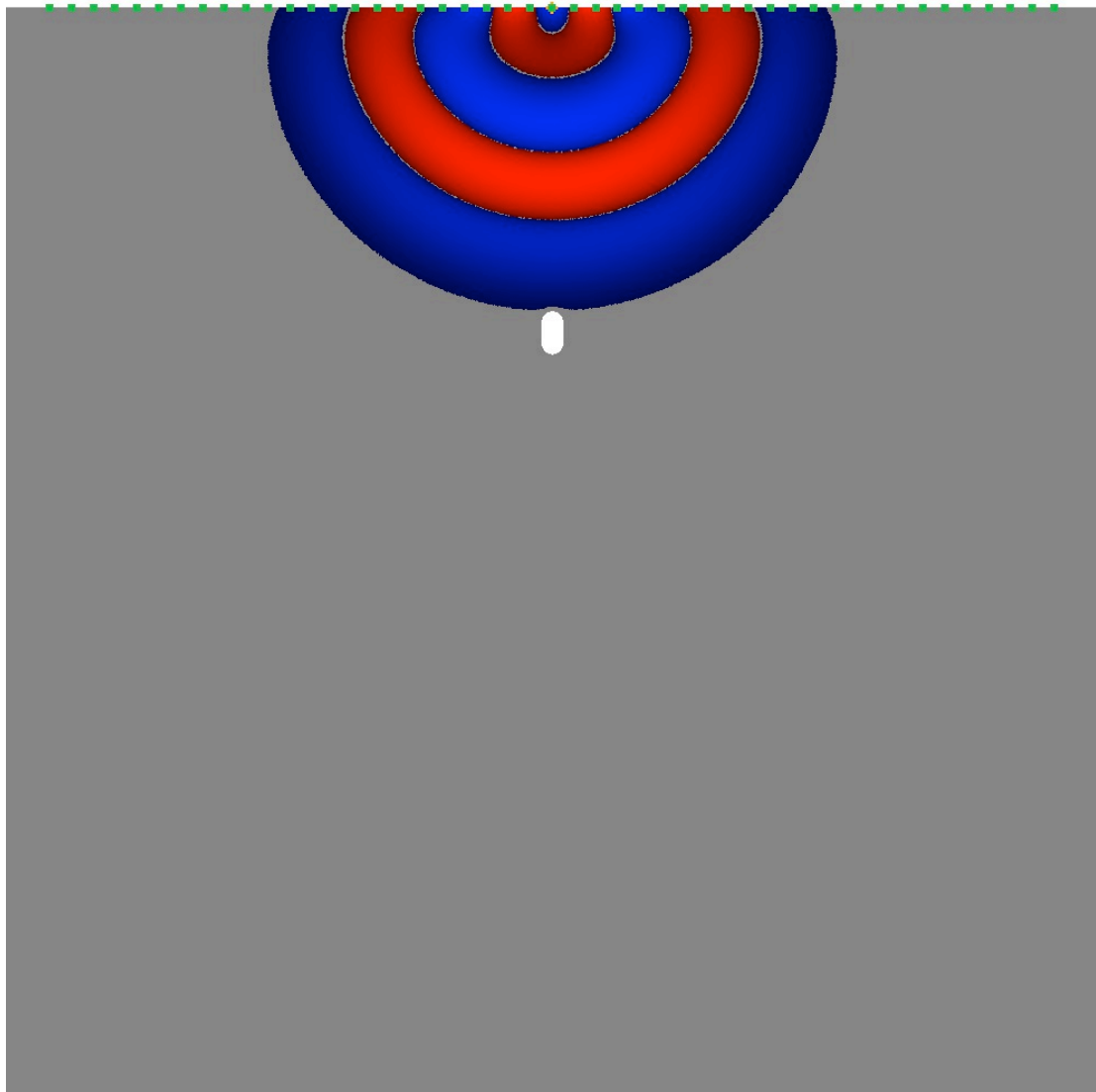
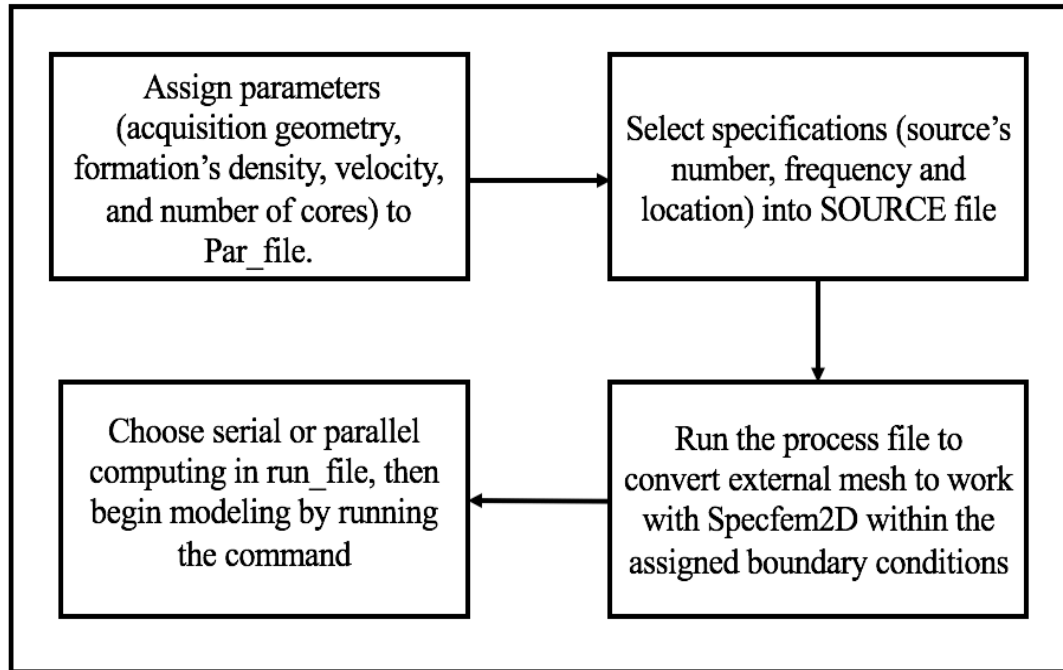


Figure 1.18: A snapshot of Specfem2D while seismic waves propagate and interact with the tunnel inside of the numerical model.

A scheme of how to run Specfem2D can be found in Table 1.4 below.

Table 1.4: Running scheme for Specfem2D.



1.5.3 Seismic Un*x

Seismic Un*x is an open seismic processing package, created by the Center for Wave Phenomena (CWP) at the Colorado School of Mines in 1987. This software provides tools and packages for seismic data processing in a Unix-like platform (Cohen et al., 2017).

For our research, we used three basic programs of Seismic Un*x, which are `suximage`, `unif2d`, `rayt2d`, and `sukdmig2d`. `Suximage` program is used for visualizing the seismograms that are generated by Specfem2D software, `Unif2d` program is used to generate 2D velocity models, which is a requirement for Kirchhoff migration, `Rayt2d` is

run for the calculation of ray tracing, also a requirement for Kirchhoff migration, and Sukdmig2d is used to apply Kirchhoff migration to our previously generated seismograms. We wrote a script that combined all these programs into a single file to apply migration efficiently (Figure 1.19).

```

#!/bin/sh
# shell for uniformly sampling velocity from a layered model
set -v
nx=101 dx=0.5 fx=0  labelx="Distance (m)"
nz=101 dz=0.5 fz=0  labelz="Depth (m)"
ninf=0 npmax=201
unif2 <input >vfile  ninf=$ninf  npmax=$npmax \
      nz=$nz dz=$dz fz=$fz nx=$nx dx=$dx fx=$fx \
      v00=3000
WIDTH=500
HEIGHT=500
WIDTHOFF1=100
HEIGHTOFF1=100
ximage <vfile  style=seismic legend=1 units=vel cmap=hsv5 \
      n1=$nz d1=$dz f1=$fz grid1=dot label1="$labelz" \
      n2=$nx d2=$dx f2=$fx grid2=dot label2="$labelx" \
      title="Velocity (m/sec)" \
      wbox=$WIDTH hbox=$HEIGHT xbox=$WIDTHOFF1 ybox=$HEIGHTOFF1 &
# shell for generating traveltimes by ray tracing
set -v
rayt2d <vfile par=rayt2d.par
# shell for Kirchhoff depth migration
insufile1='Uz_double_receivers.su'
insufile2='400z_absorbing_phase45.su'
insufile3='400z_absorbing_phase45_shift0_00875.su'
insufile4='400z_absorbing_phase45_shifted0_00875.su'
outfile1='400z_absorbing_phase45_shifted_migrated0_0075s.data'
outfile2='400z_absorbing_phase45_shifted_migrated0_01s.data'
sukdmig2d < $insufile4 par=kdmig.par> $outfile
#!/bin/sh
# shell for plotting synthetic data and migrated data
WIDTH=400
HEIGHT=600
WIDTHOFF1=10
WIDTHOFF2=440
WIDTHOFF3=860
HEIGHTOFF1=20

# Plotting migrated data
suximage< $outfile2 perc=99.5 legend=2 units=amp cmap=hsv5 \
      label1="Depth (m)" label2="Distance (m)" \
      title="Kirchhoff Depth Migration" \
      wbox=$WIDTH hbox=$HEIGHT xbox=$WIDTHOFF3 ybox=$HEIGHTOFF1 &

```

Figure 1.19: An example of visualization of a shot gather result using suximage program.

Chapter 2: Tunnel Modeling with Subsurface Acquisition Geometry

2.1 Introduction

In this chapter, several numerical models were produced based on the depth of the found clandestine tunnels by the authorities along the U.S. – Mexico border (from ice.gov) to discover the detectability of clandestine tunnels using the subsurface seismic method. To achieve this, 48 distinct models that have a tunnel located inside the model with a dimension of a 2-meter height and a 1-meter width (Figure 2.1). We placed the tunnels at two different depths (14 meters and 19 meters), different geological layering (two layered geological model), and different physical properties (velocities and densities), were generated.

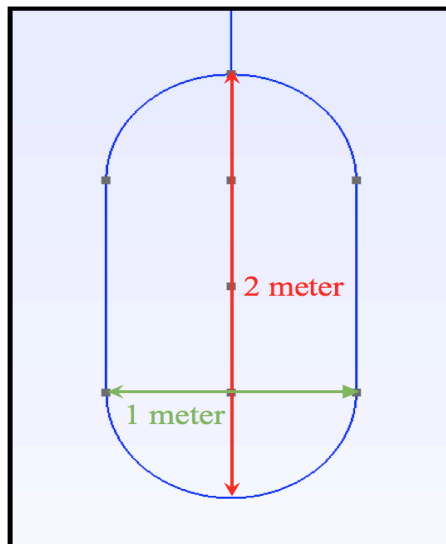


Figure 2.1: Dimensions of the tunnel in our model.

In this study, two different seismic velocities and densities were chosen to compare the seismic wave interaction with the tunnel in different geological layering for

physical parameters (i.e. velocity and density) according to the values in Table 2.1 (Mavko, 2011). The faster and denser formations were assigned as marls, which have a density of 2.6 g / cm^3 . The *P*- wave velocity is 3000 m/s, and the *S*-wave velocity is 1500 m/s. The slower formation is assumed to be composed of clays and shales, with a density of 2.4 g / cm^3 , the *P*-wave velocity 2500 m/s, and the *S*-wave velocity 800 m/s. In all the models, the shallower formation is saturated by clays and shales, and the deeper formation is marls. These values were chosen for modeling because shallow formations usually have similar densities and seismic velocities. Marls, saturated shales, and clays were selected to approximate a reasonable shallow subsurface model.

Table 2.1: Typical Seismic Velocities and Densities of Different Rock Formations (Mavko, 2011).

Type of formation	P wave velocity (m/s)	S wave velocity (m/s)	Density (g/cm ³)	Density of constituent crystal (g/cm ³)
Scree, vegetal soil	300-700	100-300	1.7-2.4	-
Dry sands	400-1200	100-500	1.5-1.7	2.65 quartz
Wet sands	1500-2000	400-600	1.9-2.1	2.65 quartz
Saturated shales and clays	1100-2500	200-800	2.0-2.4	-
Marls	2000-3000	750-1500	2.1-2.6	-
Saturated shale and sand sections	1500-2200	500-750	2.1-2.4	-
Porous and saturated sandstones	2000-3500	800-1800	2.1-2.4	2.65 quartz
Limestones	3500-6000	2000-3300	2.4-2.7	2.71 calcite
Chalk	2300-2600	1100-1300	1.8-3.1	2.71 calcite
Salt	4500-5500	2500-3100	2.1-2.3	2.1 halite
Anhydrite	4000-5500	2200-3100	2.9-3.0	-
Dolomite	3500-6500	1900-3600	2.5-2.9	(Ca, Mg) CO ₃ 2.8-2.9
Granite	4500-6000	2500-3300	2.5-2.7	-
Basalt	5000-6000	2800-3400	2.7-3.1	-
Gneiss	4400-5200	2700-3200	2.5-2.7	-
Coal	2200-2700	1000-1400	1.3-1.8	-
Water	1450-1500	-	1.0	-
Ice	3400-3800	1700-1900	0.9	-
Oil	1200-1250	-	0.6-0.9	-

2.2 Models With a 14 m Deep Tunnel

2.2.1 One Layer Case

In this section, models were generated that have a tunnel at a depth of 14-meters with a source at two different frequencies for each model: 100 Hz and 400 Hz. However, according to the wavelength (1.1) and vertical seismic resolution (1.2) formulas, only models shot with a frequency of 400 Hz allow the tunnel to be detected with the subsurface seismic method. According to these formulas, a source at 400 Hz produces a wavelength of 7.5 meters that results in 1.875 meters of vertical seismic resolution. For

this reason, we include only models with a source at 100 Hz, which is a common frequency value used for seismic exploration and we used 400 Hz as the highest source frequency to show if we can image the clandestine tunnel with a high frequency source in this section.

The acquisition geometry for a tunnel with a depth of 14 meters for the subsurface seismic method is shown in Table 2.2.

Table 2.2: The acquisition geometry parameters for the tunnel with a depth of 14 meters for subsurface seismic method.

Model Dimension	50 m x 50 m
Seismic Shot Range	11 shots, starting from 0 m to 50 m with 5 m spacing
Number of Receivers and Their Sequence	47 receivers starting from 2 m to 48 m
Frequency of Source and Its Type	100 Hz and 400 Hz, Ricker wavelet, Single Force (Coupled)
Tunnel Depth	14 m
Recording Length (millisecond)	32.5 ms
Boundary Condition	Free Surface (Top Layer) and Absorbing (Top Layer) for Each Example
Velocity Model	$V_p= 3000$ m/sec, $V_s=1500$ m/sec, Density = 2.6 g/cm ³

We ran a simple model, which has only one layer, for seismic modeling, with a density of 2.6 g/cm³, $V_p= 3000$ m/sec, and $V_s=1500$ m/sec via specfem2d software. An example of seismic modeling is shown in Figure 2.3 where the shot point is located at 25 meters with 400 Hz (Figure 2.3). This example is run with absorbing boundary and free surface boundary conditions for the surface layers of the models.

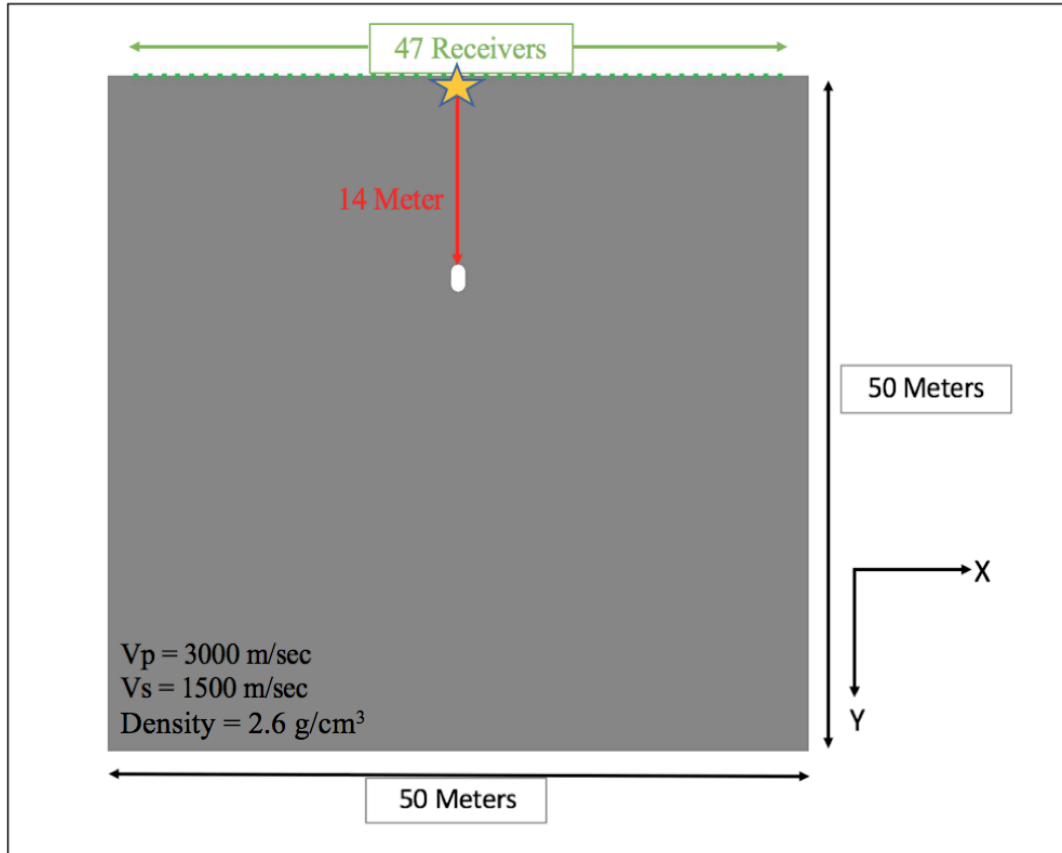


Figure 2.2: Fourteen meter deep tunnel model with one layer that has the absorbing boundary conditions for all boundaries with a single-force 400 Hz source (shown with a star) located at 25 meters on the surface.

After starting the Specfem2d that generated a model with a tunnel 14-meters deep, seismic wave propagates along the surface. Figure 2.3 shows the wave propagation for the model that has absorbing boundary condition for all its' boundaries at 5.5 ms when seismic waves arrive at the tunnel in the model.

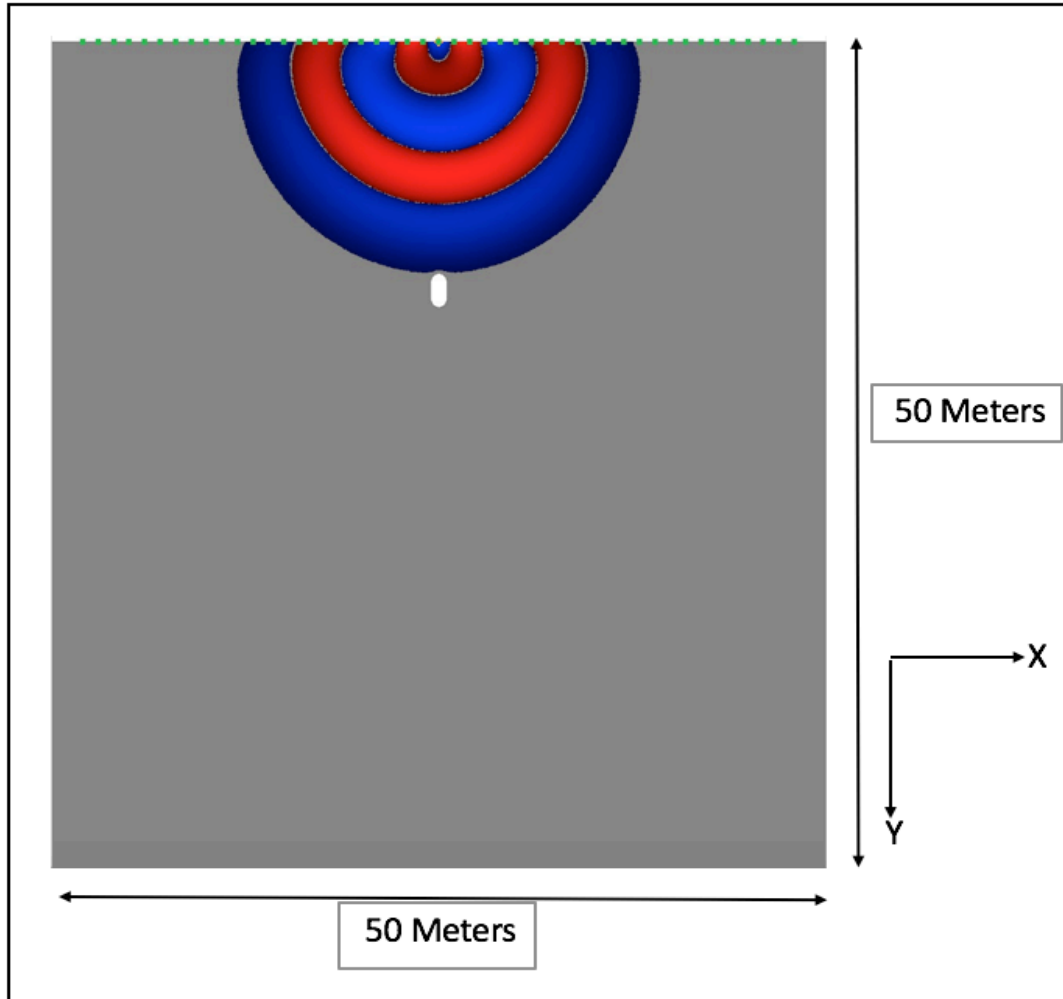


Figure 2.3: A snapshot of 14 meter deep tunnel model with one layer that has the absorbing boundary condition for all the boundaries run in Specfem2D at 5.5 ms with single-force 400 Hz source located on the surface.

After the seismic waves arrived at the tunnel, they bounced back from the void and traveled back to the surface. Figure 2.5 shows the seismic wave propagation in the model at 13.75 ms.

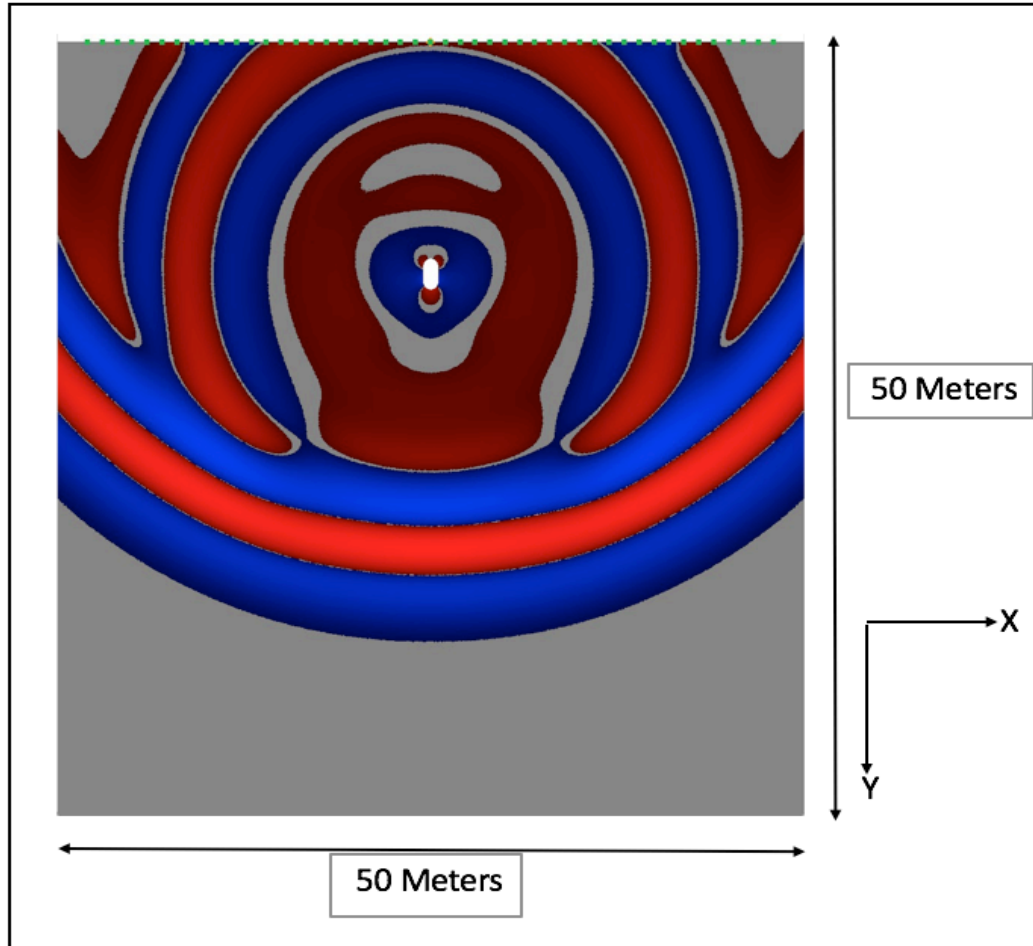


Figure 2.4: A snapshot of 14 meter deep tunnel model with one layer that has the absorbing boundary conditions for all boundaries while running in Specfem2D at 13.75 ms with a single-force 400 Hz source located at 25 meters on the surface.

The absorbing condition often requires to absorbing layers to be thick enough in order to provide an efficient absorbing boundary condition (Bélangier-Rioux et. al, 2015). Since the receivers and shots are located on the surface in our acquisition design (Figure 2.2), we cannot expect that the absorbing boundary condition is going to be working efficiently for our acquisition design. To achieve accurate results for the absorbing boundary condition case, we extended the top boundary of our models for three meters upwards so our receivers and sources are going to be located far enough from the

absorbing boundary layer that will provide an efficient absorbing boundary condition for our modeling (Figure 2.5). We used the acquisition parameters and the model whose dimension is 50 m x 54 m from Figure 2.5 for the all examples with the absorbing boundary conditions. For the free surface examples, we used the acquisition design and the model that has the dimension of 50 m x 50 m from Figure 2.2.

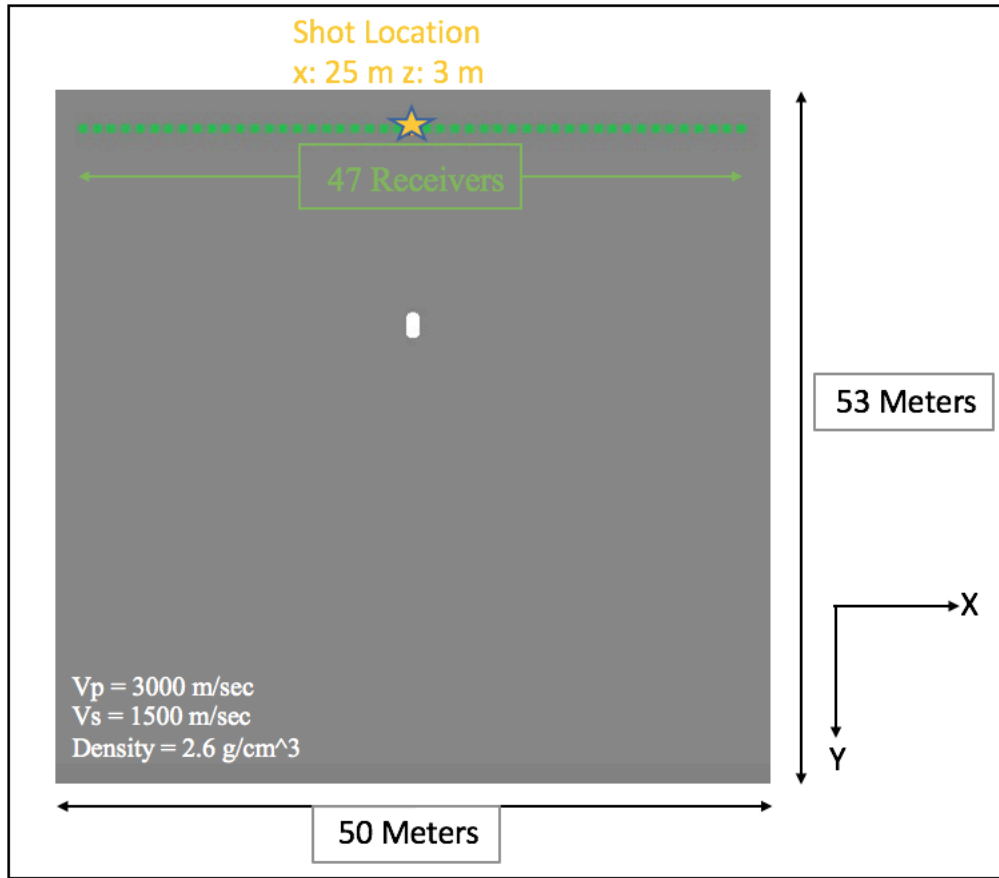


Figure 2.5: Fourteen-meter-deep tunnel model with one layer that has the absorbing boundary conditions for all boundaries with a single-force 400 Hz source (shown with a star).

After recording the seismic shooting, which was ran with the parameters in Figure 2.2 via Specfem2D, in the seismogram file (Figure 2.6) which contains our seismic modeling for the 100 Hz source at 25 meters on the x-axis with an absorbing boundary

condition of the surface, we can only recognize direct S arrivals. However, the tunnel in our model cannot be distinguished in the seismogram due to the source's low wavelength and vertical resolution.

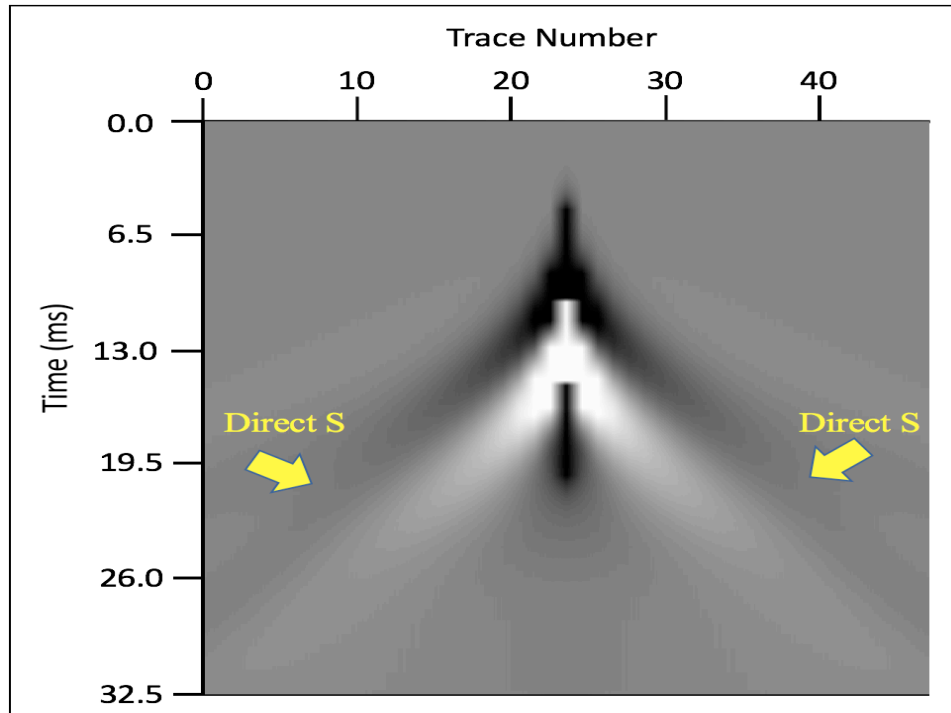


Figure 2.6: The seismogram (z-component) of a 14 meter deep tunnel model with a layer for absorbing boundary condition of all boundaries with a single-force 100 Hz source located at 25 meters distance and three meters depth (Figure 2.2).

Afterwards, all the shots were combined to determine if the low-resolution issue may be resolved by generating a set of shot gathers for the absorbing boundary condition case (Figure 2.7). We generated a homogenous one layer velocity model (Figure 2.8) to apply Kirchhoff migration to the set of seismic shot gathers that has the absorbing boundary condition for the surface of the model (Figure 2.9). According to the Kirchhoff migration result, the tunnel is not visible. The possible reason for this outcome is that the

low source frequency (100 Hz) is not high enough to locate the tunnel. As well, we see the Kirchhoff migration artifacts because of the limited number of shots and the receivers and surface effects due to direct arrivals in the migration results.

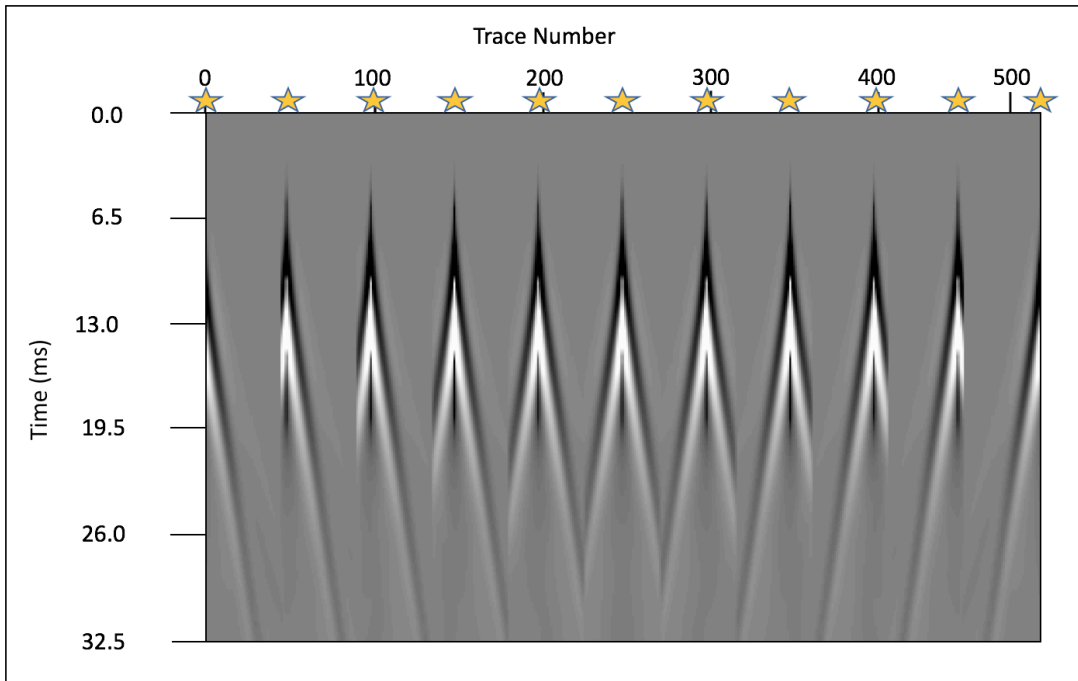


Figure 2.7: The set of seismic shot gathers (z component) for the 14 meter depth one layer model with the absorbing boundary condition for 100 Hz sources, whose shot locations were displayed with stars.

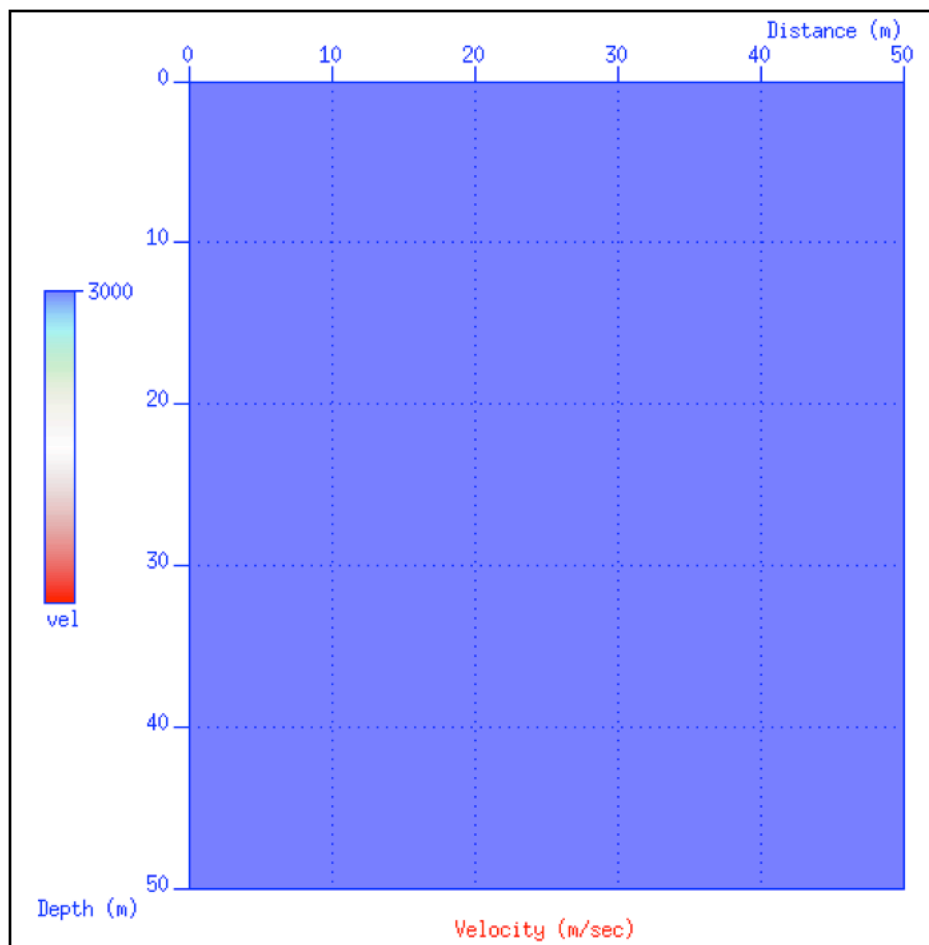


Figure 2.8: The migration velocity model for the homogenous medium that has one layer (vel represents velocity whose unit is m/sec).

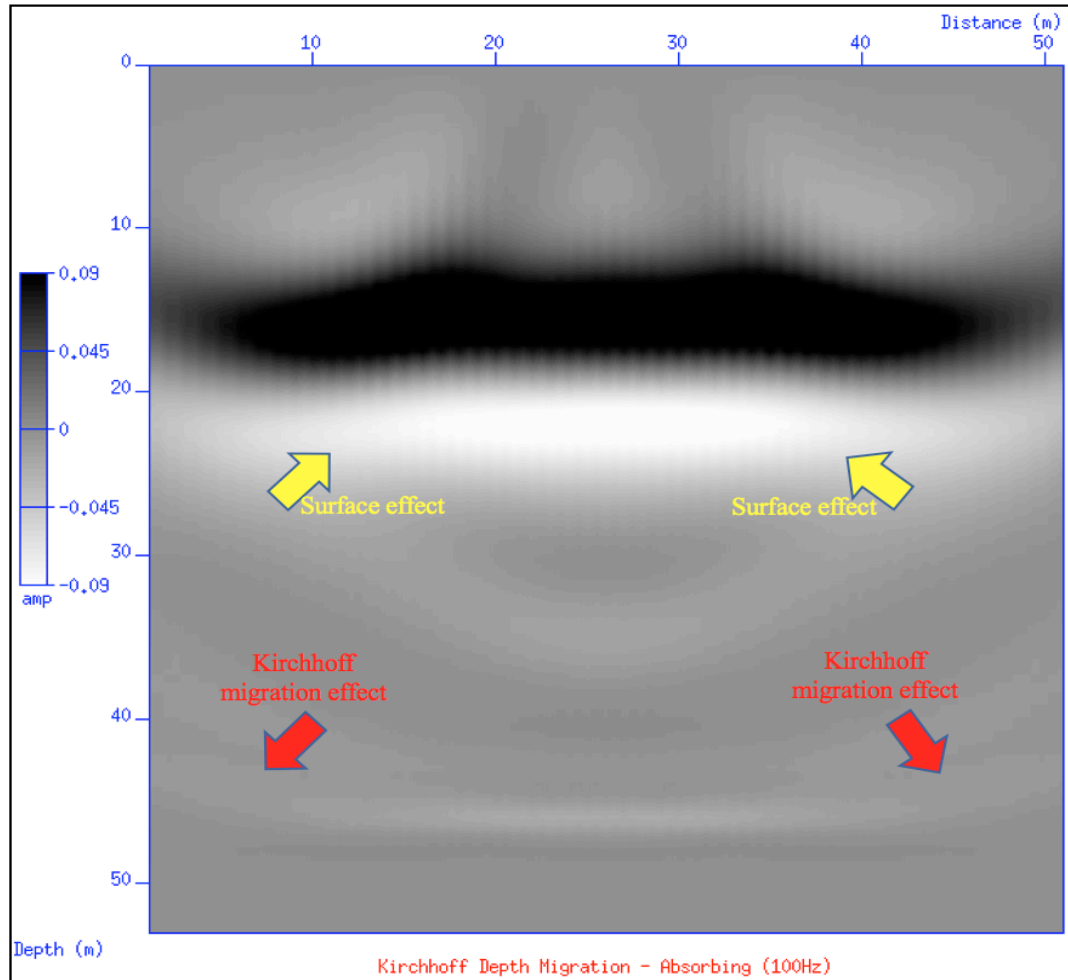


Figure 2.9: Kirchhoff migration result of a 14 meter deep tunnel model with a layer with the absorbing boundary condition for all boundaries (Amp represents the amplitude, which is a measure of the contrast in density, seismic velocities of the formations and / or underground structures. Amplitude allows us to interpret the formations and the structures in the seismic data).

Afterwards, we generated another seismic model with the parameters from Figure 2.2 as a free boundary condition for the surface layer of our model. According to the seismogram of the free boundary condition at the surface (Figure 2.10), direct S arrivals and Rayleigh waves are visible but we cannot distinguish direct S arrivals with Rayleigh waves since their velocities are too close to each other (velocity of S wave is 1500 m/sec

and velocity of Rayleigh wave is 1398 m/sec). However, the tunnel cannot be distinguished from this seismogram due to the low frequency of the source from the seismogram (Figure 2.10).

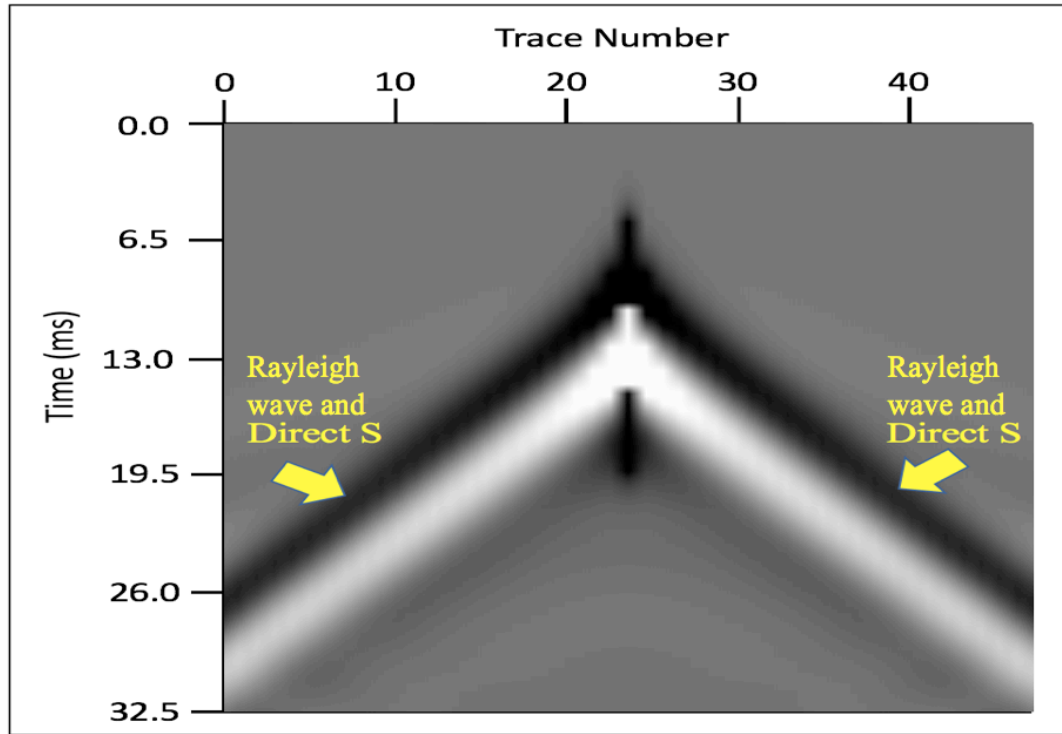


Figure 2.10: The seismogram (z-component) of a 14 meter deep tunnel model with one layer for the free surface boundary condition of the top boundary. The seismic source is a single-force 100 Hz source that located at 25 meters on the surface.

Thereafter, we combined all shots together to generate a set of shot gathers to determine if the low-resolution issue may be resolved by generating a set of shot gathers for the free surface boundary condition at the surface (Figure 2.11), and we used the same velocity model from the absorbing boundary condition case (Figure 2.8). Then we applied Kirchhoff migration to the set of shot gathers that has the free surface boundary condition at the surface of the model (Figure 2.12). According to the Kirchhoff migration

result in Figure 2.12, the tunnel is not visible. A possible reason for this outcome is that the low source frequency (100 Hz) is not high enough to locate the tunnel. As well, we also see the Kirchhoff migration artifacts (red arrows) due to the limited number of shots and the receivers and surface effect (yellow arrows) because of the direct arrivals in the migration results.

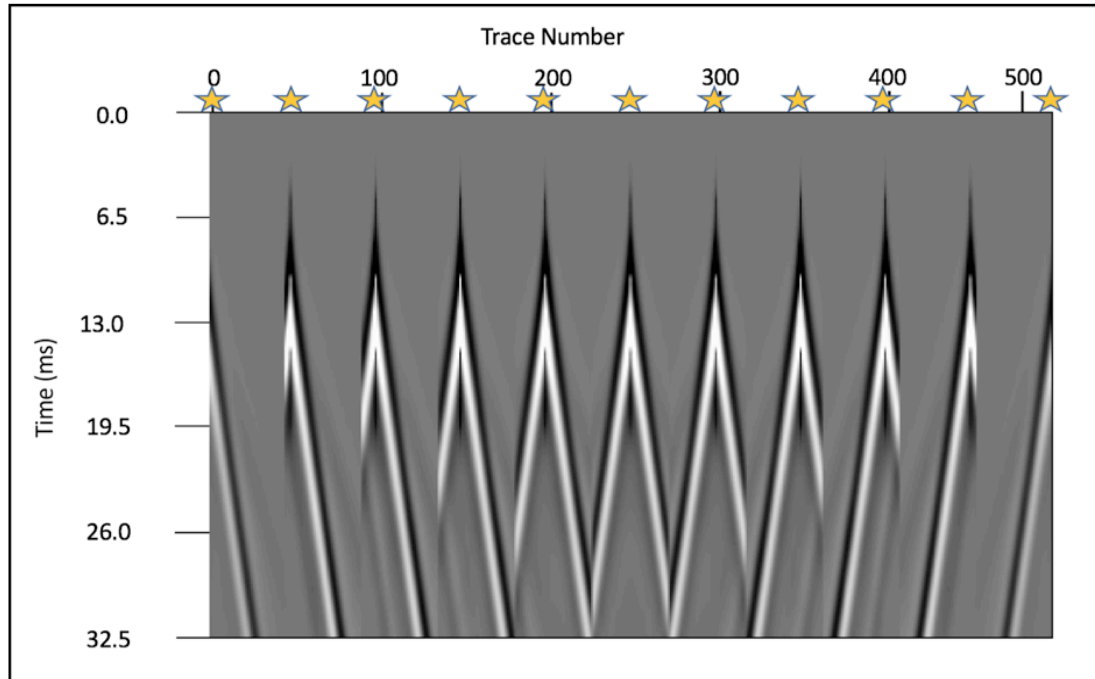


Figure 2.11: The set of shot gathers (z component) for a 14 meter depth one layer model with free surface boundary condition for 100 Hz seismic sources, whose shot locations were displayed with stars.

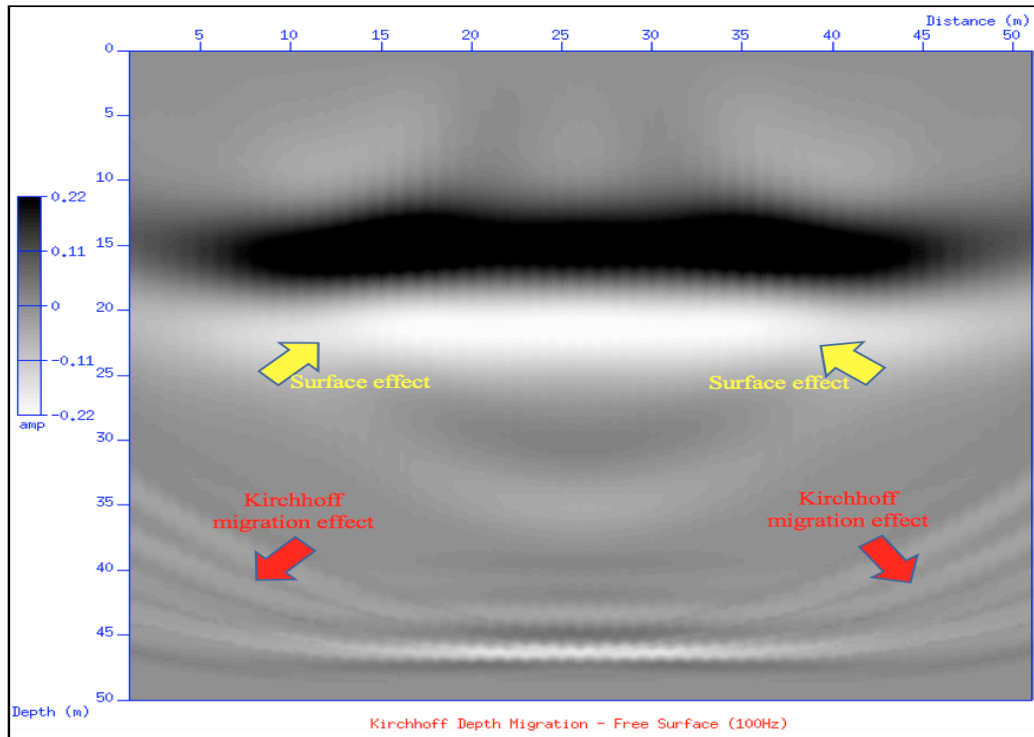


Figure 2.12: Kirchhoff migration result for the seismogram of a 14 meter deep tunnel model with a layer for the free surface boundary condition at the surface (Amp shows the amplitude that is a measure of the contrast in density, seismic velocities of the formations and / or underground structures).

After completing our research for the 14-meter deep tunnel located in one layered model with a 100 Hz source, we continued our study by modeling examples that use the same models and parameters but have a 400 Hz source frequency.

Then we ran our scripts in Specfem2D software and recorded the seismogram (Figure 2.13) which contains our seismic modeling with a 400 Hz source at 25 meters on x-axis and three meters depth. When we examine the seismogram, we can identify the direct S arrivals, the reflected P wave (PP), converted P wave (PS), and the S reflected wave (SS) from the tunnel. In this instance, we were able to identify direct arrivals and reflected waves due to the higher frequency value (400 Hz) of our source, which gives us

a higher resolution that allowed us to see the reflected waves coming from the tunnel. Since there is only one layer in our model, all the reflected waves are caused due to the existence of the tunnel in our model.

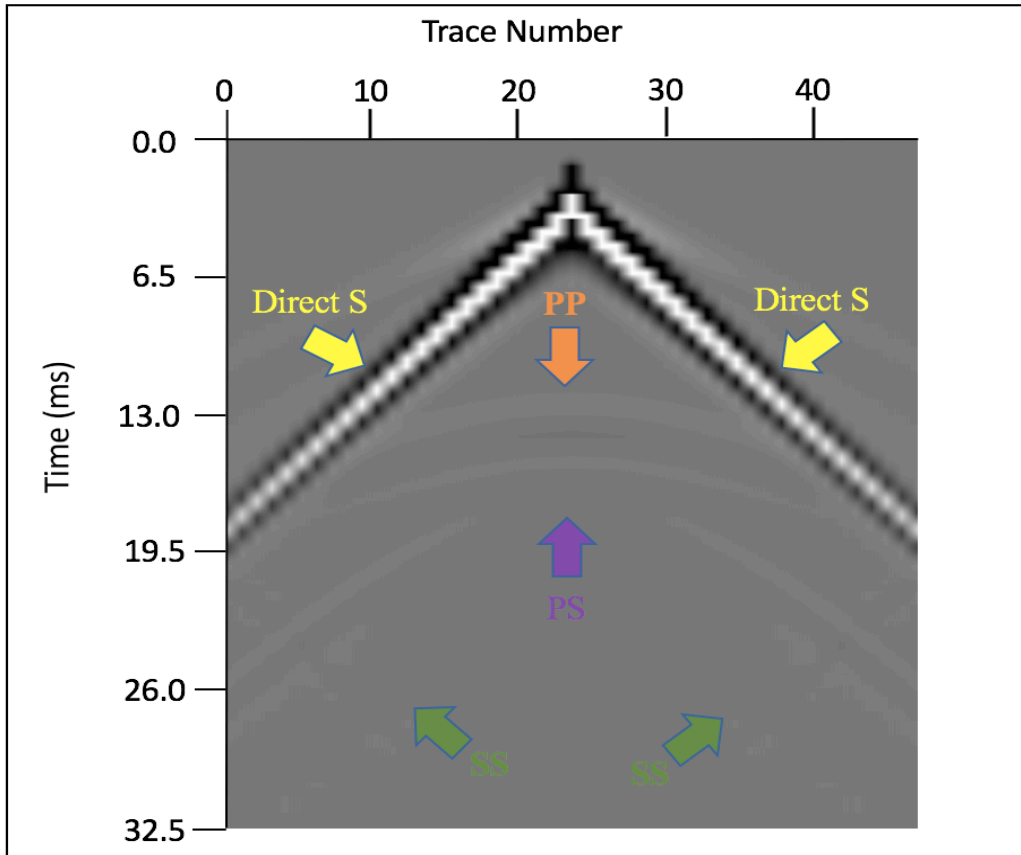


Figure 2.13: The seismogram (z-component) of a 14 meter deep tunnel model with a layer that has the absorbing boundary condition for all boundaries for a single-force 400 Hz source located at 25 meters distance on x-axis and three meters depth.

Thereafter, we generated a set of shot gathers to check that since if we can image the tunnel with a set of shot gathers (Figure 2.14) since it is hard to locate the tunnel on the seismograms one by one. Then the Kirchhoff migration was applied to our created the set of seismic shot gathers (Figure 2.14) with one layer velocity model (Figure 2.8) that we generated from the earlier section. As stated in Figure 2.14, the tunnel is located at the

exact depth (14 m) and correct thickness (2 m) with the absorbing boundary condition in the migration result. However, our result contains some artifacts caused by the Kirchhoff migration (shown with red arrows) due to the limited number of the receivers and the sources, and the surface effect (yellow arrows) which is caused due to the direct arrivals.

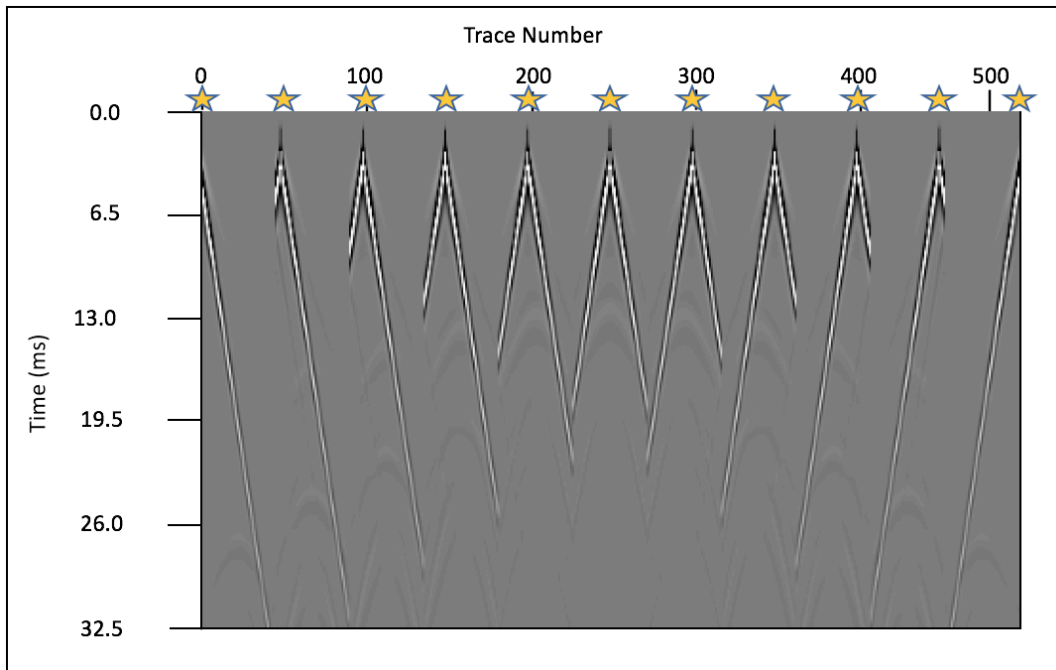


Figure 2.14: The set of seismic shot gathers (z-components) for a 14 meters depth one layer model that has the absorbing boundary condition for all boundaries with 400 Hz sources whose locations (on the surface) were marked with stars.

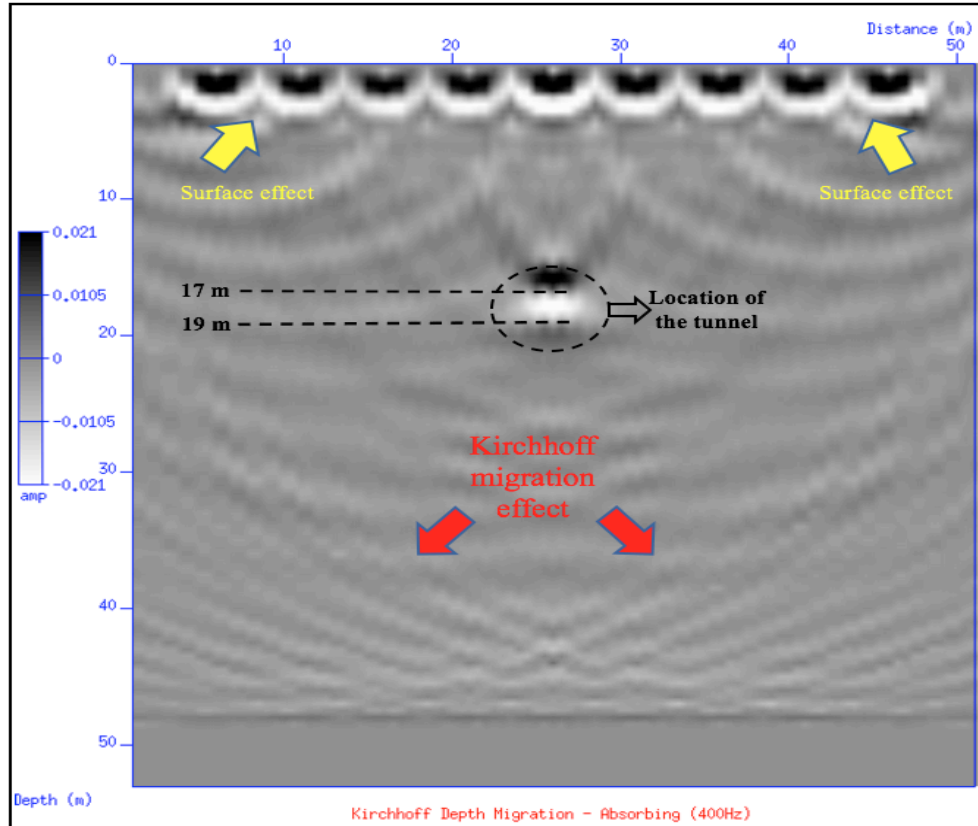


Figure 2.15 Kirchhoff migration result of the 14 meter deep tunnel model with a layer has the absorbing boundary condition for all boundaries (Amp represents the amplitude, which is a measure of the contrast in density, seismic velocities of the formations and / or underground structures).

Following the one layer model with the absorbing boundary condition and its migration result, in this section we generated another seismic model with the same parameters but for a free boundary condition. For the free boundary condition of the surface example, we can identify direct P and S wave arrivals (red and yellow arrows), the reflected P wave from the tunnel (orange arrow), converted P wave from the tunnel (blue arrow), reflected S wave from the clandestine tunnel (green arrow), and some artifacts caused by upper corners (red circle) (Figure 2.16). The tunnel can be identified from reflected waves since there is only one tunnel located in a homogenous media.

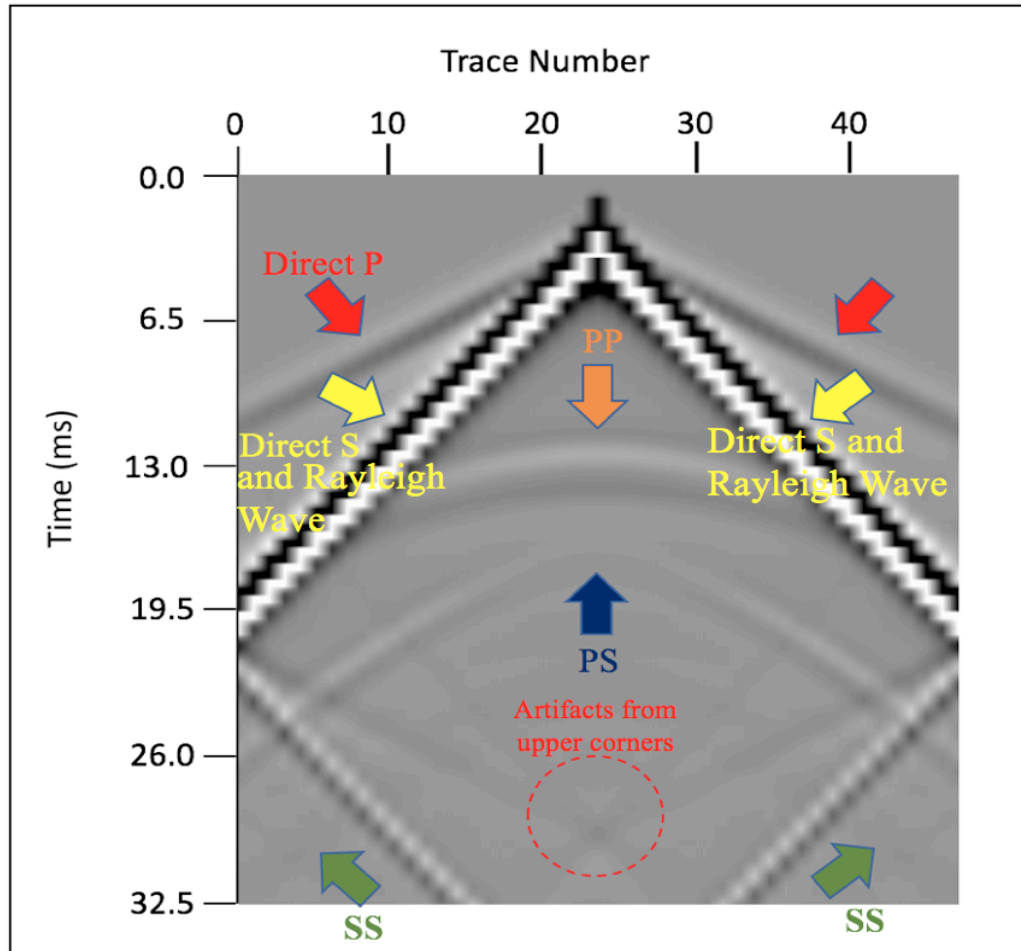


Figure 2.16: The seismogram (z-component) of 14 meter deep tunnel model with a layer with the free surface boundary condition at the surface (25 m) with a single force 400 Hz source.

In order to confirm that if we can locate the tunnel by generating a set of shot gathers for this case, we created a set of shot gathers (Figure 2.17). Then the Kirchhoff migration was applied to our set of shot gathers to image the tunnel in our model.

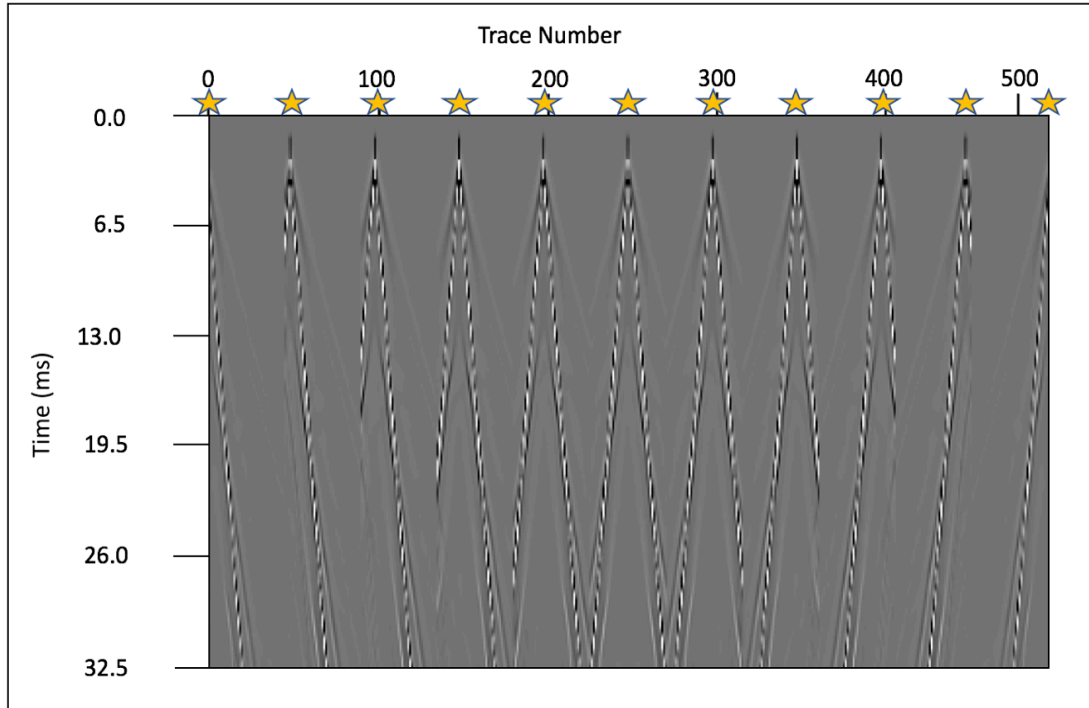


Figure 2.17: The seismic shot gather (z-component) for a 14 meter depth one layer model with the free surface boundary condition (surface). We used single-force 400 Hz seismic sources, whose shot locations are displayed with stars on the surface.

After generating a set of seismic shot gathers, we executed our Kirchhoff migration script to the shot gathers with the velocity model that we generated in the previous section (Figure 2.8). According to the result (Figure 2.18), our tunnel is located in its true depth, which is 14 meters with a correct thickness of 2 meters with the free boundary condition in the migration result. On the other hand, due to the free surface boundary condition, our result has many reflections. In addition to reflections, we have free surface artifacts (yellow arrows) because of the direct arrivals and the Kirchhoff migration artifacts (red arrows) due to insufficient number of seismic sources and receivers. However, the tunnel can still be identified clearly even though there are many artifacts existing in the results for the free surface boundary condition.

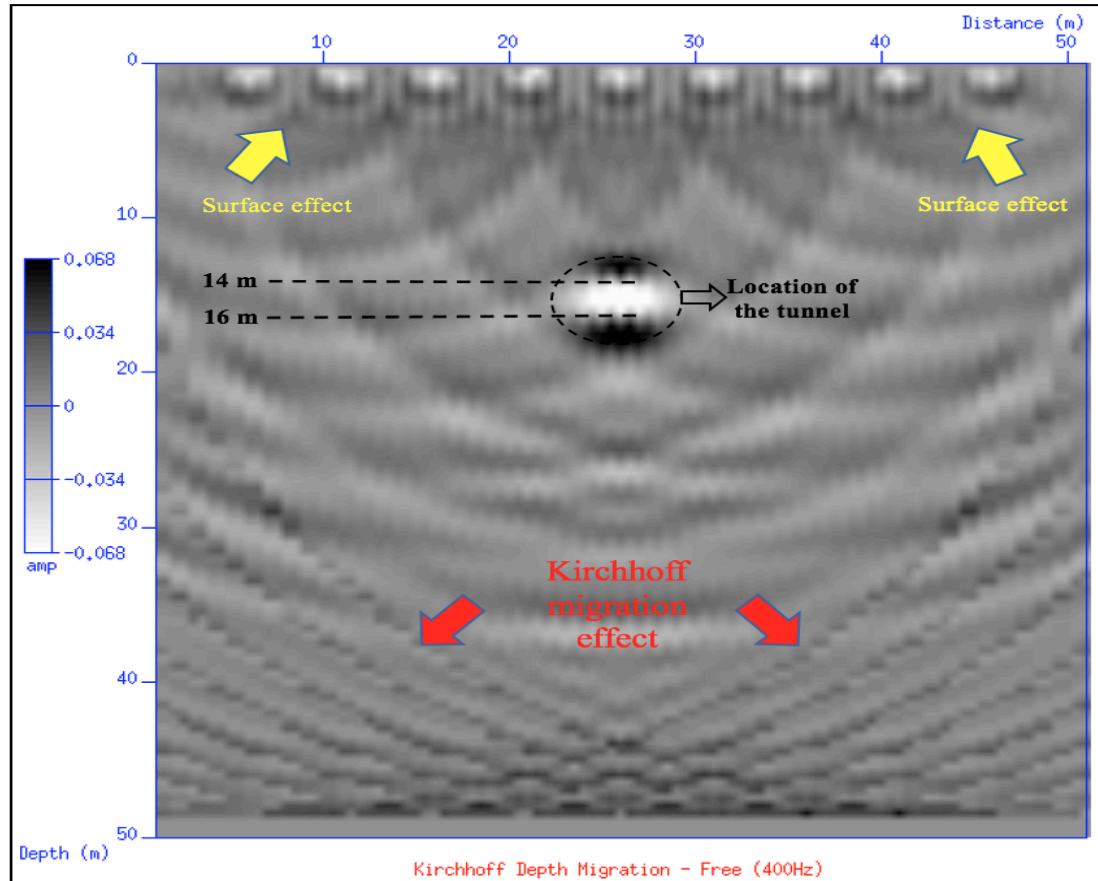


Figure 2.18: Kirchhoff migration result of the 14 meter deep tunnel model with a layer for free surface boundary condition at the surface (Amp shows the amplitude, which is a measure of the contrast in density, seismic velocities of the formations and / or underground structures).

2.2.2 Two-Layered Case

In this part, models were generated that have a tunnel at a depth of 14 meters in a two-layered model with sources at two different frequencies for each model: 100 Hz and 400 Hz. We used sources at 100 Hz at the first part of this section, because it is a very common frequency value for the seismic experiments. As a second value for the source's frequency, we chose 400 Hz as the seismic source's frequency due to the wavelength

(1.1) and vertical seismic resolution (1.2) formulas. According to given formulas, models which have been shot with a frequency of 400 Hz produce a wavelength of 7.5 meters that gives 1.875 meters of vertical seismic resolution. The acquisition geometry for a tunnel with a depth of 14 meters in a two-layered model for the subsurface seismic method is shown in Table 2.3.

Table 2.3: The acquisition geometry parameters for the tunnel at 14 meters depth for a two-layered model for the subsurface seismic method.

Model Dimension	50 m x 50 m
Seismic Shot Range	11 shots, starting from 0 m to 50 m with 5 m spacing
Number of Receivers and Their Sequence	47 receivers starting from 2 m to 48 m
Frequency of Source and Its Type	100 Hz and 400 Hz, Ricker wavelet, Single Force (Coupled)
Tunnel Depth	14 m
Recording Length (millisecond)	32.5 ms
Boundary Condition	Free (Top Layer) and Absorbing (Top Layer) for Each Example
Velocity Model	First Layer: $V_p=2500$ m/sec, $V_s=800$ m/sec, Density = 2.4 g/cm ³ Second Layer: $V_p= 3000$ m/sec, $V_s=1500$ m/sec, Density = 2.6 g/cm ³

We generated a model, which has two layers with the parameters from Table 2.3. The shallow formation which has four meters thickness has a density of 2.4 g/cm^3 , $V_p=2500 \text{ m/sec}$, $V_s=800 \text{ m/sec}$ and the deeper formation has 46 meters thickness and has a density of 2.6 g/cm^3 , $V_p=3000 \text{ m/sec}$, and $V_s=1500 \text{ m/sec}$. An example of seismic modeling is shown at Figure 2.18 where the shot point is located at 25 meters along the surface with a 400 Hz source. These generated models were run with absorbing boundary and free surface boundary conditions to evaluate which specific boundary condition gives a better result with the same model and parameters.

The absorbing boundary condition has a requirement that the absorbing layers has to be thick enough in order to work (Bélanger-Rioux et al., 2015). Since the receivers and the shots are located on the surface in our acquisition design (Figure 2.19), the absorbing boundary condition is not going to working smoothly for our acquisition design. In order to make the absorbing boundary condition work, the top boundary of our models was expanded for three meters upwards so the receivers and the sources are going to be located far enough from the absorbing boundary layer that will provide an efficient absorbing boundary condition for our modeling (Figure 2.22). We used the acquisition parameters and the model whose dimension is 50 m x 54 m from Figure 2.22 for the all examples with the absorbing boundary conditions. For the free surface examples, we used the acquisition design and the model that has the dimension of 50 m x 50 m from Figure 2.19.

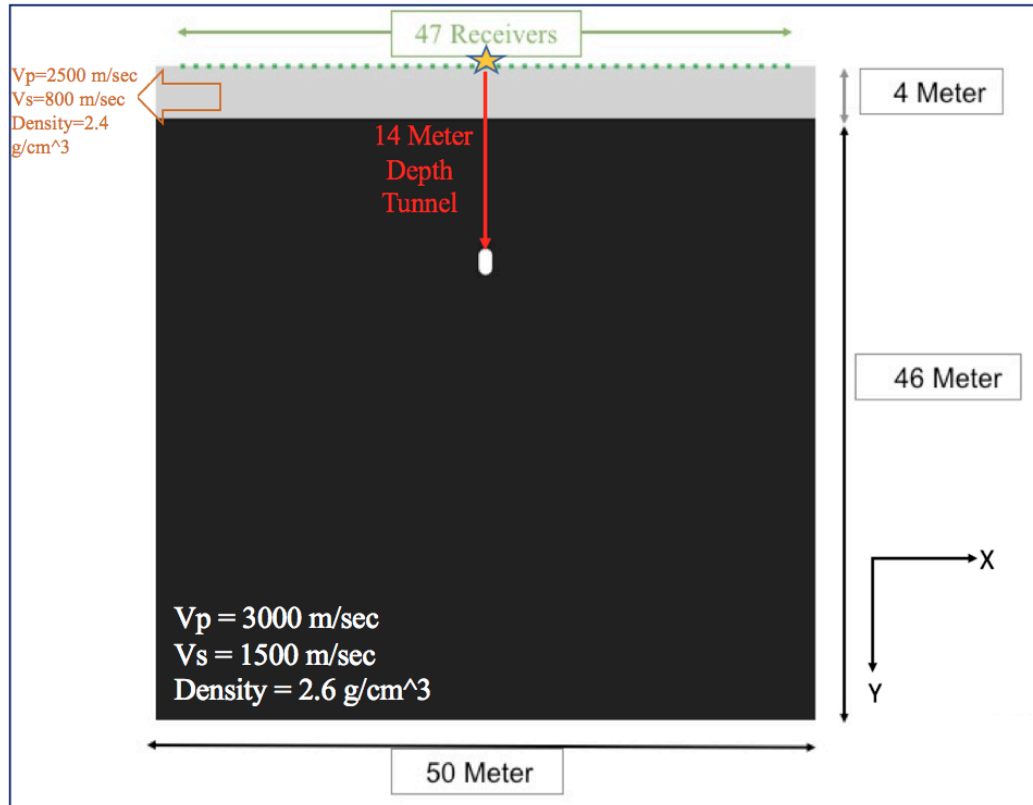


Figure 2.19: Fourteen meters depth tunnel model with two layers with the absorbing boundary condition for the all boundaries. The seismic source is a single-force with 400 Hz located on the surface (shown with the star).

After we ran our script in Specfem2D for the 14 meters depth for two-layered model, we see that seismic waves travel along the surface and through the media. Figure 2.20 shows the seismic modeling at 5.75 ms when the seismic waves arrive at the tunnel in the model.

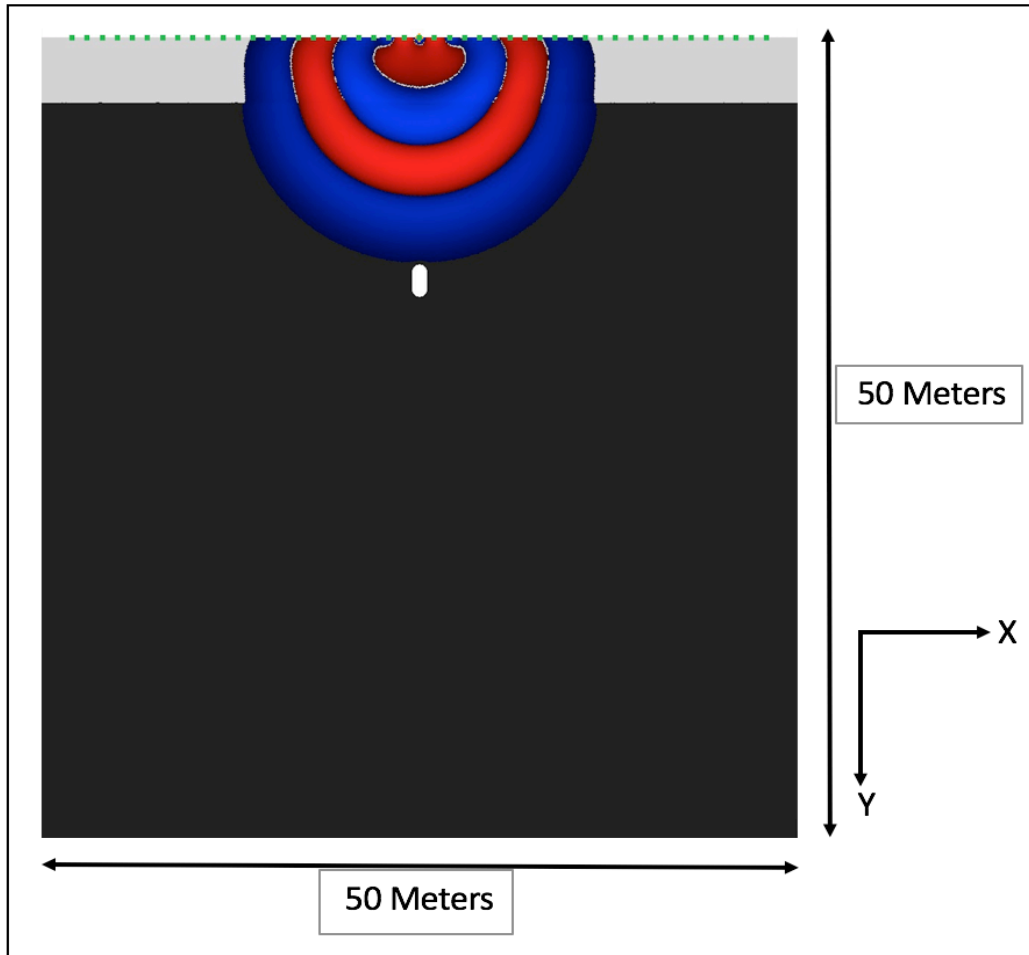


Figure 2.20: Fourteen meters depth tunnel model with two layers run in Specfem2D at 5.75 ms.

The seismic waves were reflected back towards the receivers after they reached the second layer and reaches the tunnel at 10 ms (Figure 2.21).

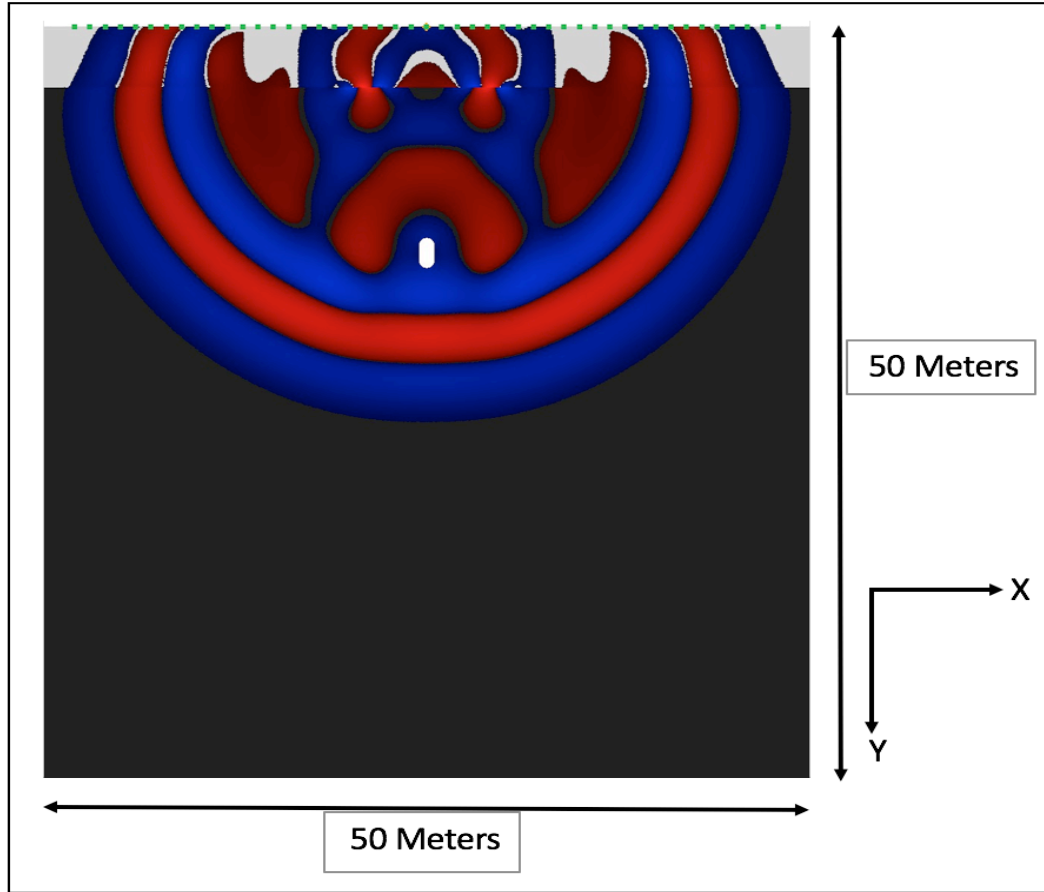


Figure 2.21: Fourteen meters depth tunnel model with one layer run in Specfem2D at 10 ms while seismic wave propagations are reflected from the deeper formation and the tunnel and travel back to the surface.

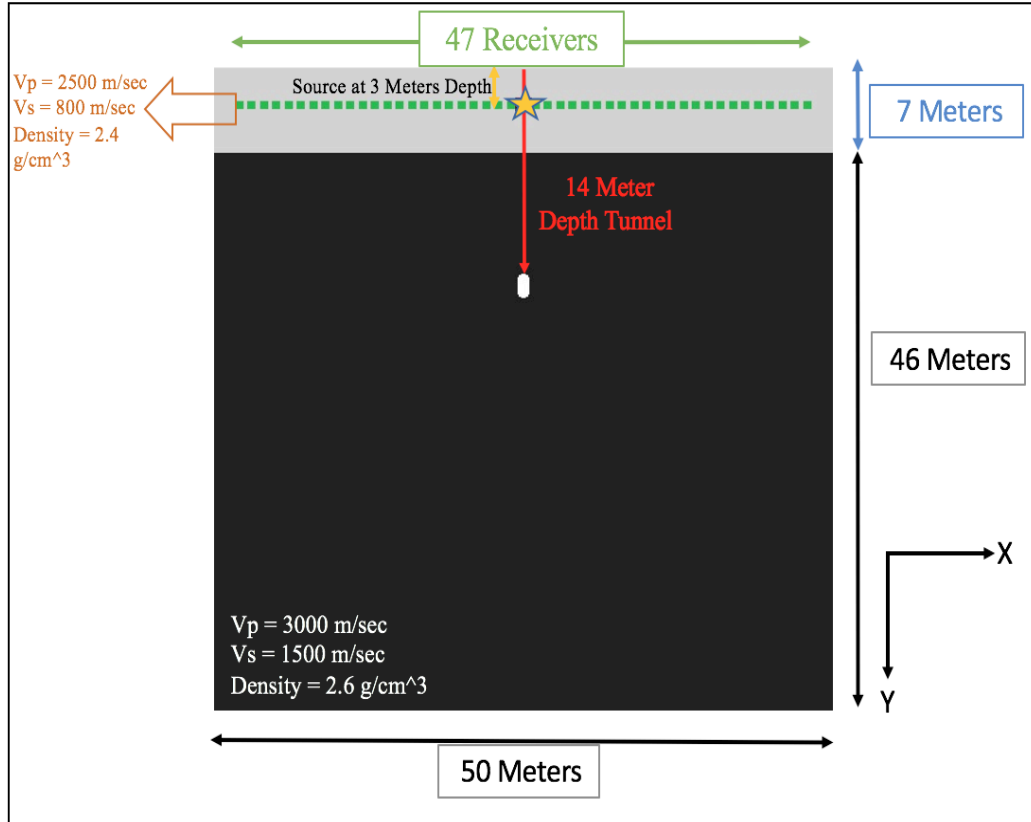


Figure 2.22: Fourteen-meter-deep tunnel model with two layers that has the absorbing boundary conditions for all boundaries with a single-force 400 Hz source at three meters depth (shown with a star).

According to the recorded seismogram (Figure 2.23) which contains our seismic modeling for a 100 Hz source at 25 meters on the surface with an absorbing boundary condition, the only waves that can be identified are direct S wave arrivals, due to the low seismic source's frequency value of 100 Hz.

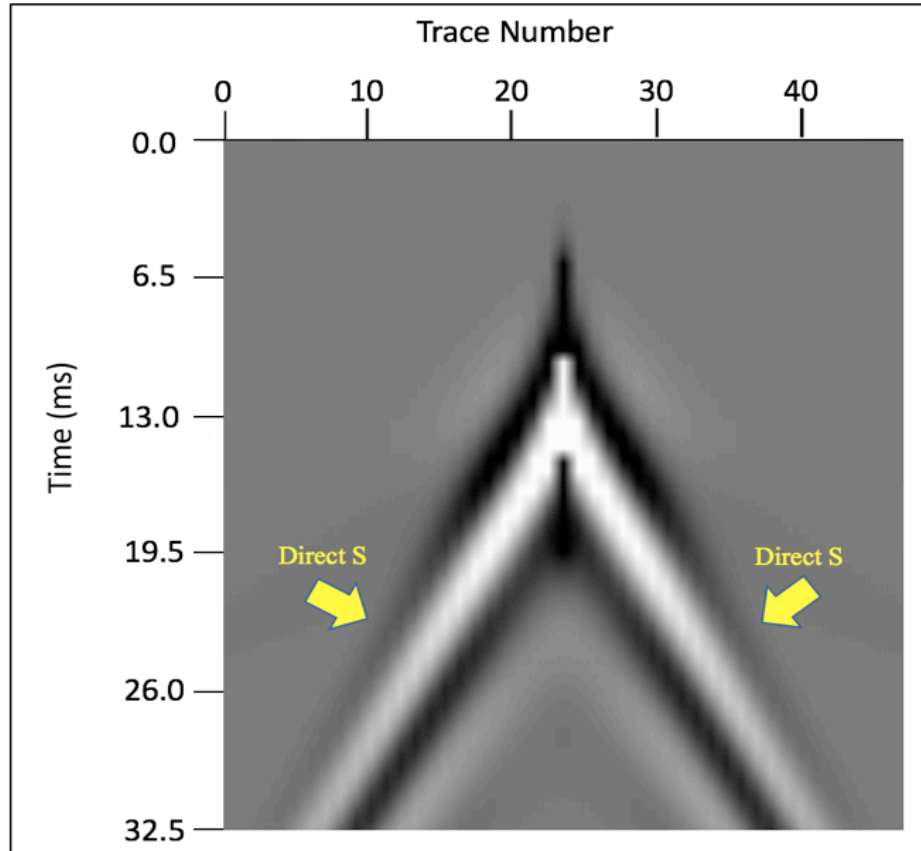


Figure 2.23: The seismogram (z-component) of a 14 meters deep tunnel model with two layers for the absorbing boundary condition at the surface with a single-force of 100 Hz source.

Afterwards, we generated a velocity model for a two-layered model (Figure 2.24). We then combined all the shots together to generate a set of shot gathers (Figure 2.25) to apply the seismic migration to image the clandestine tunnel with an absorbing boundary condition for all boundaries of the model (Figure 2.26). As seen in the migration result, the tunnel is not visible. The possible reason of this outcome is that the low source frequency (100 Hz) is not high enough to locate and detect the tunnel. The only distinguishable features in the migration result are the surface effects (yellow arrows),

which are because of the direct arrivals and the Kirchhoff migration artifacts (red arrows), which are caused by the limited number of the seismic shots and the receivers.

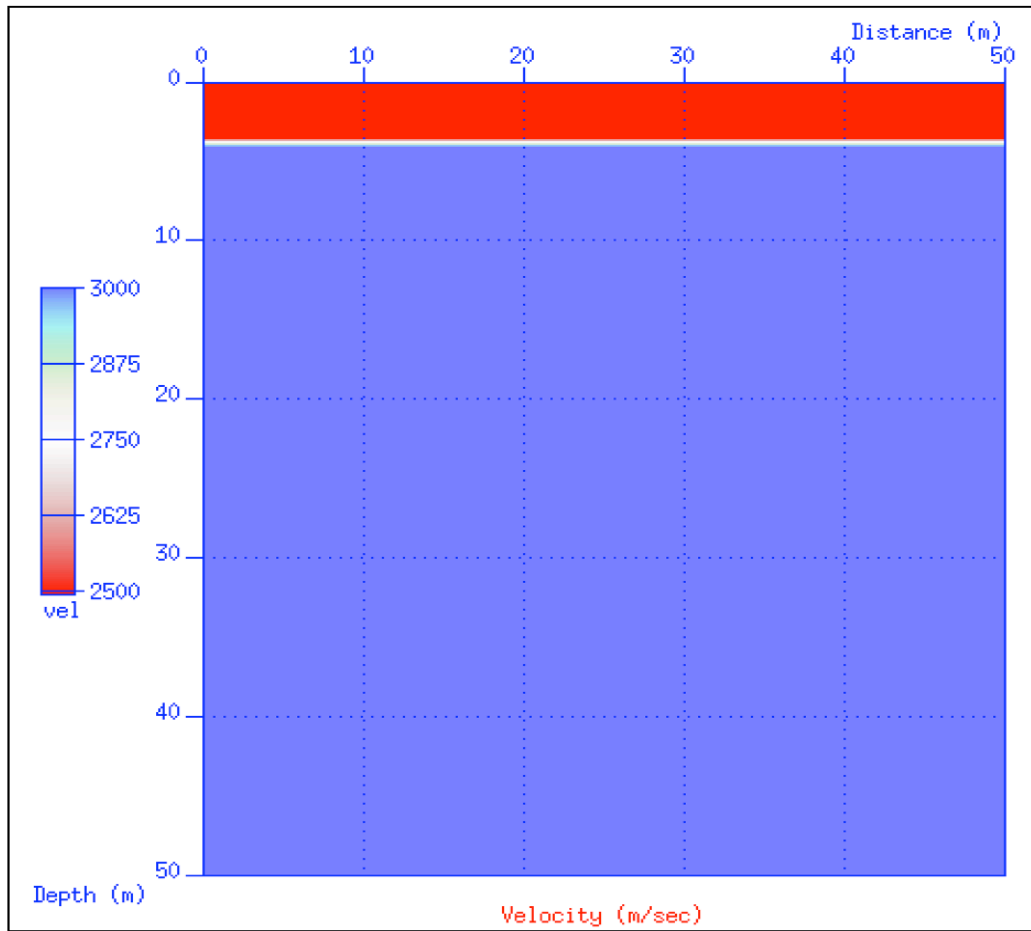


Figure 2.24: The migration velocity model for the two-layered medium (vel represents velocities whose values are between 2500 m/sec to 3000 m/sec).

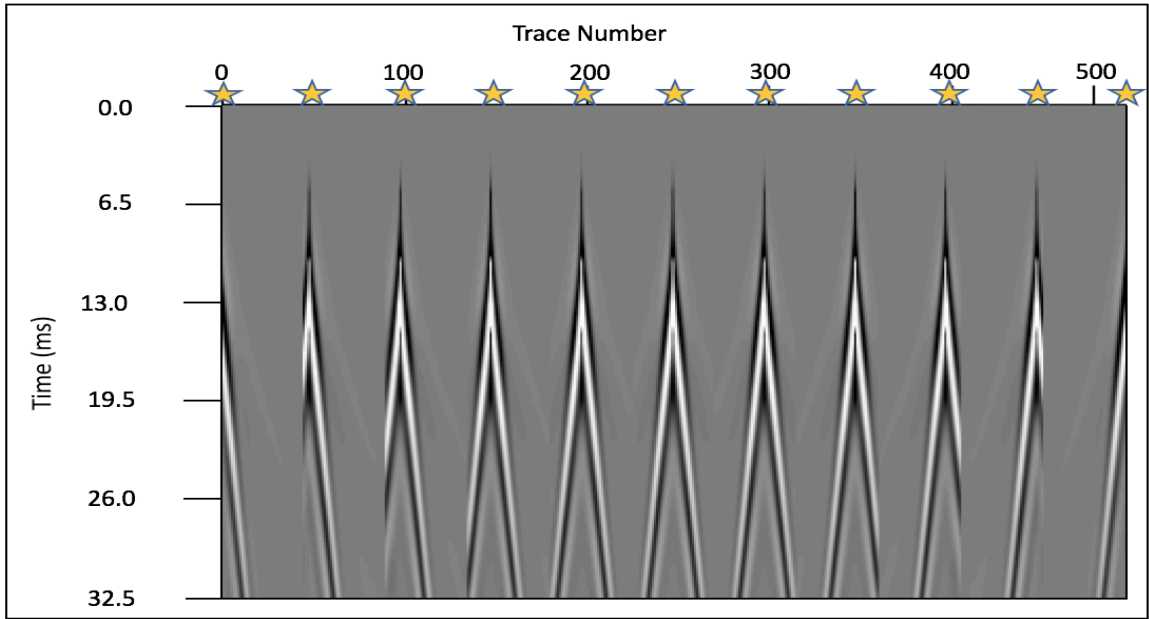


Figure 2.25: The seismic shot gather (z-component) for 14 meters depth two-layered model with the absorbing boundary condition for all the boundaries. Sources are single-forces with 100 Hz, shot locations were shown with stars.

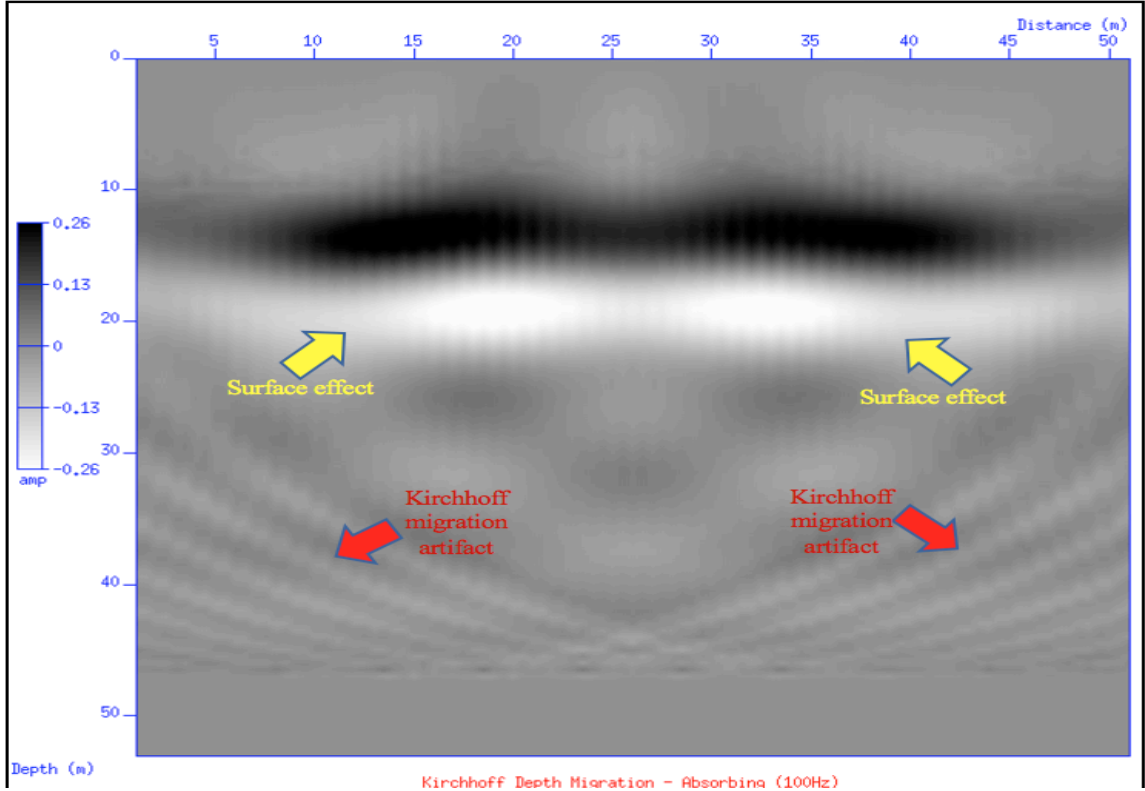


Figure 2.26: Kirchhoff migration result of the 14 meters depth tunnel model with two layers for an absorbing boundary condition for all boundaries with 100 Hz seismic sources (Amp represents the amplitude, which is a measure of the contrast in density, seismic velocities of the formations and / or underground structures. Amplitude allows us to interpret the formations and the structures in the seismic data).

After finalizing the case with 100 Hz source for the absorbing boundary condition, we used the same model and source for the free surface boundary condition to compare it with the absorbing boundary condition case. For this purpose, we created seismic modeling by using the model from Figure 2.22 and the parameters from Table 2.3 for a free absorbing boundary condition case. After generating the seismogram, we can only see direct P (red arrows) and S wave arrivals (yellow arrows) in our result (Figure 2.27). According to our calculations, we also see the Rayleigh waves with the direct S arrivals since the Rayleigh wave's velocity is 1398 m/sec and direct S arrival's velocity is 1500 m/sec. Since we cannot separate them on the seismogram since their speeds are too close to each other, we tag the Rayleigh waves and direct S arrivals together (Figure 2.27).

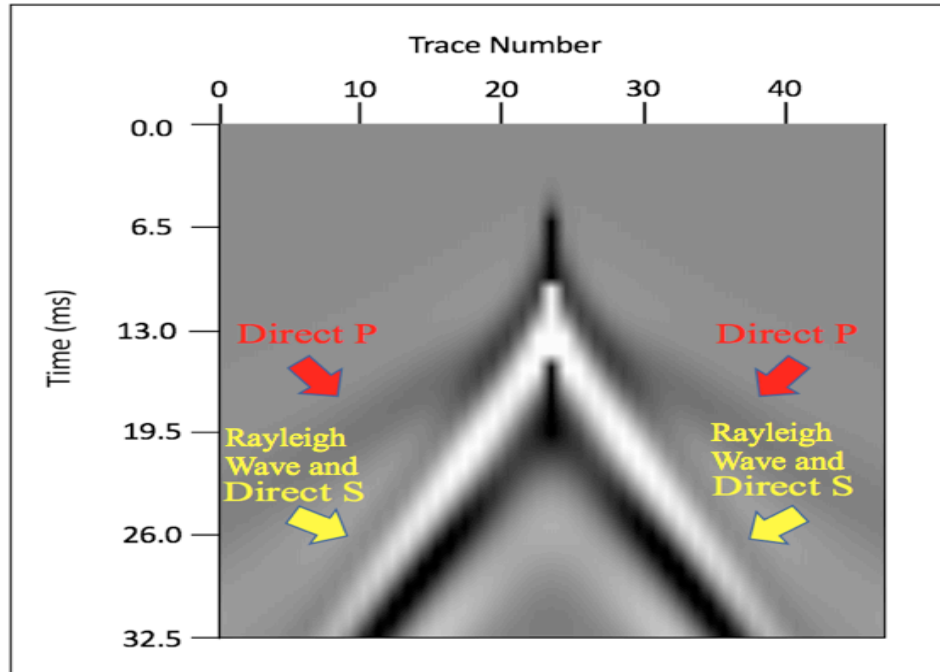


Figure 2.27: The seismogram (z-component) of a 14 meters depth model for a free surface boundary condition with a parallel layer for a 100 Hz seismic source at 25 meters on the surface.

Then, we generated a set of shot gathers with a free surface boundary condition (top boundary) (Figure 2.28) to run the seismic migration to check if we can locate the tunnel with the migration with 100 Hz sources. According to the Kirchhoff migration result in Figure 2.29, we almost have an identical result as the one we have in the previous section for a one layered model. In the migration result, we can only identify the surface effects (yellow arrows), which are caused of the direct arrivals and the Kirchhoff migration artifacts (red arrows) due to insufficient number of the sources and the receivers. We cannot see our tunnel in the migration result due to the low frequency value of the sources and their long wavelength and low vertical resolution.

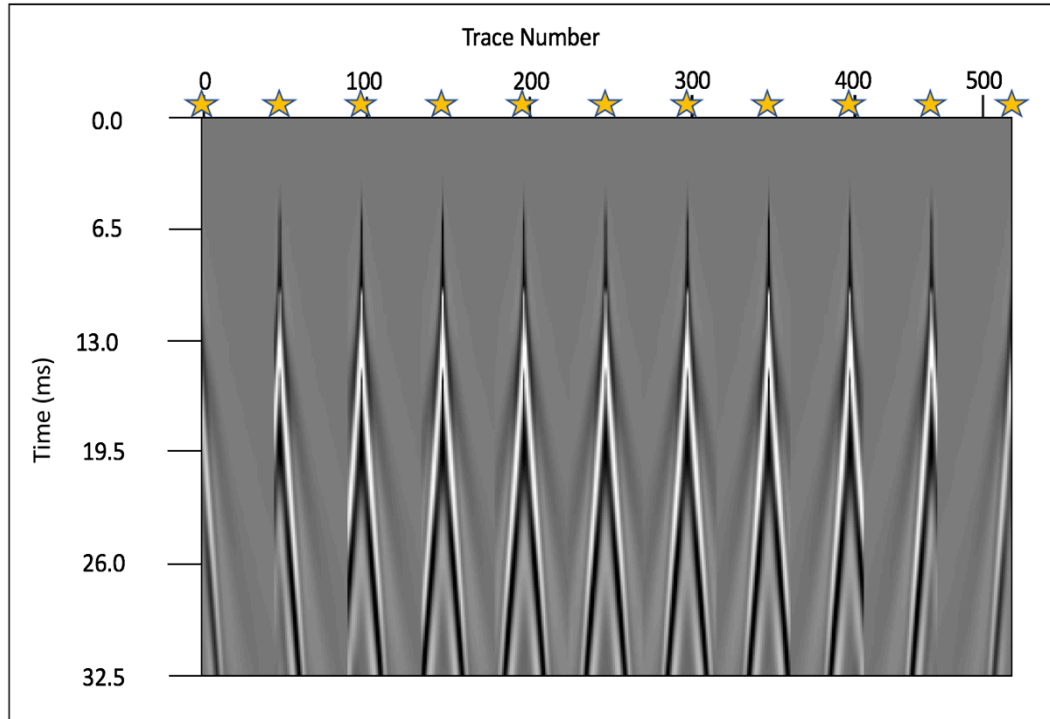


Figure 2.28: The set of shot gathers for the free boundary condition (surface) for 14 meters depth tunnel with a parallel layer with the seismic sources of 100 Hz (shown with stars).

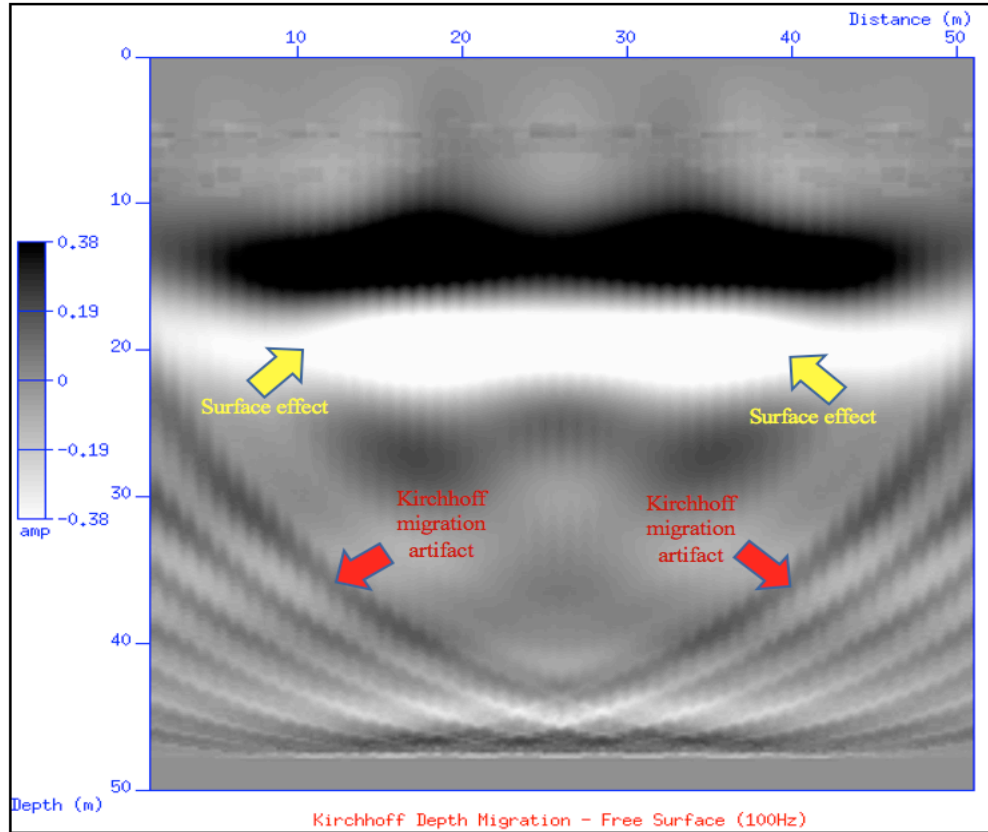


Figure 2.29: Kirchhoff migration result of the 14 meters depth tunnel model with two layers for the free surface boundary condition (surface) with single-force seismic sources of 100 Hz.

After completing models for the source which has a frequency of 100 Hz, we continued our research for examples with sources that have a 400 Hz frequency. We generated a seismic model with an absorbing boundary condition with a seismic source of 400 Hz located at three meters depth from the surface, the recorded seismogram is shown below (Figure 2.30). Yellow arrows indicate the direct S wave arrivals, the orange arrow shows the reflected P wave from the shallow layer, and the white arrows show reflected S wave from the tunnel.

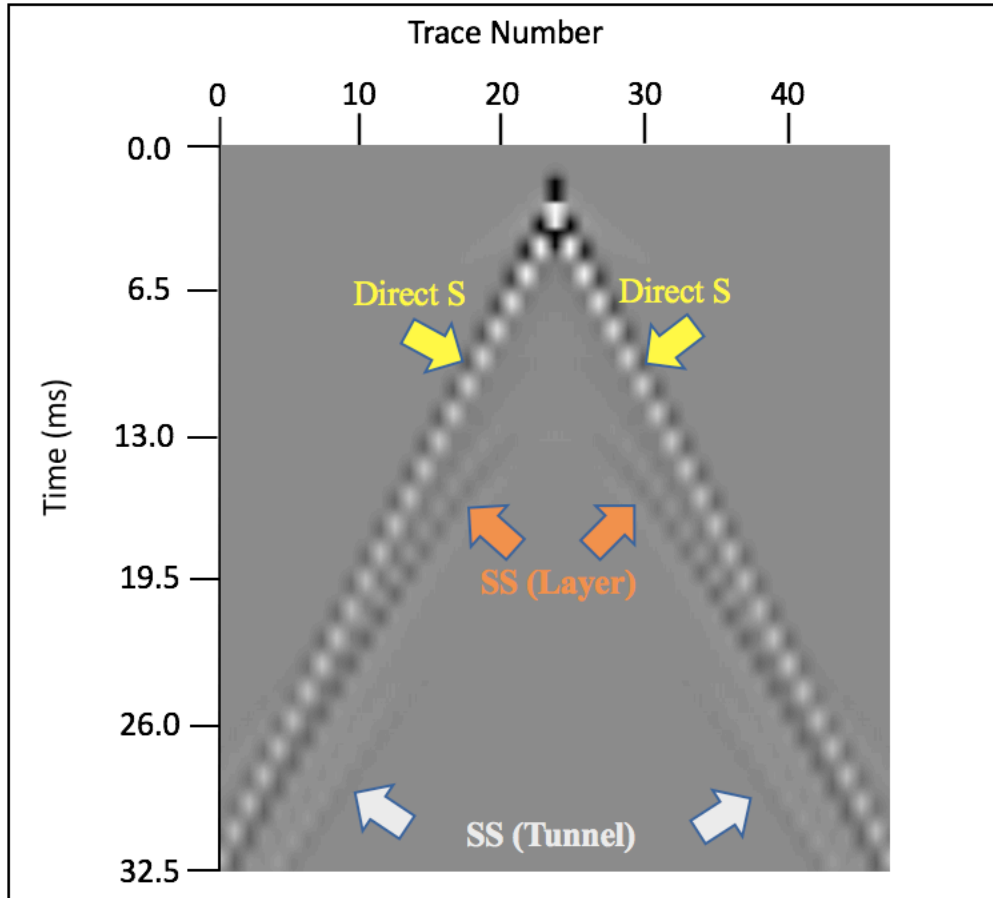


Figure 2.30: The seismogram (z-component) of a 14 meters depth model with two layers for the absorbing boundary condition (all boundaries) with a single-force 400 Hz source at three meters depth from the surface.

After identifying the reflected waves, we generated a set of shot gathers for this case (Figure 2.29). Then we used the two layers seismic velocity model (Figure 2.24) from the earlier case. After generating the set of shot gathers, we applied the Kirchhoff migration to the created shot gathers (Figure 2.30).

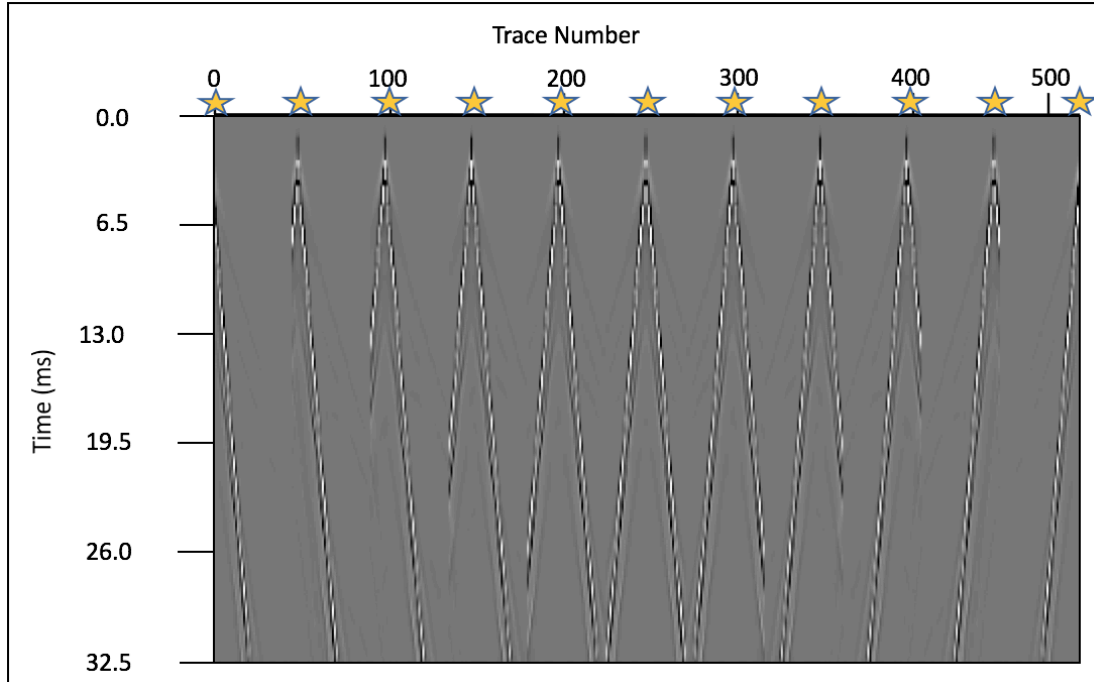


Figure 2.31: The set of shot gathers of 14 meters depth tunnel model with two layers that have the absorbing boundary condition (all boundaries) with single-force 400 Hz seismic sources (shown with stars) on the surface.

According to the migration result in Figure 2.30, we can locate the tunnel in its correct location and thickness. The black circle shows the location of the tunnel between 14 meters and 16 meters. We also see the Kirchhoff migration artifacts (red arrows) because of the limited numbers of the shots and the receivers and the surface effect (yellow arrows) due to the direct arrivals.

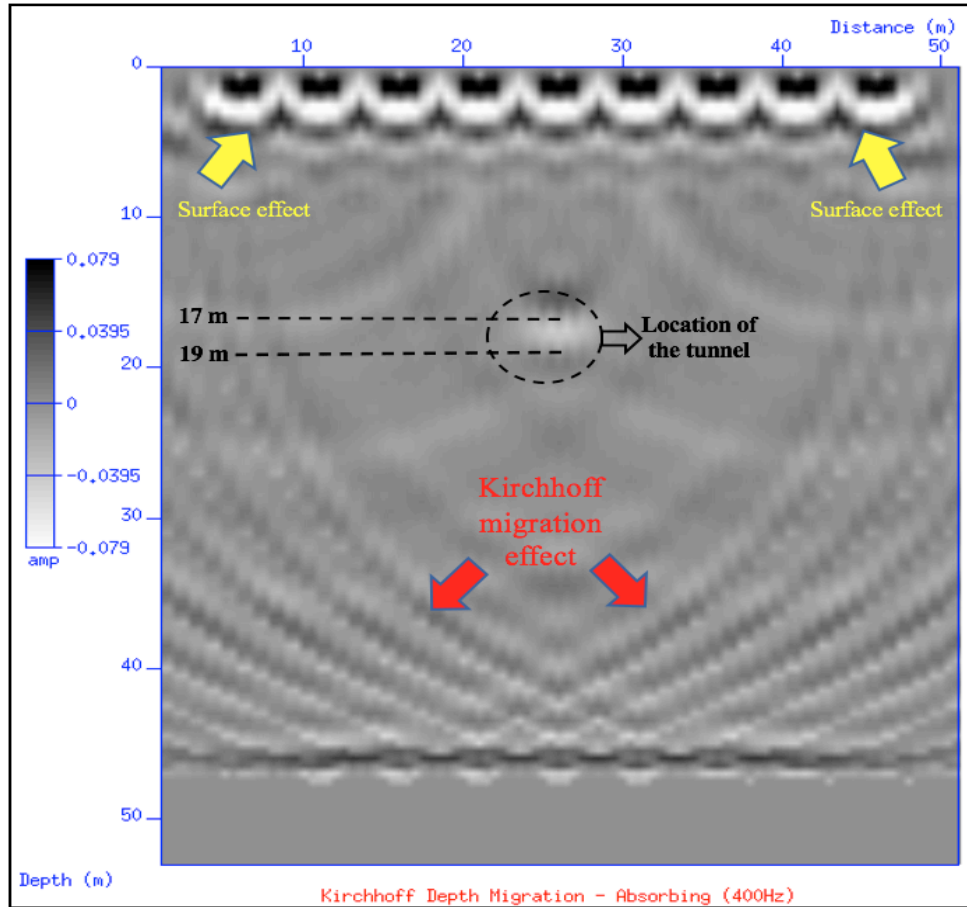


Figure 2.32: Kirchhoff migration result of the 14 meters depth tunnel model with two layers model for the absorbing boundary condition (all boundaries) (Amp shows the amplitude, which is a measure of the contrast in density, seismic velocities of the formations and / or underground structures).

Following the absorbing surface case, we used the same models and parameters from Figure 2.19 to test our model for the free surface boundary condition. We generated a seismogram via Specfem2D for a 14 meters depth tunnel with two-layers model with free surface condition at the surface (Figure 2.33). In this seismogram, red arrows show direct P wave arrivals, yellow arrows indicate direct S wave arrivals, the orange arrow shows the reflected P wave from the layer, the blue arrows display the reflected P wave

from the tunnel, the purple arrow shows the converted P wave from the tunnel, and the green arrows shows the reflected S wave from the layer.

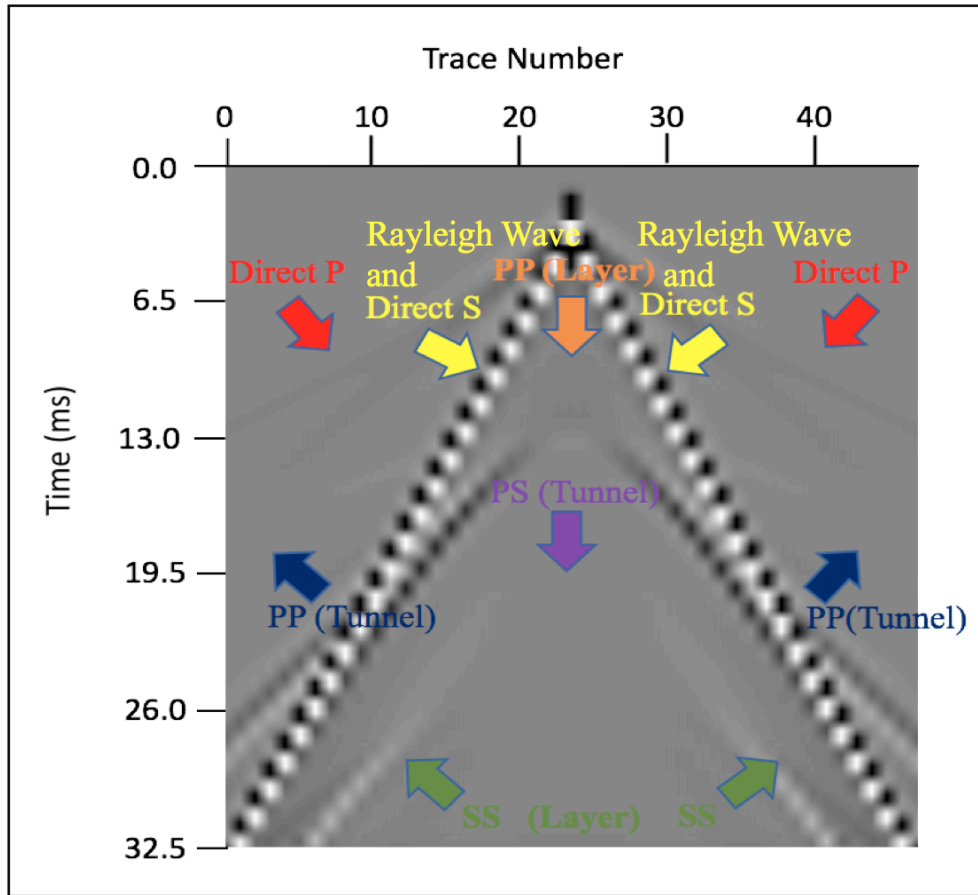


Figure 2.33: The seismogram (z-component) of a 14 meters depth tunnel model with two layers for the free surface condition (surface) with a single-force 400Hz seismic source at 25 meters on x-axis at the surface.

After identifying the waves in the seismogram, we created a set of shot gathers (Figure 2.34) for the free surface boundary condition at the surface, then we applied the Kirchhoff migration to the set of shot gathers to image the clandestine tunnel (Figure 2.35).

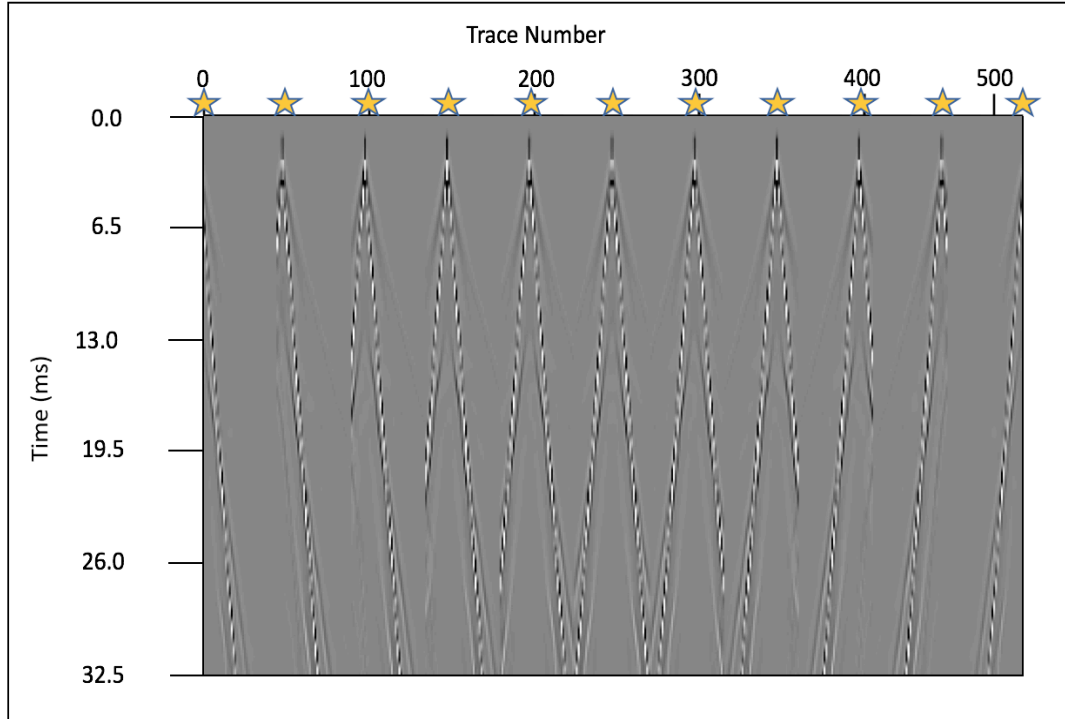


Figure 2.34: The set of shot gathers of 14 meters depth tunnel with two layers for the free surface boundary condition with single-force seismic sources of 400 Hz (shown with stars).

According to the migration results in Figure 2.35, we can see the clandestine tunnel clearly in its right position (14 meters depth) and with the correct thickness (two meters). However, we cannot clearly identify the shallow layer, which is possibly due to the low frequency of the source, short thickness of the shallow formation, and free surface boundary condition. In addition to problems to locate the shallow formation, we can clearly see Kirchhoff migration artifacts (red arrows) due to the limited number of shots and receivers, and surface effects because of the direct arrivals.

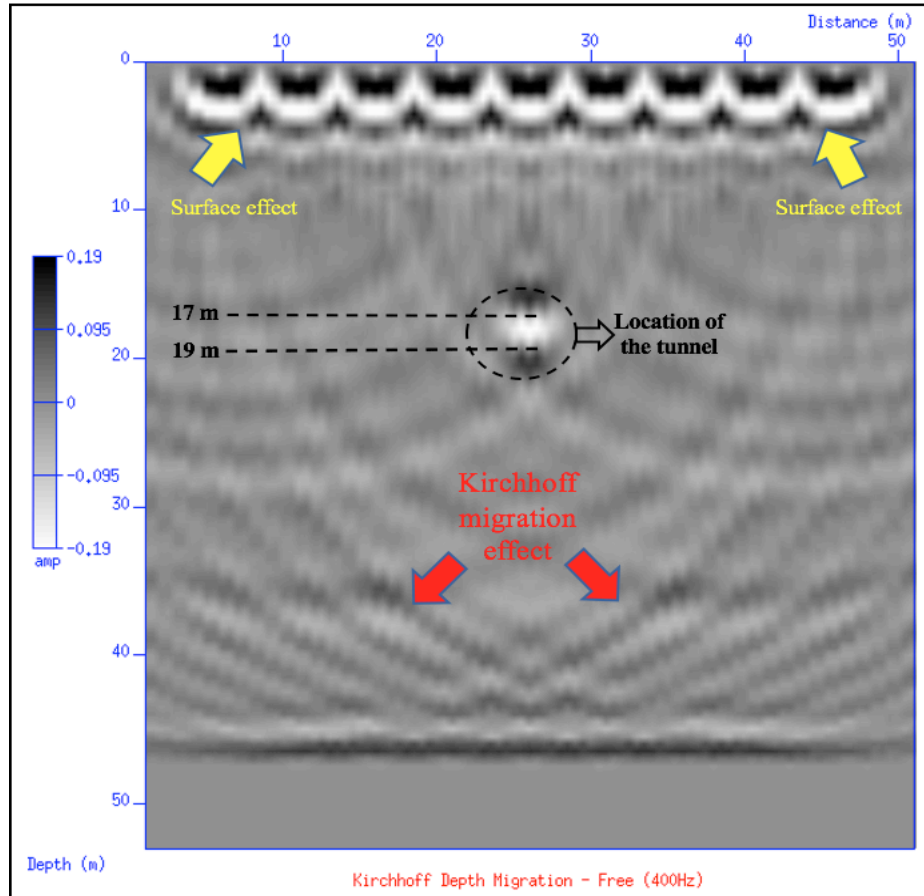


Figure 2.35: The seismic shot gather for the free surface boundary condition for 14 meters depth tunnel with a parallel layer and a seismic source at 400 Hz (Amp represents the amplitude, which is a measure of the contrast in density, seismic velocities of the formations and / or underground structures).

2.3 Model of Tunnel Located at 19 Meters

2.3.1 One Layer Case

In this section, the same tunnel and parameters from “2.2 Model of Tunnel located at 14 Meters” are used. The tunnel was placed at a depth of 19-meters to observe if by increasing the depth of the tunnel, it may be detected in the seismograms. The

models were generated with two different source frequencies each: 100 Hz and 400 Hz. However, due to the wavelength (1.1) and vertical seismic resolution formulas (1.2), the same issue from the previous section were encountered, and only models shot with a frequency of 400 Hz produced some reflections to help locate the tunnel in the seismogram with the subsurface seismic method. However, we still included the modeling result with 100 Hz frequency to cross check our results with a different seismic source's frequency value. As a result, in this section we included the results of the models with sources of 100 Hz and 400 Hz.

We generated a simple model that has only one layer for this seismic modeling, whose density is 2.6 g/cm^3 , $V_p= 3000 \text{ m/sec}$, and $V_s=1500 \text{ m/sec}$. The shot point is located at 25 meters with 400 Hz (Figure 2.34). The purpose of running this uncomplicated model is to see if the tunnel can be recognized in the easiest settings. Otherwise we can draw the conclusion that this method cannot be fully used to locate the clandestine tunnels.

The acquisition geometry for a tunnel with a depth of 14 meters for the subsurface seismic method is shown in Table 2.4.

Table 2.4: The acquisition geometry parameters for the tunnel with a depth of 19 meters for subsurface seismic method

Model Dimension	50 m x 50 m
Seismic Shot Range	11 shots, starting from 0 m to 50 m with 5 m spacing
Number of Receivers and Their Sequence	47 receivers starting from 2 m to 48 m
Frequency of Source and Its Type	100 Hz and 400 Hz, Ricker wavelet, Single Force (Coupled)
Tunnel Depth	19 m
Recording Length (millisecond)	32.5 ms
Boundary Condition	Free Surface (Top Layer) and Absorbing (Top Layer) for Each Example
Velocity Model	$V_p= 3000$ m/sec, $V_s=1500$ m/sec, Density = 2.6 g/cm ³

We ran this simple model that has only one layer and has a density of 2.6 g/cm³, $V_p= 3000$ m/sec, and $V_s=1500$ m/sec (Table 2.4). An example of seismic modeling is shown in Figure 2.36 where shot point is located at 25 meters with 400 Hz (Figure 2.36). We ran some examples with absorbing boundary and free surface boundary conditions

for the surface layers of the models to compare the ideal results with more realistic results.

On the other hand, the absorbing boundary condition needs absorbing layers to be thick enough in order to them to work efficiently (Bélanger-Rioux et. al, 2015). As we have the receivers and the shots on the surface in our acquisition design (Figure 2.36), the absorbing boundary condition is not going to working efficiently for this acquisition design. We expanded the top boundary of our model in Figure 2.36 for three meters higher in order to make the absorbing boundary condition work for our acquisition design (Figure 2.37). We used the acquisition parameters from Table 2.4 and the model, whose dimension is 50 m x 54 m from Figure 2.37 for the all examples with the absorbing boundary conditions. For the free surface examples, we used the acquisition design and the model that has the dimension of 50 m x 50 m from Figure 2.36.

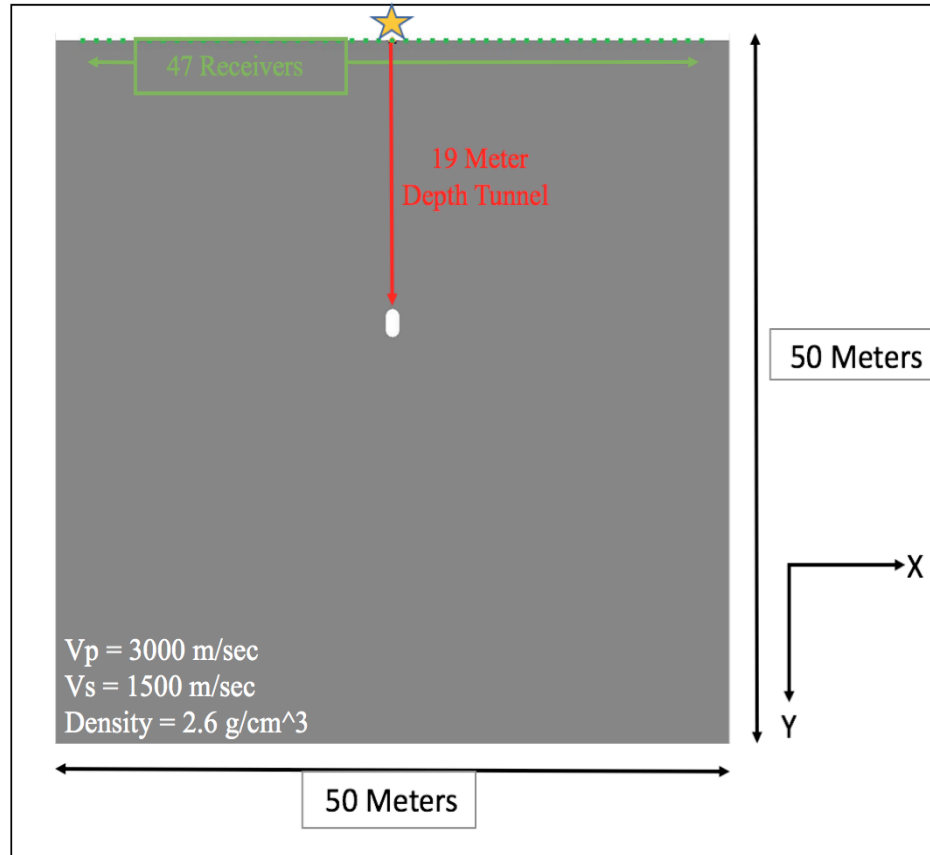


Figure 2.36: 14 meter depth tunnel model with one layer. The source (shown with the star) is a single-force with 400 Hz located at 25 meters on x-axis .

We ran our seismic modeling according to the parameters in Table 2.4 and Figure 2.37. After recording the seismogram that has the absorbing boundary condition for all boundaries with 100 Hz source in Figure 2.38, we can only see direct S wave arrivals due to the low frequency (100 Hz) of the source.

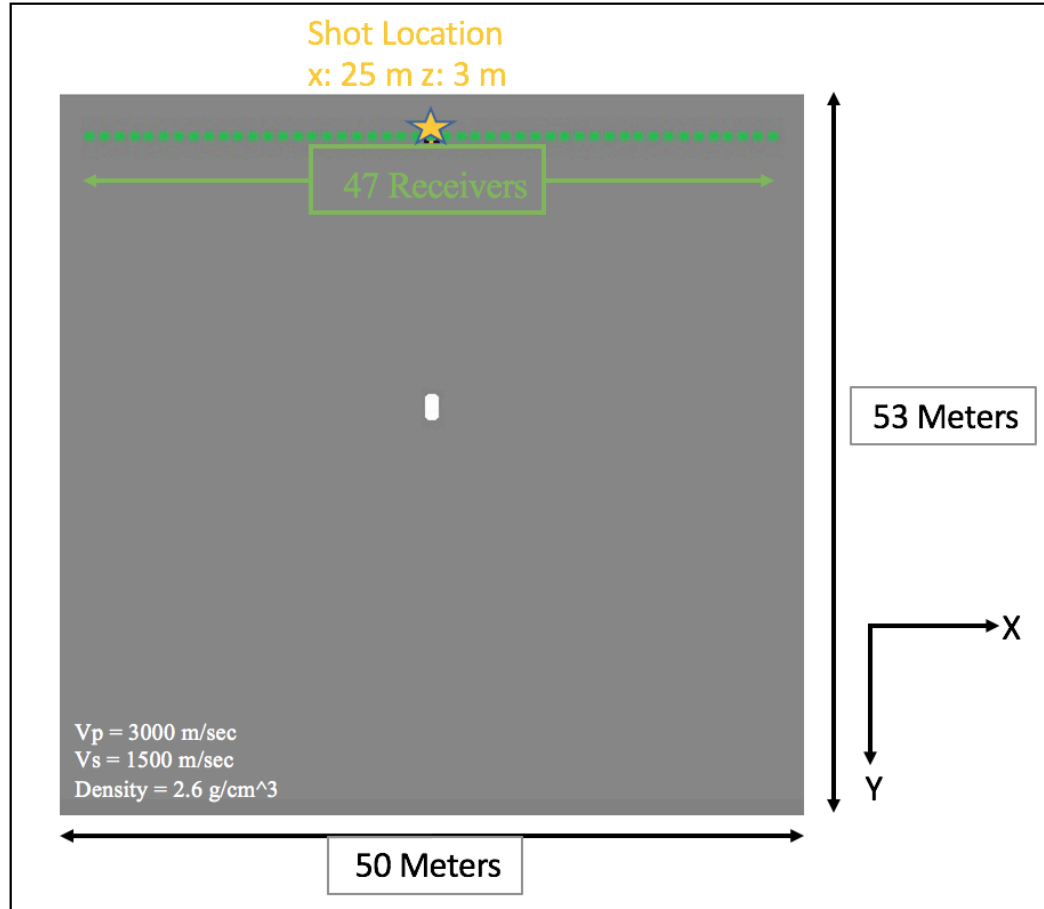


Figure 2.37: Fourteen meters depth tunnel model with one layer. The shot location (25 meters on x-axis) is shown with the star.

After examining the waves in the seismogram, we created a set of shot gathers for this case (Figure 2.39). Subsequently, we used this generated the set of shot gathers for applying the Kirchhoff migration to image the clandestine tunnel located at 19 meters depth with the one layer velocity model (Figure 2.8). According to the migration result in Figure 2.40, we cannot locate the tunnel after migrating the reflections. We can only identify the surface effects, which are caused by the direct arrivals and the Kirchhoff migration effects due to the limited number of the sources and the receivers.

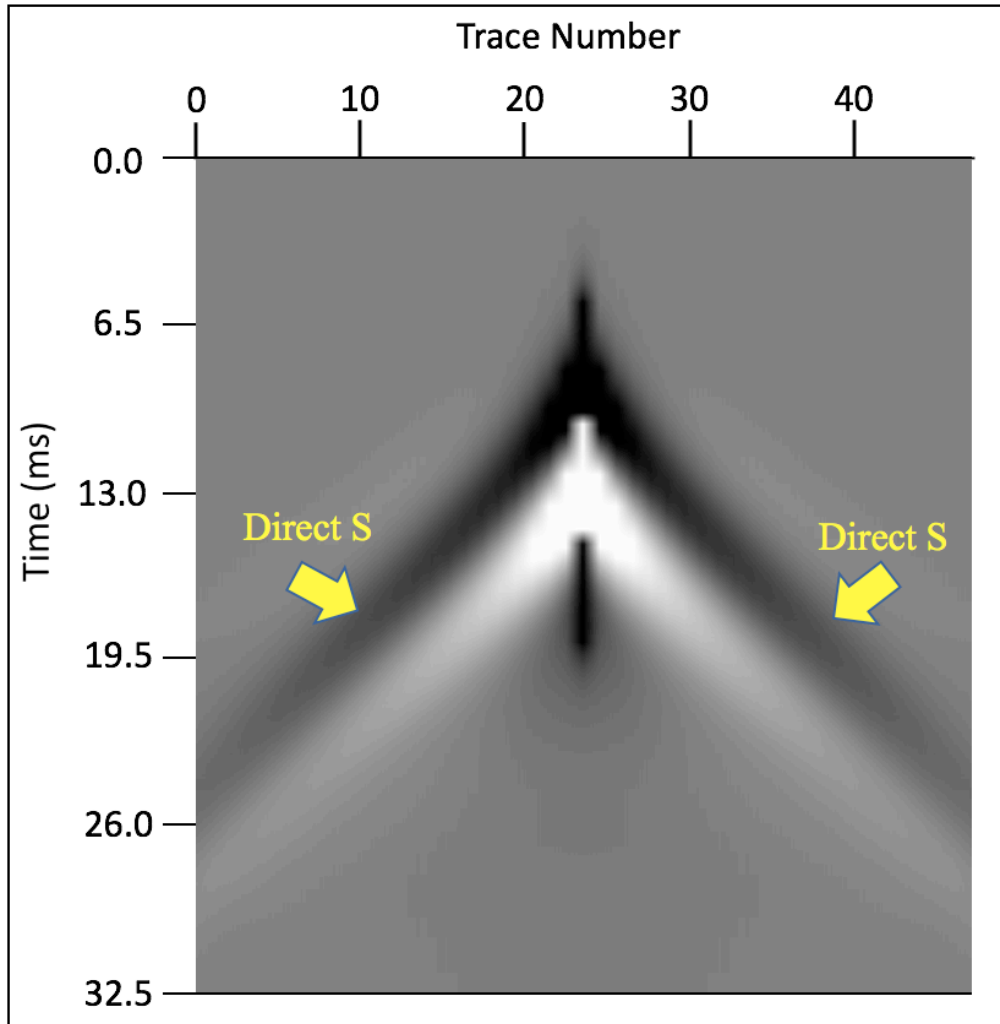


Figure 2.38: The seismogram (z-component) of 14 meters depth model with one layer for the absorbing boundary condition (all boundaries) with a single-force 100 Hz seismic source located at 25 meters on x-axis, three meters depth from the surface.

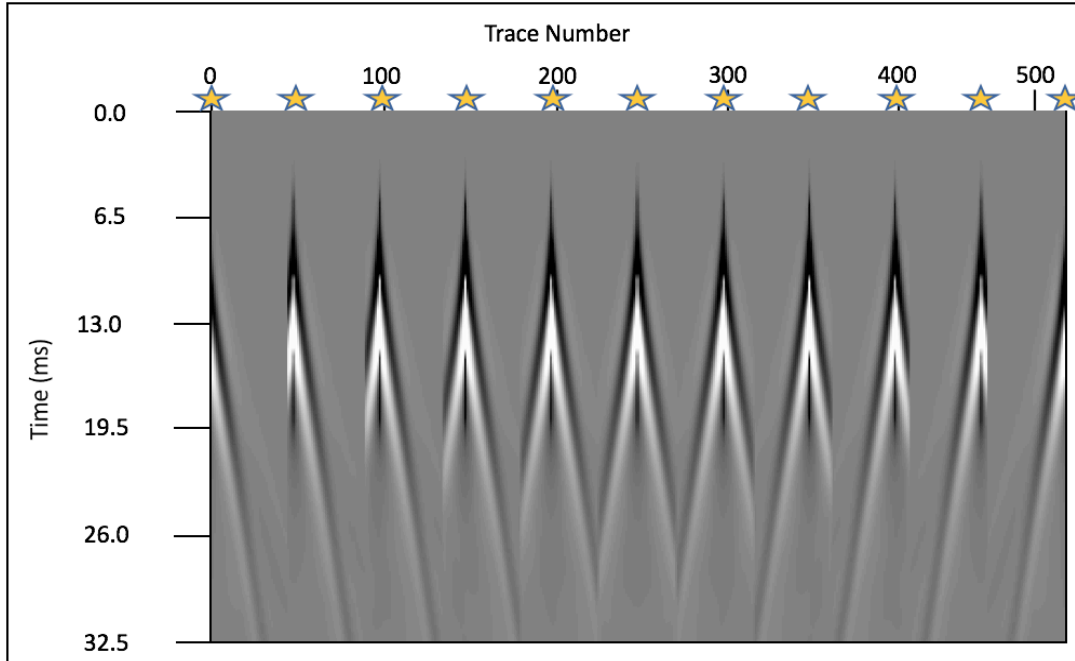


Figure 2.39: The set of shot gathers (z-component) for the 19 meters depth tunnel model with one layer of the absorbing boundary condition (for all boundaries) with single-force 100 Hz sources (shown with stars).

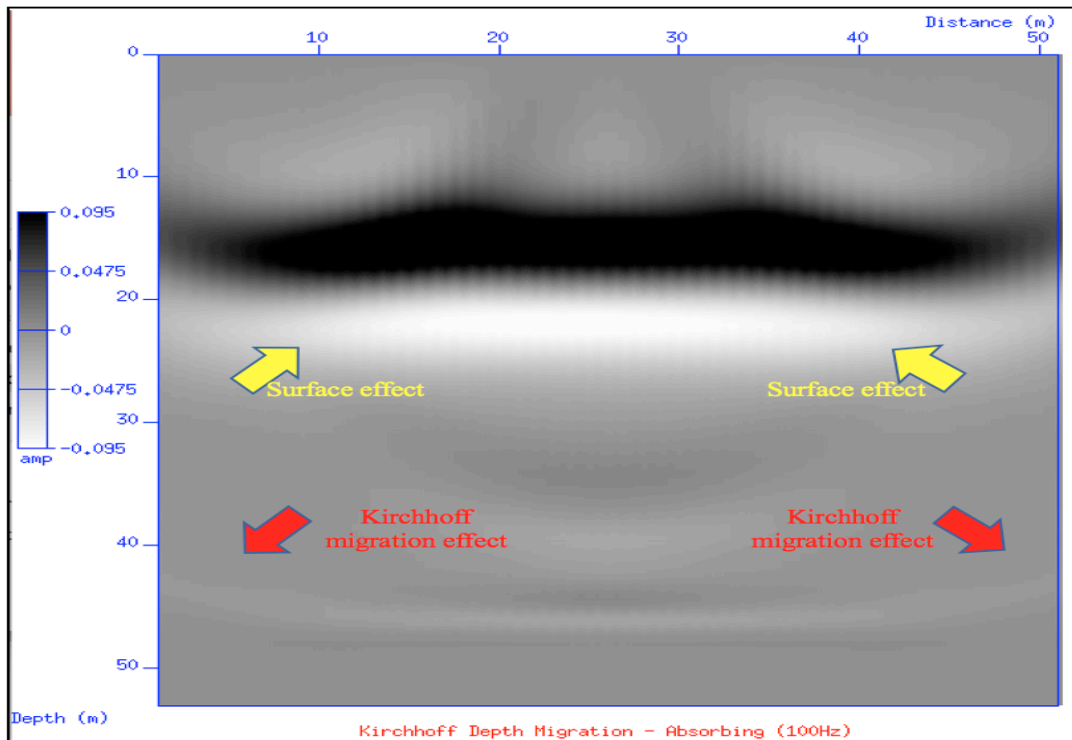


Figure 2.40: The Kirchhoff migration result for 19 meters depth one layer model with absorbing boundary condition with the 100 Hz source (Amp represents the amplitude, which is a measure of the contrast in density, seismic velocities of the formations and / or underground structures).

Afterwards, we ran Specfem2D software to simulate the model from Figure 2.36 with the parameters from Table 2.4 for the free surface boundary condition. After executing the script in Specfem2d, we recorded the seismogram in Figure 2.41. According to the seismogram, only direct S wave arrivals and the Rayleigh waves can be seen due to the low frequency of the source. However, we cannot distinguish the Rayleigh waves (1398 m/sec) from the direct S arrivals (1500 m/sec) due to their close velocities with each other.

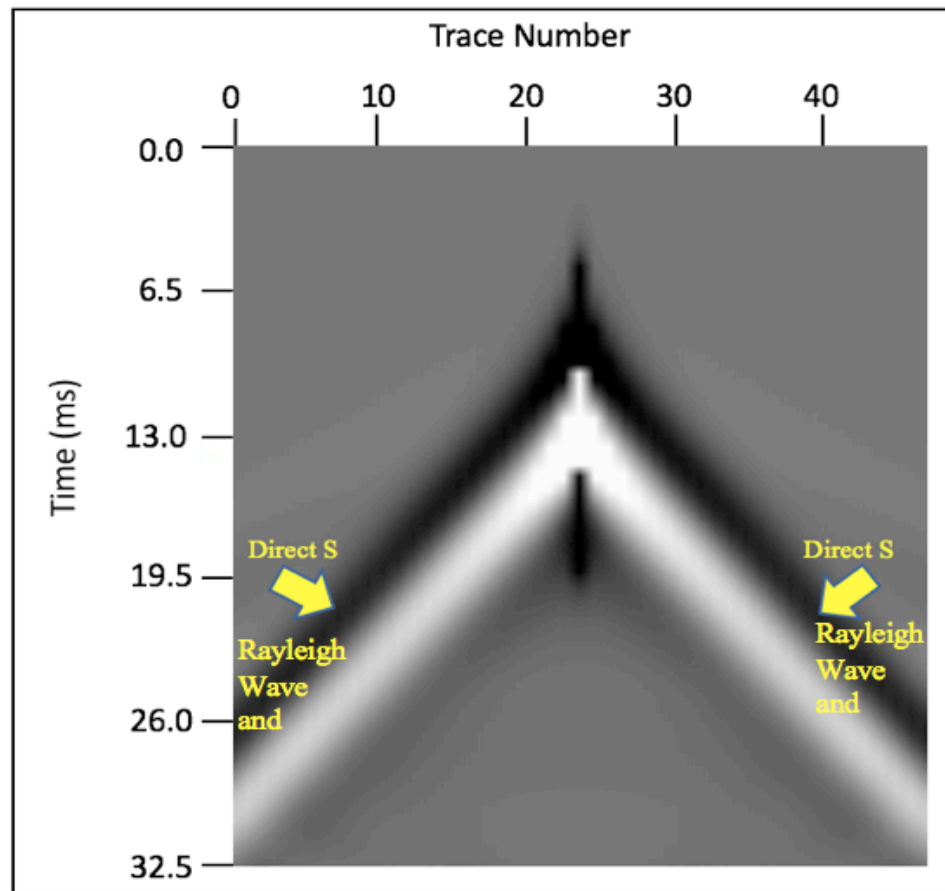


Figure 2.41: The seismogram (z-component) of 19 meters depth model with one layer for the free surface boundary condition (surface) with a single-force 100 Hz source located at 25 meters on the surface.

Then we generated a set of shot gathers (Figure 2.42) to see that if we can locate the tunnel in our model. We applied Kirchhoff migration (Figure 2.43) to our shot gather to see if we can identify the tunnel after migration.

According to the migration result in the Figure 2.43, the tunnel is not visible in the migration results. The only visible features are the free surface effects (yellow arrows) due to the direct arrivals, Rayleigh waves and Kirchhoff migration artifacts (red arrows) because of the insufficient amount of the seismic shots and the receivers.

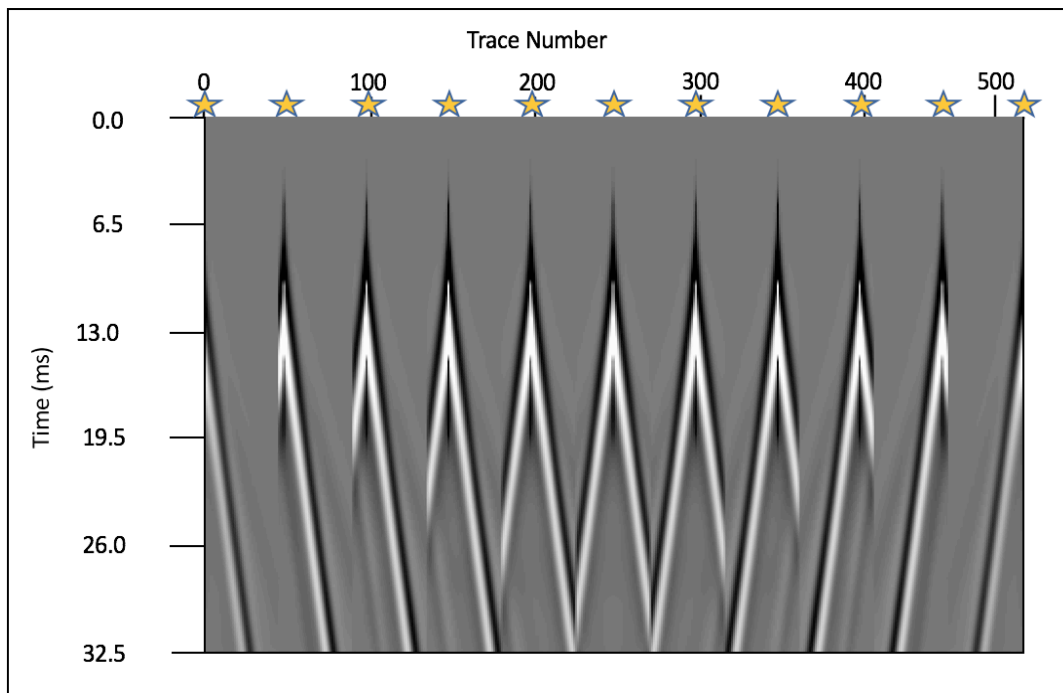


Figure 2.42: The set of shot gathers (z-component) for 19 meters depth one layer model with the free surface condition with the single-force 100 Hz sources (shown with stars).

Following the 100 Hz examples, we extended our research for the models with 400 Hz sources. We generated a model that has one layer with the absorbing boundary condition at the surface with the 400 Hz source (Figure 2.44). In the seismogram below, yellow arrows indicate the direct S wave arrivals, the orange arrow displays the reflected P wave reflection from the tunnel, and the purple arrow shows the converted P wave reflection from the tunnel.

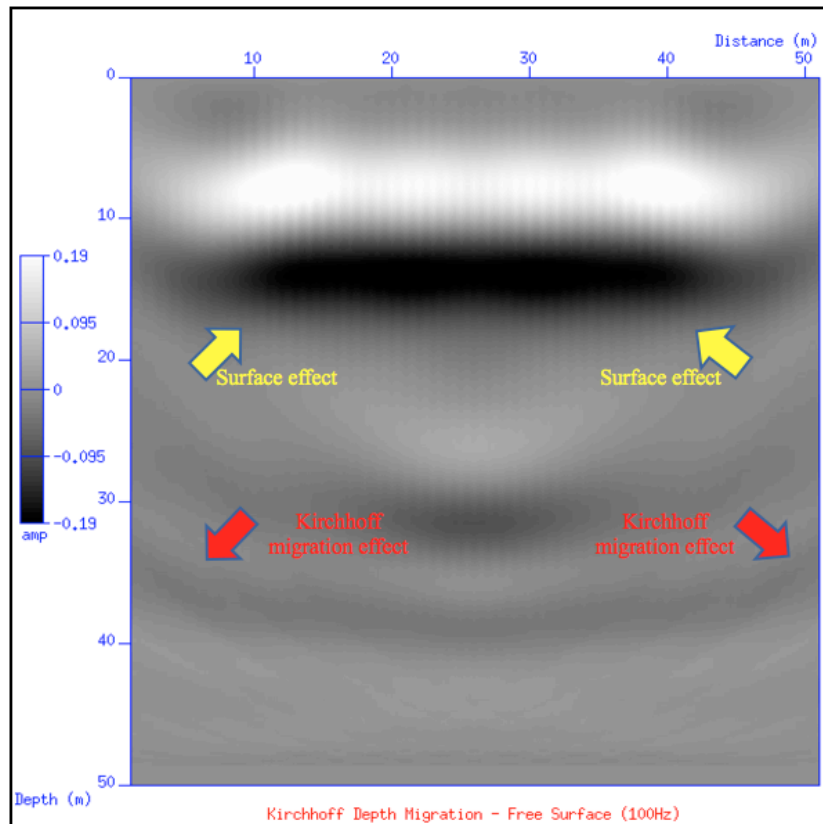


Figure 2.43: The seismic shot gather (z-component) for 19 meters depth one layer model with free surface condition for 100 Hz source. The shot locations were showed with stars (Amp shows the amplitude, which is a measure of the contrast in density, seismic velocities of the formations and / or underground structures).

After examining the seismogram (Figure 2.44), we created a set of shot gathers (Figure 2.45) for this example, and we applied Kirchhoff migration to image the tunnel (Figure 2.46).

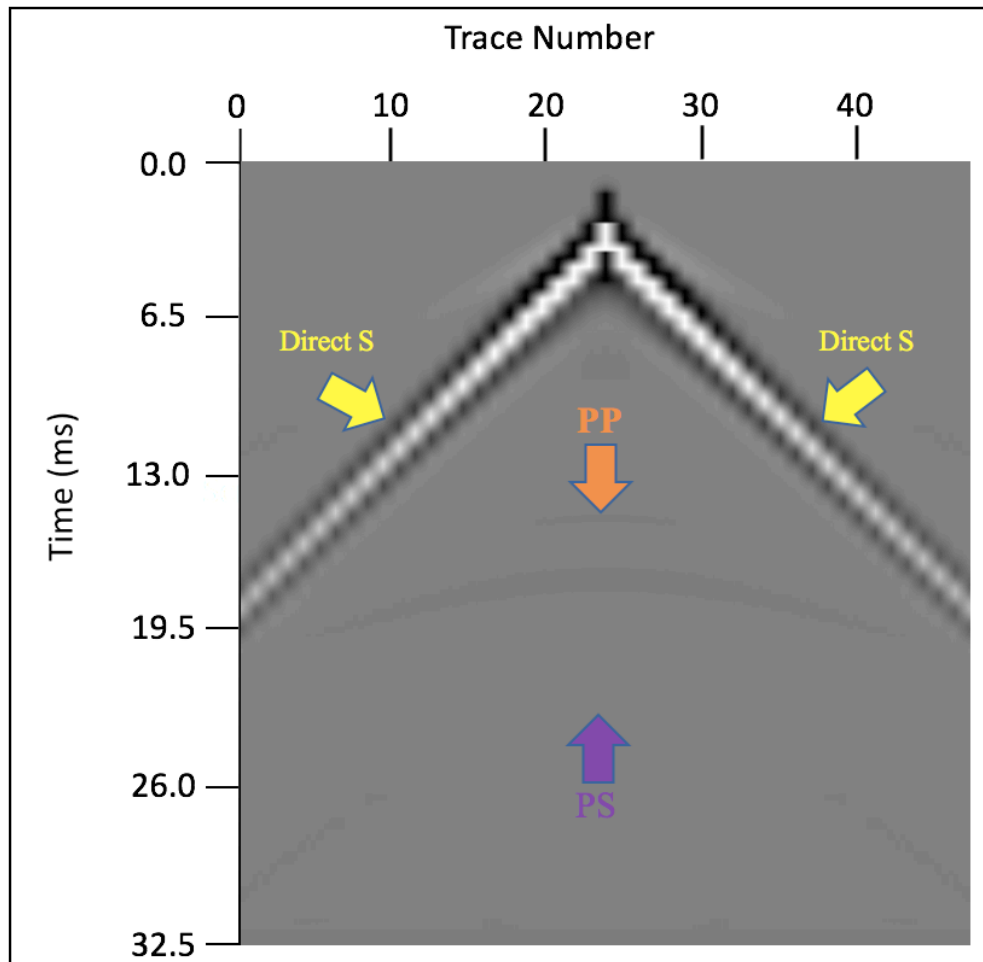


Figure 2.44: The seismogram for the model that has a tunnel at 19 Meters depth with one layer for the absorbing boundary condition (all boundaries) with a single-force 400 Hz source located at 25 m on x-axis and three meters depth.

According to the migration in Figure 2.43, the depth of the tunnel (19 meters) and its thickness (two meters) match exactly with our initial model. Additionally, there are

surface artifacts (yellow arrows) due to direct arrivals and Kirchhoff migration artifacts because of the number of the receivers and the seismic sources.

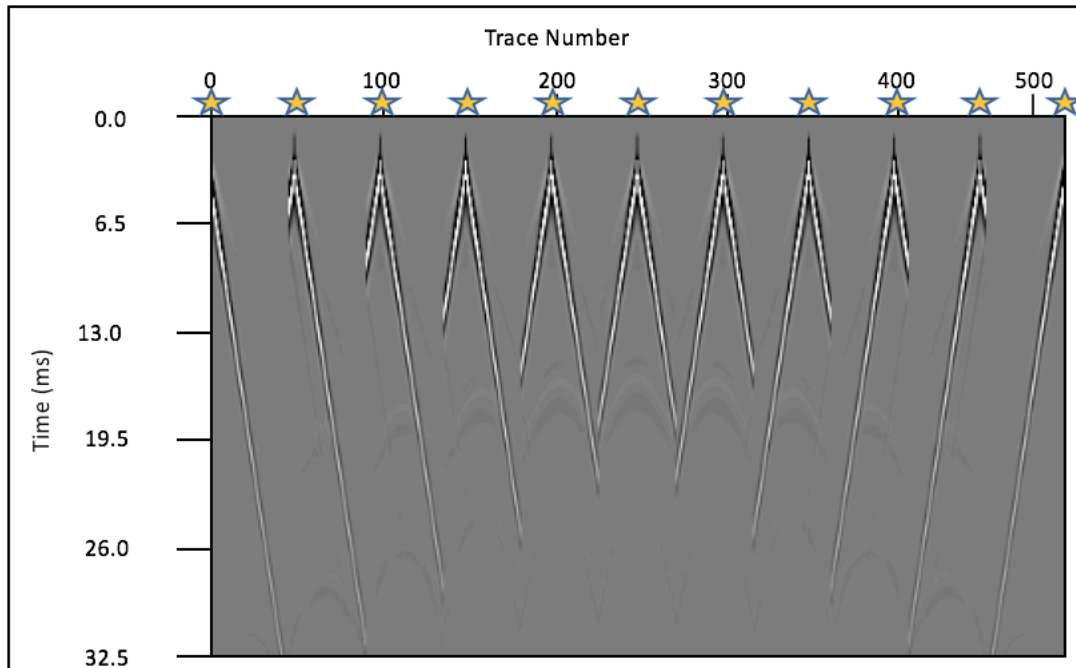


Figure 2.45: The set of shot gathers for the model that has a tunnel at 19 meters depth with the single-force 400 Hz sources (shown with stars).

After completing the migration for the absorbing boundary condition case, we continued our research by generating an example for the free surface boundary condition using the parameters from Table 2.4. and the model from Figure 2.36. When we run our script in Specfem2d, we receive the recorded seismogram in Figure 2.47 for the example with the free surface boundary condition. According to Figure 2.47, the red arrows represent direct P wave arrivals and the yellow arrows show direct S wave arrivals, the blue arrow indicates the reflected P wave from the tunnel, the orange arrow shows the converted P wave from the tunnel, and the red circle shows the artifacts caused by the upper corner of the model.

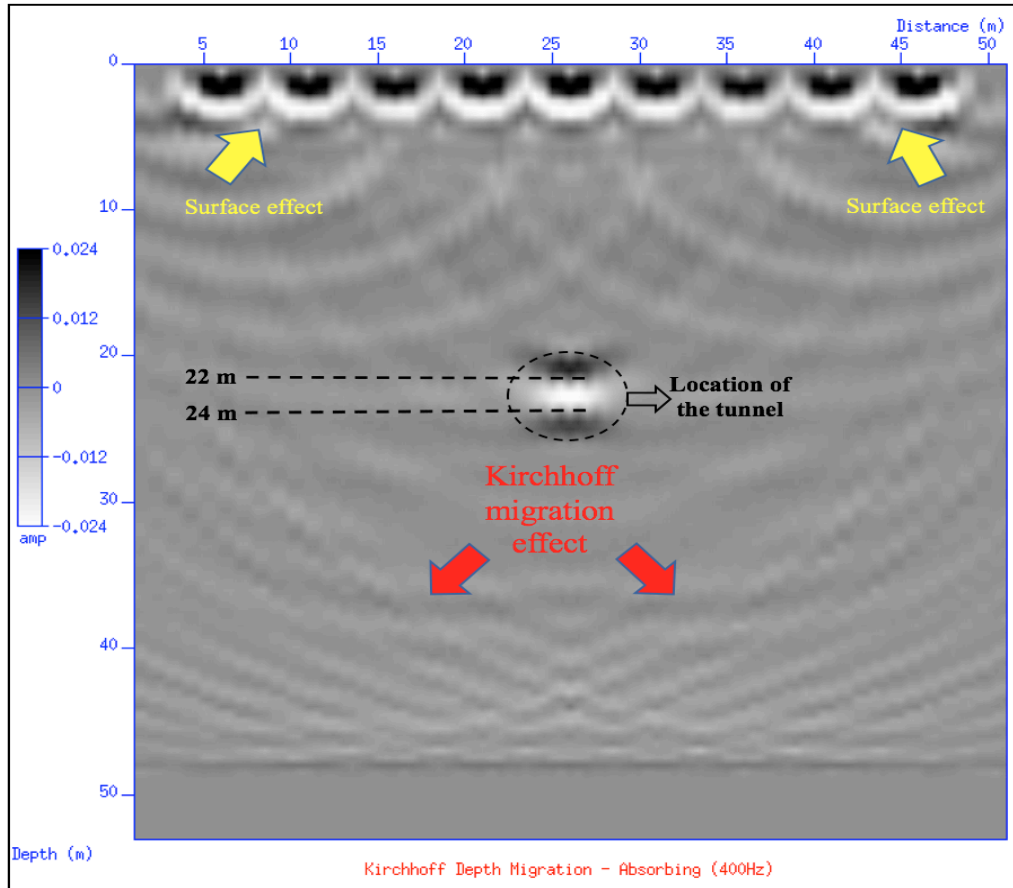


Figure 2.46: The Kirchhoff migration result for the model that has a tunnel at 19 meters depth (with extended top boundary-22 meters depth tunnel) with the single-force 400 Hz sources at the three meters depth from the surface (Amp shows the amplitude, which is a measure of the contrast in density, seismic velocities of the formations and / or underground structures).

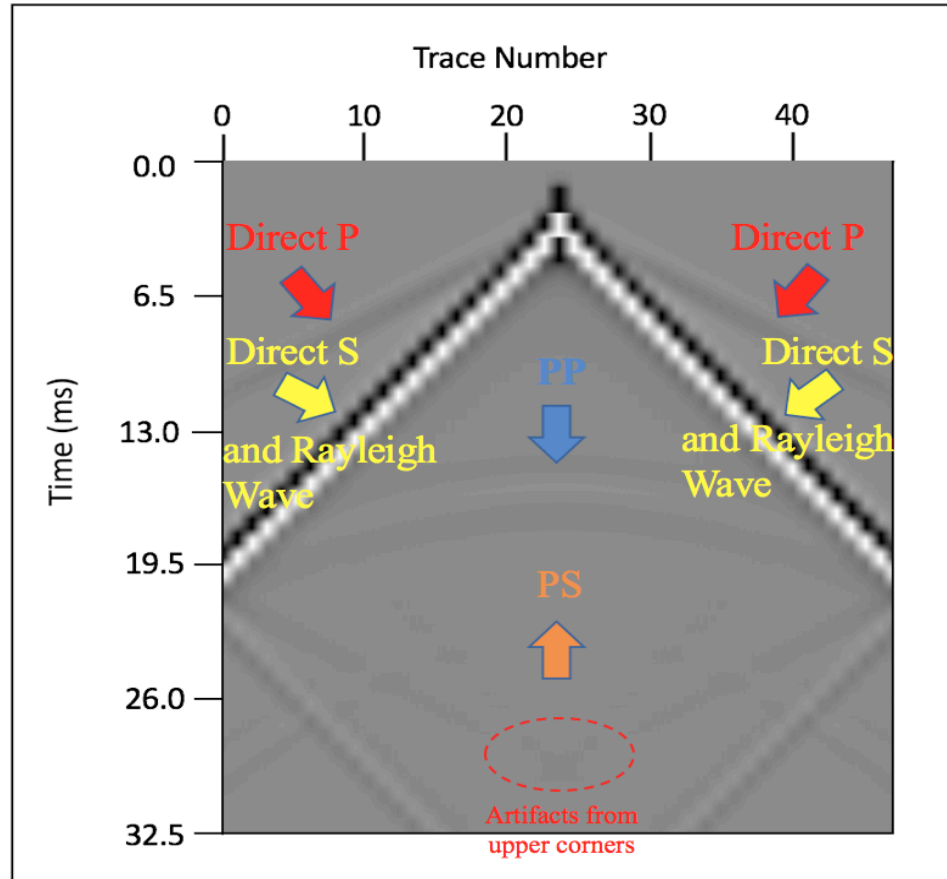


Figure 2.47: The seismogram for the model that has a tunnel at 19 meters depth with one layer and the free surface condition (surface) with the single-force 400 Hz sources located at the surface.

After identifying the reflections in the seismogram, we extended our research by generating a set of shot gathers (Figure 2.48) so we can apply our Kirchhoff migration script to the set of shot gathers to locate the tunnel in the migration result (Figure 2.49).

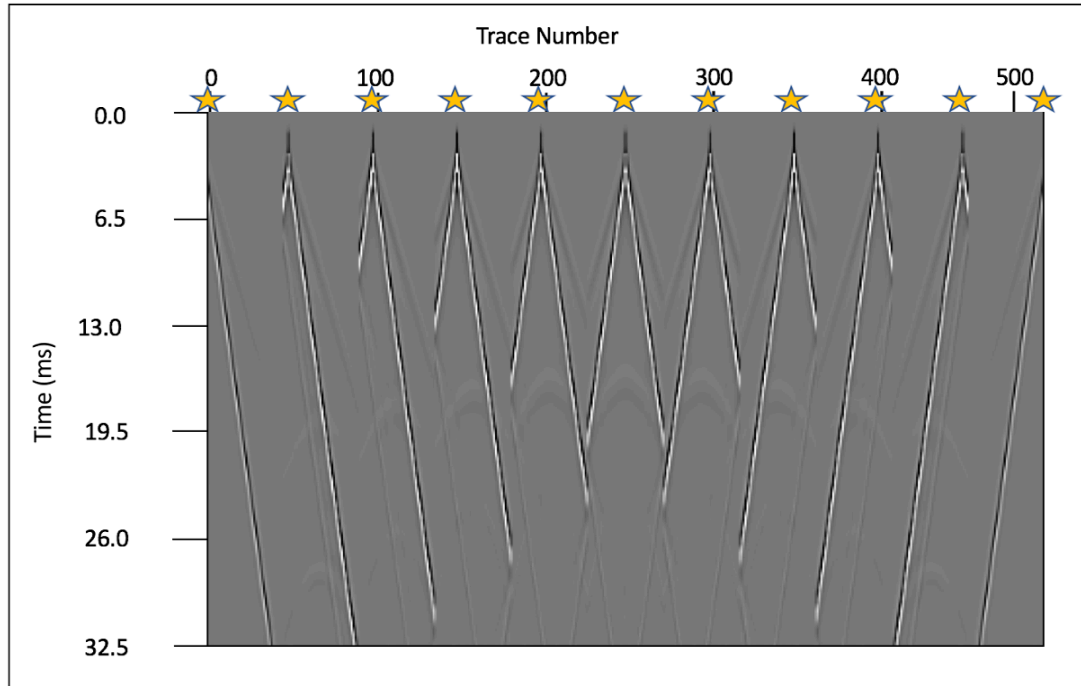


Figure 2.48: The set of shot gathers for the model that has a tunnel at 19 meters depth with single-force sources of 400 Hz (shown with stars).

According to the migration results shown in Figure 2.49, we can identify the tunnel with its correct location (19 meters depth) and thickness (two meters). We can also see the surface effect (yellow arrows) due to direct arrivals and the Rayleigh waves in the result, as well as the Kirchhoff migration artifacts (red arrows) because of the limited number of shots and the receivers in the data. Also, due to the free surface feature, we see a result with more artifacts (reflections) in comparison to the example with the absorbing boundary condition in the result file.

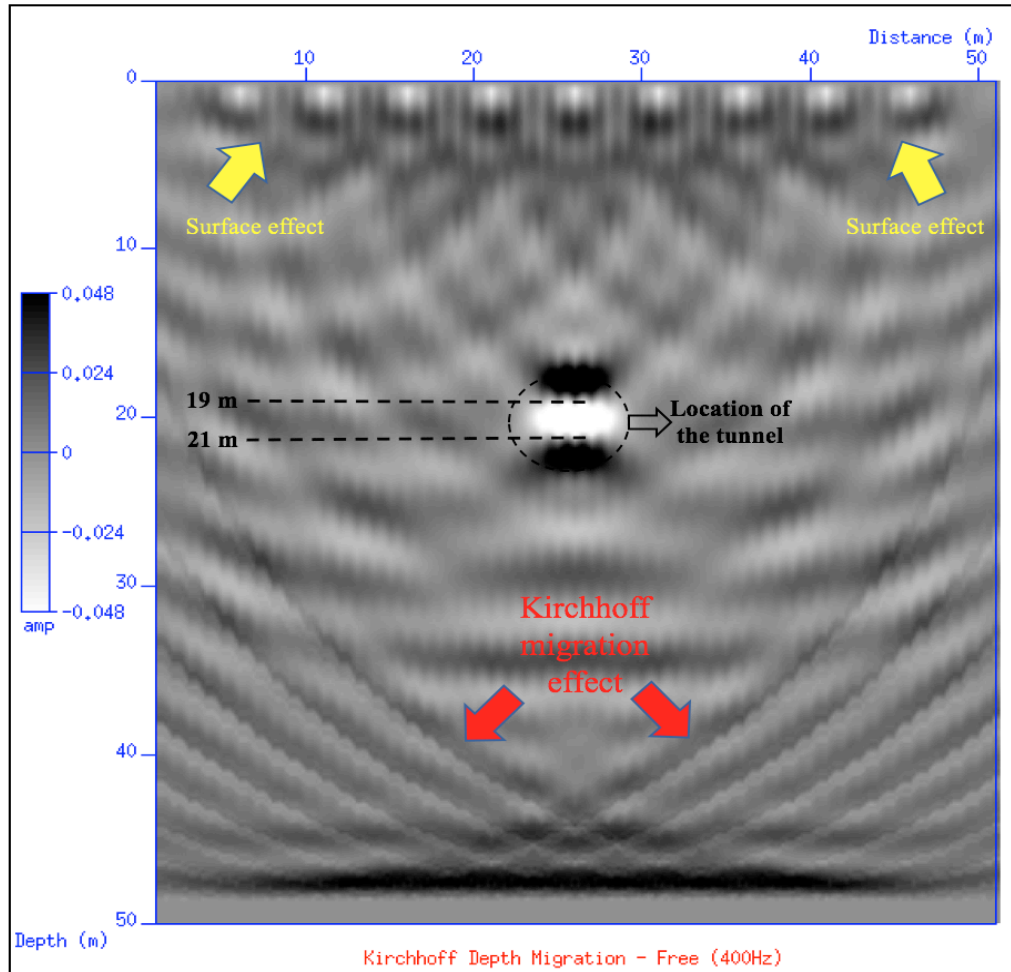


Figure 2.49: The Kirchhoff migration result for the model that has a tunnel at 19 meters depth with the 400 Hz source at the surface with the absorbing boundary condition (Amp represents the amplitude, which is a measure of the contrast in density, seismic velocities of the formations and / or underground structures).

2.3.2 Two-Layered Case

In this section, we generated models that have a tunnel at a depth of 19 meters in a two-layered model with sources at two different frequencies for each model: 100 Hz and 400 Hz. We chose a 100 Hz frequency value for our source because it is a very common frequency value for the seismic experiments. As a second value for the source's

frequency, we chose 400 Hz as the seismic source's frequency that will provide us smaller wavelength and higher vertical resolution according to the wavelength (1.1) and vertical seismic resolution (1.2) formulas. We include only models with sources at 100 Hz and 400 Hz frequencies in this section to compare the results with each other to find out which frequency value will work better for locating the clandestine tunnel in our model. The acquisition geometry for a tunnel with a depth of 14 meters in a two-layered model for the subsurface seismic method is shown in Table 2.5.

A basic model was generated that has two layers: the first layer is a shallow formation that has 4 meters thickness and a density of 2.4 g/cm^3 , $V_p=2500 \text{ m/sec}$, $V_s=800 \text{ m/sec}$, the second layer, which is the deeper formation, has 46 meters thickness which has a density of 2.6 g/cm^3 , $V_p=3000 \text{ m/sec}$, and $V_s=1500 \text{ m/sec}$. An illustration of the acquisition geometry is shown in Figure 2.47 where the shot point is located at 25 meters along the surface with a 400 Hz source. These generated models were run with both absorbing boundary and free surface boundary conditions to figure out which specific boundary condition gives a better result with the same model and parameters to locate the tunnels.

However, the absorbing boundary condition requires that the absorbing layers has to be thick enough in order to observe the seismic waves (Bélanger-Rioux et. al, 2015). According to the acquisition geometry in Figure 2.50, the receivers and the shots are located on the absorbing boundary, in this case, the absorbing boundary condition is not going to work efficiently for our acquisition design. In order to make the absorbing boundary condition work, we extended the top boundary of our models for three meters

upwards so the receivers and the sources are going to be located far enough from the absorbing boundary layer that will provide us an efficient absorbing boundary condition for our modeling (Figure 2.51). We used the acquisition parameters and the model whose dimension is 50 m x 54 m from Figure 2.48 for the all examples with the absorbing boundary conditions. For the free surface examples, we used the acquisition design and the model that has the dimension of 50 m x 50 m from Figure 2.50.

Table 2.5: The acquisition geometry parameters for the tunnel at 19 meters depth with two-layers model for the subsurface seismic method.

Model Dimension	50 m x 50 m
Seismic Shot Range	11 shots, starting from 0 m to 50 m with 5 m spacing
Number of Receivers and Their Sequence	47 receivers starting from 2 m to 48 m
Frequency of Source and Its Type	100 Hz and 400 Hz, Ricker wavelet, Single Force (Coupled)
Tunnel Depth	19 m
Recording Length (millisecond)	32.5 ms
Boundary Condition	Free (Top Layer) and Absorbing (Top Layer) for Each Example
Velocity Model	First Layer: $V_p=2500$ m/sec, $V_s=800$ m/sec, Density = 2.4 g/cm ³ Second Layer: $V_p= 3000$ m/sec, $V_s=1500$ m/sec, Density = 2.6 g/cm ³

The seismic modeling was generated in accordance with the parameters in Table 2.5 and Figure 2.48. After recording the seismogram which has the absorbing boundary condition for all boundaries with a 100 Hz source at three meters depth in Figure 2.52, we can only see direct S wave arrivals due to the low frequency (100 Hz) of the source.

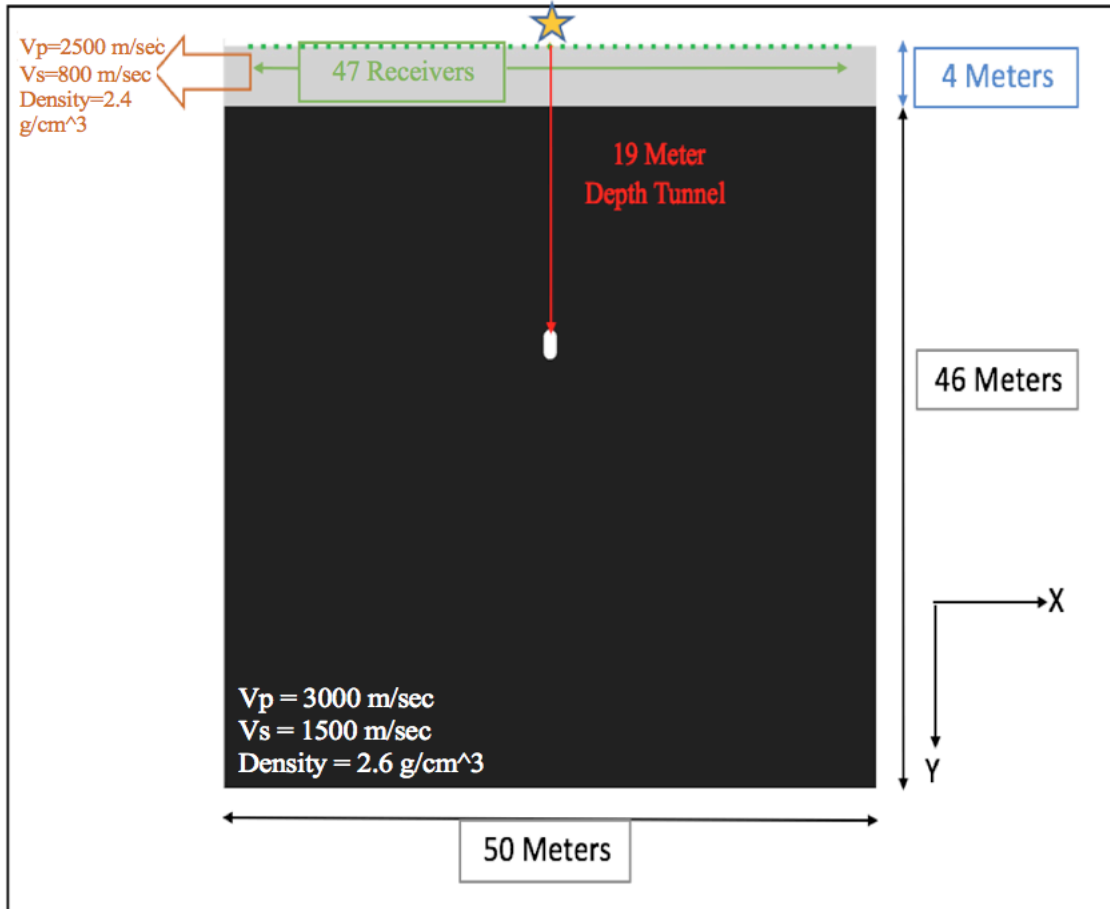


Figure 2.50: Nineteen meters depth tunnel model with two layers for the absorbing boundary case. The source is a single-force with 400 Hz located at 25 meters on x-axis and shown with the star.

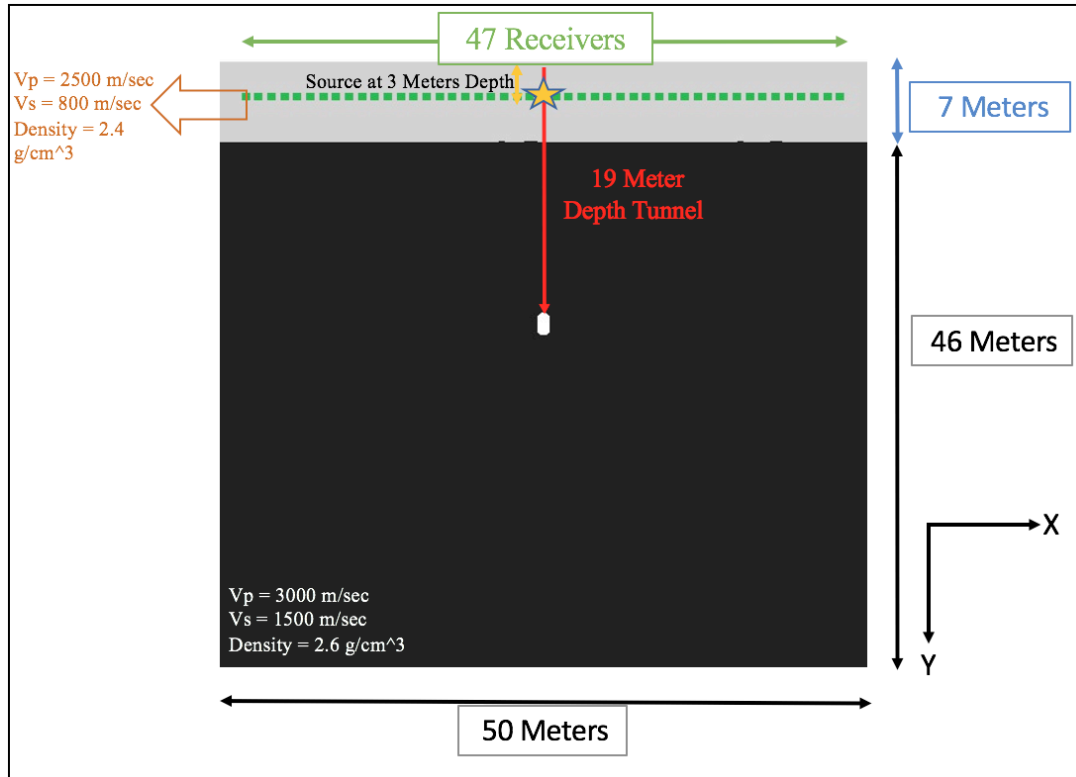


Figure 2.51: Nineteen-meter-deep tunnel (22 meters with the extended top) model with two layers that has the absorbing boundary conditions for all boundaries with a single-force 400 Hz source at three meters depth (shown with a star).

After examining the waves in the seismogram, we created a set of shot gathers (Figure 2.53) for a 19 meters depth tunnel (22 meters with the extended top) model with two layers to apply seismic migration and put the reflectors in their right position to image the clandestine tunnel in our model. We used the two-layered velocity model from Figure 2.24 for the migration. Afterwards, we applied Kirchhoff migration to the set of shot gathers (Figure 2.54). According to the migration result, the clandestine tunnel is not visible in the result. The possible reason for this outcome is that the frequency of our sources is too low to image the tunnel. In addition to that we can identify the surface

effect (yellow arrows) due to the direct arrivals and Kirchhoff migration effects (red arrows) because of the limited number of the shots and the receivers.

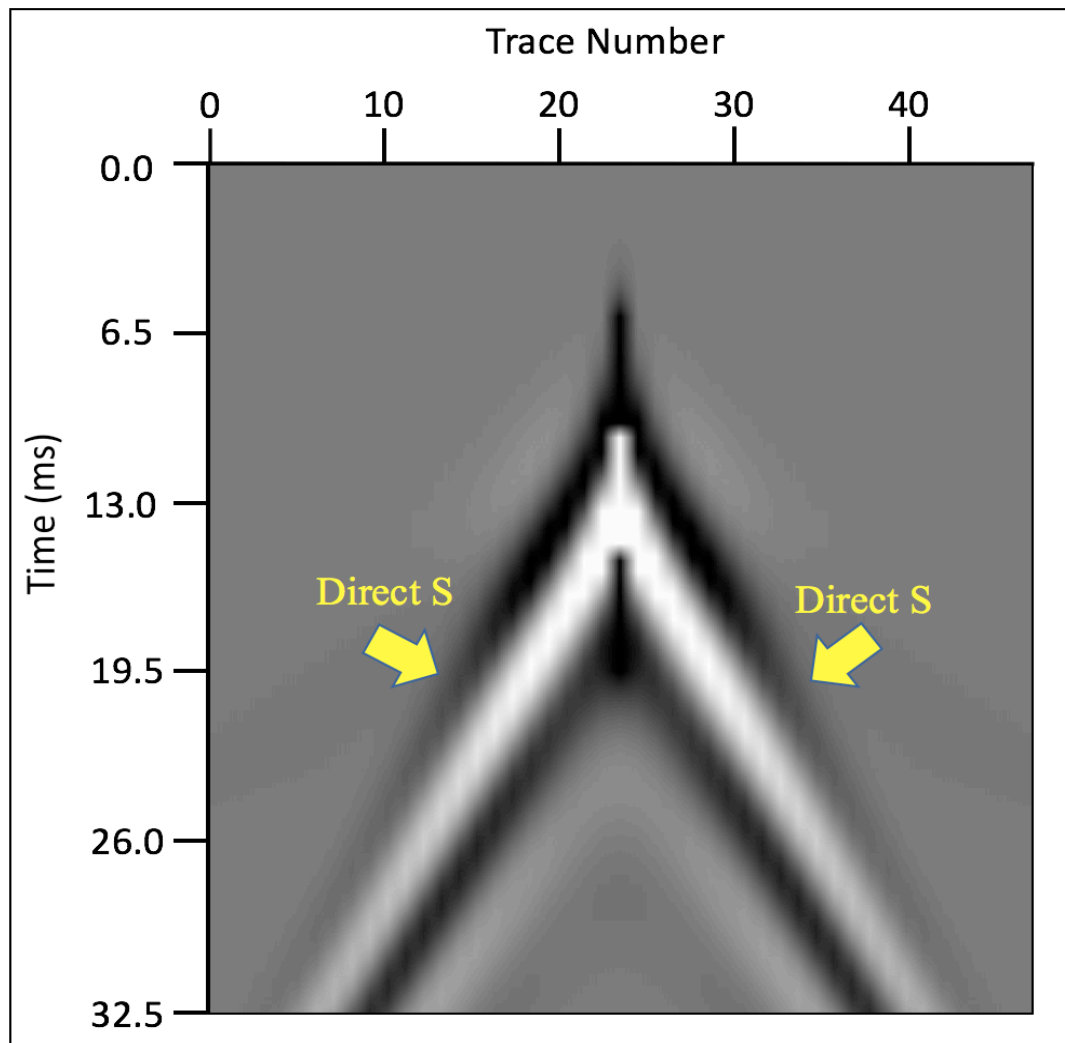


Figure 2.52: The seismogram (z-component) of the 19 meters depth tunnel model (22 meters with extended top) with two layers for the absorbing boundary condition with a single-force 100 Hz source at the three meters depth.

After reviewing the result for the absorbing boundary condition, we used the model from Figure 2.48 with the parameters from Table 2.5 to generate another model for the free surface case. We ran the Specfem2D with the required parameters and saved the

seismogram for this modeling (Figure 2.55). When we examine the recorded seismogram for the free surface boundary condition (surface) case, only the direct P wave and the direct S wave and the Rayleigh waves can be identified. However, since direct S wave's velocity is 1500 m/sec and the Rayleigh wave's velocity is 1398 m/sec for our modeling, we cannot separate these two waves from their arrival times because they are overlapping with each other. Another noticeable effect of this example is that the direct S waves are more visible in comparison to the result with the absorbing boundary condition (Figure 2.49).

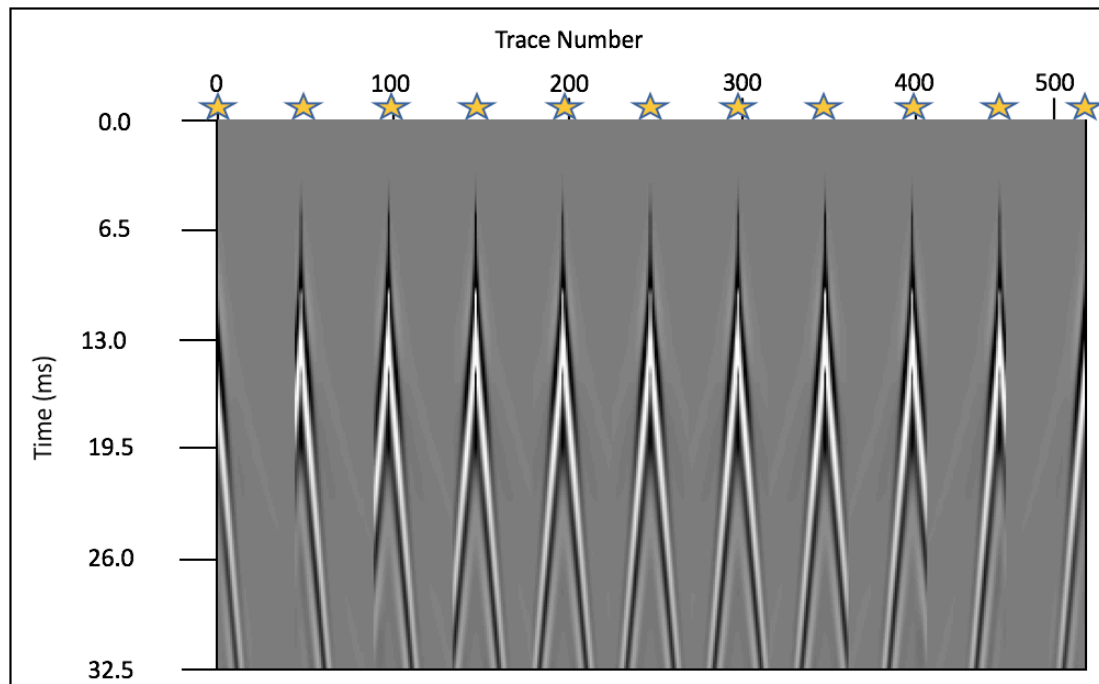


Figure 2.53: The set of shot gathers (z-component) for the 19 meters depth two-layered model with an absorbing boundary condition for single-force 100 Hz sources, shot locations are shown with stars.

Having identified the waves in Figure 2.55, we created a set of shot gathers for this example in order to apply Kirchhoff migration to it to image the tunnel in our model

clearly. Therefore, after generating the set of shot gathers (Figure 2.56), we used the two-layered velocity model (Figure 2.24) and applied our migration script to the seismic shot gather (Figure 2.57). According to the migration result, we cannot identify the tunnel due to low frequency of the sources (100 Hz). We can only see the free surface effect (yellow arrows), which occurs due to direct arrivals and we can identify the Kirchhoff migration's effect, which is due to the number of receivers and seismic shot intervals. As a summary, the tunnel cannot be located in this result.

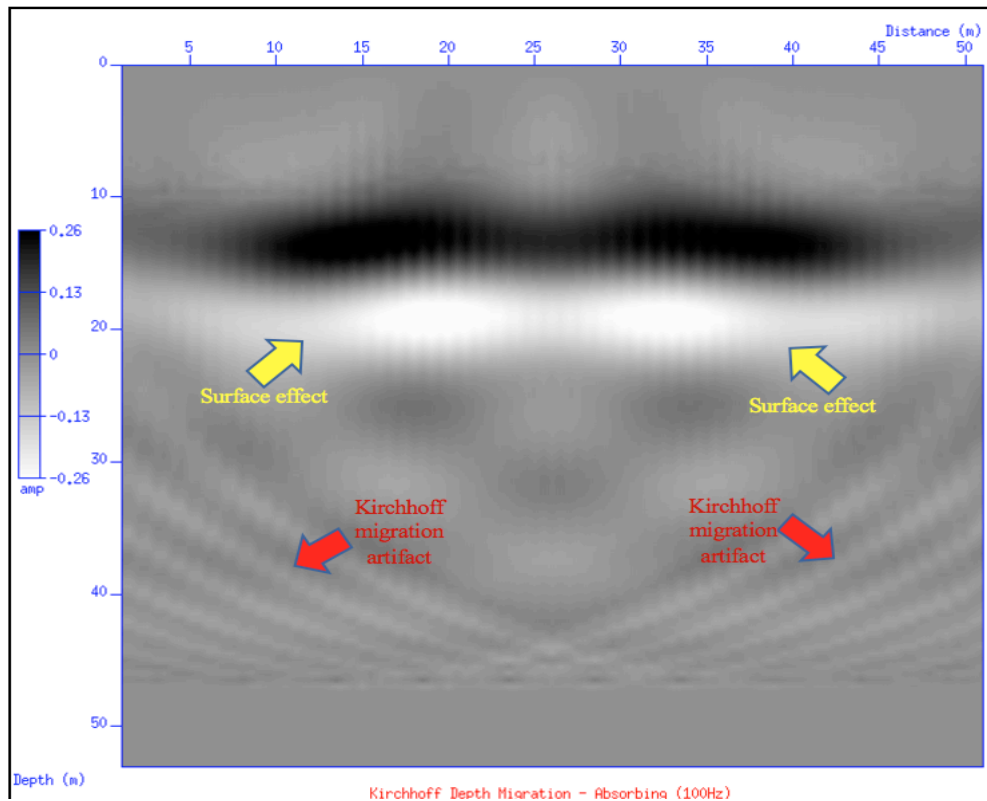


Figure 2.54: Kirchhoff migration result of the 19 meters depth tunnel model with two layers for the absorbing boundary condition (all boundaries) with single-force 100 Hz sources on the surface (Amp represents the amplitude, which is a measure of the contrast in density, seismic velocities of the formations and / or underground structures).

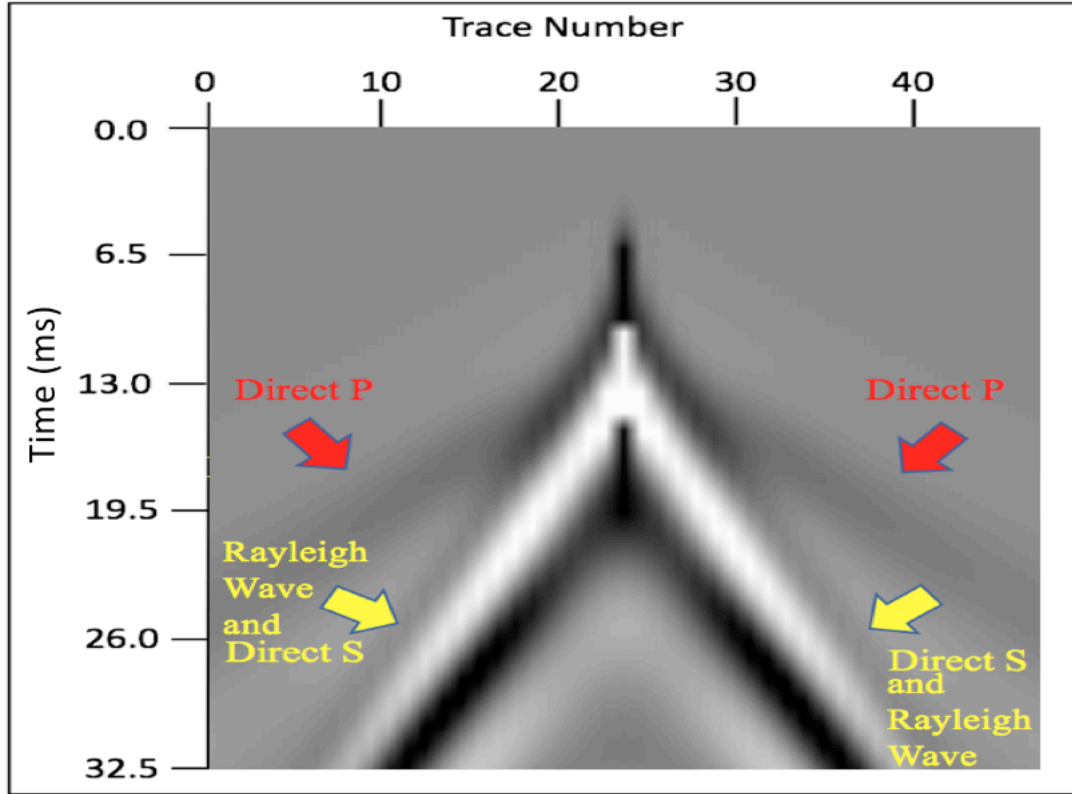


Figure 2.55: The seismogram (z-component) of the 19 meters depth model with free surface boundary condition with two layers for a 100 Hz seismic source 25 meters on x-axis at the surface.

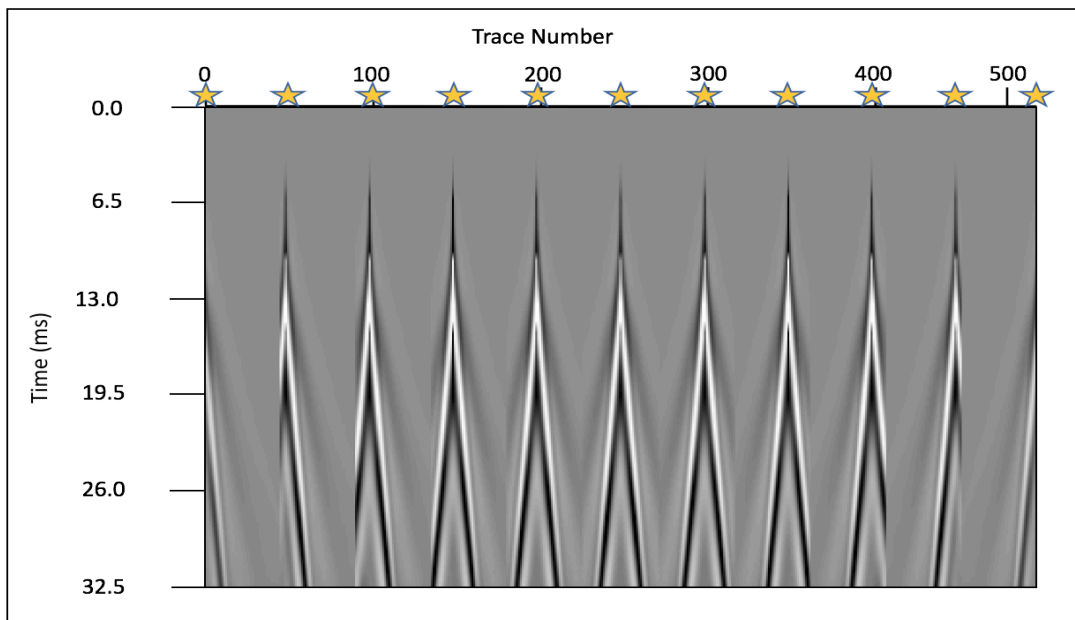


Figure 2.56: The set of shot gathers for the free boundary condition for the 19 meters depth tunnel with two layers with seismic sources (shown with stars) of 100 Hz located on the surface.

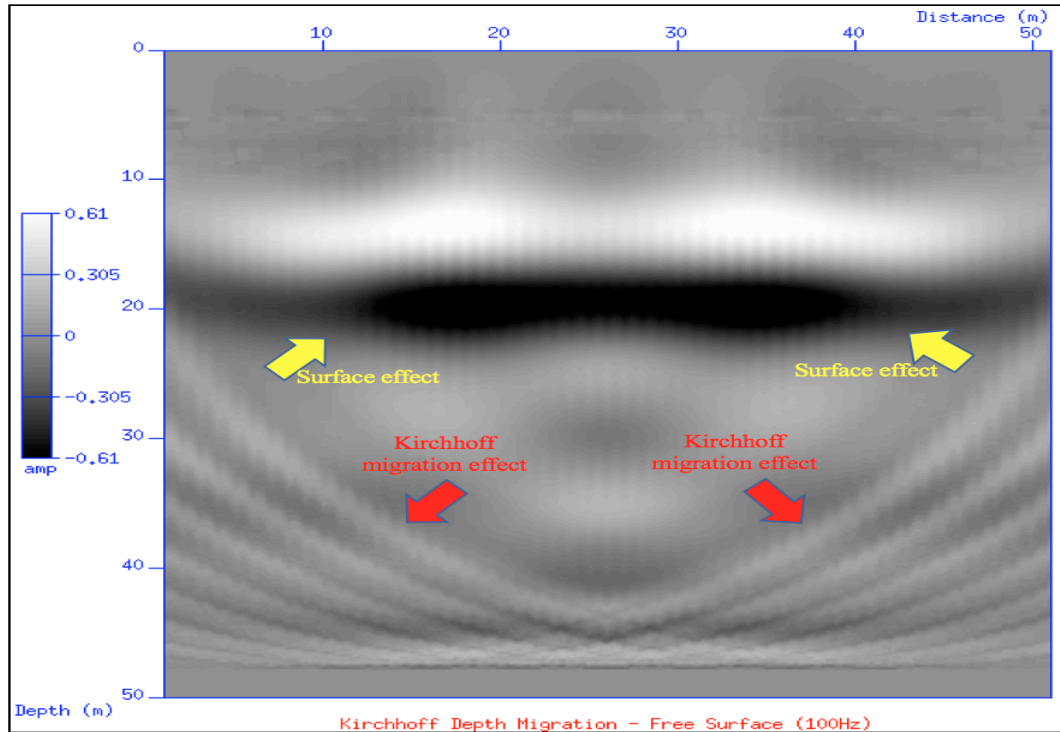


Figure 2.57: Kirchhoff migration result of the 19 meters depth tunnel model with two layers for the free surface boundary condition at the surface with 100 Hz sources. (Amp shows the amplitude, which is a measure of the contrast in density, seismic velocities of the formations and / or underground structures).

After finalizing the imaging of the 19 meters depth tunnel model with two layers with 100 Hz source, we extended our research using 400 Hz sources for our modeling. For this objective, we ran a model with the same parameters from the early section with 400 Hz of source with the absorbing boundary condition (for all boundaries). According to the recorded seismogram (Figure 2.58), we can identify the reflections from the tunnel with the 400 Hz source. Yellow arrows indicate the direct S wave arrivals, the orange arrow shows the reflected P wave from the shallow layer, the blue arrows display the

reflected P wave from the tunnel, the purple arrow shows the converted P wave from the tunnel, the green arrows indicate the reflected S wave from the shallow layer, the black arrows display the converted P wave from the shallow layer, and the white arrows show the reflected S wave from the tunnel.

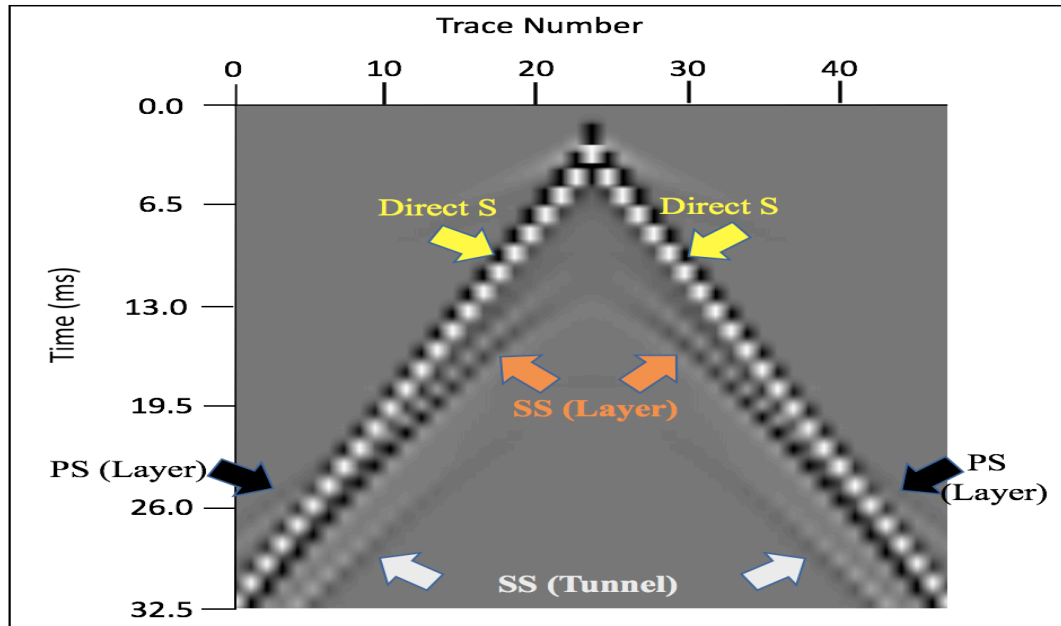


Figure 2.58: The seismogram (z-component) of the 19 meters depth tunnel model for the absorbing boundary condition with a parallel layer and a single-force 400 Hz source located at 25 meters on the surface.

After identifying the reflections in the seismogram (Figure 2.58), we created a set of shot gathers (Figure 2.59) to check that if we can image the tunnel from the generated set of shot gathers. However, we cannot identify any tunnel from the gathers in Figure 2.59. Then we applied the seismic migration to our generated set of shot gathers to image the tunnel with 400 Hz of sources. We used the two-layered velocity model from the earlier chapter (Figure 2.24). According to the results in Figure 2.60, we can identify the tunnel at the correct depth 22 meters (19 meters before the extension of the model) with

its precise thickness (two meters). In addition to these findings, we can also see the surface effects (yellow arrows) due to the direct arrivals and the Kirchhoff migration artifacts (red arrows) because of the limited number of the sources and the receivers. As it can be seen in the migration result, it is possible to locate the tunnel with the absorbing boundary condition (surface) with 400 Hz sources.

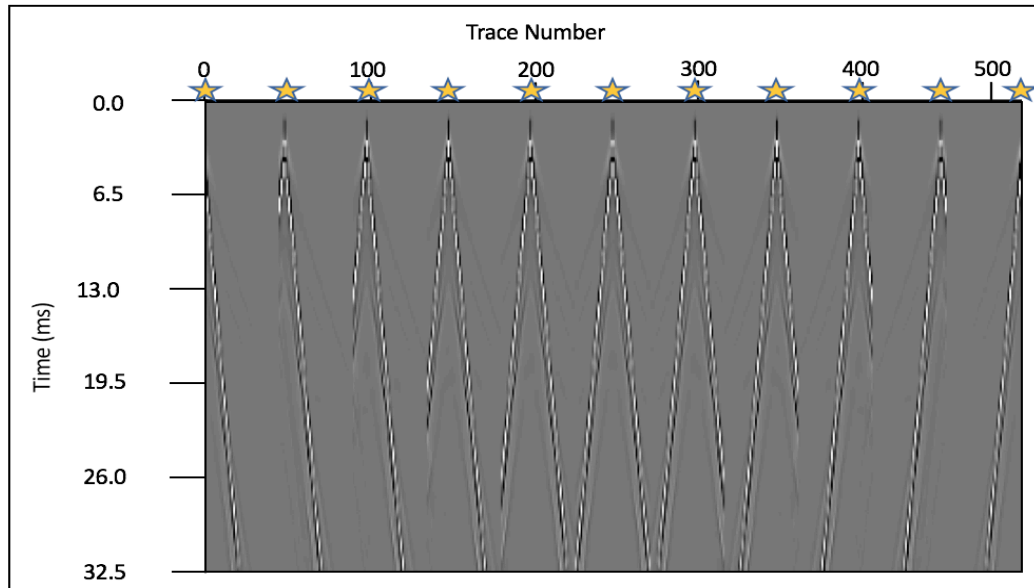


Figure 2.59: The set of shot gathers of the absorbing boundary condition for the 19 meters depth tunnel with a parallel layer seismic source at 400 Hz.

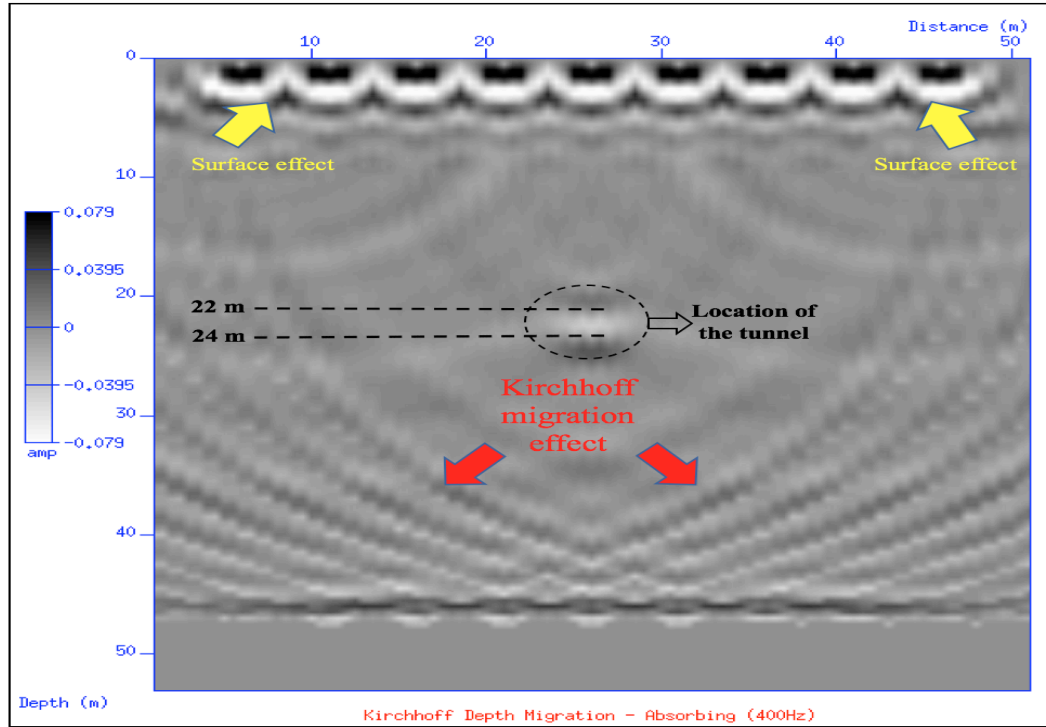


Figure 2.60: Kirchhoff migration result of the 19 meters depth tunnel (22 meters depth due to the extension) model with two layers model with the absorbing boundary condition at the surface (Amp shows the amplitude, which is a measure of the contrast in density, seismic velocities of the formations and / or underground structures).

Afterwards, we made another model for the free surface case by using the same parameters from the Figure 2.47. According to the seismogram that was generated (Figure 2.61), the red arrows show direct P wave arrivals, yellow arrows indicate direct S wave arrivals and the Rayleigh waves, the orange arrow shows the reflected S wave from the shallow layer, the black arrows display the converted P wave from the shallow layer, and the white arrows show the reflected S wave from the tunnel. We cannot distinguish the Rayleigh wave whose velocity is 758 m/sec to the direct S arrival whose velocity is 800 m/sec for the shallow layer. Since there is only small velocity difference between these two waves, they are overlapping in the seismogram.

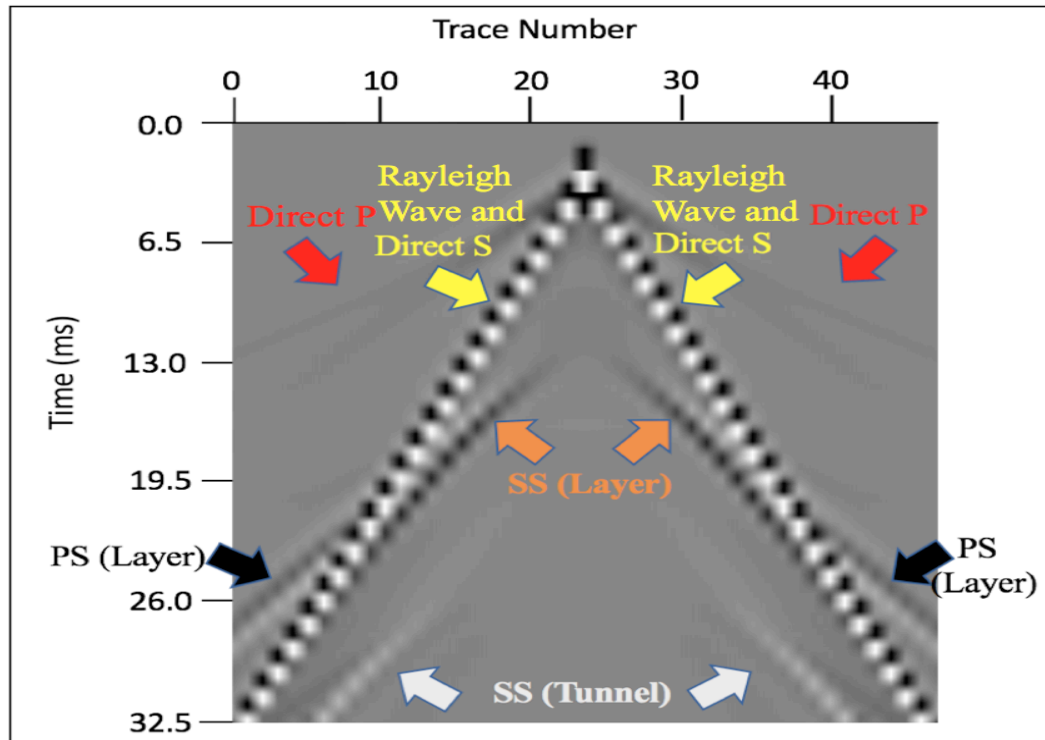


Figure 2.61: The seismogram (z-component) of the 19 meters depth tunnel model for the free surface condition with a parallel layer and a 400 Hz seismic source at 25 meters on the surface.

Upon analyzing the reflection in Figure 2.61, we generated a set of shot gathers (Figure 2.62) to see that if we can image the tunnel if we combine all shots into a gather. However, we cannot identify the tunnel from Figure 2.62. Then by using the two-layered velocity model (Figure 2.24), we applied Kirchhoff migration to our set of shot gathers (Figure 2.63).

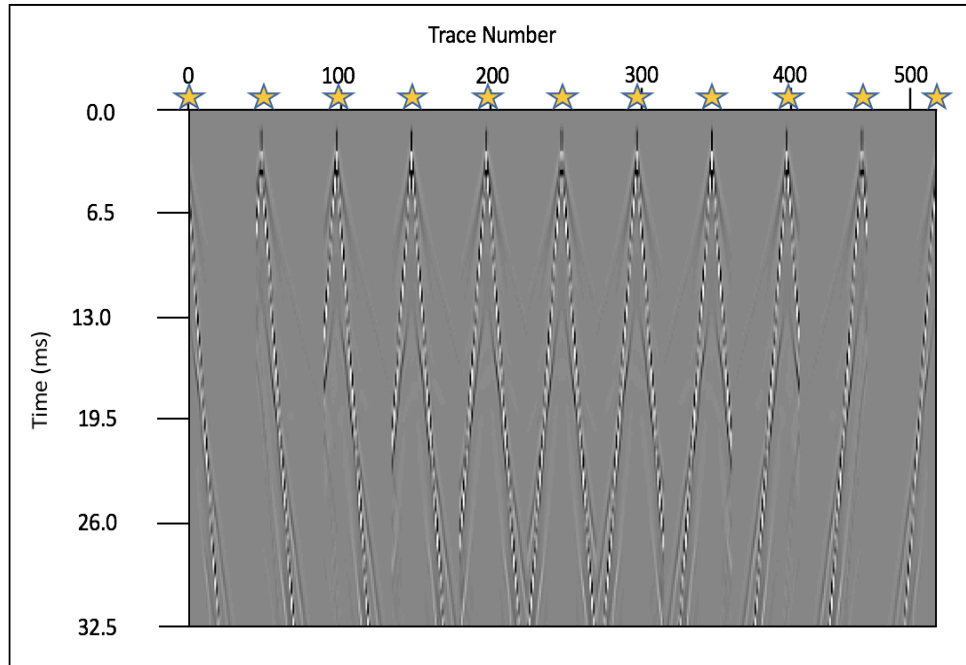


Figure 2.62: The seismic shot gather for the free surface boundary condition for the 19 meters depth tunnel with a parallel layer and a seismic source of 400 Hz.

According to the result in Figure 2.63, we can locate the tunnel in its correct location (19 m to 21 m). In addition to the detecting the tunnel, we can identify the surface effects caused by the direct arrivals and the Kirchhoff migration effect due to limited number of shots and receivers.

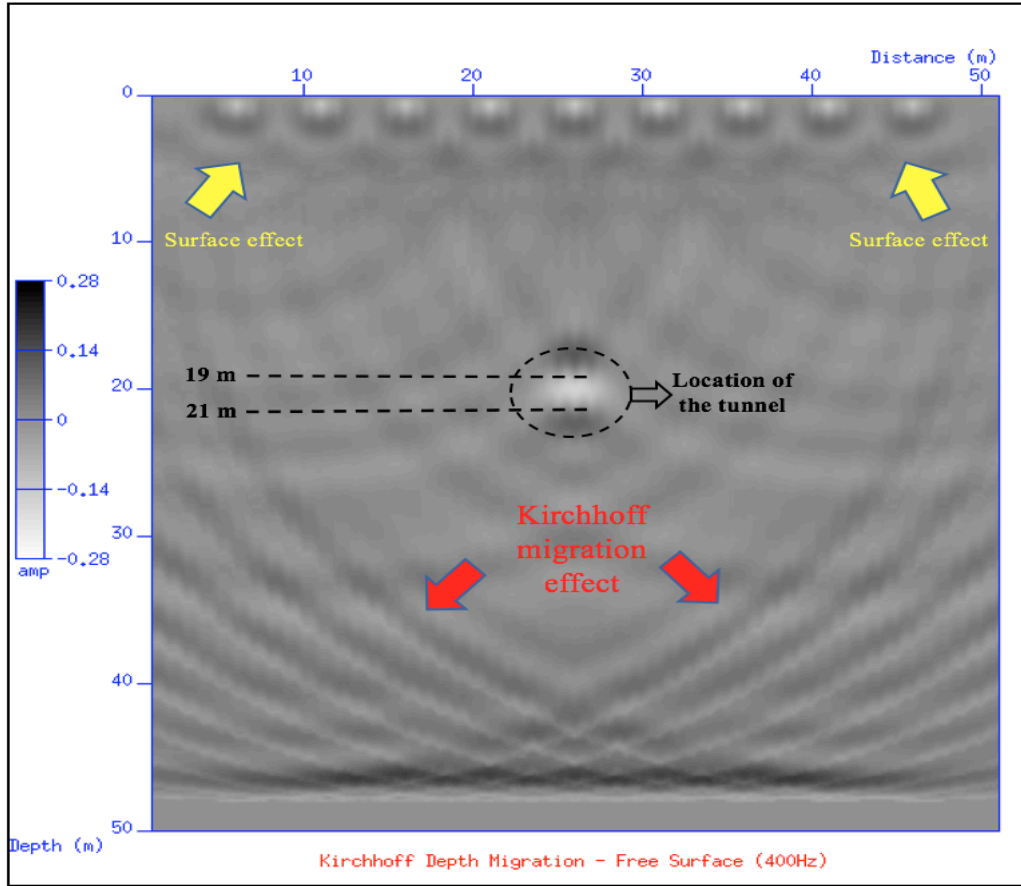


Figure 2.63: The seismic shot gather for the free surface boundary condition for the 19 meters depth tunnel with a parallel layer seismic source at 400 Hz (Amp represents the amplitude, which is a measure of the contrast in density, seismic velocities of the formations and / or underground structures).

Chapter 3: Tunnel Modeling with Cross-Well Seismic Method

3.1 Introduction

Since the subsurface seismic acquisition geometry did not provide reliable results except for the examples with the 400 Hz source, we expanded our research to include the cross-well seismic acquisition geometry. This acquisition design uses higher frequencies (3 kHz – 5 kHz) than the subsurface seismic method, which gives us a chance to increase the seismic resolution. A higher frequency source will decrease the wavelength of the seismic waves, which in turn will increase the vertical seismic resolution. This will give us an advantage to locate and identify the tunnels with higher accuracy. In addition, the cross-well seismic is not affected by ground rolls and surface noises as much as the subsurface seismic since the receivers are located inside of the medium.

3.2 Example of Sources and Receivers Are Located in The Formation

In this part of the research, we created some of our numerical models for cross-well seismic without any wells. The cross-well seismic offers great promise for the detection of tunnels. However, the original method itself generates multiples since a high frequency source is located inside of the water in a well, and the formation properties (velocity, density) around the well contrast considerably with the water's density and velocity. To illustrate this problem, we modeled an acquisition geometry for the cross-well seismic method with wells (Figure 3.1). In this model, we have two wells, the one on the left is used for the source and the one on the right is used for the receivers. The parameters are given below for this acquisition geometry in Table 3.1.

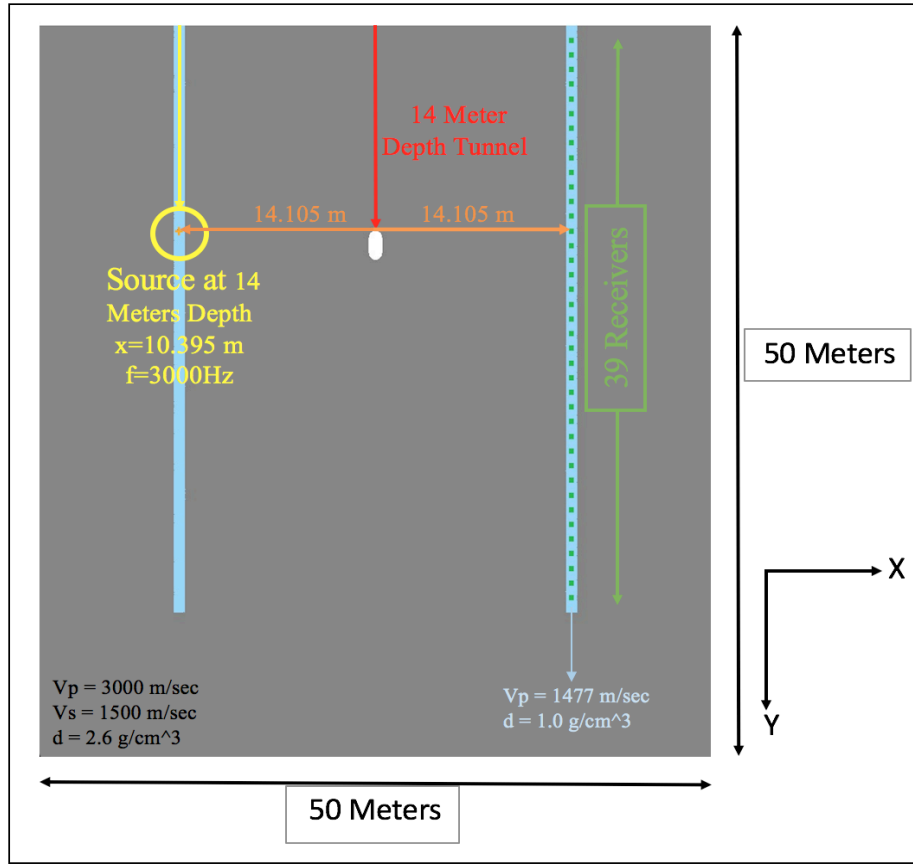


Figure 3.1: The geometry of the cross-well seismic with wells.

Table 3.1: The acquisition geometry for the cross-well seismic method.

Model Dimension	50 m x 50 m
Seismic Shot Range	1 shot, x=10.395 m and z=14 m
Number of Receivers and Their Sequence	39 receivers starting from 2 m to 38 m depth
Frequency of Source and Its Type	3000 Hz, Ricker wavelet, Single Force (Coupled)
Tunnel Depth	14 m
Recording Length (millisecond)	32.5 ms
Boundary Condition	Absorbing Boundary Condition (Surface)
Velocity Model	For the layer: $V_p = 3000$ m/sec, $V_s = 1500$ m/sec, Density = 2.6 g/cm ³ For water: $V_p = 1477$ m/sec, Density= 1.0 g/cm ³

After assigning the required parameters in the Specfem2D software, we begin the seismic modeling. Figure 3.2 illustrates the seismic modeling at 10 ms. We then record the seismogram of this seismic modeling. According to the seismogram (Figure 3.3), we can see the arrivals of the seismic waves that passed through the tunnel at 10 ms (red circled area). As it can be seen in Figure 3.2 and Figure 3.3, the existence of water generates multiples.

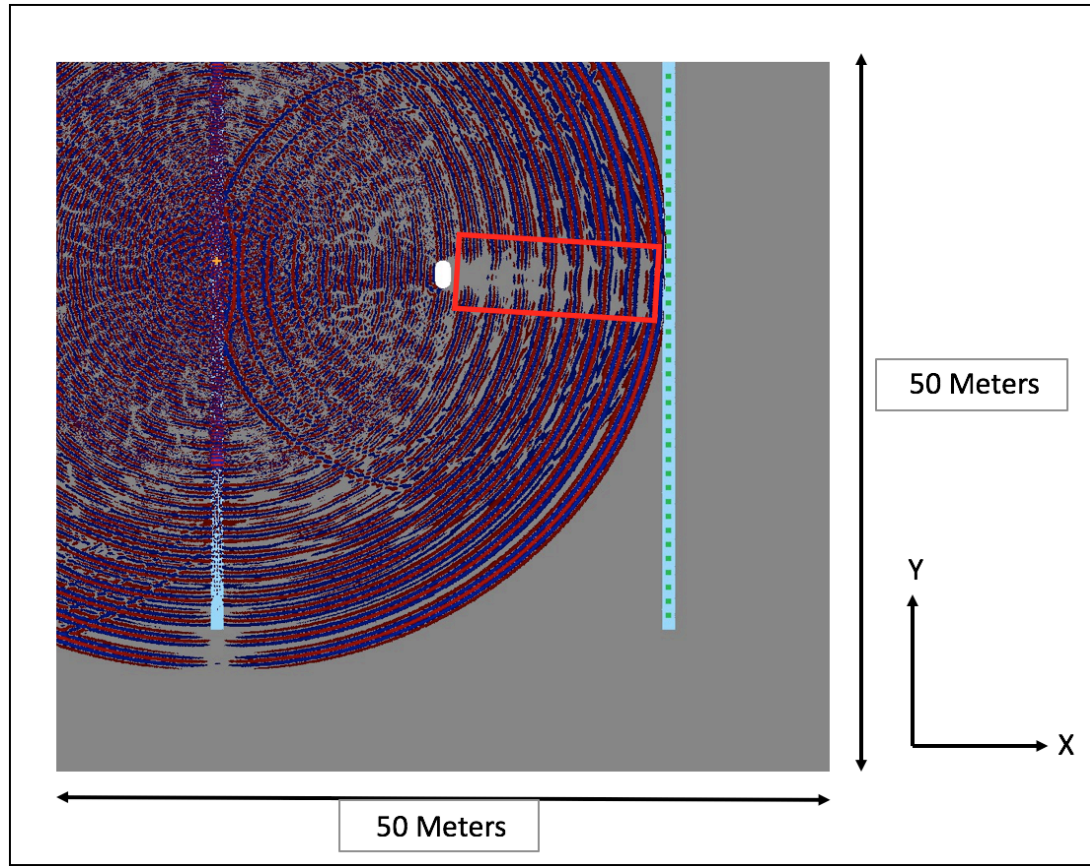


Figure 3.2: The 14 meters depth tunnel model with one layer run in Specfem2D at 10 ms.

This problem may be solved by placing the source and receivers into formations without any wells. Since receivers can be attached to the wall of the well by compressing air into the receivers, we can use this example in the real case applications. For this purpose, we created a different model with the same parameters with a change in that we located the source and the receivers directly inside of the model without any well (Figure 3.4). Then we ran Specfem2D software to start the seismic modeling. Figure 3.5 illustrates the generated seismic waves' interaction with the tunnel at 10 ms. When we examine the recorded seismogram in Figure 3.6, we can see the seismic waves that are affected by the existence of the tunnel in the model in the red circle zone. In addition to

that, when we compare the seismograms of the cross-well example with wells (Figure 3.3) with the seismograms of the cross-well example without wells (Figure 3.6), we can clearly see that the cross-well without wells gives a better result than the cross-well with wells.

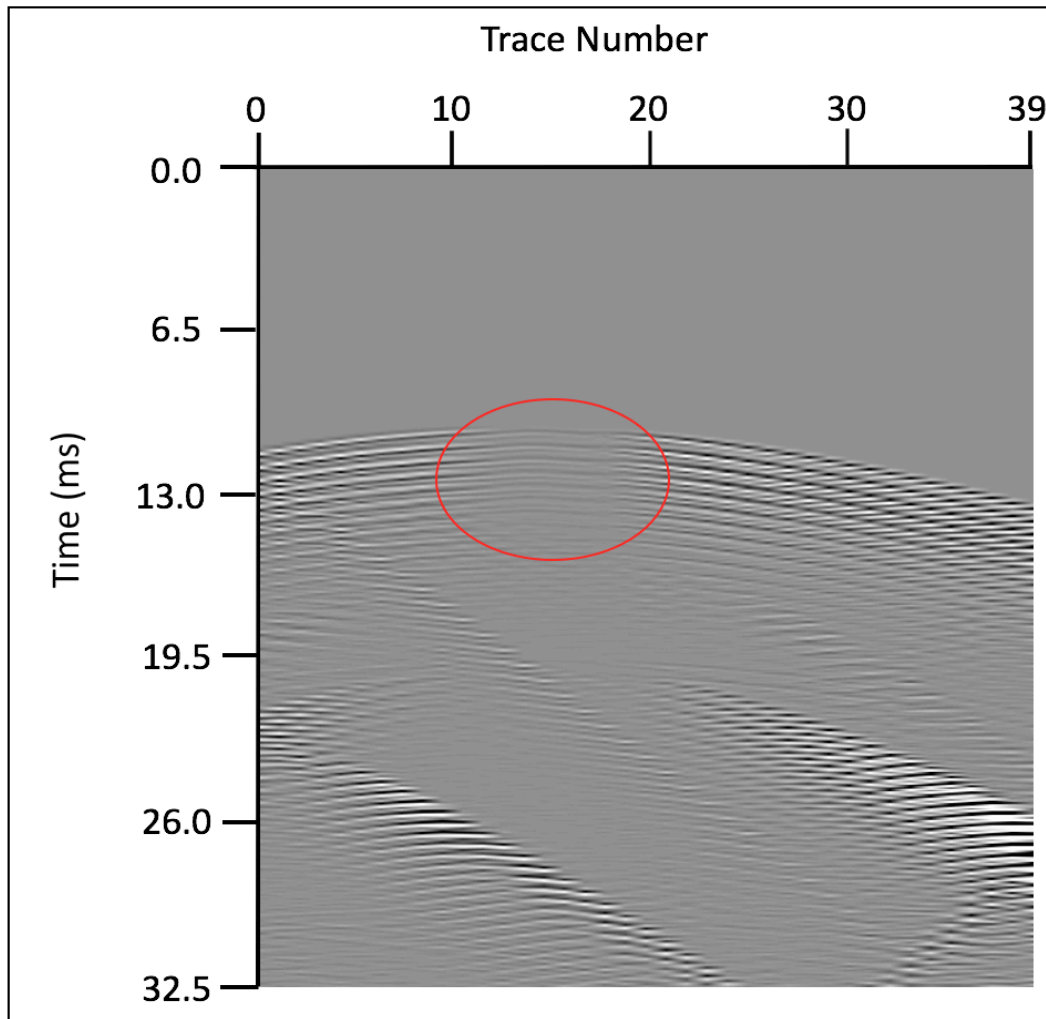


Figure 3.3: The seismogram z-component of the 14 meter depth tunnel model with one layer.

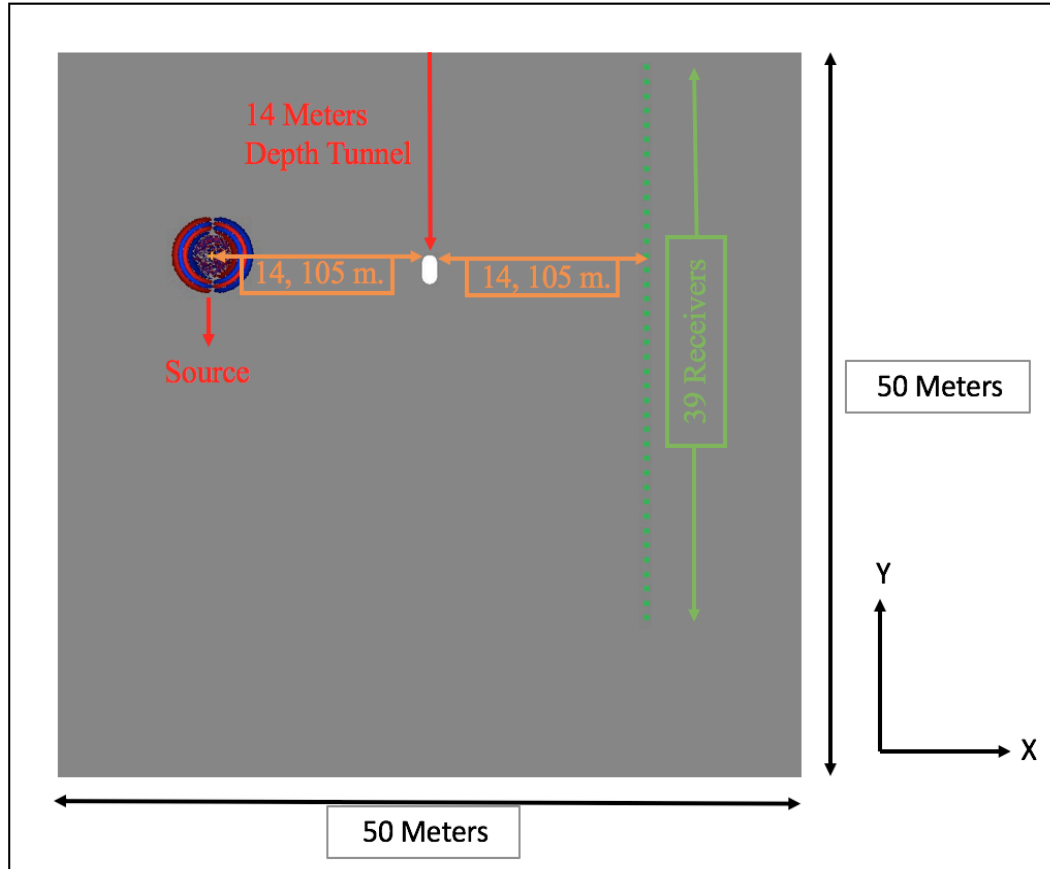


Figure 3.4: The geometry of the cross-well seismic method without wells.

After comparing these two simple examples, we continued our research with the cross-well seismic without wells.

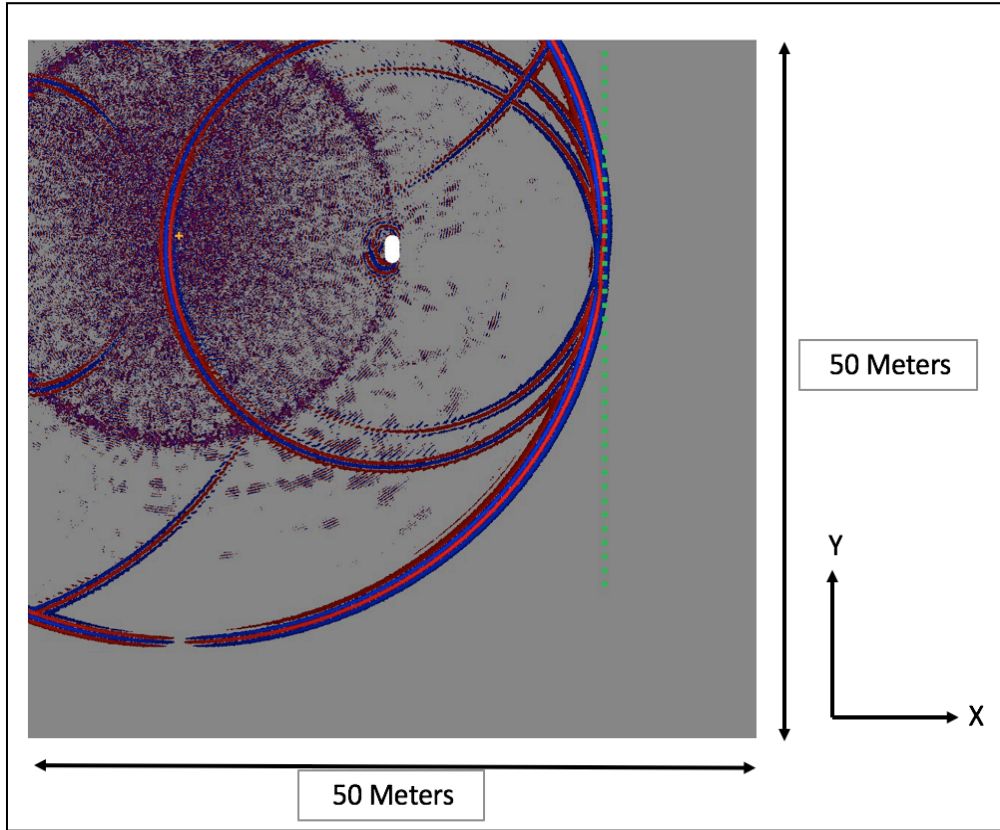


Figure 3.5: 14 meters depth tunnel model with one layer run in Specfem2D at 10 ms.

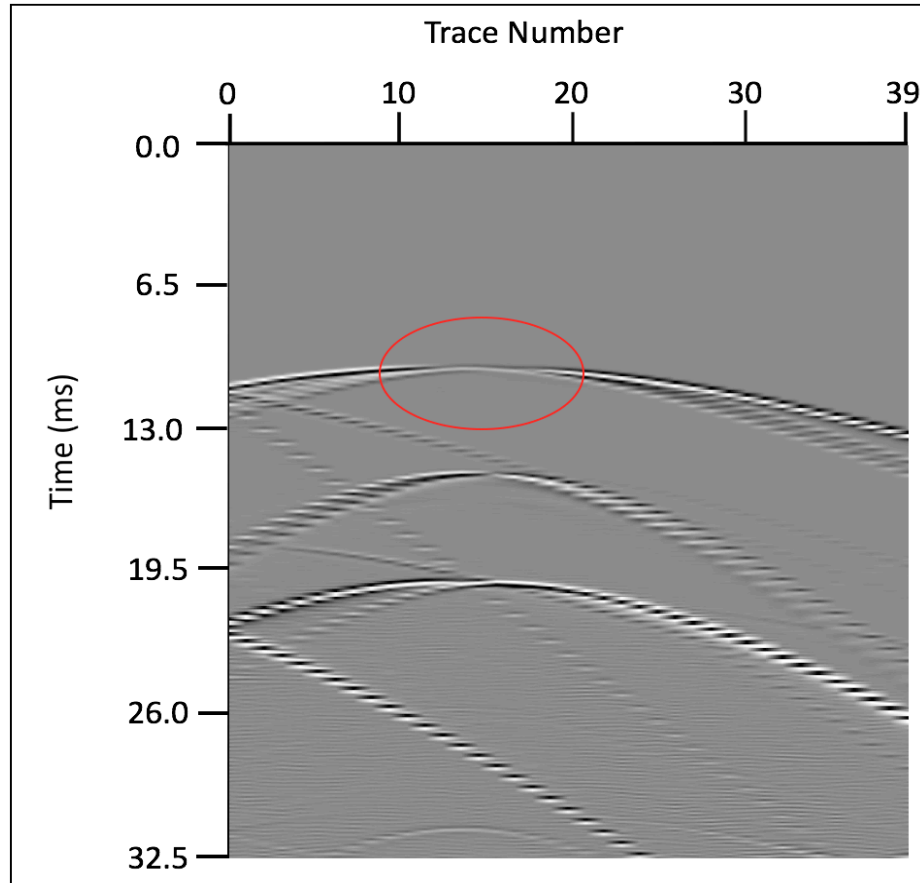


Figure 3.6: The seismogram z-component of the 14 meters depth tunnel model with one layer.

3.2.1 Model of Tunnel Located at 14 Meters Depth

3.2.1.1 One Layer Case

In this part, we generated some numerical models that have a tunnel at a depth of 14 meters with a source at two different frequencies for each model: 3000 Hz and 4000 Hz. We chose two different frequencies for the source to examine which source gives more accurate results for the cross-well without wells to locate the clandestine tunnels.

Since we received better results with the absorbing boundary condition in the earlier chapter, we only generated models with absorbing boundary condition in this section.

The acquisition geometry for the 14 meters depth tunnel for the subsurface seismic method is shown in Table 3.2.

Table 3.2: The acquisition geometry parameters for the 14 meters depth tunnel with one layer for the cross-well seismic without wells.

Model Dimension	50 m x 50 m
Seismic Shot Range	11 shots, starting from 0 m to 50 m with 5 m spacing on z-axis
Number of Receivers and Their Sequence	47 receivers starting from 2 m to 48 m
Frequency of Source and Its Type	3000 Hz and 4000 Hz, Ricker wavelet, Single Force (Coupled)
Tunnel Depth	14 m
Recording Length (millisecond)	32.5 ms
Boundary Condition	Absorbing Boundary (Top Layer) for Each Example
Velocity Model	$V_p= 3000$ m/sec, $V_s=1500$ m/sec, Density = 2.6 g/cm ³

We ran a simple model, which has only one layer, for seismic modeling, with a density of 2.6 g/cm³, $V_p= 3000$ m/sec, and $V_s=1500$ m/sec to test if our acquisition geometry works with a simple case via Specfem2D software. An example of seismic modeling is shown in Figure 3.7 where the shot point is located at 15 meters with 3000 Hz. This example is run with the absorbing boundary at the surface layer of the model.

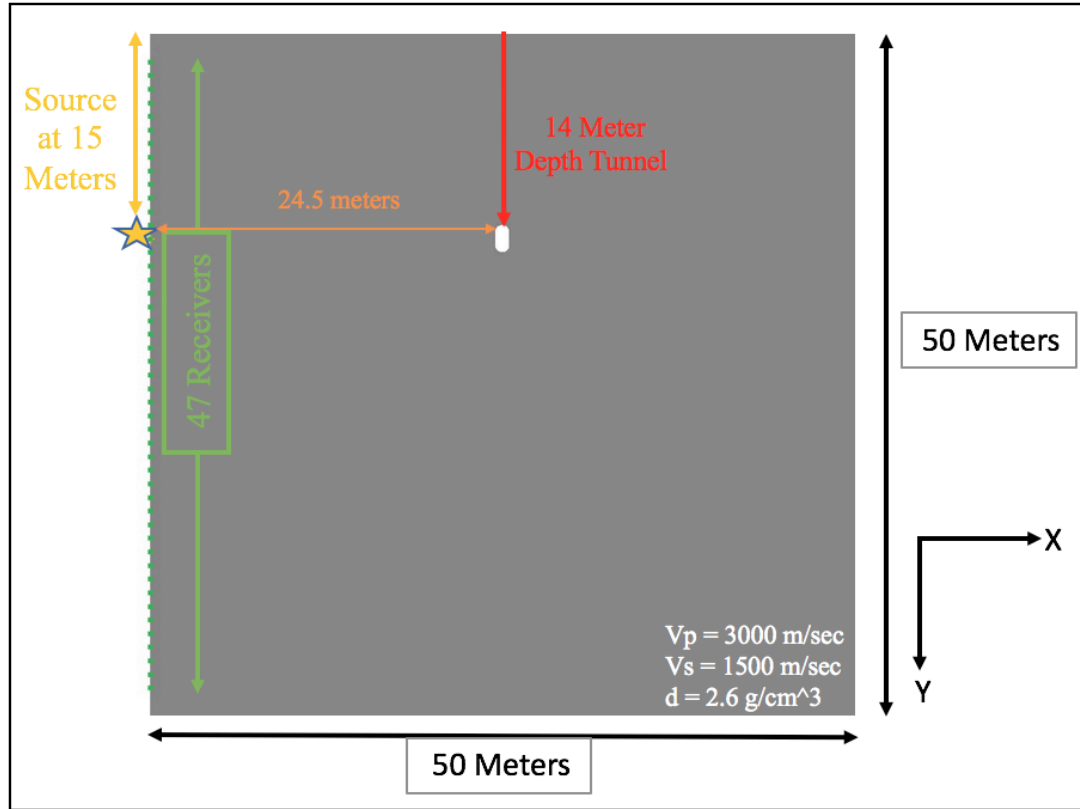


Figure 3.7: The acquisition geometry and model parameters of the 14 meters depth tunnel model with one layer.

After completing the seismic modeling, we examined the recorded seismogram (Figure 3.8). In the seismogram, we can see the reflections clearly compared to the results in the subsurface tunnel imaging section due to the high frequency of the source (3000 Hz). In the seismogram, we can identify direct P arrivals and direct S arrivals, the reflected P wave (PP) from the tunnel, and the converted P wave (PS) from the tunnel. We also noticed that there are some recordings in our seismogram from the waves which were generated as a result of corner effect (dark blue arrow). And due to the reflected wave from surface because of the imperfect absorbing boundary condition, this wave reflected from the tunnel and was recorded in the seismogram (black arrow).

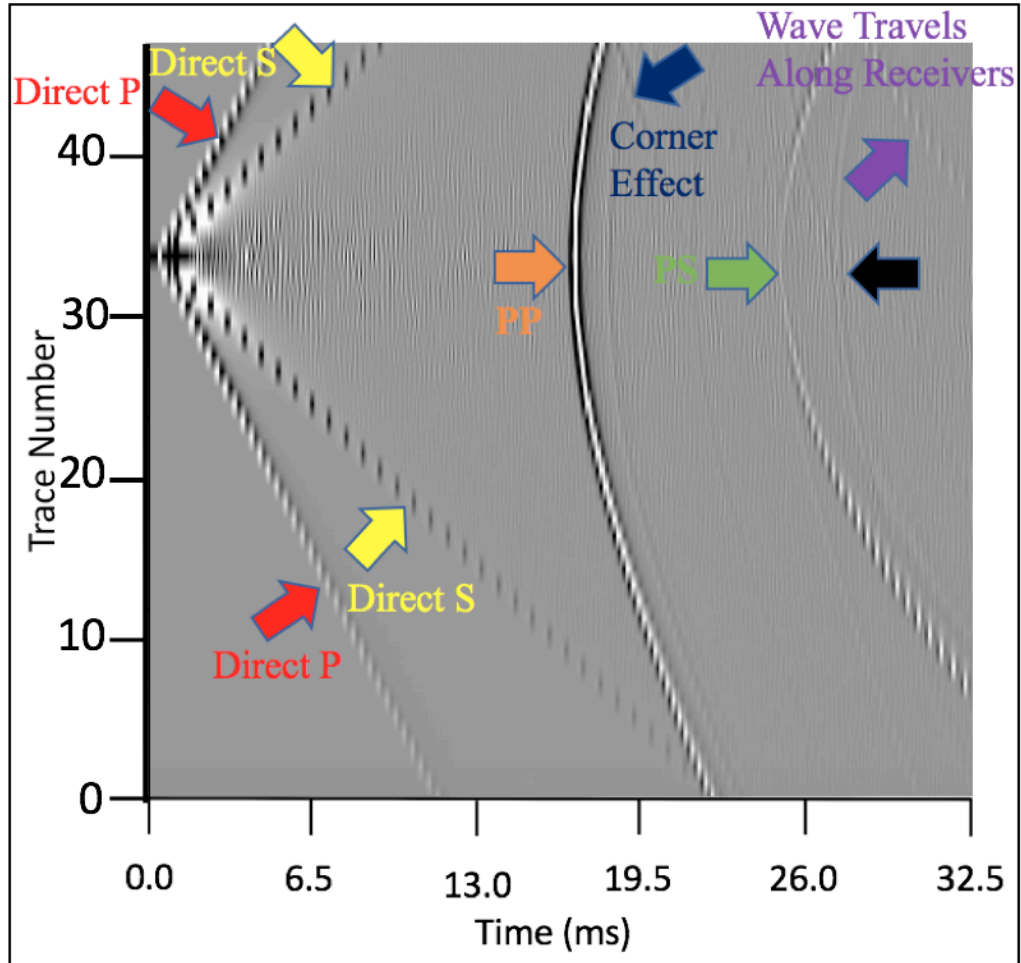


Figure 3.8: The seismogram (z-component) of the 14 meters depth tunnel model for the absorbing boundary condition with one layer and a 3000 Hz seismic source at 15 meters depth on the left side of the model.

Having reviewed the seismogram, we generated a seismic shot gather (Figure 3.8) so we can apply the migration code to image the tunnel with the one layer velocity model (Figure 2.7) that we created from the earlier chapter. Then we applied Kirchhoff migration to the seismic shot gather. According to the result, the cross-well method without a well gives the most accurate result for imaging the tunnel. This method gives the right location of the tunnel in height (two meters) and width (one meter), which we

could not see for the subsurface tunnel imaging method in the earlier chapter. On the other hand, we can still identify the same artifacts of Kirchhoff migration (yellow arrow) caused by the limited number of receivers and sources, and surface effects (white arrows) because of the direct arrivals. We can conclude that these effects are not dependent on the frequency of the source.

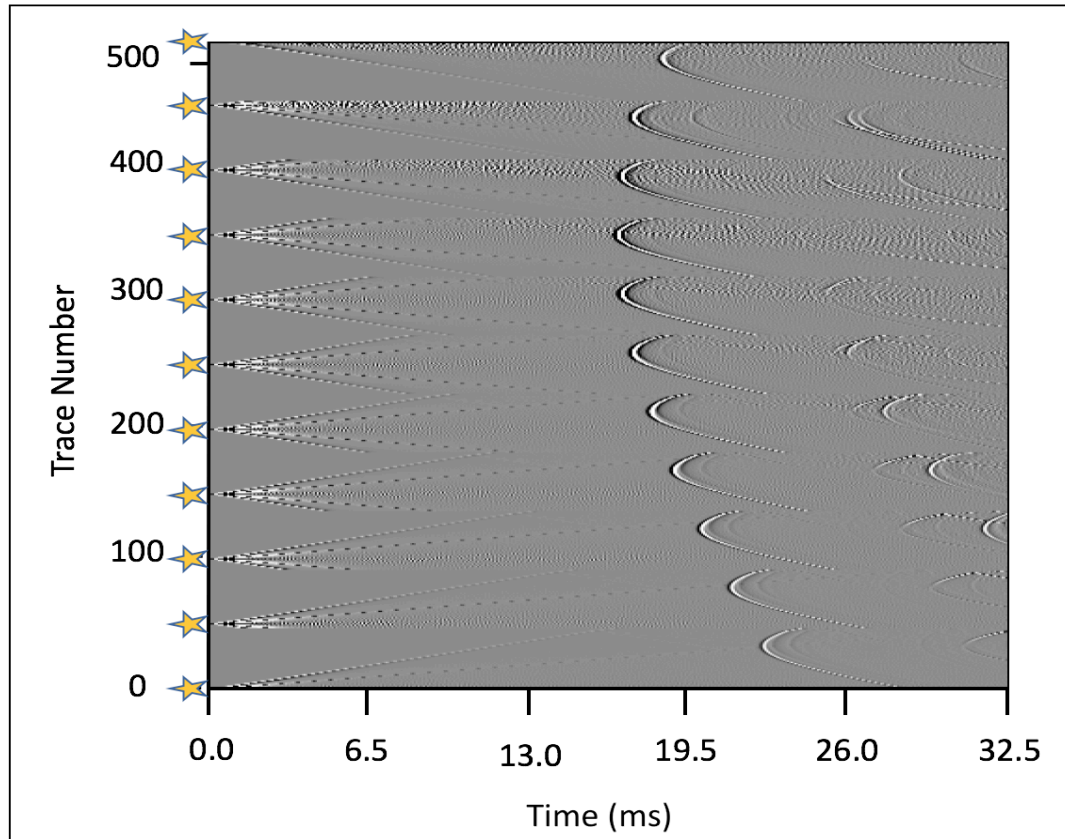


Figure 3.9: The seismic shot gather for the absorbing surface boundary condition for the 14 meters depth tunnel with a parallel layer and a seismic source of 3000 Hz.

Upon finishing examining the model that has the 14 meters depth tunnel with one layer with the absorbing boundary condition, we continue our research by generating a model using the same parameters from the absorbing boundary case with 4000 Hz of

source. For this objective, we ran our script in Specfem2D software, and then we reviewed the seismogram of the model with 4000 Hz (Figure 3.11).

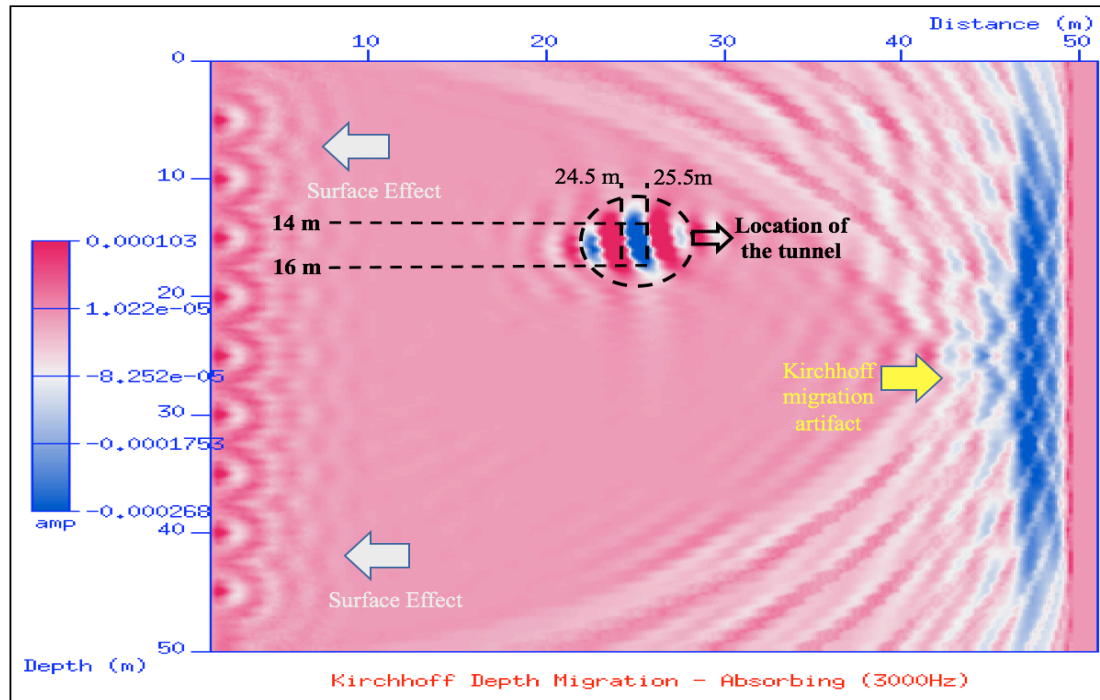


Figure 3.10: Kirchhoff migration result of the 14 meters depth tunnel model with the one layer model with the absorbing surface boundary condition (all boundaries) with single-force 3000 Hz sources are located on the left boundary (Amp represents the amplitude, which is a measure of the contrast in density, seismic velocities of the formations and / or underground structures).

After we examine the recorded seismogram with the 4000 Hz source, we can see direct P arrivals and direct S arrivals, the reflected P wave (PP) from the tunnel, and the converted P wave (PS) from the tunnel. There are some recordings in our seismogram from the waves which were generated due to corner effect (dark blue arrow). The black arrow shows a wave that is a result of the reflected wave from the top surface, and due to imperfect absorbing boundary condition, this wave reflected from the tunnel and was recorded in the seismogram (black arrow). We see more numerical modeling dispersion

in this example than in the example that has a 3000 Hz source, especially between the direct wave arrivals and converted P wave. A possible reason for this conclusion is that 4000 Hz is high for this example.

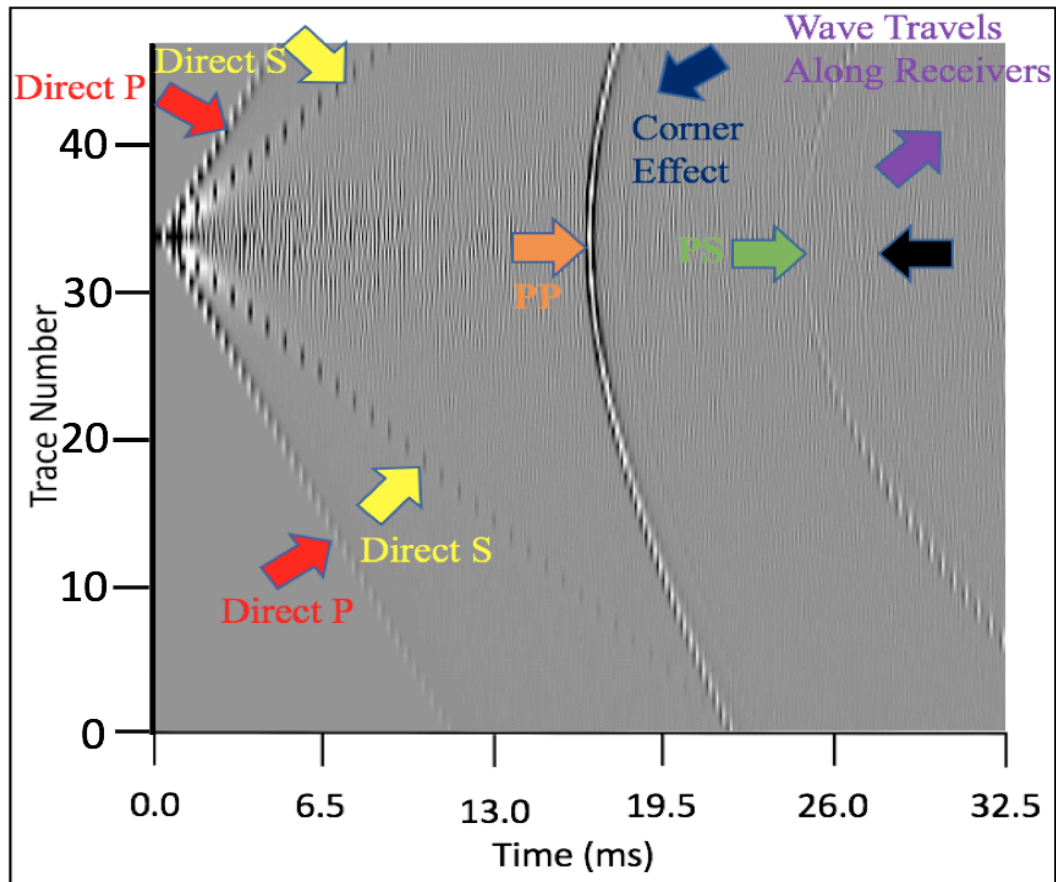


Figure 3.11: The seismogram (z-component) of the 14 meters depth tunnel model with the absorbing boundary (surface) with one layer and a 4000 Hz seismic source at 15 meters depth on the left side of the model.

After examining the recorded seismogram, we generated a seismic shot gather (Figure 3.12) on which to apply the migration. With the correct velocity model for the one layer from Figure 2.7, we ran Kirchhoff migration. According to the migration result (Figure 3.13), we can locate the clandestine tunnels at the appropriate location with its correct height (two meters) and weight (one meter). In addition to the tunnel, we can see

the artifacts of the surface (white arrows) because of the direct arrivals, and Kirchhoff migration's artifacts (yellow arrow) due to the insufficient amount of shots and receivers in our acquisition design. The 4000 Hz source increases the noise at the surface effect. For that reason, we can conclude that the 3000 Hz source is more suitable for this model with this acquisition geometry.

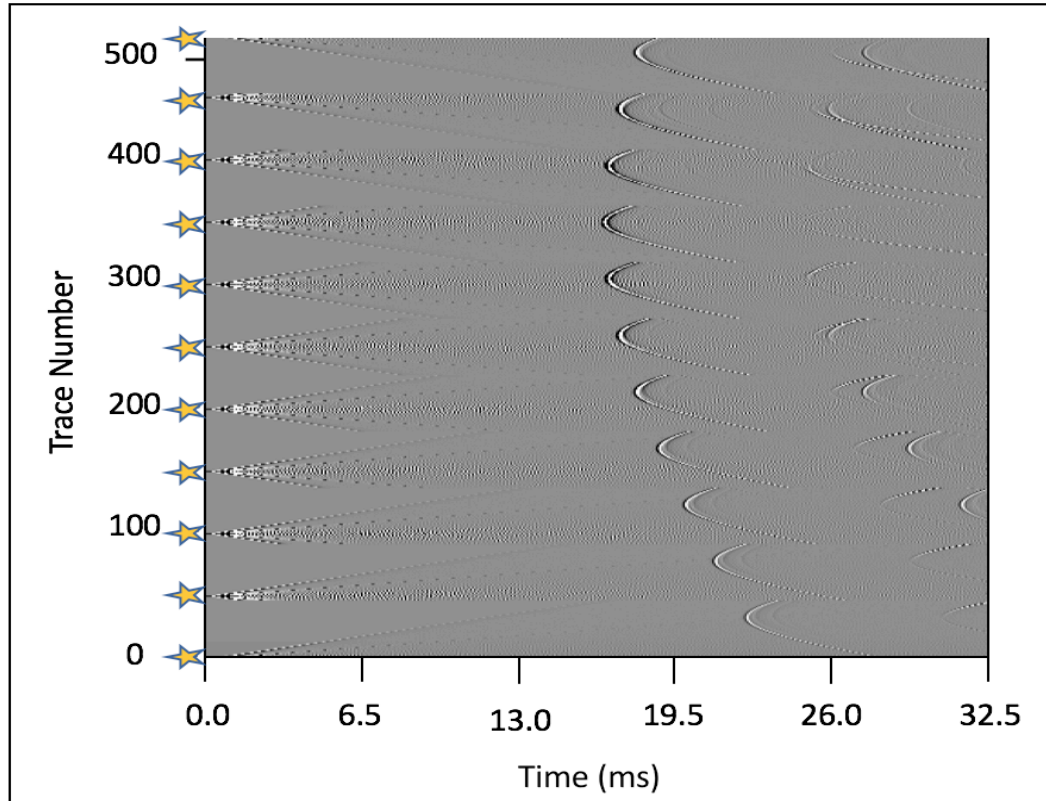


Figure 3.12: The seismic shot gather for the absorbing surface boundary condition for the 14 meters depth tunnel with a parallel layer and a seismic source of 4000 Hz.

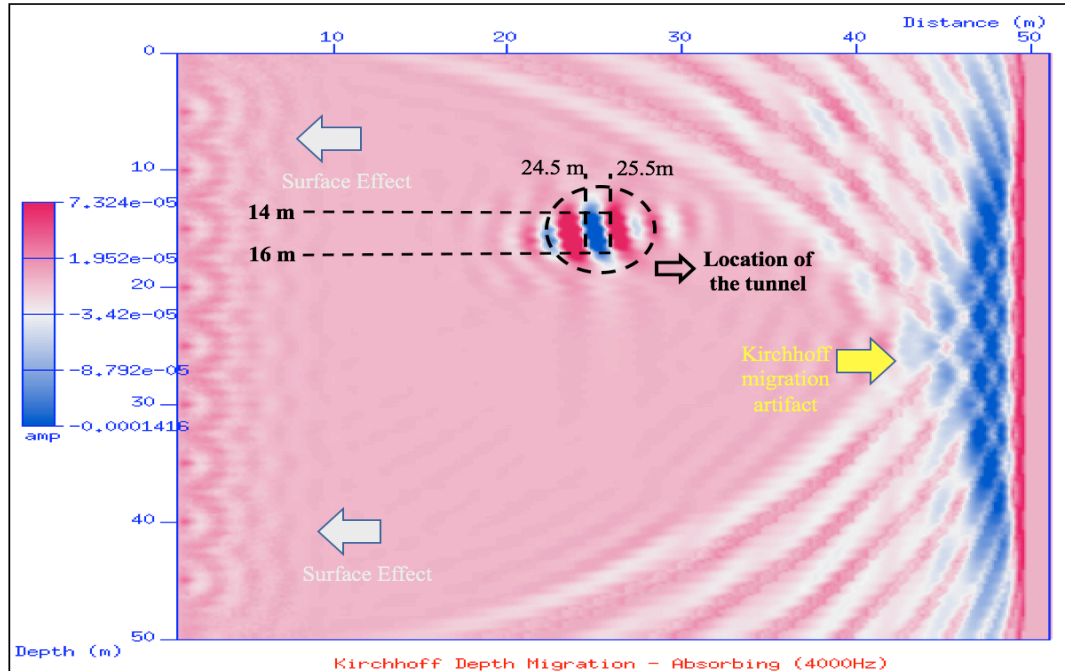


Figure 3.13: Kirchhoff migration result of the 14 meters depth tunnel model with the one layer model with the absorbing surface boundary condition at the surface and 4000 Hz sources (Amp shows the amplitude, which is a measure of the contrast in density, seismic velocities of the formations and / or underground structures).

3.2.1.2 Two-Layered Case

In this section, we generated some numerical models that have two layers with a tunnel at a depth of 14 meters. A single-force seismic source (double couple) was used at two different frequencies for each model: 3000 Hz and 4000 Hz. Using two different sources for the same model gives us the opportunity to find the optimal source's frequency that gives the most accurate result for the cross-well without wells to image the clandestine tunnels in our results. Since we generated the results in the one layer case section with the absorbing boundary condition, we continued creating the models with the absorbing boundary condition in this section.

The acquisition geometry for the 14 meters depth tunnel with two layers for the cross-well subsurface seismic method without wells is shown in Table 3.3. And a figure of this acquisition geometry is shown in Figure 3.14.

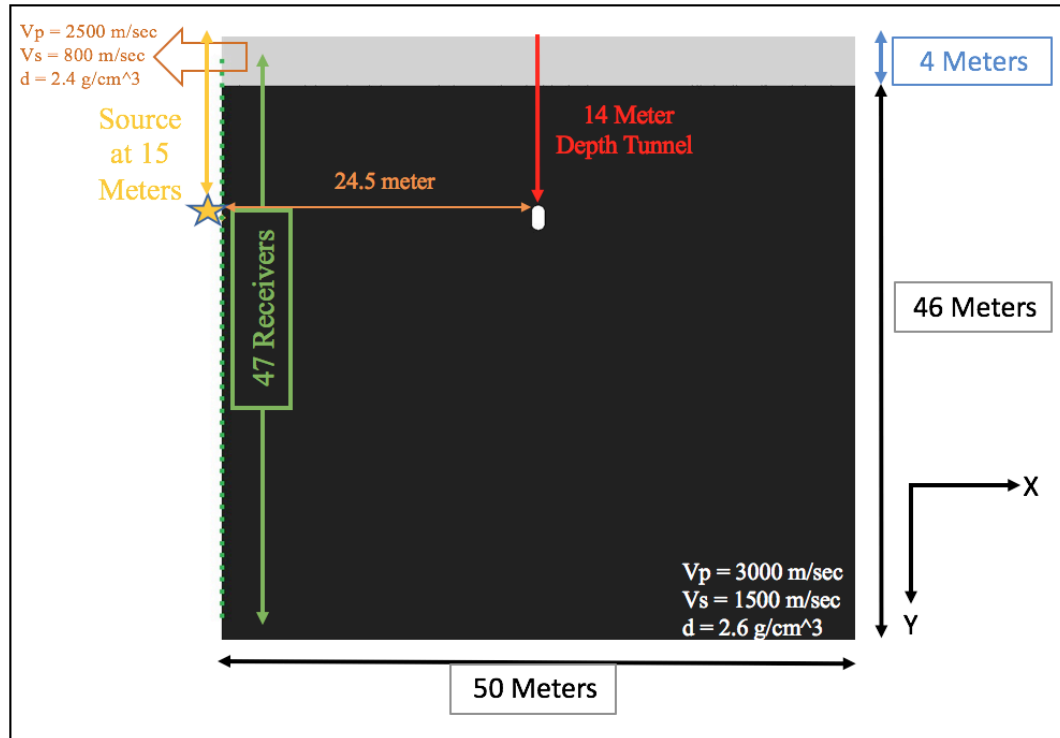


Figure 3.14: The acquisition geometry design for the 14 meters depth tunnel with two layers for the cross-well seismic without wells.

Table 3.3: The acquisition geometry parameters for the 14 meters depth tunnel with two layers for the cross-well seismic without wells.

Model Dimension	50 m x 50 m
Seismic Shot Range	11 shots, starting from 0 m to 50 m with 5 m spacing on z-axis
Number of Receivers and Their Sequence	47 receivers starting from 2 m to 48 m
Frequency of Source and Its Type	3000 Hz and 4000 Hz, Ricker wavelet, Single Force (Coupled)
Tunnel Depth	14 m
Recording Length (millisecond)	32.5 ms
Boundary Condition	Absorbing Boundary (Top Layer) for Each Example
Velocity Model	<p>First Layer: $V_p=2500$ m/sec, $V_s=800$ m/sec, Density = 2.4 g/cm³</p> <p>Second Layer: $V_p= 3000$ m/sec, $V_s=1500$ m/sec, Density = 2.6 g/cm³</p>

We generated the first seismic model in accordance with the parameters in Table 3.3 and Figure 3.14 for this section. After recording the seismogram which has the absorbing boundary condition at the surface with a 3000 Hz source located at 15 meters depth on the left boundary of the model in Figure 3.15, we can see direct P (red arrows)

and S wave arrivals (yellow arrows), the reflected P wave from the tunnel (orange arrow), the converted P wave from the tunnel (green arrow), and the white arrow illustrates the direct arrivals from the shallow layer. There are some recordings in our seismogram from the waves which were generated as a result of corner effect (dark blue arrow). The black arrow illustrates a wave that is a result of the reflected wave from the top surface due to imperfect absorbing boundary condition; this wave was then reflected from the tunnel and recorded in the seismogram.

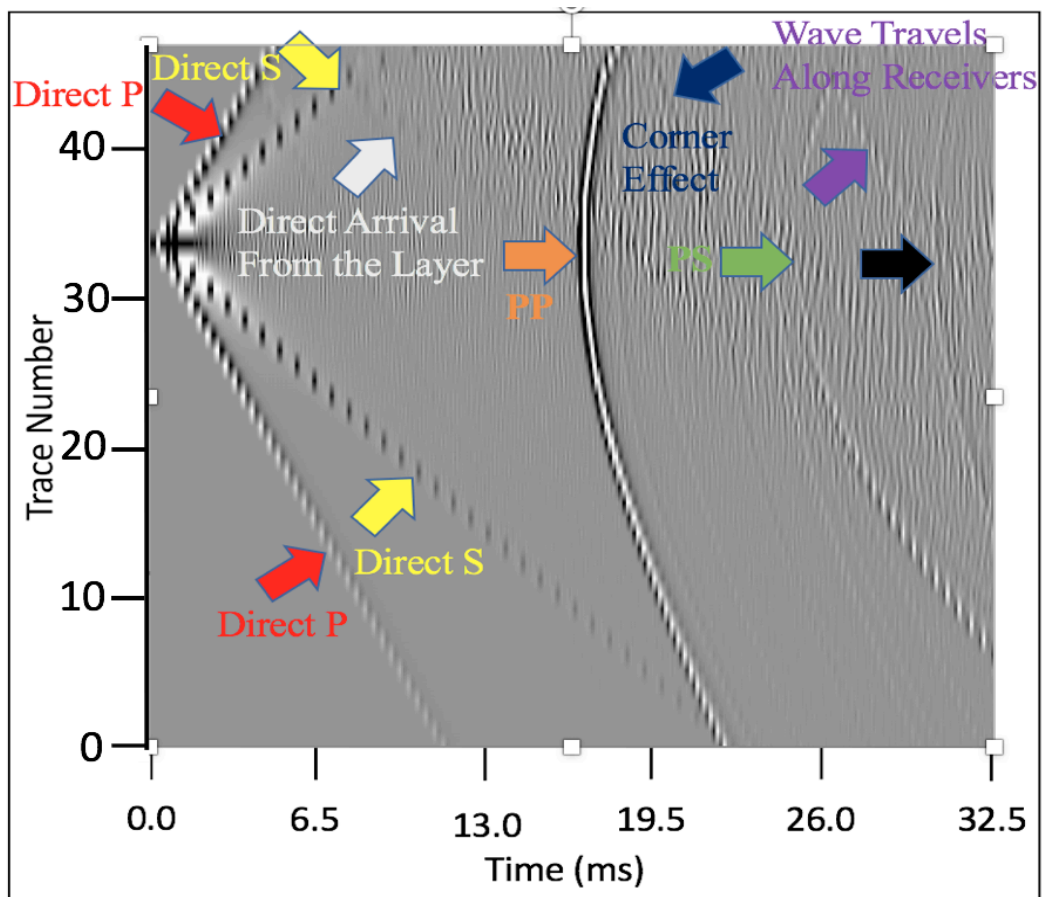


Figure 3.15: The seismogram (z-component) of the 14 meters depth tunnel model with the absorbing boundary condition (surface) with two layers and a 3000 Hz seismic source at 15 meters depth on the left side of the model.

After examining the seismogram, we generated a set of shot gathers (Figure 3.16) so we can apply the migration code to image the tunnel with the two-layered velocity model (Figure 2.22) that we created from the earlier chapter.

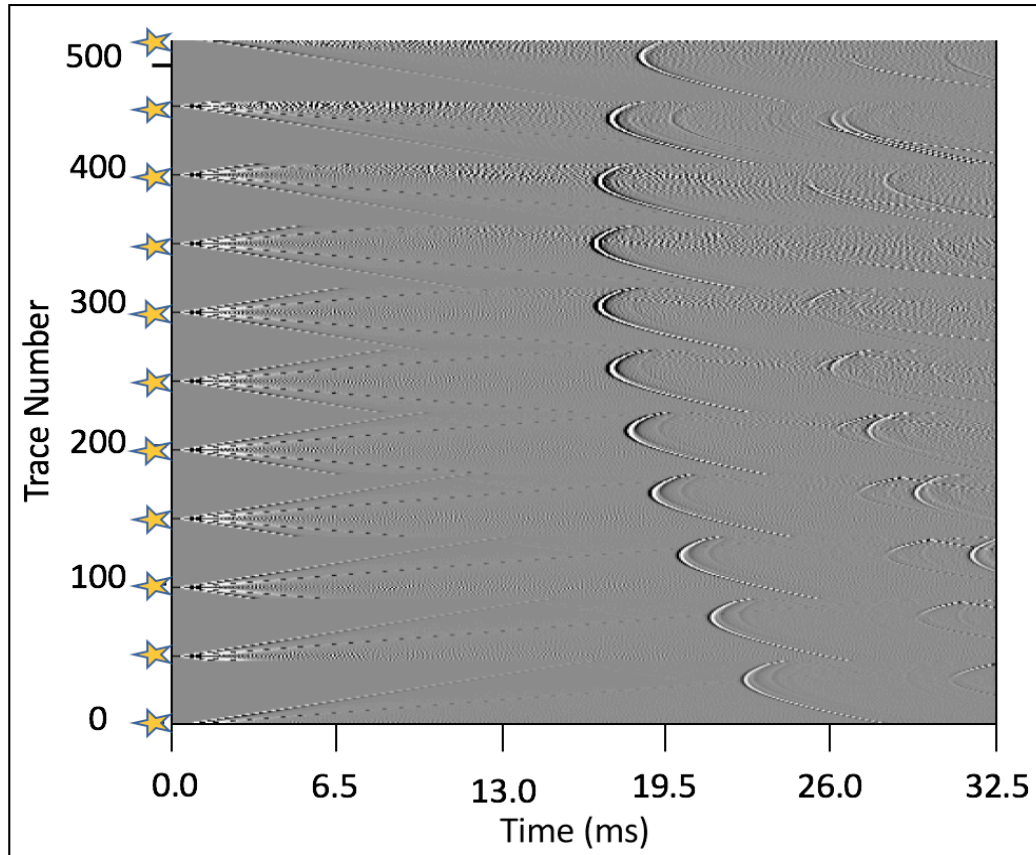


Figure 3.16: The set of shot gathers with the absorbing surface boundary condition (all boundaries) for the 14 meters depth tunnel with two layers for the seismic sources of 3000 Hz.

Then we applied Kirchhoff migration to the seismic shot gather (Figure 3.17). According to the result, the cross-well acquisition geometry without a well gives some accurate results for imaging the tunnel. This geometry presents the right location of the tunnel; however, the height of the tunnel appears to be one meter longer than it is supposed to be. The migration result correlates with the exact value of the width of the

tunnel (one meter); we could not see such a detailed result in the subsurface tunnel imaging method results. In addition to these findings, we can also see the surface effect, which is caused by the direct arrivals, and the Kirchhoff migration artifacts because of the limited number of shots and receivers.

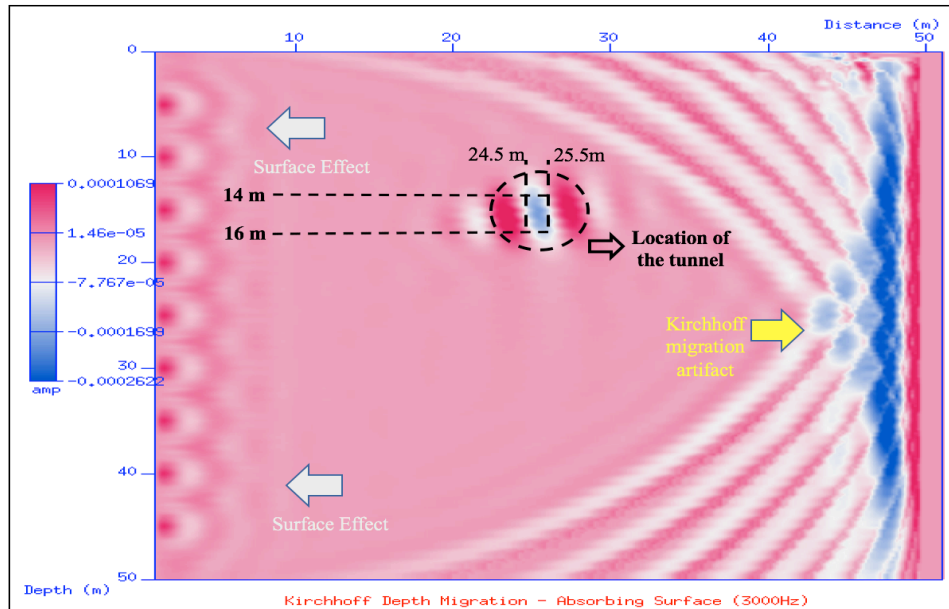


Figure 3.17: Kirchhoff migration result of the 14 meters depth tunnel model with two layers with the absorbing surface boundary condition at the surface and 3000Hz sources (Amp represents the amplitude, which is a measure of the contrast in density, seismic velocities of the formations and / or underground structures. Amplitude allows us to interpret the formations and the structures in the seismic data).

After completing the seismic modeling for 3000 Hz, we extended our research to seismic modeling with a 4000 Hz source. We created a model with the same parameters from the model with 3000 Hz source and modeled this new example with 4000 Hz of source to determine which frequency value produces a better result for our seismic modeling. For this objective, we ran our script in Specfem2D software, and then we reviewed the seismogram of the model with the 4000 Hz source (Figure 3.18). In the

seismogram, we can identify direct P arrivals and direct S arrivals, the reflected P wave (PP) from the tunnel, and the converted P wave (PS) from the tunnel. We also observed the waves which were generated as a result of corner effect (dark blue arrow). The black arrow presents the reflected wave from surface because of the imperfect absorbing boundary condition; this wave was reflected from the tunnel and recorded in the seismogram.

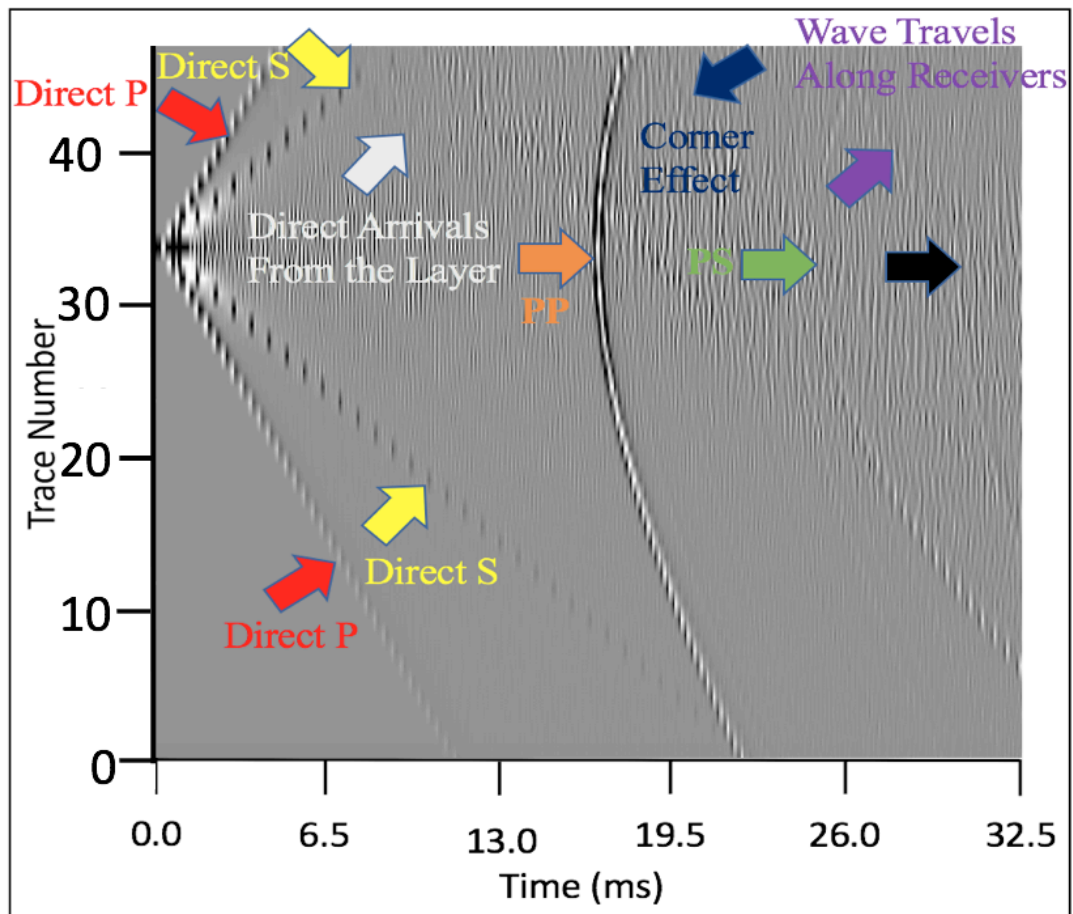


Figure 3.18: The seismogram (z-component) of the 14 meters depth tunnel model with two layers and with the absorbing boundary condition (surface) and a 4000 Hz seismic source at 15 meters depth on the left side of the model.

After reviewing the reflections in the seismogram, we created a set of shot gathers (Figure 3.19) for the 4000 Hz source case so that we can apply our Kirchhoff migration script to the generated seismogram.

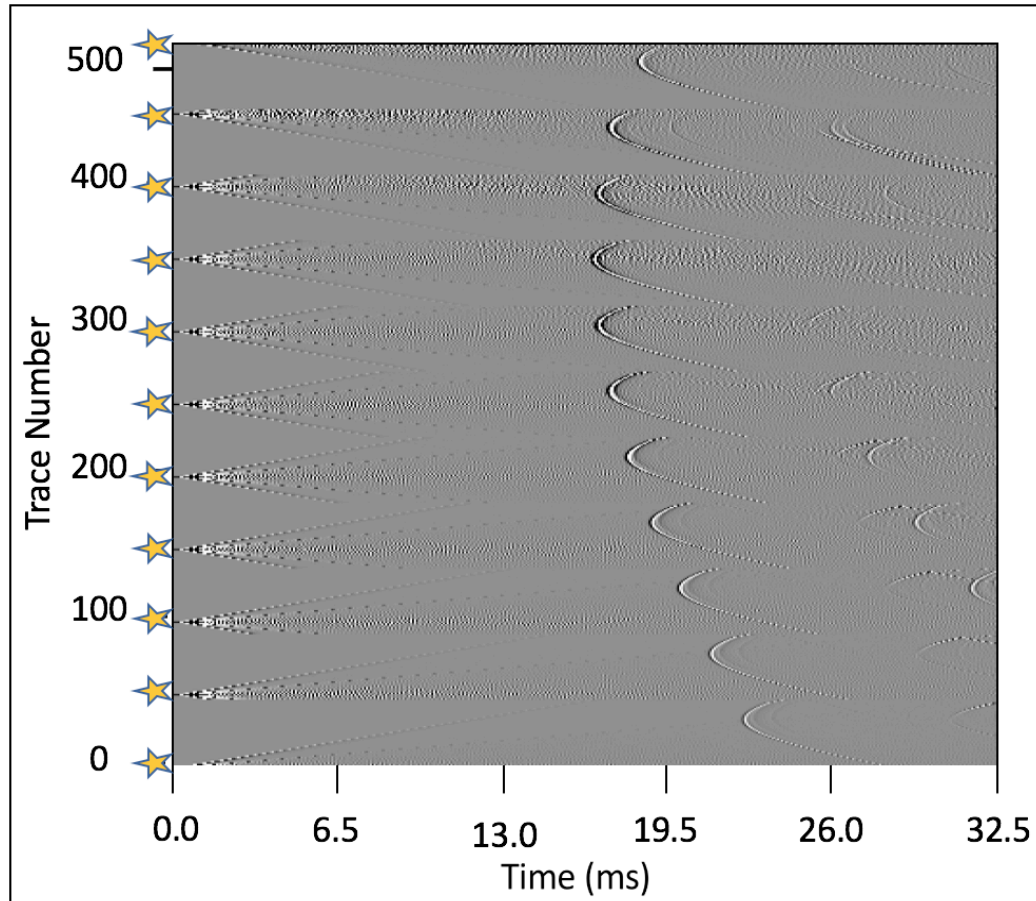


Figure 3.19: The set of shot gathers with the absorbing surface boundary condition (surface) for the 14 meters depth tunnel with two layers with seismic sources of 4000 Hz.

We then recorded the results after applying Kirchhoff migration to our seismic shot gather of 4000 Hz, we recorded the results. According to the result of the migration (Figure 3.20), the cross-well method without a well provides the correct location of the tunnel (the red circle). Although the width (one meter) of the tunnel is correct, the tunnel is one meter longer than its precise length (two meters). We cannot locate the shallow

layer from the migration result. A possible reason for this outcome is the thickness of the shallow formation (four meters), and for the fact that there is only one seismic shot recording inside of this shallow layer. In addition to these findings, we can identify the same artifacts from the earlier results for Kirchhoff migration that were caused by the limited number receivers and shot points, and the surface effect was caused by the direct arrivals. We can conclude that these effects are not dependent on the frequency of the source after comparing the same model with the 3000 Hz source and 4000 Hz source examples.

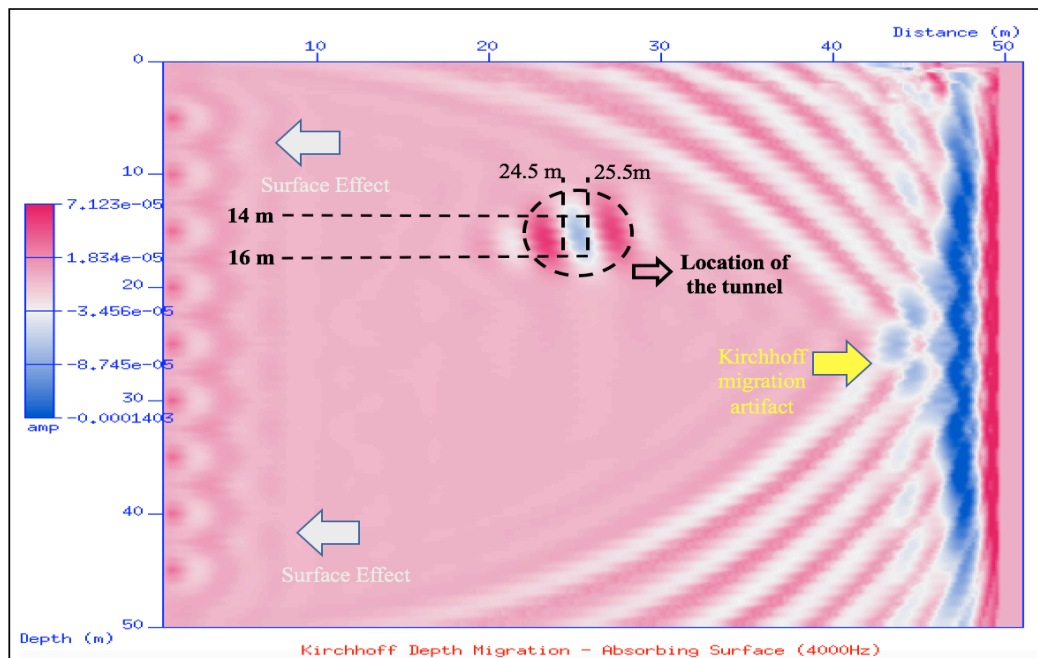


Figure 3.20: Kirchhoff migration result of the 14 meters depth tunnel model with two layers with the absorbing surface boundary condition at the surface and 4000 Hz sources (Amp shows the amplitude, which is a measure of the contrast in density, seismic velocities of the formations and / or underground structures).

3.2.2 Model of Tunnel Located at 19 Meters Depth

3.2.2.1 One Layer Case

After completing the chapters with the 14 meters depth tunnel, in this section, we created numerical models that have a clandestine tunnel at a depth of 19 meters with a source at two different frequencies for each model: 3000 Hz and 4000 Hz, in order to see if we can locate the tunnel when its depth is at 19 meters. We chose two different frequencies for the source to determine which source yields a better result for the cross-well method without wells to locate the clandestine tunnels. Since we received superior results with the absorbing boundary condition in the earlier chapters, we only generated models with the absorbing boundary condition in this section.

The acquisition geometry for the 14 meters depth tunnel with one layer formation for the cross-well seismic method without wells is shown in Table 3.4.

Table 3.4: The acquisition geometry parameters for the 14 meters depth tunnel with one layer for the cross-well seismic without wells.

Model Dimension	50 m x 50 m
Seismic Shot Range	11 shots, starting from 0 m to 50 m with 5 m spacing on z-axis
Number of Receivers and Their Sequence	47 receivers starting from 2 m to 48 m
Frequency of Source and Its Type	3000 Hz and 4000 Hz, Ricker wavelet, Single Force (Coupled)
Tunnel Depth	19 m
Recording Length (millisecond)	32.5 ms
Boundary Condition	Absorbing Boundary (Top Layer) for Each Example
Velocity Model	$V_p= 3000$ m/sec, $V_s=1500$ m/sec, Density = 2.6 g/cm ³

We ran a simple model, which has only one layer, for this seismic modeling, with a density of 2.6 g/cm³, $V_p= 3000$ m/sec, and $V_s=1500$ m/sec to test if our acquisition geometry works with a simple case. In the case that we do not receive any reliable results for the simple case, we will not be able to achieve any decent results for more complicated models. An example of our seismic modeling is shown in Figure 3.21 where

the shot point is located at 20 meters with 3000 Hz. This example is run with the absorbing boundary at the surface layer of the model.

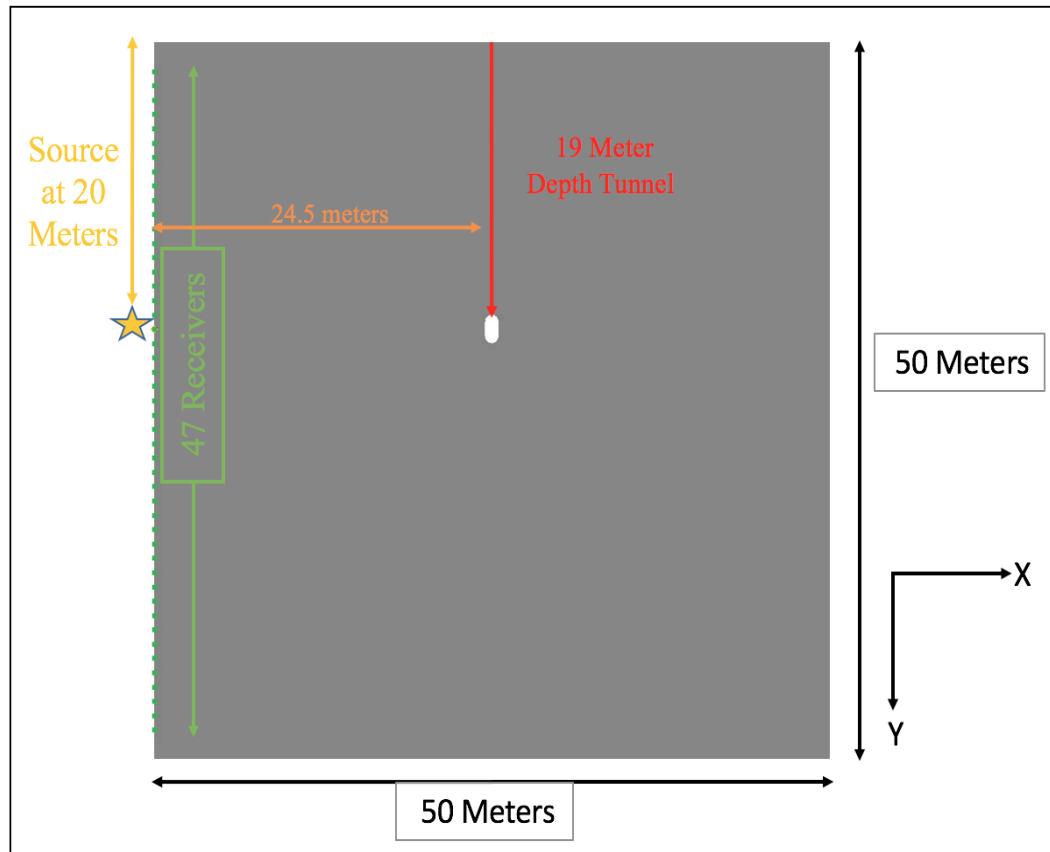


Figure 3.21: The acquisition geometry and parameters of the 14 meters depth tunnel model with one layer.

Upon completing this seismic modeling, we reviewed the recorded seismogram (Figure 3.22). In the seismogram, we can see the reflections clearly compared to the results in the subsurface tunnel imaging section due to the high frequency of the source (3000 Hz). In the seismogram, we can identify direct P and S arrivals, the reflected P wave (PP) from the tunnel, and the converted P wave (PS) from the tunnel. We also noticed that there are some recordings in our seismogram from the waves which were

generated as a result of corner effect (dark blue arrow). As a result of the reflected wave from surface from the imperfect absorbing boundary condition, this wave reflected from the tunnel and was recorded in the seismogram (black arrow).

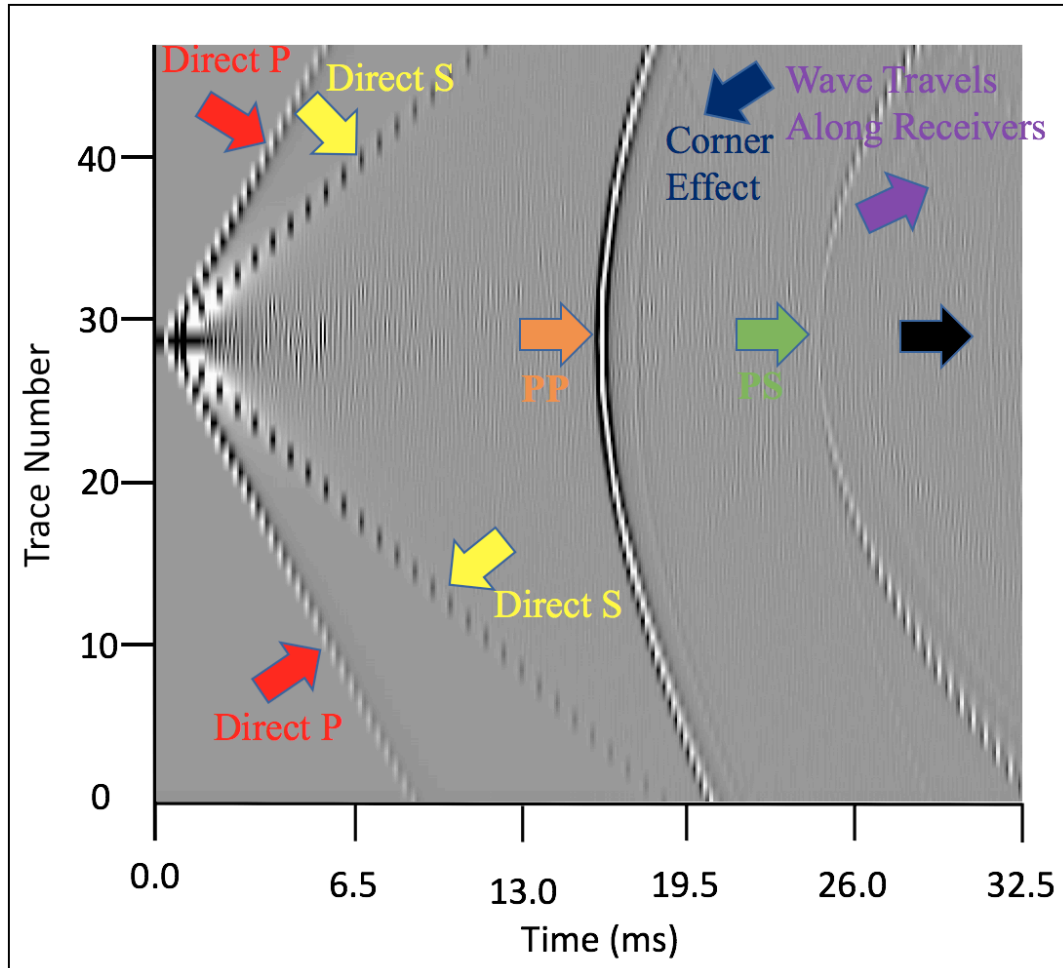


Figure 3.22: The seismogram (z-component) of the 14 meters depth tunnel model for the absorbing boundary condition with one layer and a 3000 Hz seismic source at 15 meters depth on the left side of the model.

Having reviewed the seismogram, we generated a set of shot gathers (Figure 3.23) so we can apply the migration code to image the tunnel with the one layer velocity model (Figure 2.7), generated in the earlier chapter. Then we applied Kirchhoff migration to our

generated seismic shot gather. According to the migration result, the cross-well method without a well gives the most accurate result for imaging the tunnel. This method gives the right location of the tunnel in height (two meters) and width (one meter), which we could not see for the subsurface tunnel imaging method in the earlier chapter. On the other hand, we can still identify the same artifacts of Kirchhoff migration, the Ricker wavelet, and surface effect. We can conclude that these effects are not dependent on the frequency of the source.

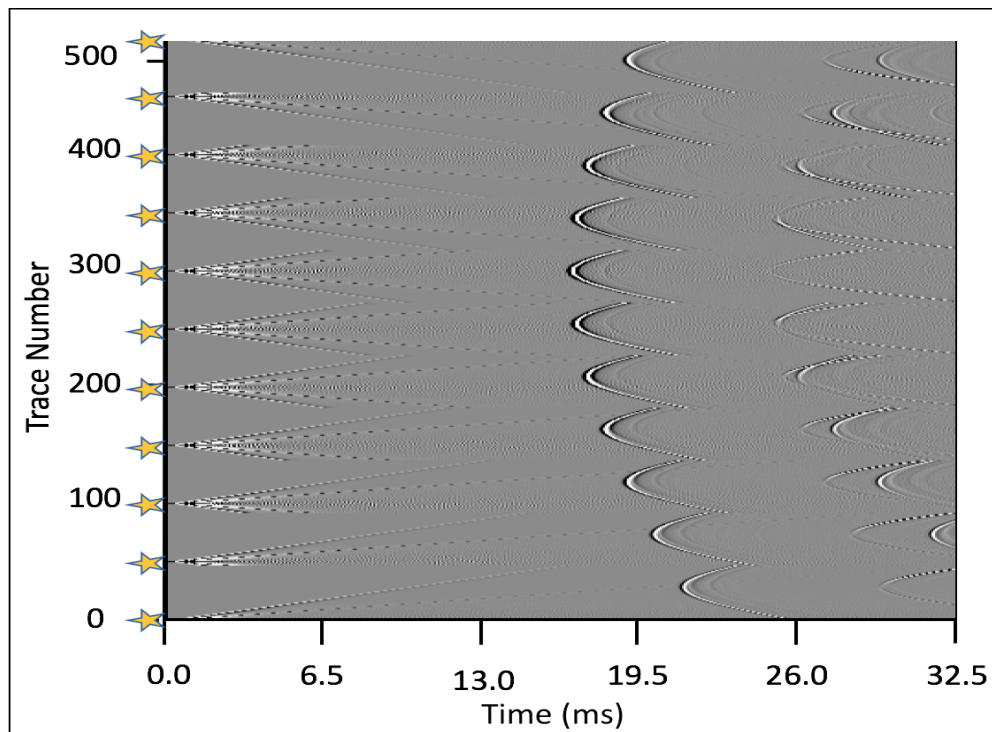


Figure 3.23: The set of shot gathers for the absorbing surface boundary condition for the 19 meters depth tunnel within one layer and seismic sources of 3000 Hz.

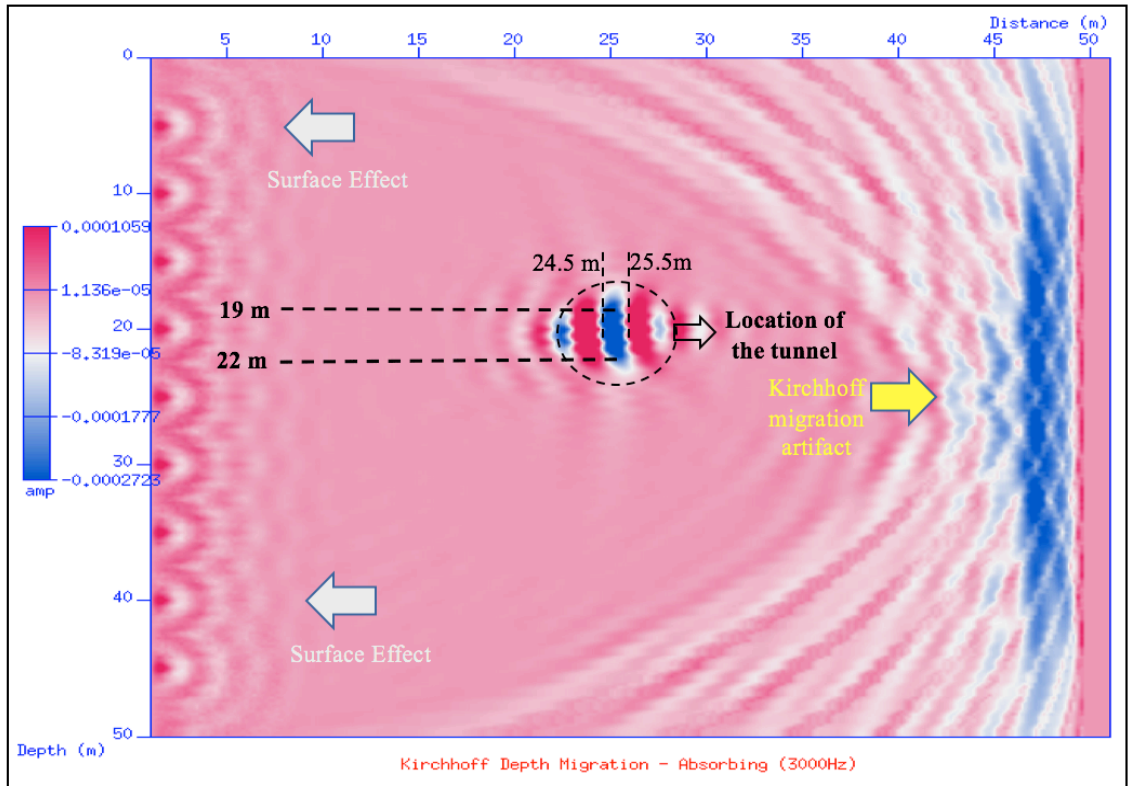


Figure 3.24: Kirchhoff migration result of the 19 meters depth tunnel model with one layer with the absorbing surface boundary condition at the surface and 3000 Hz sources (Amp represents the amplitude, which is a measure of the contrast in density, seismic velocities of the formations and / or underground structures).

Upon finishing examining the migration of the 19 meters depth tunnel model with one layer with the absorbing boundary condition, we continue our research by generating a model using the same parameters from the absorbing boundary case with 3000 Hz source. For this objective, we assigned the source's frequency to 4000 Hz, ran our script in Specfem2D software, and then reviewed the seismogram of the model with 4000 Hz (Figure 3.25).

After we examine the recorded seismogram with the 4000 Hz source, we can see direct P and S arrivals, the reflected P wave (PP) from the tunnel, and the converted P

wave (PS) from the tunnel. There are some recordings in our seismogram from the waves which were generated due to corner effect (dark blue arrow). The black arrow shows a wave that is a result of the reflected wave from the top surface. Due to the imperfect absorbing boundary condition, this wave reflected from the tunnel and was recorded in the seismogram (black arrow). We see more numerical modeling dispersion (between direct arrivals and PP wave) in this example than in the example that has a 3000 Hz source, especially between the direct wave arrivals and converted P wave. A likely explanation for this outcome is that 4000 Hz is too high for this example.

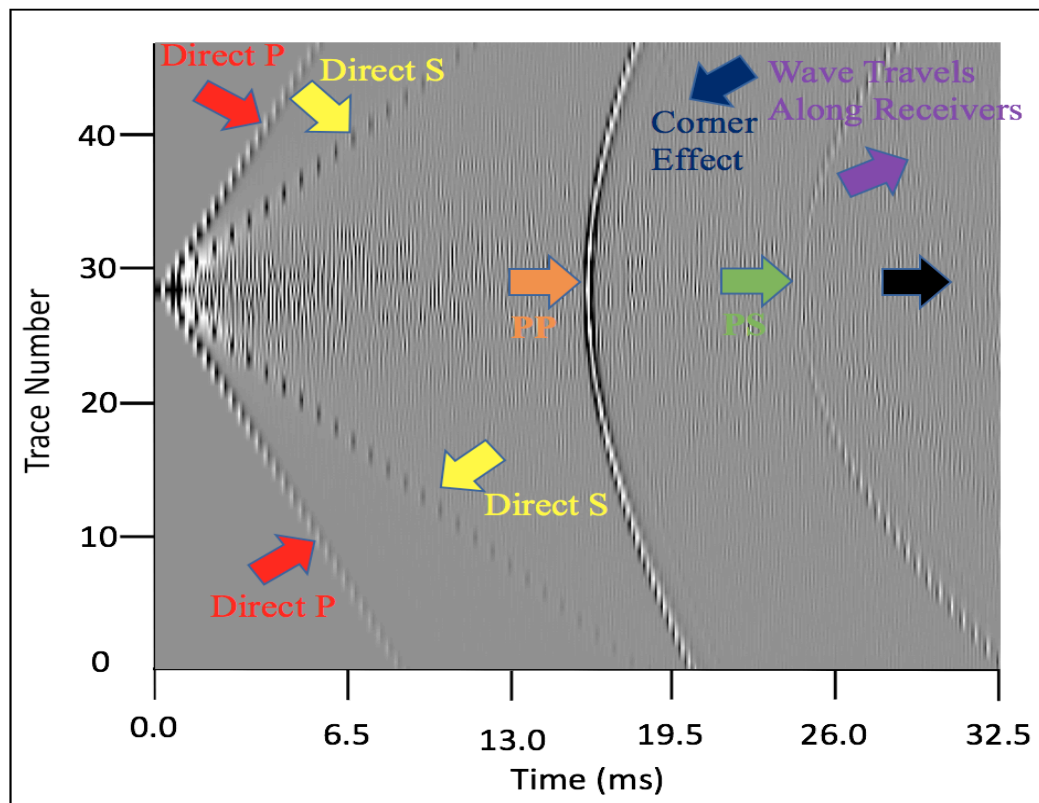


Figure 3.25: The seismogram (z-component) of the 19 meters depth tunnel model with the absorbing boundary condition (surface) with one layer and a 4000 Hz seismic source at 20 meters depth on the left side of the model.

After examining the recorded seismogram, we created a seismic shot gather (Figure 3.26) to apply migration to image the clandestine tunnel located at a depth of 19 meters. We ran Kirchhoff migration on the correct velocity model with one layer from Figure 2.7. According to the migration result (Figure 3.27), we can locate the clandestine tunnels at the appropriate location with the correct height (two meters) and width (one meter). In addition to the tunnel, we can see the surface effects (white arrows) caused by the direct arrivals, and the Kirchhoff migration's effect (yellow arrow) due to the limited number of receivers and shot in our acquisition design.

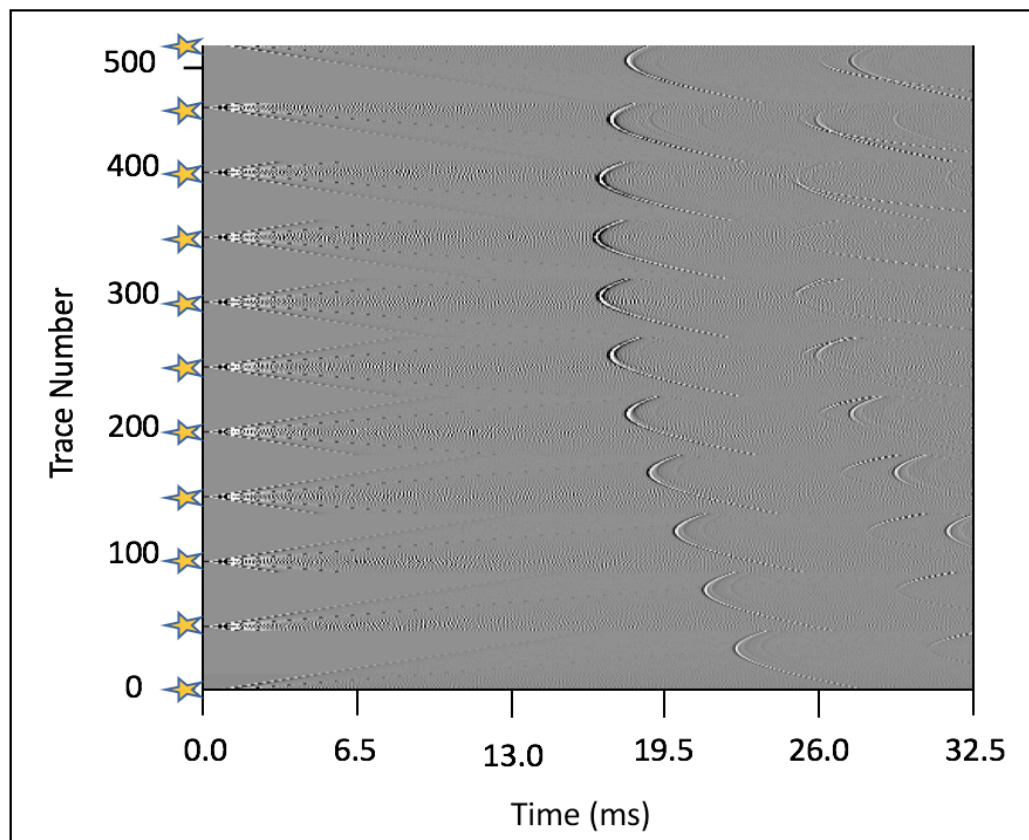


Figure 3.26: The set of shot gathers for the absorbing surface boundary condition for the 19 meters depth tunnel with a parallel layer and a seismic source of 4000 Hz.

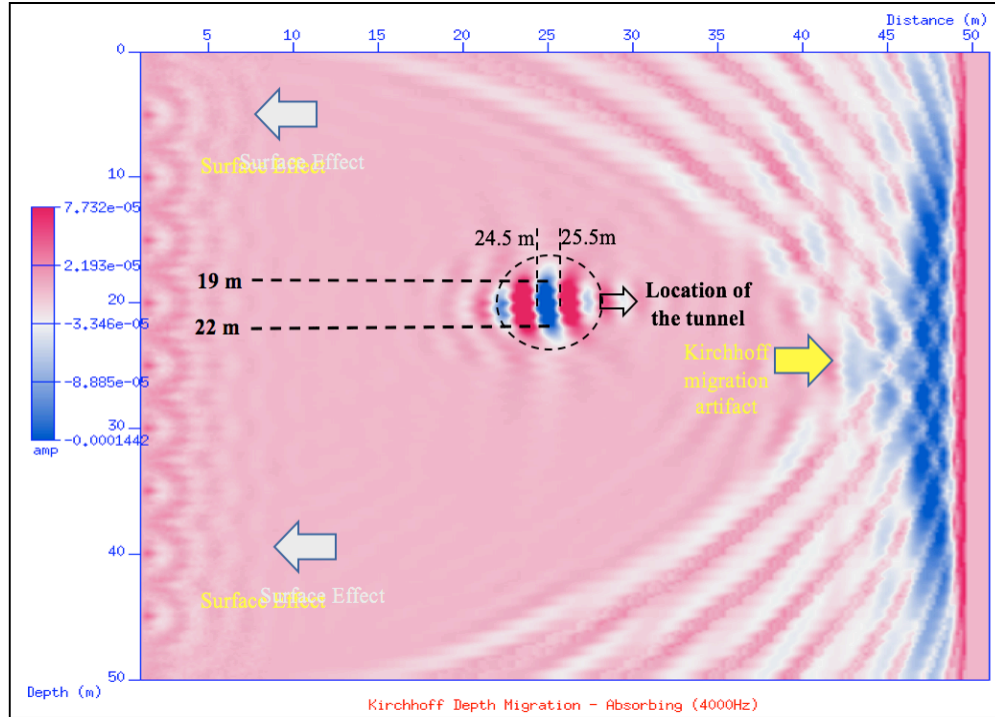


Figure 3.27: Kirchhoff migration result of the 19 meters depth tunnel model with one layer with the absorbing surface boundary condition at the surface and 4000 Hz sources (Amp shows the amplitude, which is a measure of the contrast in density, seismic velocities of the formations and / or underground structures).

3.2.2.2 Two-Layered Case

Upon completing the one layer case examples, we extended our research to generating models that have two layers, including the tunnels located at 19 meters depth inside of the models. The acquisition geometry and parameters are given in Table 3.5, and an illustrated figure of the acquisition design and its parameters are shown in Figure 3.28 below.

Table 3.5: The acquisition geometry parameters for the 19 meters depth tunnel with two layers for the cross-well seismic method without wells.

Model Dimension	50 m x 50 m
Seismic Shot Range	11 shots, starting from 0 m to 50 m with 5 m spacing on z-axis
Number of Receivers and Their Sequence	47 receivers starting from 2 m to 48 m
Frequency of Source and Its Type	3000 Hz and 4000 Hz, Ricker wavelet, Single Force (Coupled)
Tunnel Depth	19 m
Recording Length (millisecond)	32.5 ms
Boundary Condition	Absorbing Boundary (Top Layer) for Each Example
Velocity Model	<p>First Layer: $V_p=2500$ m/sec, $V_s=800$ m/sec, Density = 2.4 g/cm³</p> <p>Second Layer: $V_p= 3000$ m/sec, $V_s=1500$ m/sec, Density = 2.6 g/cm³</p>

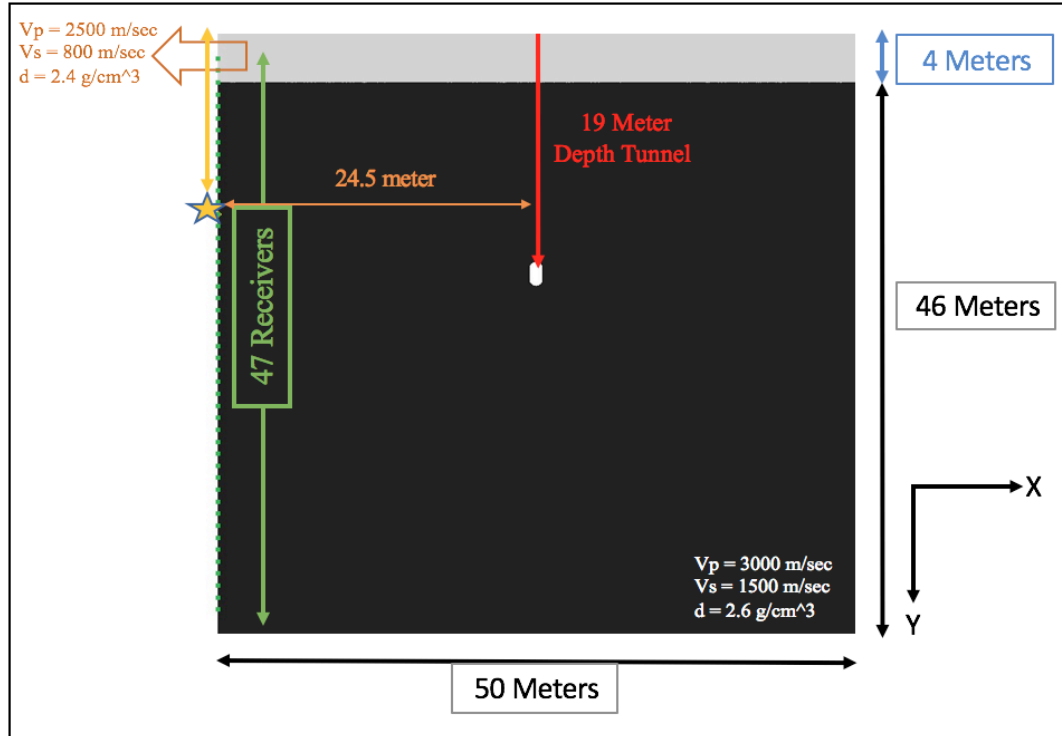


Figure 3.28: The acquisition geometry design for the 19 meters depth tunnel with two layers for the cross-well seismic method without wells.

After assigning the required parameters, we ran the Specfem2D according to the given parameters and saved the seismogram. According to the recorded seismogram in Figure 3.29, we can recognize the direct P and S arrivals, the reflected P wave (PP) from the tunnel, and the converted P wave (PS) from the tunnel. There are also waves which were generated as a result of the corner effect (dark blue arrow), and the black arrow represents the reflected wave from the surface. Due to the imperfect absorbing boundary, this wave reflected from the tunnel and was recorded in the seismogram.

After examining the seismogram, we generated a set of shot gathers (Figure 3.30) so that we can apply the migration code to image the tunnel with the two-layered velocity model (Figure 2.22) that we created.

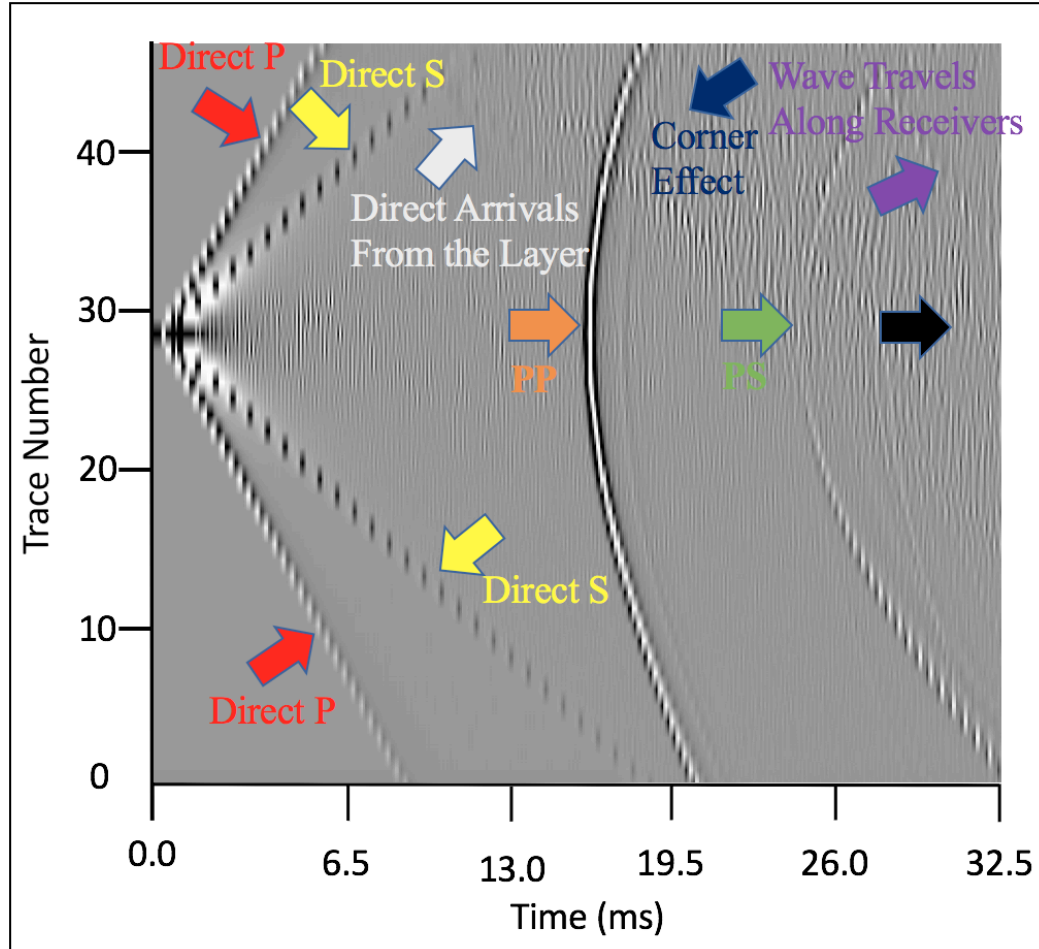


Figure 3.29: The seismogram (z-component) of the 19 meters depth tunnel model with the absorbing boundary (surface) with two layers and a 3000 Hz seismic source at 20 meters depth on the left side of the model.

Afterwards, the Kirchhoff migration was applied to the set of shot gathers (Figure 3.31). According to the Kirchhoff result, the location of the tunnel was correct; however, the tunnel is one meter longer than its designed initial model. In addition to these findings, we can also locate the surface effect, which is caused by the direct arrivals, and Kirchhoff migration artifacts because of the limited number of receivers and shot points. On the other hand, we cannot identify the shallow layer from the migration result due to

the shallow layer's thickness (four meters), from having only one shot inside of this shallow layer (at 0 meters depth), and slow seismic speeds of the shallow formation.

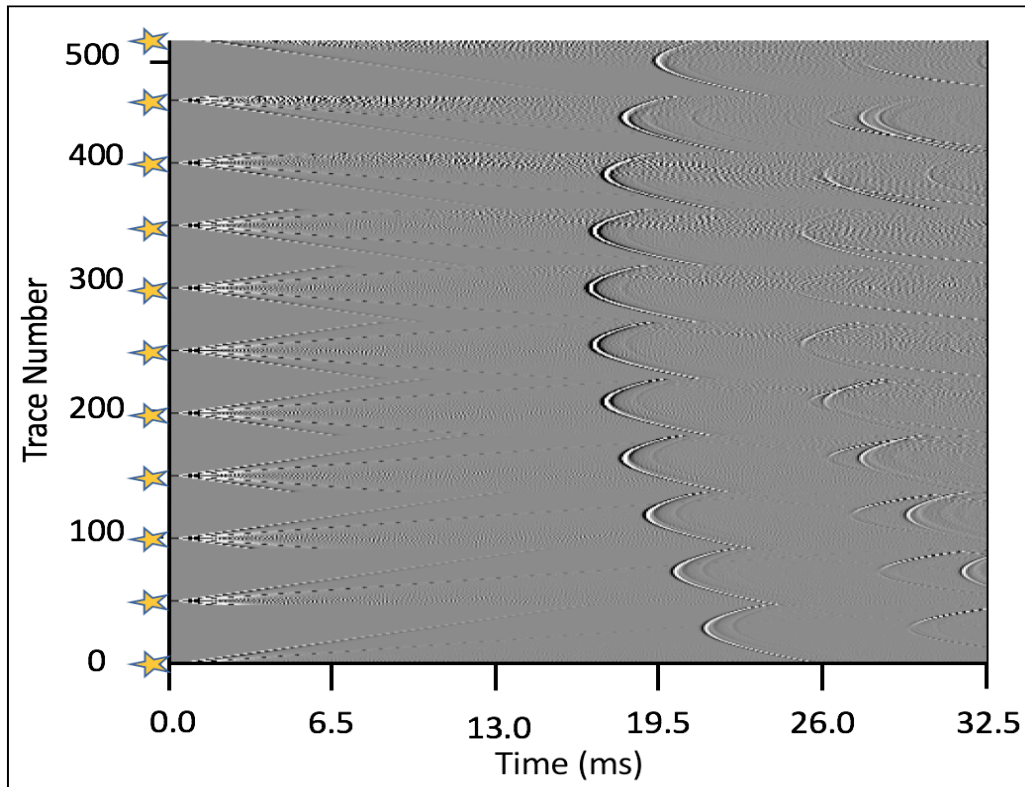


Figure 3.30: The set of shot gathers with the absorbing surface boundary condition (surface) for the 19 meters depth tunnel with two layers for the seismic sources of 3000 Hz.

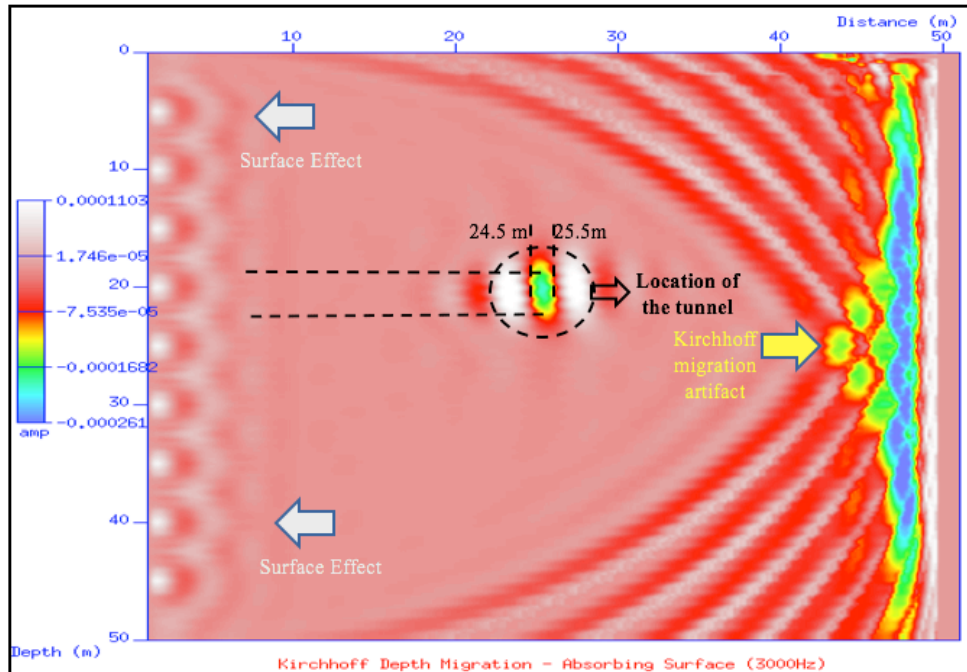


Figure 3.31: Kirchhoff migration result of the 14 meters depth tunnel model with two layers with the absorbing boundary condition (for all boundaries) and single-force 3000 Hz sources are located on the left boundary (Amp shows the amplitude, which is a measure of the contrast in density, seismic velocities of the formations and / or underground structures).

Following the completion of generating and examining models with a 3000 Hz source, we ran new examples of seismic modeling with 4000 Hz sources using the same parameters from the 3000 Hz case. Our intent to generate more models with different frequencies is so that we might find the most accurate frequency value for our model. For this objective, we ran our script to record the seismogram of the first sample, which is a two-layered model that has a tunnel at 19 meters depth with a 4000 Hz source (Figure 3.32). After examining the recorded seismogram, we can see the direct P and S arrivals, the reflected P wave (PP) from the tunnel, and the converted P wave (PS) from the tunnel. The dark blue arrow shows the waves generated from the corner effect, and the

black arrow presents the reflected wave from the surface due to the imperfect absorbing boundary condition. Afterwards this wave reflected from the tunnel and was recorded in the seismogram.

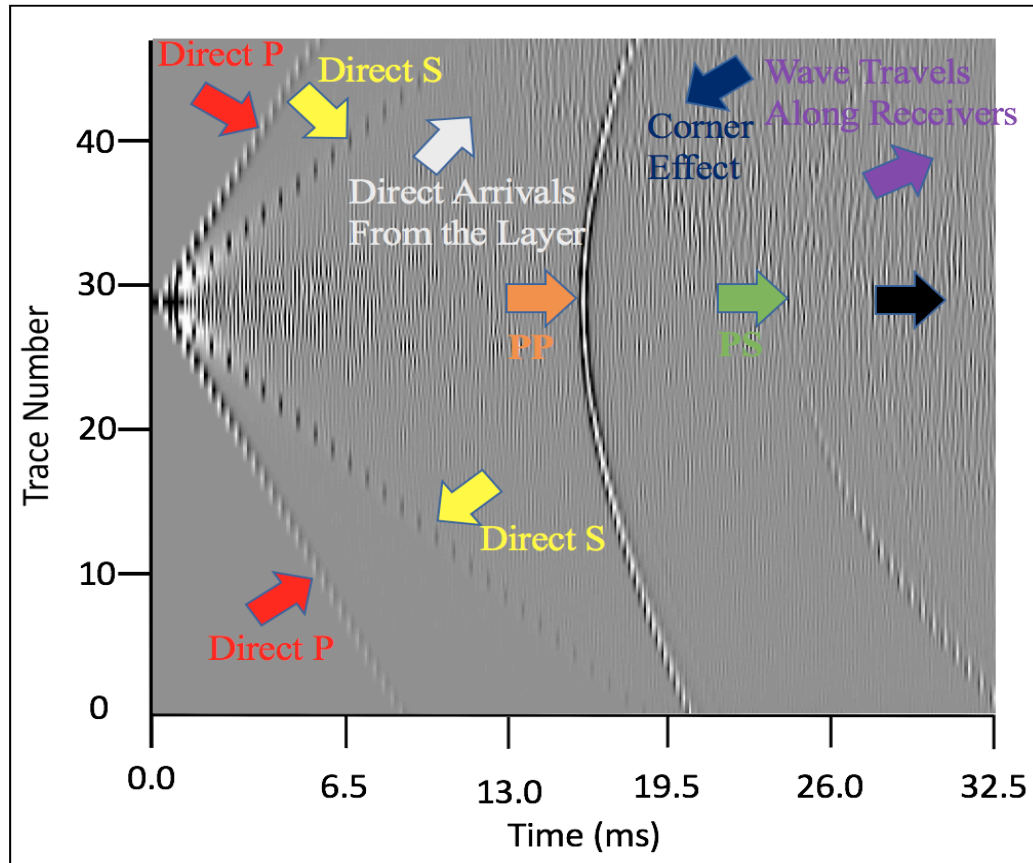


Figure 3.32: The seismogram (z-component) of the 19 meters depth tunnel model with the absorbing boundary condition (surface) with two layers and a 4000 Hz seismic source at 20 meters depth on the left side of the model.

Subsequently, we created a set of shot gathers (Figure 3.32) to be able to apply the seismic migration to our generated shot gather. According to the migration results (Figure 3.33), the location of the tunnel had a small error in that the tunnel is 1.5 meters longer than its designed initial model. Also, we located the surface effect, which is caused by the direct arrivals, and Kirchhoff migration artifacts that are caused by the

insufficient number of receivers and shots. In addition, the shallow layer is not recognizable from the migration result, due to a thin shallow layer with only one shot inside (at 0 meters depth), the slow seismic speeds of the shallow formation, and the high frequency of the source (4000 Hz).

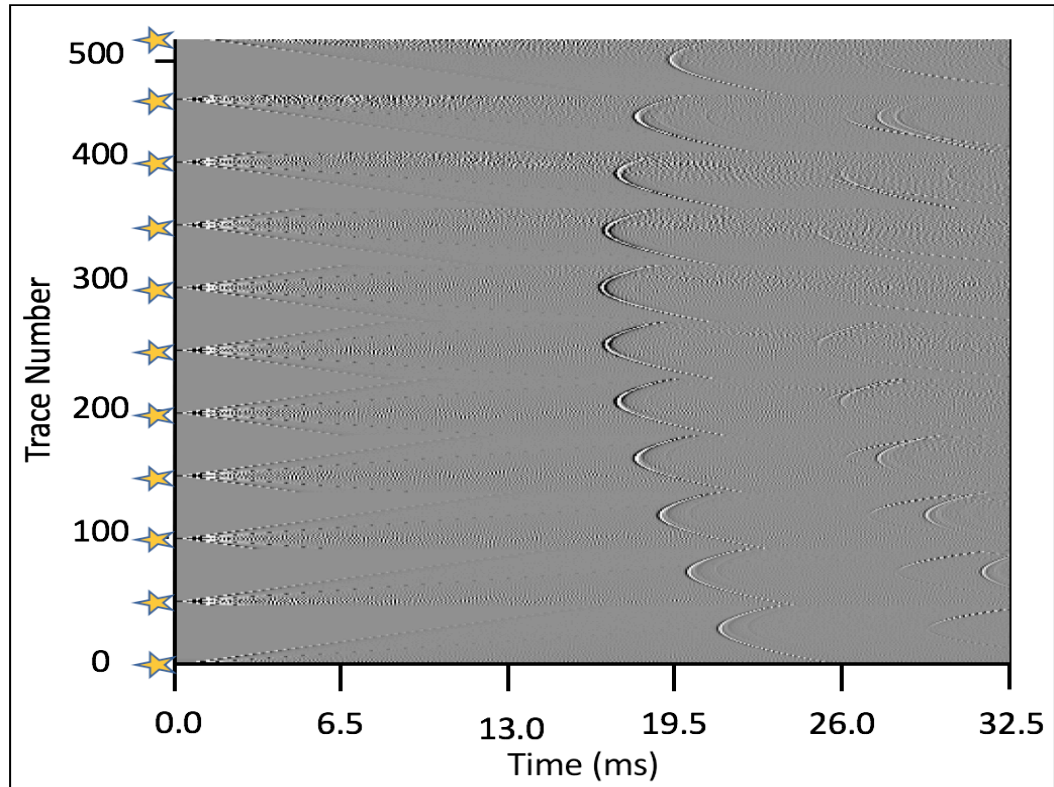


Figure 3.33: The set of shot gathers with the absorbing surface boundary condition (for all boundaries) for the 19 meters depth tunnel with two layers. The seismic sources are single-force 4000 Hz sources that are located on the left boundary of the model.

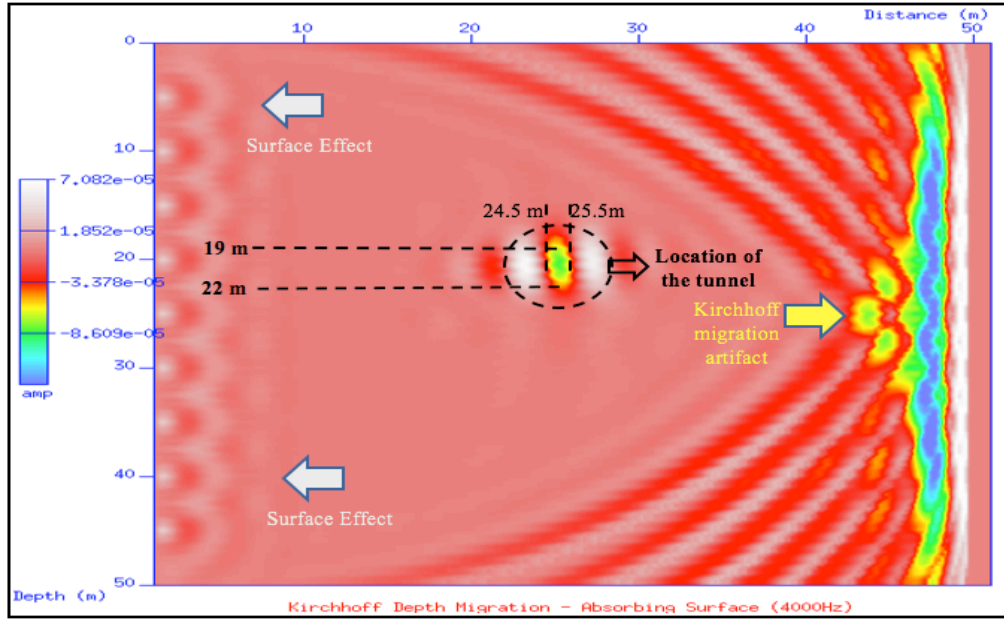


Figure 3.34: Kirchhoff migration result of the 19 meters depth tunnel model with two layers with the absorbing surface boundary condition (for all boundaries) and the seismic sources are single-force 4000 Hz sources located on the left boundary of the model (Amp represents the amplitude, which is a measure of the contrast in density, seismic velocities of the formations and / or underground structures).

Chapter 4: Recommended Acquisition Design to Locate Tunnels

4.1 Introduction

In the previous chapters, by comparing all the results from earlier chapters, we concluded that the cross-well seismic method when the source and receivers are located inside of a medium without wells gave the best results for locating the clandestine tunnels. We tried to find the ideal acquisition design parameters and seismic source frequency to detect the tunnels in our numerical model, which is generated with real parameters (seismic, velocity and density) for the cross-well seismic method.

For this objective, we produced some numerical models to discover a recommended acquisition design based on a tunnel at 14 meters depth, since the cross-well method without wells can easily detect tunnels if they are close enough to the receivers and sources. To test this, we modeled one layer and two layered models with a tunnel located at 14 meters depth and ran these different models with two different frequencies of 3000 Hz and 4000 Hz sources, then compared the models to each other to find the best acquisition design for locating the clandestine tunnels. We also used attenuation for our models to make our numerical modeling more realistic. We chose our quality factor as 30 since it is in the range of clays and marls (Table 4.1), and used this value to our numerical models.

Table 4.1: Orders of magnitudes of Q-factors of rocks of P-Waves (Modified and retrieved from Lavergne, 1989).

Type of Formation	Q - Factor
Clays and marls	30 - 70
Sands and sandstones	70 - 150
Limestones and dolomites	100 - 600
Granit and basalts	200 - 600

4.1.1 Model of Tunnel Located at 14 Meters Depth

In this part of our research, we used two different acquisition designs. The first acquisition design has the receivers and the shots on the left boundary of the model to record the reflections from the tunnel. In the second acquisition design, the seismic sources are located on the left boundary of the model and the receivers are located on the right boundary of the model. With the second acquisition geometry, we aim to prove the existence of the tunnel in our model from the direct waves going through the tunnel, and use the design's results for supporting the first acquisition geometry that we created. Since we received better results with the absorbing boundary condition for the models

that we created in the earlier chapters, we only generated models with absorbing boundary condition in this section. However, we applied the free surface boundary condition to the final model to test if our proposed acquisition design can locate the tunnels in the most realistic design that we created in this research.

4.1.1.1 One Layer Case

In this section, we generated models with one layer. Each has a tunnel at 14 meters depth in the middle of the model with two different acquisition designs, and two different frequencies (3000 Hz and 4000 Hz), shown below in Table 4.2. The acquisition design for targeting the reflection waves from the tunnel is shown in Figure 4.1 and the other acquisition design that we created focusing on the direct waves is shown in Figure 4.2.

Table 4.2: The acquisition geometry parameters for the 14 meters depth tunnel with one layer for the cross-well seismic method without wells.

Model Dimension	25 m x 50 m
Seismic Shot Range	11 shots, starting from 0 m to 50 m with 5 m spacing on z-axis (on the left boundary)
Number of Receivers and Their Sequence	47 receivers starting from 2 m to 48 m on z-axis (on the left and right boundaries for each example)
Frequency of Source and Its Type	3000 Hz and 4000 Hz, Ricker wavelet, Single Force (Coupled)
Tunnel Depth	14 m
Recording Length (millisecond)	32.5 ms
Boundary Condition	Absorbing Boundary (Top Layer) for Each Example
Velocity Model	$V_p = 1100$ m/sec, $V_s = 575$ m/sec, $d = 1.66$ g/cm ³

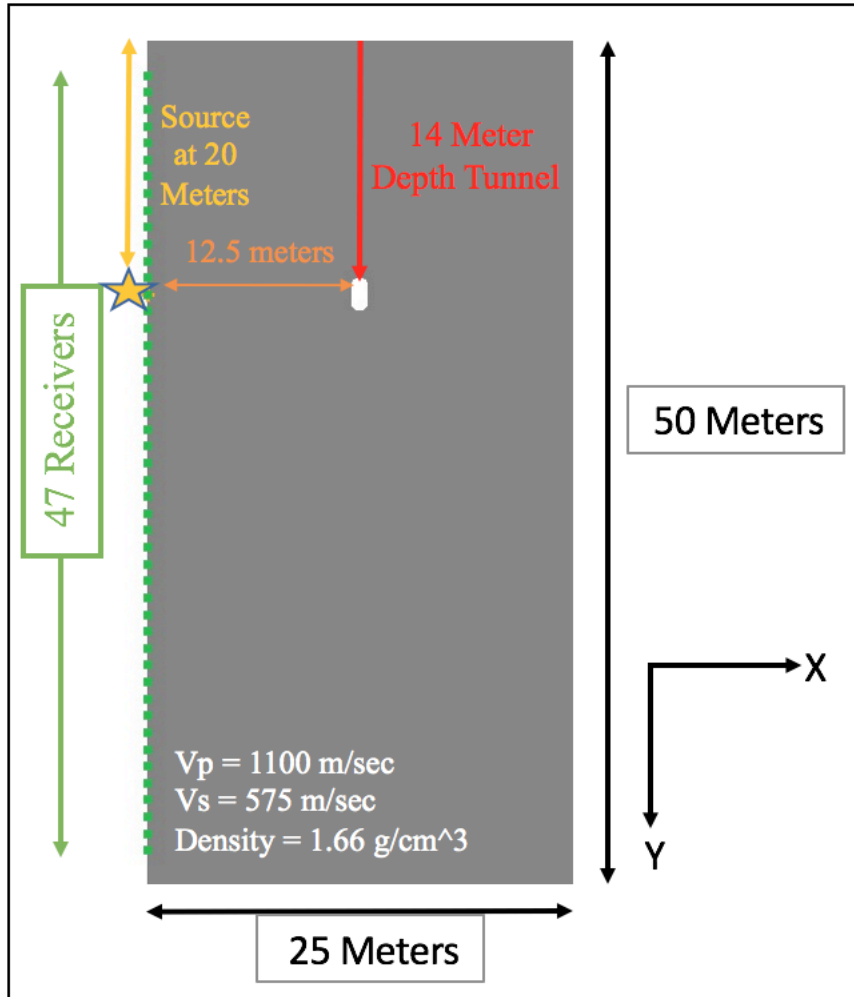


Figure 4.1: The acquisition geometry and parameters of the 14 meters depth tunnel model with one layer when the receivers and the source are located on the left boundary of the model.

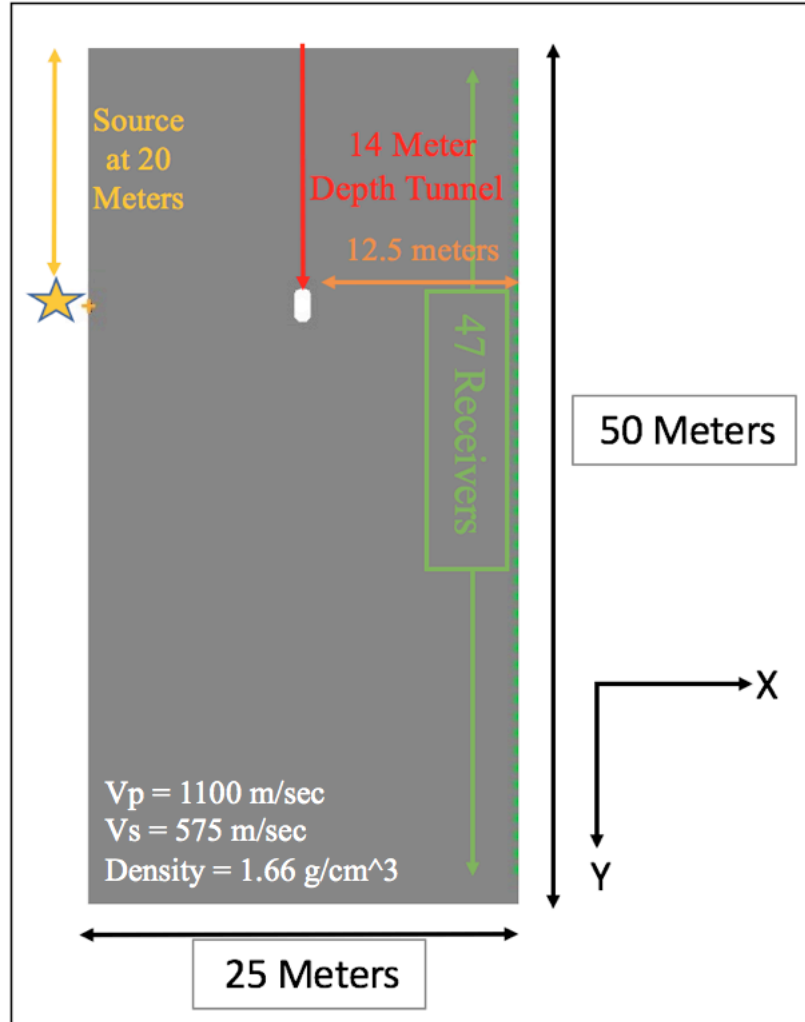


Figure 4.2: The acquisition geometry and parameters of the 14 meters depth tunnel model with one layer when the source is located on the left boundary and the receivers are placed on the right boundary of the model.

We then assigned the required parameters into Specfem2D software and ran our script to generate the seismograms for the 14 meters depth tunnel model with the absorbing boundary condition (surface) with one layer and a 3000 Hz source. After running the software, we recorded the seismogram to generate two sets of shot gathers for the direct waves case and the reflection case. Having generated the set of shot gathers, we

applied the Kirchhoff migration script to our set of shot gathers. According to the migration result (Figure 4.3), we cannot locate the tunnel due to the Kirchhoff migration effect, because the tunnel's amplitude is suppressed by the migration effect.

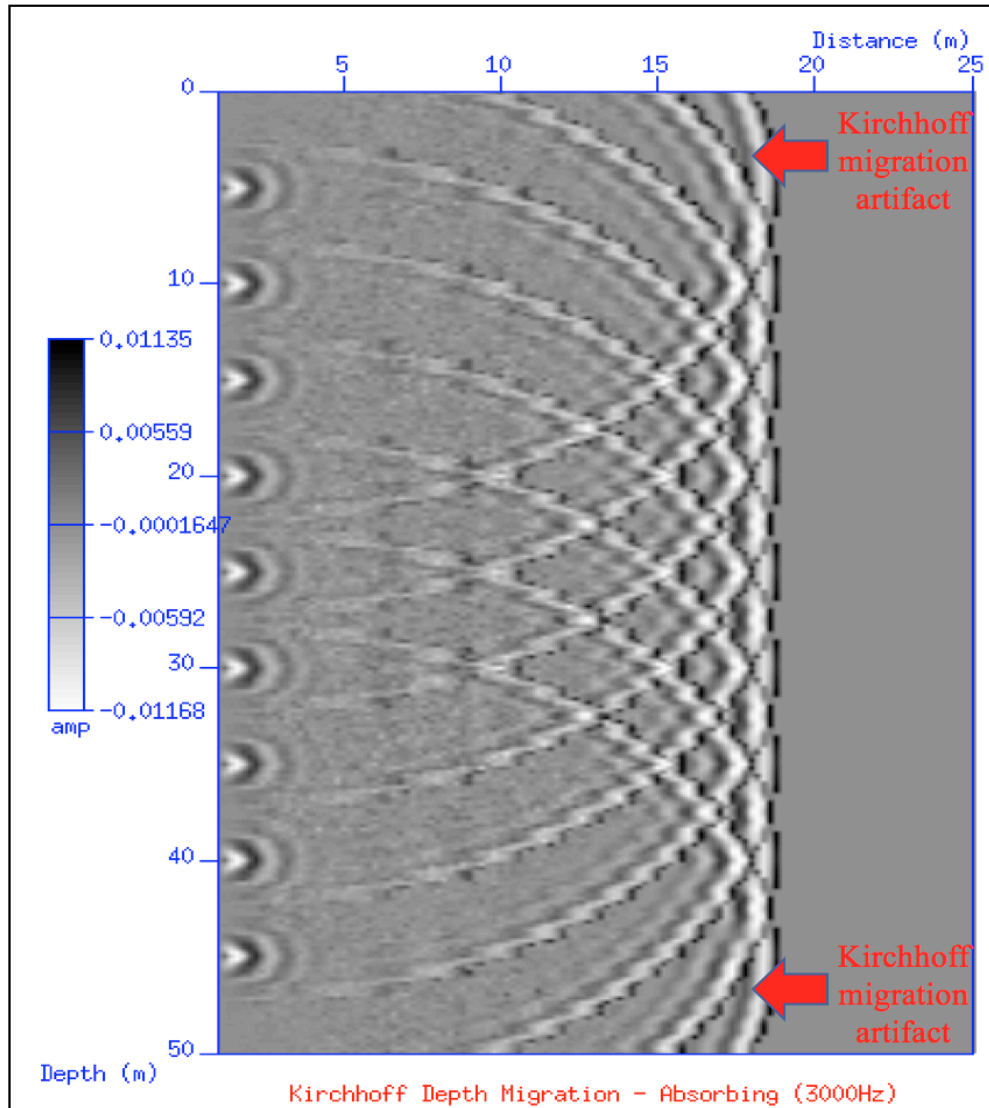


Figure 4.3: Kirchhoff migration result for the model in which single-force 3000 Hz sources and the receivers are located on the left boundary of the model (Amp represents the amplitude, which is a measure of the contrast in density, seismic velocities of the formations and / or underground structures).

When we examine the migration result for the model that has the sources on the left boundary and the receivers on the right boundary, we can locate the location of the tunnel precisely at 12.5 meters on the x-axis and between 14 m to 16 m. Since we do not have anything other than the tunnel in the model, we can conclude that discontinuity on the migrated seismic waves is caused by the existence of the tunnel (yellow zone). In addition, the red arrows indicate the Kirchhoff migration effect on the result, and the blue arrows show the absorbing boundary condition effect that absorbed the migrated seismic waves from both sides.

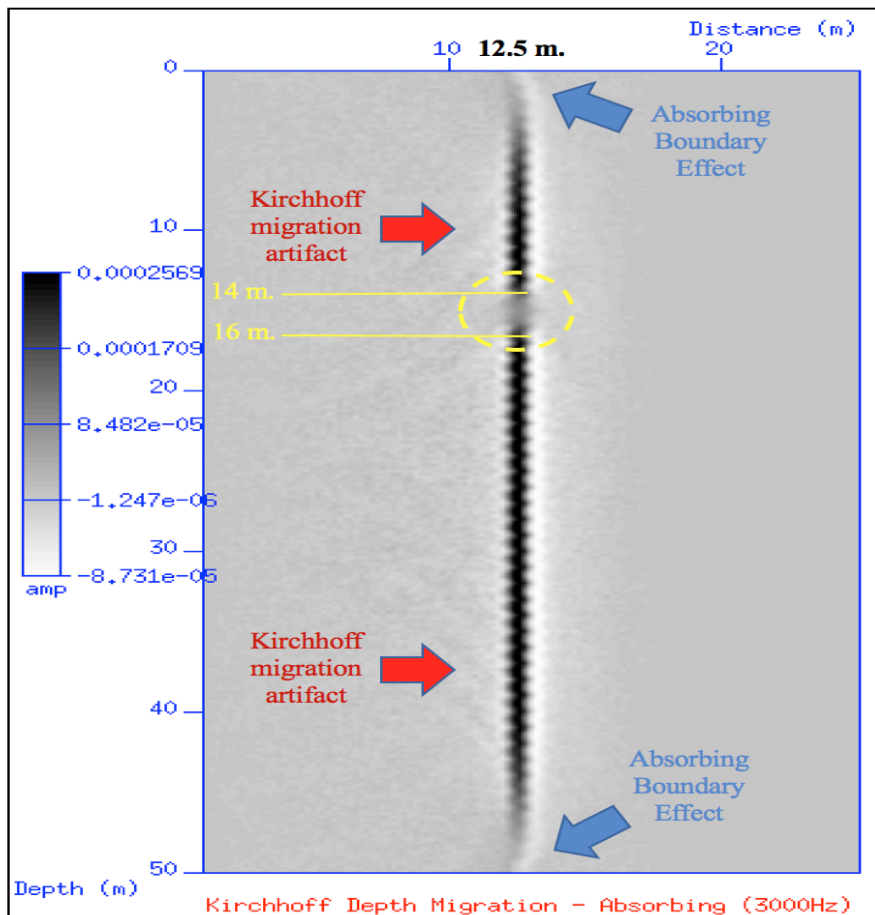


Figure 4.4: Kirchhoff migration result for the model in which single-force 3000 Hz sources are located on the left boundary and the receivers are placed on the right

boundary of the model (Amp shows the amplitude, which is a measure of the contrast in density, seismic velocities of the formations and / or underground structures).

The task to generate and review the models with a 3000 Hz source completed, we ran new examples of seismic modeling with 4000 Hz sources using the same parameters from the 3000 Hz case. Then we assigned the required parameters into the Specfem2D software and ran our script to generate seismograms for the 14 meters depth tunnel model with the absorbing boundary condition (surface) with one layer and a 4000 Hz source. Next, we recorded the seismogram to generate two sets of shot gathers for the direct waves case and the reflection case. Then we generated the set of shot gathers and applied the Kirchhoff migration script to our set of shot gathers. According to the migration result (Figure 4.5), the tunnel's amplitude was suppressed by the migration effect; therefore, we cannot locate the tunnel due to the Kirchhoff migration effect in the result. After reviewing the case that has the receivers and sources on the left boundary of the model, we continued our research by reviewing the recorded seismogram for the other case.

According to the result of the recorded seismogram in Figure 4.6, we can accurately locate the tunnel's location from our recorded seismic wave propagation. The yellow circle indicates the location of discontinuity of the migrated waves that show two meters length and one meter wide. Since we have only one tunnel with one layer in our model, we can conclude that the discontinuity was caused by the tunnel.

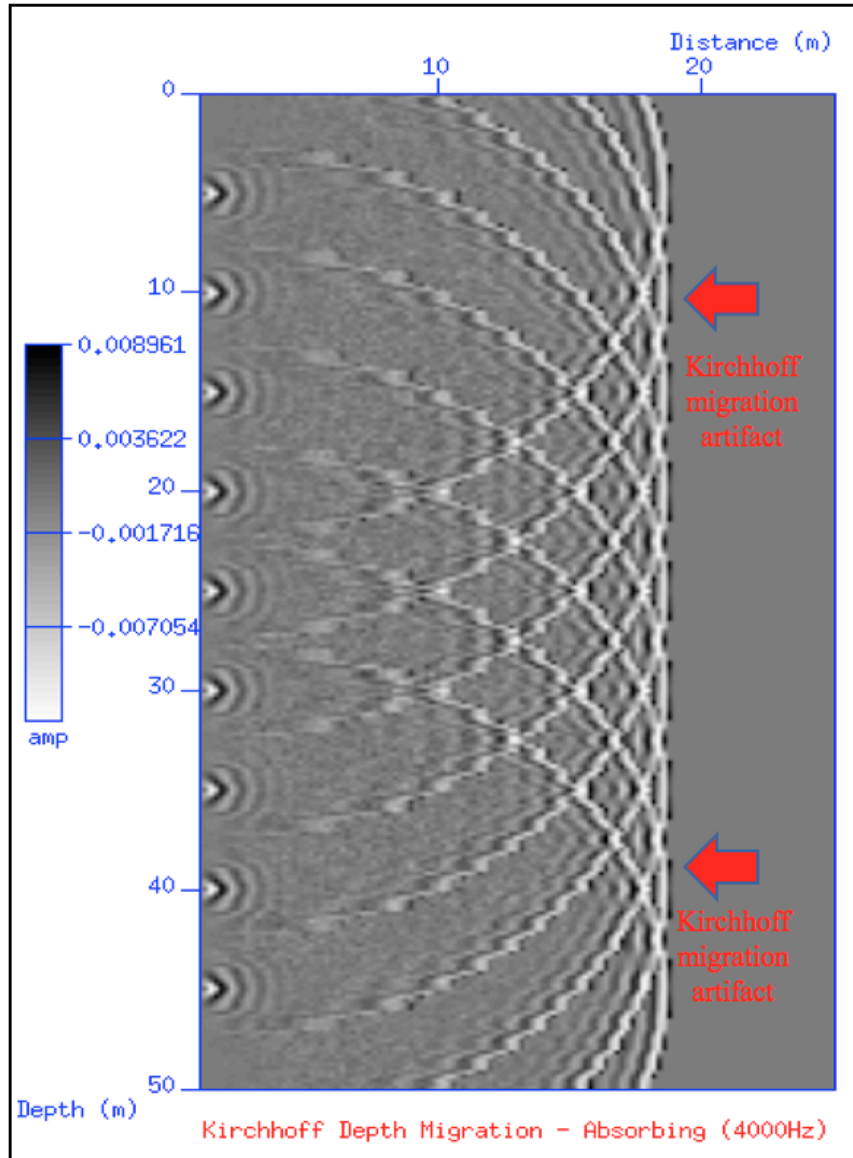


Figure 4.5: Kirchhoff migration result for the model in which single-force 4000 Hz sources and the receivers are located on the left boundary of the model (Amp shows the amplitude, which is a measure of the contrast in density, seismic velocities of the formations and / or underground structures).

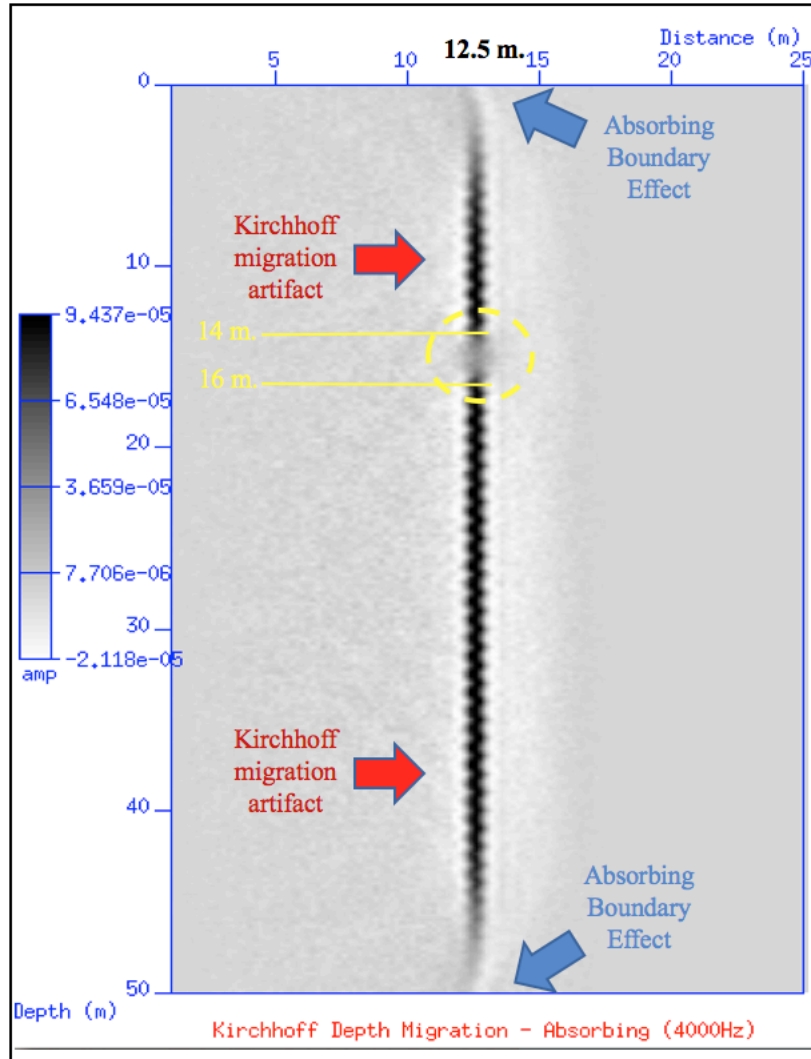


Figure 4.6: Kirchhoff migration result for the model in which single-force 4000 Hz sources are placed on the left boundary of the model and the receivers are located on the right boundary of the model (Amp represents the amplitude, which is a measure of the contrast in density, seismic velocities of the formations and / or underground structures).

4.1.1.2 Two-Layered Case

Upon completing the one layer case examples, we extended our research to generating models that have two layers, with tunnels located at 14 meters depth inside of the models. The acquisition design of the two-layered model for targeting the reflection

waves from the tunnel is shown in Figure 4.7 and the other acquisition design of the two-layered model that we created focusing on the direct waves is shown in Figure 4.8. Other acquisition parameters are given in Table 4.3.

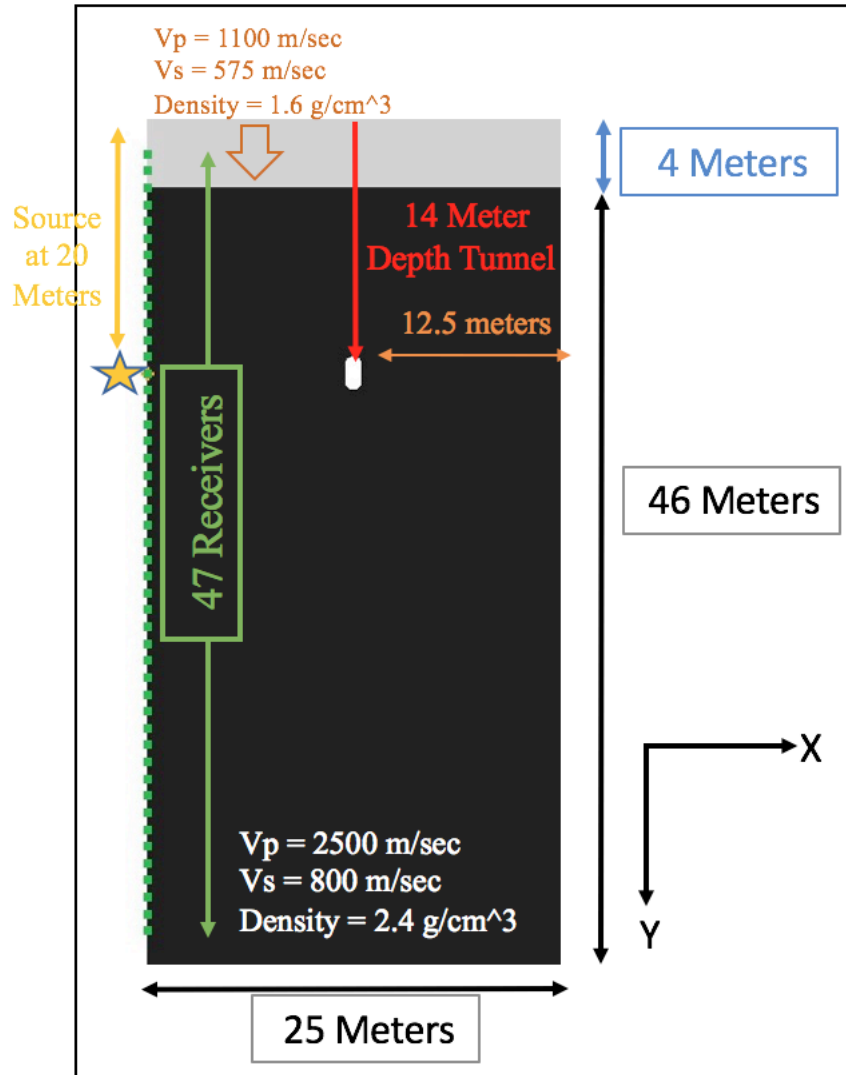


Figure 4.7: The acquisition geometry and parameters of the 14 meters depth tunnel model with two layers when the receivers and the source are located on the left boundary of the model.

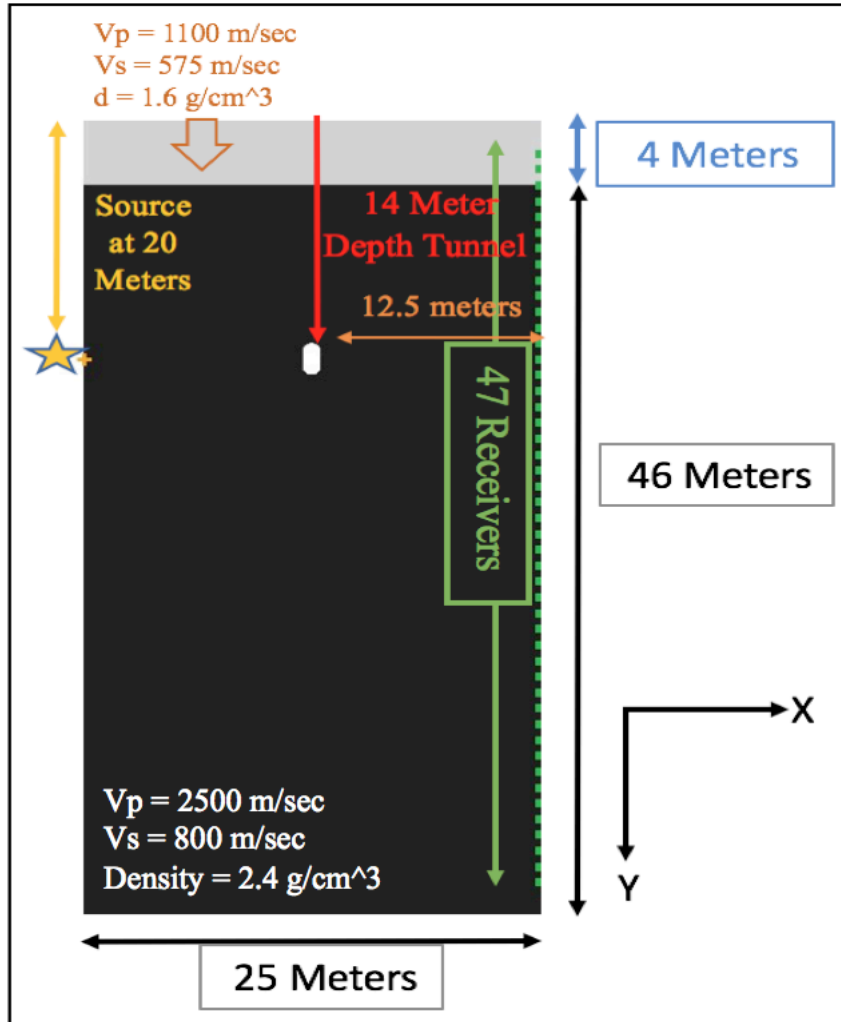


Figure 4.8: The acquisition geometry and parameters of the 14 meters depth tunnel model with two layers when the source is located on the left boundary and the receivers are placed on the right boundary of the model.

Table 4.3: The acquisition geometry parameters for the 14 meters depth tunnel with one layer for the cross-well seismic without wells.

Model Dimension	25 m x 50 m
Seismic Shot Range	11 shots, starting from 0 m to 50 m with 5 m spacing on z-axis (on the left boundary)
Number of Receivers and Their Sequence	47 receivers starting from 2 m to 48 m on z-axis (on the left and right boundaries for each example)
Frequency of Source and Its Type	3000 Hz and 4000 Hz, Ricker wavelet, Single Force (Coupled)
Tunnel Depth	14 m
Recording Length (millisecond)	32.5 ms
Boundary Condition	Absorbing Boundary (Top Layer) for Each Example
Velocity Model	First Layer: $V_p = 1100$ m/sec, $V_s = 575$ m/sec, Density = 1.66 g/cm ³ Second Layer: $V_p=2500$ m/sec, $V_s=800$ m/sec, Density = 2.4 g/cm ³

After we begin the seismic modeling according to the given parameters from Table 4.3 for the acquisition design of the 14 meters depth tunnel model with two layers when the receivers and the source are located on the left boundary of the model, we record the seismograms and generate a set of shot gathers file for this example. Then we

applied Kirchhoff migration to the velocity model that we generated for the two-layered model (Figure 4.9).

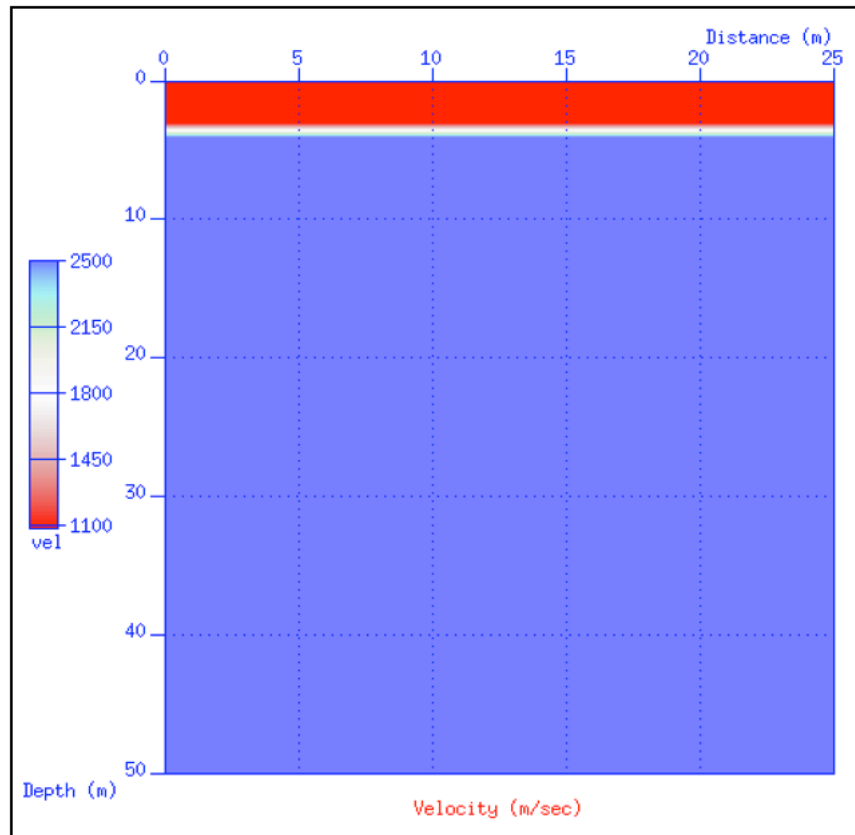


Figure 4.9: The velocity model of the two-layered model (vel represents velocities whose values are between 1100 m/sec to 2500 m/sec).

According to the migration result (Figure 4.10), the effects of Kirchhoff migration that is caused by the limited number of shots and receivers suppress the image of the tunnel in the result file since the tunnel is too close to the receivers' line. Due to these effects, we cannot locate the clandestine tunnel in our migration result. We also cannot locate the shallow formation (bentonite) due to its low seismic velocity values and its thickness.

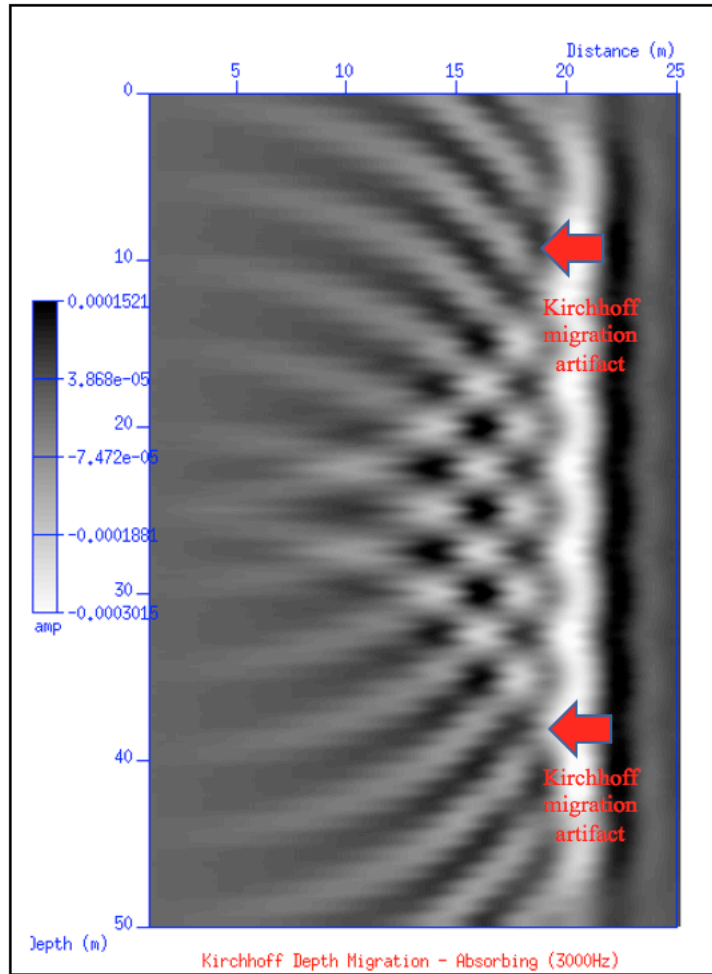


Figure 4.10: Kirchhoff migration result for the model that has two layers in which single-force 3000 Hz sources and receivers are located on the left boundary of the model (Amp shows the amplitude, which is a measure of the contrast in density, seismic velocities of the formations and / or underground structures).

After examining Figure 4.10, we reviewed the migration result in Figure 4.11.

According to Figure 4.11, we can locate the tunnel with its correct location (12.5 meters on the distance-axis and 14 m to 16 m on the depth-axis) and thickness (yellow zone). In addition to this finding, we can also locate the shallow formation's effect on our migrated seismic waves. Due to its low velocities, the slope of the seismic waves is increasing because in this shallow zone, the seismic waves travel slower in comparison to the deeper

formation. We can also see the Kirchhoff migration effects and absorbing boundary effect that absorbs the seismic waves in our result.

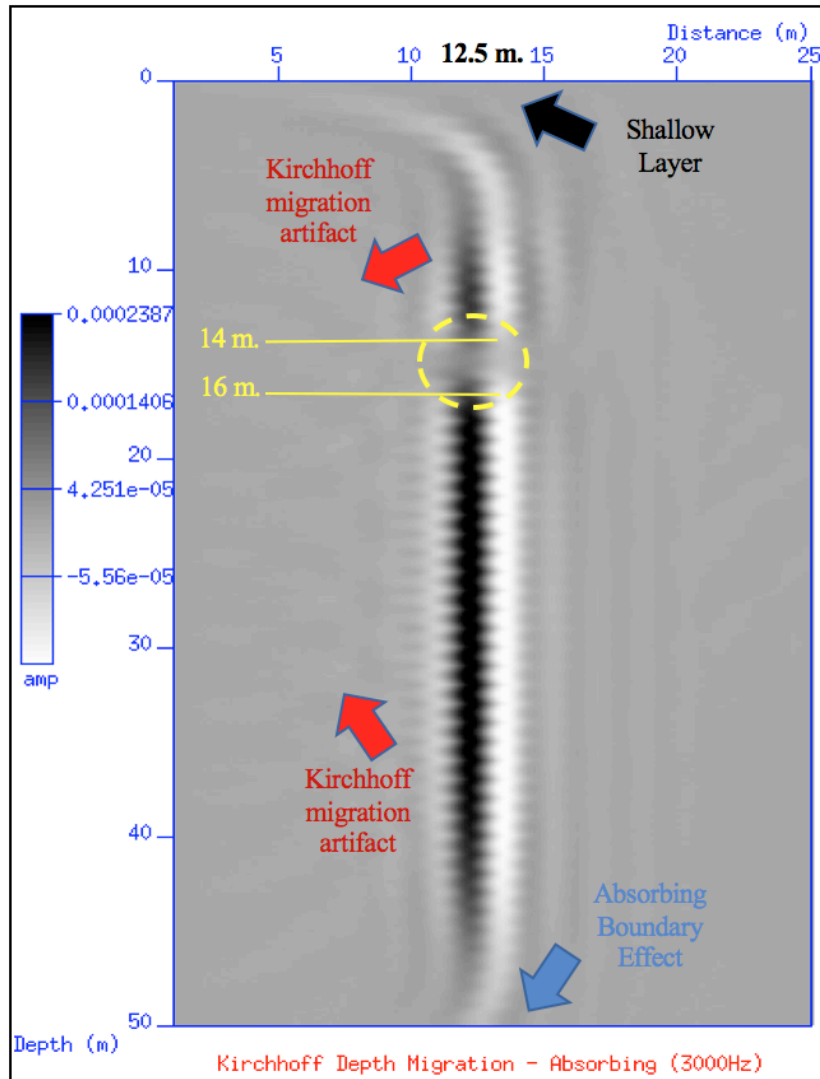


Figure 4.11: Kirchhoff migration result for the model that has two layers in which single-force 3000 Hz sources are placed on the left boundary of the model and the receivers are located on the right boundary of the model (Amp represents the amplitude, which is a measure of the contrast in density, seismic velocities of the formations and / or underground structures).

After interpreting the migration results of the examples with a 3000 Hz source, we continue to examine the models which were run with a 4000 Hz source. According to the

migration result in Figure 4.12, we cannot locate the tunnel because of the strong artifacts from the Kirchhoff migration due to limited number of seismic shots and the receivers.

Since the tunnel is too close to the receivers, it is influenced by these artifacts.

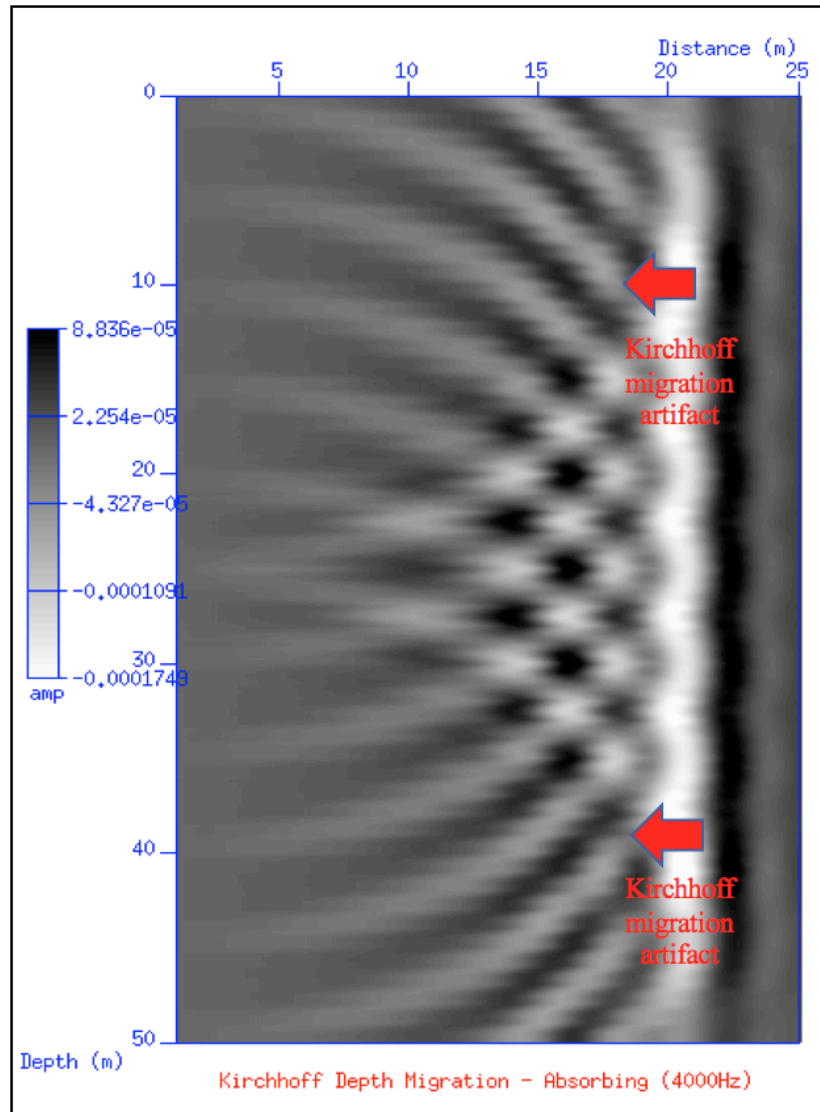


Figure 4.12: Kirchhoff migration result for the model that has two layers in which single-force 4000 Hz sources and the receivers are located on the left boundary of the model (Amp shows the amplitude, which is a measure of the contrast in density, seismic velocities of the formations and / or underground structures).

After reviewing the migration results of the model that has two layers which has the sources and the receivers on the left boundary, we continue to examine the next migration result, which is for the model that has the shots on the left boundary and the receivers on the right boundary (Figure 4.13). According to the Kirchhoff migration result, the tunnel can be imaged with this geometry setting and parameters (yellow zone). This acquisition design gives the accurate location of the tunnel with its true dimensions (height and width). We can also see the effect of the shallow layer on our migrated seismic wave (black arrow). Due to the slow velocities of the shallow formation, the seismic waves travel at slower speeds prompt a delay of the seismic waves' arrival to the seismogram. In addition to the tunnel and shallow formation's effect, we can distinguish the Kirchhoff migration effects (red arrows) and absorbing boundary condition effect (blue arrow).

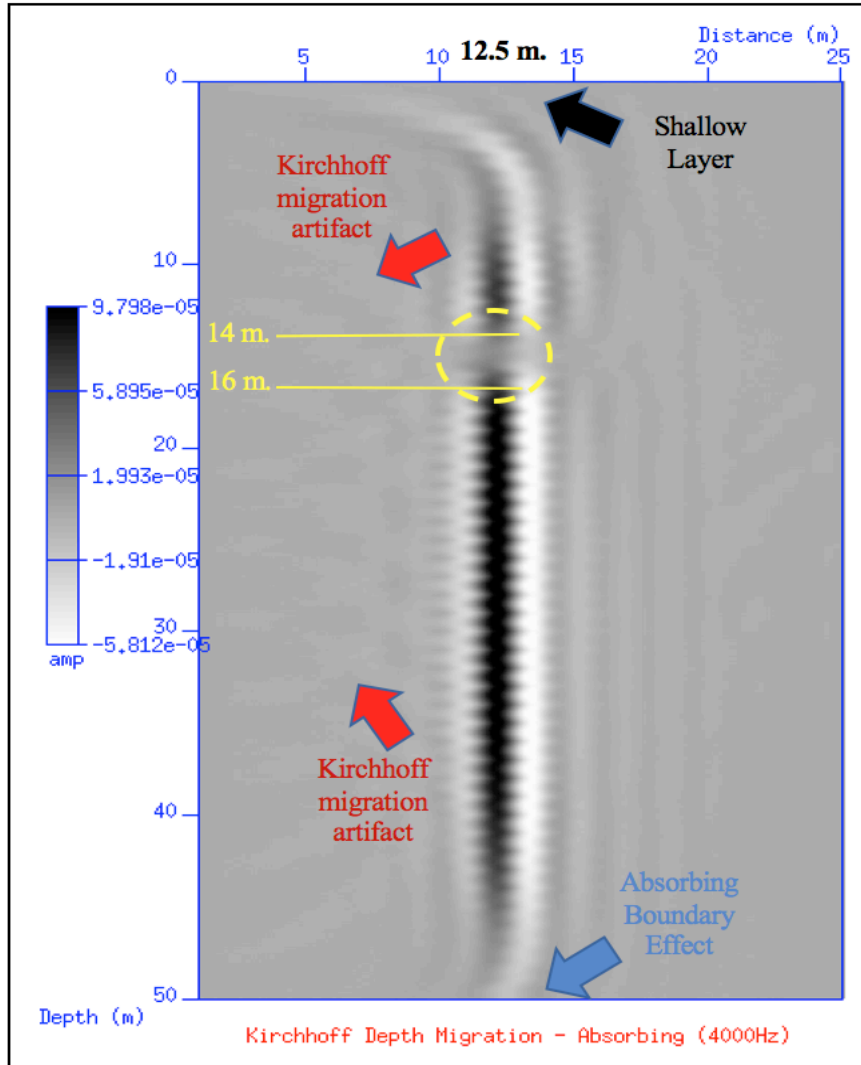


Figure 4.13: Kirchhoff migration result for the model that has two layers in which single-force 4000 Hz sources are placed on the left boundary of the model and the receivers are located on the right boundary of the model with 3000 Hz source (Amp shows the amplitude, which is a measure of the contrast in density, seismic velocities of the formations and / or underground structures).

Chapter 5: Discussion

For the subsurface imaging method in the Chapter 2, direct wave arrivals suppress some of the reflections from the layers and the tunnels, especially with free surface boundary condition. To solve this problem, we also used absorbing boundary condition. However, even with the absorbing boundary condition, we can still detect some waves which behave like surface waves, depending on their incident angle to the surface with the absorbing boundary condition in the figures and the seismograms. The reason for this problem is the imperfect absorbing boundary condition which causes some numerical model mistakes even under perfect parameters and conditions.

For the recommended acquisition design Chapter, 25 meters distance on the x-axis is too short, which causes the Kirchhoff migration's effects to cover almost 25 meters on the x-axis (distance). Due to this reason, we cannot see the tunnel on the migration results of the acquisition geometry that has the sources and the receivers on the left boundary of the model since amplitude values of the tunnel are suppressed by the Kirchhoff migration effects. On the other hand, we cannot increase 25 meters to any higher value since we are using bentonite's parameters (P and S waves' velocities) to model a real case scenario. In a case where there was an increase in the distance between the receivers and the tunnel, there likely would be a problem because the reflections are not going to reach our receivers due to the low velocity values of the bentonite, which will require a longer recording time. To solve this issue, we can increase our nt (total number of time steps) value, which is 65,000 for the current bentonite modeling. So, with a longer duration of recording time, we can increase the distance between the tunnel and

the receivers and record the reflections from the tunnel to be used in the migration in order to get away from the Kirchhoff migration artifacts. Seismic Unix unfortunately does have a limitation for the maximum nt value, and this software does not allow us to image or apply migration for any nt value beyond 65,000. However, to generate high resolution figures for seismic modeling and seismograms, because we are working on shallow seismic imaging, which requires high resolution to detect small details such as the clandestine tunnels, we need to keep our dt (time duration between each time step) value as low as possible to achieve high resolution in our recorded figures and seismograms. On the other hand, decreasing the dt value in Specfem2D causes the program to crash while it is running. This makes seismic modeling impossible with lower dt values.

Chapter 6: Conclusion

In conclusion, after creating a variety of models and using these models in different seismic methods (subsurface seismic method, cross-well method) with different frequencies, we concluded that subsurface seismic method's low source frequency causes a limitation where we can only detect the location of the tunnel correctly by the depth (z-axis) in our migration results. However, we cannot identify the width of the tunnel with subsurface imaging due this method's low frequencies (100 Hz and 400 Hz). On the other hand, cross-well seismic method where the source and the receivers are in the model yields better resolution and more accurate results for our study due to its high frequency values. We tried different numerical models with an array of dimensions and decided that in order to image the clandestine tunnels, the best frequency value for the source is 3000 Hz, which will give a high vertical resolution and the value of the source will be less affected from the attenuation. The recommended acquisition geometry is to place the source and receivers a maximum of 25 meters away from the tunnel with 50 meters depth. Longer distances between the source to the tunnel, and receivers to the tunnel, will make the tunnel more difficult to locate in the real cases.

Chapter 7: Future Work

Numerical modeling for exploration seismology is a subject with broad opportunities. In fact, many different seismic imaging problems can be transferred into numerical models and run simulations to gain anticipated results. For this purpose:

1. A proposal will be written to fund physical modeling and seismic survey for the detection of clandestine tunnels.
2. If funding is received, upon completing the physical modeling and field survey(s), numerical modeling results and physical modeling results will be combined for application in a real data set to prove the detectability of underground tunnels using cross-well seismic imaging, the operation of this method becoming a monitoring system against new tunnels.
3. As final future work, a detailed paper will be written with all findings to be sent to the *Geophysics* journal.

Chapter 8: References

- Ballard, R. F. (1982). Tunnel detection. Vicksburg, Mississippi: U.S. Army Engineer Waterways Experiment Station.
- Bélangier-Rioux, R., & Demanet, L. (2015). Compressed Absorbing Boundary Conditions via Matrix Probing. *SIAM Journal on Numerical Analysis*, 53(5), 2441-2471.
- Biondi, B. (2005). Angle-domain common image gathers for anisotropic migration. *SEG Technical Program Expanded Abstracts*, 1922-1925.
- Bourbié, T., & Coussy, O. (1987). *Acoustics of Porous Media*. Paris: Éditions Technip.
- Cohen, J. K. and Stockwell, Jr. J. W., (2017), CWP/SU: Seismic Un*x Release No. 44R5: an open source software package for seismic research and processing, Center for Wave Phenomena, Colorado School of Mines.
- Dodds, K. (2016, November). Underground: Klaus Dodds is Professor of Geopolitics at Royal Holloway, University of London and author of *Geopolitics: A Very Short Introduction*. *Geographical*, 88(11), 21.
- Elawadi, E., Salem, A., & Ushijima, K. (2001). Detection of cavities and tunnels from gravity data using a neural network. *Exploration Geophysics*, 32(4), 204.
doi:10.1071/eg01204
- Farid, A., Martinez-Lorenzo, J. A., Alshawabkeh, A. N., & Rappaport, C. M. (2012). Experimental Validation of a Numerical Forward Model for Tunnel Detection Using Cross-Borehole Radar. *Journal of Geotechnical and Geoenvironmental Engineering*, 138(12), 1537-1541.
- Fischer, P. F., & Patera, A. T. (1989). Parallel Spectral Element Methods for The Incompressible Navier-Stokes Equations. *Solution of Superlarge Problems in Computational Mechanics*, 49-65.
- Geuzaine, C., & Remacle, J. (2009). Gmsh: A 3-D finite element mesh generator with built-in pre- and post-processing facilities. *International Journal for Numerical Methods in Engineering*, 79(11), 1309-1331.
- Google Earth Pro 7.1.5.1557. (November 17, 2016). Otay Mesa, United States of America. 32°33'31.85"N, 116°58'24.35"W, Eye alt 36072 ft
- Guo, J., & Luo, C. (2014). Application of Tunnel Seismic Image Approach to the Advanced Geological Prediction for Tunnel. *Journal of Multimedia*, 9(7).

Snell's law. (n.d.). Retrieved April 14, 2017, from http://www.glossary.oilfield.slb.com/Terms/s/snells_law.aspx

Kirchhoff migration. (n.d.). Retrieved June 14, 2017, from http://www.glossary.oilfield.slb.com/Terms/k/kirchhoff_migration.aspx

Komatitsch, D. (1997, May). Méthodes spectrales et éléments spectraux pour l'équation de l'élastodynamique 2D et 3D en milieu hétérogène (Spectral and spectral-element methods for the 2D and 3D elastodynamics equations in heterogeneous media). PhD thesis, Institut de Physique du Globe, Paris, France.

Lavergne, M. (1989). Seismic methods. London: Graham & Trotman.

Lytle, R., Laine, E., Lager, D., & Davis, D. (1977). Finding a tunnel using cross-borehole electromagnetic probing. Antennas and Propagation Society International Symposium.

Mahrer, K. D., & List, D. F. (1995). Radio frequency electromagnetic tunnel detection and delineation at the Otay Mesa site. *Geophysics*, 60(2), 413-422.

Marion, B. (2014, January). Cross-Well Imaging Offers Higher Resolution. *The American Oil & Gas Reporter*.

Mavko, G. (2011). Parameters That Influence Seismic Velocity. Conceptual Overview of Rock and Fluid Factors that Impact Seismic Velocity and Impedance. Stanford Rock Physics Laboratory. pp. 73-112. Retrieved from <https://pangea.stanford.edu/courses/gp262/Notes/8.SeismicVelocity.pdf>

McKirdy, E. (2017, March 08). Mosul offensive: Assyrian artifacts discovered in abandoned ISIS tunnels. Retrieved April 09, 2017, from <http://www.cnn.com/2017/03/08/middleeast/mosul-isis-assyrian-antiquities-discovered/index.html>

Miller, R., Ivanov, J., Park, C. (2003). After Action Review, Otay Mesa, California, Tunnel Search Mission. Retrieved from [http://expservices.ku.edu/sites/expservices.drupal.ku.edu/files/docs/2003/Miller%20et%20al.%20\(2003\)%20Otay%20Mesa,%20California,%20Tunnel%20Search%20Mission.pdf](http://expservices.ku.edu/sites/expservices.drupal.ku.edu/files/docs/2003/Miller%20et%20al.%20(2003)%20Otay%20Mesa,%20California,%20Tunnel%20Search%20Mission.pdf)

Nixon, R. (2016, September 01). As Donald Trump Calls for Wall on Mexican Border, Smugglers Dig Tunnels. Retrieved April 06, 2017, from <https://www.nytimes.com/2016/09/02/us/us-mexico-border-wall-tunnels.html>

Patera, A. T. (1984). A spectral element method for fluid dynamics: Laminar flow in a channel expansion. *Journal of Computational Physics*, 54(3), 468-488.

Rechtien, R. D., Greenfield, R. J., & Ballard, R. F. (1995). Tunnel signature prediction for a cross-borehole seismic survey. *Geophysics*, 60(1), 76-86.

Schneider, W. A. (1971). Developments in seismic data-processing and analysis. *Geophysics*, 36, 1043–1073.

Sloan, S. D., Peterie, S. L., Miller, R. D., Ivanov, J., Schwenk, J. T., & Mckenna, J. R. (2015). Detecting clandestine tunnels using near-surface seismic techniques. *Geophysics*, 80(5).

Smith, D. (2017, January 25). Trump signs order to begin Mexico border wall in immigration crackdown. Retrieved July 24, 2017, from <https://www.theguardian.com/us-news/2017/jan/25/donald-trump-sign-mexico-border-executive-order>

Tisato, N., & Marelli, S. (2013). Laboratory measurements of the longitudinal and transverse wave velocities of compacted bentonite as a function of water content, temperature, and confining pressure. *Journal of Geophysical Research: Solid Earth*, 118(7), 3380-3393.

U.S. Immigration and Customs Enforcement (ICE). (n.d.). Retrieved April 10, 2017, from <https://www.ice.gov/news-release-original-images/Feds%20dismantle%20one%20of%20longest%20underground%20tunnels%20ever%20found%20%20along%20California%20border/35278>